

Soft-Demodulation of QPSK and 16-QAM for Turbo Coded WCDMA Mobile Communication Systems

Yusep Rosmansyah

Submitted for the Degree of
Doctor of Philosophy
from the
University of Surrey

Unis

Centre for Communication Systems Research
School of Electronics and Physical Sciences
University of Surrey
Guildford, Surrey GU2 7XH
United Kingdom

Summary

The UMTS HSDPA (Universal Mobile Telecommunication System High Speed Downlink Packet Access) standard has been developed to offer wireless mobile downlink data rate in excess of 10 megabits per second. This is possible thanks primarily to the incorporation adaptive modulation and coding (AMC) involving QPSK and 16-QAM and a binary turbo code (TC), hybrid automatic retransmission request (HARQ), and space-time transmit diversity (STTD).

Maximising the coded performance of a binary TC, such as employed in the aforementioned system, can be partly achieved by providing the TC decoder with good soft-demodulated bits and channel state information (CSI). Unfortunately, there is not much detailed information regarding the soft-demodulation in the literature. Furthermore, the available solution to include the CSI during decoding leads to unnecessary implementation complexity.

This thesis proposes several soft-demodulation methods that include the CSI in every soft-demodulated bit. This way, the best performance of the TC is maintained and at the same time there are no requirements of having separate CSI input to the TC constituent decoder and the corresponding TC decoder modifications, as otherwise necessitated by the approaches in the literature. This approach can simplify a typical HSDPA receiver implementation given that there are many subsystems separating the demodulator and the TC decoder.

The approximate complexity of the proposed soft-demodulation methods is calculated and their performance is evaluated in different communication environments. It is found that one particular approximate soft-demodulation method gives a good performance-versus-complexity compromise throughout. It incurs less than 10% of the complexity of the exact method, yet delivers almost as good performance.

To be able to evaluate the performance of the proposed soft-demodulation methods in more realistic environments, as well as to demonstrate the proposed simplification in the receiver implementation, a UMTS link simulator is developed, including the professional version that is currently used by an industrial partner. In addition, similar evaluation and demonstration in a more complicated HARQ system, namely a simplified HSDPA link simulator, is also developed. A more efficient HARQ redundancy sequence is proposed. It is found that in most channels, the performance of the same approximation soft-demodulation method mentioned above is almost as good as that of the exact method and is better than the approximation method available in the literature.

Acknowledgements

Praise be to Allah, the Cherisher and Sustainer of the worlds.

I would like to express my special thanks to my supervisors Dr. Peter Sweeney and Prof. Rahim Tafazolli for their guidance and support during the whole period of my research in the Centre for Communication Systems Research (CCSR). A word of thanks also goes to Prof. Barry Evans for giving me chance to conduct the research in the Centre.

I wish to express my appreciation to my colleagues, particularly Dr. Reza Hoshyar, Mr. Atta ul Quddus and Dr. David Burgess, for their help and cooperation. Specifically, some of the ideas suggested by Dr. Hoshyar are gratefully acknowledged. The same appreciation goes to the Centre's computing and administration staff for their help and support: Mr. Adam Kirby, Mr. C. Clark, Mr. T. Roberts, Mr. D. Brock, Miss E. Darut, Mrs. S. Evans, Mrs. A. Rubin and Miss. J. Wright.

My gratitude also goes to Prof. A.S. Ahmad, Prof. K. Soemintapoera, Prof. W. Merati and Prof. L. Hendrajaya of ITB-Indonesia for their encouragement and support that enabled me to pursue this research.

Last but not least, I am very grateful to my parents, parents-in-law, my son Fahma, and – most importantly – my wife Yusi for their motivation, understanding and support.

To
my wife Yusi

Contents

Summary	ii
Acknowledgements	iii
Contents.....	v
List of Figures	ix
List of Tables.....	xiii
Glossary of Terms	xiv
Chapter 1 Introduction	1
1.1 Introduction	1
1.2 Motivation and Objectives of the Research.....	2
1.3 Original Achievements	3
1.4 Organisation of the Thesis.....	4
Chapter 2 Overview of the Elements of Wireless Mobile Communication Systems	5
2.1 Introduction	5
2.2 QPSK and 16-QAM Modulation Schemes	5
2.2.1 Introduction	5
2.2.2 QPSK	6
2.2.3 16-QAM	7
2.3 Wireless Mobile Channels.....	8
2.3.1 Introduction.....	8
2.3.2 Channel Modelling.....	10
2.4 Space-Time Transmit Diversity.....	10
2.4.1 Introduction.....	10
2.4.2 Block Coded STTD.....	11
2.5 WCDMA Mobile Communication Systems	12
2.5.1 Introduction.....	12
2.5.2 CDMA.....	13
2.5.2.1 Basic Concept.....	13
2.5.2.2 Basic Transmitter.....	13

2.5.2.3 Basic Receiver	14
2.5.2.4 Rake Receiver.....	14
2.5.2.5 Other Features.....	15
2.5.3 WCDMA.....	16
2.5.4 UMTS.....	17
2.5.5 HSDPA.....	18
2.6 Turbo Codes	18
2.6.1 Introduction.....	18
2.6.2 Encoding	19
2.6.3 Decoding	20
2.6.3.1 MAP and its Simplified Algorithms	22
2.6.4 Parameter Selections	28
2.6.4.1 Constituent Encoder	28
2.6.4.2 Constituent Decoder	28
2.6.4.3 Interleaver.....	28
2.6.4.4 Trellis Termination.....	29
2.6.4.5 Iteration Stopping	29
2.6.4.6 Puncturing.....	29
2.6.4.7 Channel State Information (CSI)	29
2.7 Current Developments in Soft-Demodulation Methods	30
2.8 Summary.....	32
Chapter 3 Link Simulator Development	33
3.1 Introduction	33
3.2 Design.....	34
3.3 Implementation	38
3.4 Validation Process	39
3.4.1 Channel Models	39
3.4.1.1 AWGN and Uncorrelated Rayleigh.....	39
3.4.1.2 Correlated Rayleigh.....	40
3.4.2 Comparison of Uncoded BER Performance with Theoretical Analysis	44
3.4.3 Comparison of TC Performance with Literature.....	46
3.4.4 Comparison of UMTS Simulator Performance with That of Nokia and Ericsson.....	48
3.5 Summary.....	52
Chapter 4 Soft-Demodulation Methods	53
4.1 Introduction	53

4.2	Soft-Demodulation of Binary Modulation in an AWGN Environment.....	54
4.3	Design of Soft-Demodulation Methods in Rayleigh Environments	56
4.4	Approximation “Method M”	59
4.5	Approximation “Method R”.....	60
4.6	Performance Evaluation.....	67
4.6.1	QPSK	68
4.6.1.1	AWGN Channel	68
4.6.1.2	Uncorrelated Rayleigh Channel.....	68
4.6.1.3	Correlated Rayleigh Channel.....	70
4.6.2	16-QAM	71
4.6.2.1	AWGN Channel	71
4.6.2.2	Uncorrelated Rayleigh Channel.....	73
4.6.2.3	Correlated Rayleigh Channel.....	74
4.6.2.4	Effects of Bit Interleaving	76
4.6.2.5	Effects of Interleaving Length.....	79
4.6.2.6	Effects of Doppler Spread	81
4.6.3	Performance versus Complexity Assessment	82
4.7	Summary.....	84
Chapter 5 Soft-Demodulation Applications in WCDMA and STTD Coded Systems		.86
5.1	Introduction	86
5.2	Design of Soft-Demodulation Methods in WCDMA and STTD Systems	86
5.2.1	WCDMA System	86
5.2.2	STTD System.....	89
5.3	Performance Evaluation in WCDMA System.....	89
5.3.1	QPSK	90
5.3.1.1	Validation	90
5.3.1.2	Performance in Various Channels	91
5.3.2	16-QAM	91
5.3.2.1	Validation	91
5.3.2.2	AWGN.....	92
5.3.2.3	Correlated Rayleigh.....	93
5.3.2.4	Vehicular A Environment.....	94
5.4	Performance Evaluation in STTD WCDMA System.....	95
5.4.1	QPSK	95
5.4.1.1	Validation	95
5.4.1.2	Performance in Various Channels	96

5.4.2	16-QAM	97
5.4.2.1	Validation	97
5.4.2.2	AWGN.....	98
5.4.2.3	Correlated Rayleigh.....	99
5.4.2.4	Vehicular A Environment.....	100
5.5	Summary.....	102
	Chapter 6 Soft-Demodulation Applications in HSDPA HARQ System	104
6.1	Introduction	104
6.2	General Description of an HSDPA System.....	104
6.2.1	The HSDPA HARQ	105
6.2.2	Soft-bit Calculation in HARQ Combining.....	106
6.2.3	HARQ First Rate Matching Stage.....	106
6.2.4	HARQ Second Rate Matching Stage	107
6.2.5	Bit Interleaving for HS-DSCH.....	108
6.2.6	Constellation Re-arrangement for 16-QAM	109
6.2.7	Redundancy and Constellation Version Coding	110
6.2.8	Parallel HARQ	111
6.3	HSDPA HARQ Link Simulator.....	112
6.4	Simplified HSDPA HARQ Link Simulator.....	113
6.5	Performance Evaluation.....	118
6.5.1	RV Value Sequence of (6, 1, 3, 5)	118
6.5.1.1	AWGN Channel	118
6.5.1.2	Uncorrelated Rayleigh Channel.....	125
6.5.1.3	Correlated Rayleigh Channel.....	131
6.5.2	RV Value Sequence of (6, 2, 1, 5)	137
6.5.2.1	AWGN Channel	138
6.5.2.2	Uncorrelated Rayleigh Channel.....	142
6.5.2.3	Correlated Rayleigh Channel.....	147
6.6	Summary.....	151
	Chapter 7 Conclusion.....	152
7.1	Conclusion.....	152
7.2	Future Work.....	154
	List of Publications.....	156
	References	158

List of Figures

Figure 2-1: QPSK signal constellation.	7
Figure 2-2: 16-QAM signal constellation.	8
Figure 2-3: Basic CDMA transmitter.	14
Figure 2-4: Basic CDMA receiver.	14
Figure 2-5: Rake receiver.	15
Figure 2-6: Turbo encoder.	20
Figure 2-7: Turbo decoder.	21
Figure 3-1: Simulator Structure.	35
Figure 3-2: 3GPP UMTS bit framing [TGP02b].	36
Figure 3-3: 3GPP HSDPA bit framing [TGP02b].	37
Figure 3-4: Snapshot of W-CDMA Version 3 for Windows 2000/XP.	38
Figure 3-5: AWGN pdf, with mean = 0 and variance = 0.25.	40
Figure 3-6: Correlated Rayleigh power plot.	42
Figure 3-7: Correlated Rayleigh magnitude pdf.	42
Figure 3-8: Correlated Rayleigh squared-magnitude lcr.	43
Figure 3-9: Correlated Rayleigh squared-magnitude afd.	44
Figure 3-10: Performance of Uncoded QPSK in AWGN channel.	45
Figure 3-11: Performance of Uncoded 16-QAM in AWGN channel.	46
Figure 3-12: Performance of UMTS TC(1, 15/13, 15/13) in AWGN channel.	47
Figure 3-13: Performance of TC(1, 5/7, 5/7) in AWGN channel.	48
Figure 3-14: Simulator Performance of Speech 12.2 kbps Service in 3GPP Static (AWGN) channel.	50
Figure 3-15: Simulator Performance of Speech 12.2 kbps in 3GPP Case 1 channel.	51
Figure 3-16: Simulator Performance in Data 64 kbps in 3GPP Static (AWGN) channel.	51
Figure 3-17: Simulator Performance of Data 64 kbps Service in 3GPP Case 1 channel.	52
Figure 4-1: A Simple Low-Pass Equivalent Link Layer Model.	55
Figure 4-2: 16-QAM signal constellation and its corresponding 4-PAM.	59
Figure 4-3: 16-QAM LLR of MSB at $E_s/N_0 = 0$ dB.	61
Figure 4-4: 16-QAM LLR of LSB at $E_s/N_0 = 0$ dB.	63
Figure 4-5: Correction factors of E operator in Method E at $E_s/N_0 = 0$ dB.	64
Figure 4-6: 16-QAM LLR of MSB at (a) $E_s/N_0 = 10$ dB and (b) $E_s/N_0 = 20$ dB.	65
Figure 4-7: 16-QAM LLR of LSB at (a) $E_s/N_0 = 10$ dB and (b) $E_s/N_0 = 20$ dB.	66
Figure 4-8: QPSK Performance in AWGN channel.	68

Figure 4-9: QPSK Performance in Uncorrelated Rayleigh channel	70
Figure 4-10: QPSK BER Performance in Correlated Rayleigh channel	71
Figure 4-11: 16-QAM Performance in AWGN channel.....	72
Figure 4-12: 16-QAM Performance in Uncorrelated Rayleigh channel.....	74
Figure 4-13: 16-QAM Performance in Correlated Rayleigh channel, $f_D = 222$ Hz	75
Figure 4-14: Basic Link Model Incorporating Bit-Interleaving	76
Figure 4-15: Effects of Bit Interleaving on 16-QAM Performance in Uncorrelated Rayleigh channel, using Method E soft-demodulation, Interleaving Length 3012.....	77
Figure 4-16: Effects of Bit Interleaving on 16-QAM Performance in Uncorrelated Rayleigh channel, using Method R soft-demodulation, Interleaving Length 3012	77
Figure 4-17: Effects of Bit Interleaving on 16-QAM Performance in Correlated Rayleigh channel, using Method E soft-demodulation, Interleaving Length 3012	78
Figure 4-18: Effects of Bit Interleaving on 16-QAM Performance in Correlated Rayleigh channel, using Method R soft-demodulation, Interleaving Length 3012.....	79
Figure 4-19: Effects of Interleaving Length on 16-QAM Performance in Uncorrelated Rayleigh channel.....	80
Figure 4-20: Effects of Interleaving Length on 16-QAM Performance in Correlated Rayleigh channel.....	80
Figure 4-21: Effects of Doppler Spread on 16-QAM Performance in Correlated Rayleigh channel.	81
Figure 5-1: Turbo Coded QPSK Performance Validation	90
Figure 5-2: Turbo Coded QPSK Performance in CDMA environment.....	91
Figure 5-3: Turbo Coded 16-QAM Performance Validation.	92
Figure 5-4: Turbo Coded 16-QAM Performance in AWGN channel.	93
Figure 5-5: Turbo Coded 16-QAM Performance in Correlated Rayleigh channel.....	94
Figure 5-6: Turbo Coded 16-QAM Performance in Vehicular A channel.	95
Figure 5-7: Turbo Coded QPSK Performance in AWGN channel.....	96
Figure 5-8: Turbo Coded QPSK Performance in STTD WCDMA system.....	97
Figure 5-9: Turbo Coded 16-QAM Performance Validation.	98
Figure 5-10: Turbo Coded 16-QAM Performance in STTD System, AWGN channel.....	99
Figure 5-11: Turbo Coded 16-QAM Performance in UMTS STTD System, Correlated Rayleigh channel.	100
Figure 5-12: Turbo Coded 16-QAM Performance in STTD System, Vehicular A channel, 6-finger rake.	101
Figure 5-13: Turbo Coded 16-QAM Performance in STTD System, Vehicular A channel, 4-finger rake.	101
Figure 6-1: Two stage rate matching of the HS-PDSCH HARQ.	106

Figure 6-2: HS-DSCH channel interleaving	108
Figure 6-3: Illustration of Constellation Re-arrangement for 16-QAM	110
Figure 6-4: Parallel HARQ operation [TGP01].....	111
Figure 6-5: Timing relationship of UMTS and HSDPA frames implemented in the simulator...	113
Figure 6-6: SAW HARQ model implemented in the simplified simulator.....	114
Figure 6-7: Block sizes in simplified SAW HARQ.....	115
Figure 6-8: 16-QAM BER Performance in AWGN Channel, 3-Retx, 4-Itr	120
Figure 6-9: 16-QAM BLER Performance in AWGN Channel, 3-Retx, 4-Itr.....	121
Figure 6-10: 16-QAM BER Performance in AWGN Channel, 3-Retx, 8-Itr	121
Figure 6-11: 16-QAM BLER Performance in AWGN Channel, 3-Retx, 8-Itr.....	122
Figure 6-12: 16-QAM BER Performance in AWGN Channel, 4-Retx, 4-Itr	122
Figure 6-13: 16-QAM BLER Performance in AWGN Channel, 4-Retx, 4-Itr.....	123
Figure 6-14: 16-QAM BER Performance in AWGN Channel, 4-Retx, 8-Itr	123
Figure 6-15: 16-QAM BLER Performance in AWGN Channel, 4-Retx, 8-Itr.....	124
Figure 6-16: Retransmission Efficiency in AWGN Channel	125
Figure 6-17: 16-QAM BER Performance in Uncorrelated Rayleigh Channel, 3-Retx, 4-Itr	126
Figure 6-18: 16-QAM BLER Performance in Uncorrelated Rayleigh Channel, 3-Retx, 4-Itr.....	127
Figure 6-19: 16-QAM BER Performance in Uncorrelated Rayleigh Channel, 3-Retx, 8-Itr	127
Figure 6-20: 16-QAM BLER Performance in Uncorrelated Rayleigh Channel, 3-Retx, 8-Itr.....	128
Figure 6-21: 16-QAM BER Performance in Uncorrelated Rayleigh Channel, 4-Retx, 4-Itr	128
Figure 6-22: 16-QAM BLER Performance in Uncorrelated Rayleigh Channel, 4-Retx, 4-Itr.....	129
Figure 6-23: 16-QAM BER Performance in Uncorrelated Rayleigh Channel, 4-Retx, 8-Itr	129
Figure 6-24: 16-QAM BLER Performance in Uncorrelated Rayleigh Channel, 4-Retx, 8-Itr.....	130
Figure 6-25: Retransmission Efficiency in Uncorrelated Rayleigh Channel.....	131
Figure 6-26: 16-QAM BER Performance in Correlated Rayleigh Channel, 3-Retx, 4-Itr	133
Figure 6-27: 16-QAM BLER Performance in Correlated Rayleigh Channel, 3-Retx, 4-Itr.....	133
Figure 6-28: 16-QAM BER Performance in Correlated Rayleigh Channel, 3-Retx, 8-Itr	134
Figure 6-29: 16-QAM BLER Performance in Correlated Rayleigh Channel, 3-Retx, 8-Itr.....	134
Figure 6-30: 16-QAM BER Performance in Correlated Rayleigh Channel, 4-Retx, 4-Itr	135
Figure 6-31: 16-QAM BLER Performance in Correlated Rayleigh Channel, 4-Retx, 4-Itr.....	135
Figure 6-32: 16-QAM BER Performance in Correlated Rayleigh Channel, 4-Retx, 8-Itr	136
Figure 6-33: 16-QAM BLER Performance in Correlated Rayleigh Channel, 4-Retx, 8-Itr.....	136
Figure 6-34: Retransmission Efficiency in Correlated Rayleigh Channel.....	137
Figure 6-35: 16-QAM BER Performance in AWGN Channel, 3-Retx, 4-Itr	138
Figure 6-36: 16-QAM BLER Performance in AWGN Channel, 3-Retx, 4-Itr.....	139
Figure 6-37: 16-QAM BER Performance in AWGN Channel, 3-Retx, 8-Itr	139
Figure 6-38: 16-QAM BLER Performance in AWGN Channel, 3-Retx, 8-Itr.....	140

Figure 6-39: 16-QAM BER Performance in AWGN Channel, 4-Retx, 4-Itr	140
Figure 6-40: 16-QAM BLER Performance in AWGN Channel, 4-Retx, 4-Itr.....	141
Figure 6-41: 16-QAM BLER Performance in AWGN Channel, 4-Retx, 8-Itr.....	141
Figure 6-42: 16-QAM BLER Performance in AWGN Channel, 4-Retx, 8-Itr.....	142
Figure 6-43: 16-QAM BER Performance in Uncorrelated Rayleigh Channel, 3-Retx, 4-Itr	143
Figure 6-44: 16-QAM BLER Performance in Uncorrelated Rayleigh Channel, 3-Retx, 4-Itr....	143
Figure 6-45: 16-QAM BER Performance in Uncorrelated Rayleigh Channel, 3-Retx, 8-Itr	144
Figure 6-46: 16-QAM BLER Performance in Uncorrelated Rayleigh Channel, 3-Retx, 8-Itr....	144
Figure 6-47: 16-QAM BER Performance in Uncorrelated Rayleigh Channel, 4-Retx, 4-Itr	145
Figure 6-48: 16-QAM BLER Performance in Uncorrelated Rayleigh Channel, 4-Retx, 4-Itr....	145
Figure 6-49: 16-QAM BER Performance in Uncorrelated Rayleigh Channel, 4-Retx, 8-Itr	146
Figure 6-50: 16-QAM BLER Performance in Uncorrelated Rayleigh Channel, 4-Retx, 8-Itr....	146
Figure 6-51: 16-QAM BER Performance in Correlated Rayleigh Channel, 3-Retx, 4-Itr	147
Figure 6-52: 16-QAM BLER Performance in Correlated Rayleigh Channel, 3-Retx, 4-Itr.....	148
Figure 6-53: 16-QAM BER Performance in Correlated Rayleigh Channel, 3-Retx, 8-Itr	148
Figure 6-54: 16-QAM BLER Performance in Correlated Rayleigh Channel, 3-Retx, 8-Itr.....	149
Figure 6-55: 16-QAM BER Performance in Correlated Rayleigh Channel, 4-Retx, 4-Itr	149
Figure 6-56: 16-QAM BLER Performance in Correlated Rayleigh Channel, 4-Retx, 4-Itr.....	150
Figure 6-57: 16-QAM BER Performance in Correlated Rayleigh Channel, 4-Retx, 8-Itr	150
Figure 6-58: 16-QAM BLER Performance in Correlated Rayleigh Channel, 4-Retx, 8-Itr.....	151

List of Tables

Table 2-1: UMTS WCDMA Basic Parameters	17
Table 2-2: Notations and conditions for the SMAP algorithm.....	22
Table 3-1: Simulation assumptions of Nokia and Ericsson [TGP99a, TGP99b].....	49
Table 4-1: Approximate complexity calculation and comparison	82
Table 4-2: Summary of Relative Coding Gain and Approximate Complexity.....	84
Table 6-1: Parameters for HARQ second rate matching	108
Table 6-2: Constellation Re-arrangement for 16-QAM.....	109
Table 6-3: RV Values for 16-QAM	110
Table 6-4: RV Values for QPSK	111
Table 6-5: RV Values for Maximum Number Retransmissions of 4	115
Table 6-6: Actual Operations of RV Value Sequence of (6, 2, 1, 5) used in [TGP03].....	116
Table 6-7: Actual Operations of the Proposed RV Value Sequence of (6, 1, 3, 5)	117
Table 6-8: Approximate E_b/N_0 Gain Relative to the Use of 3 Retransmissions, 4 TC Decoding Iterations in AWGN Channel at BER of 10^{-5} and BLER of 10^{-3}	119
Table 6-9: Approximate E_b/N_0 Gain Relative to the Use of 3 Retransmissions, 4 TC Decoding Iterations in Uncorrelated Rayleigh Channel at BER of 10^{-5} and BLER of 10^{-3}	126
Table 6-10: Approximate E_b/N_0 Gain Relative to the Use of 3 Retransmissions, 4 TC Decoding Iterations in Correlated Rayleigh Channel at BER of 10^{-5} and BLER of 10^{-3}	132

Glossary of Terms

16-QAM	16-ary Quadrature Amplitude Modulation
3GPP	3 rd Generation Partnership Project
afd	Average Fade Duration
ACK	(Positive) Acknowledgement
AMC	Adaptive Modulation and Coding
ARQ	Automatic Retransmission Request
BER	Bit Error Rate
BICM	Bit Interleaved Coded Modulation
BLER	Block Error Rate
BPSK	Binary Phase Shift Keying
CC	Convolutional Code
CC HARQ	Code Combining HARQ
CCSR	Centre for Communication Systems Research
CDMA	Code Division Multiple Access
CRC	Cyclic Redundancy Check
CSI	Channel State Information
ECC	Error Control Coding
EDGE	Enhanced Data rates for Global Evolution
EGC	Equal Gain Combining
ETSI	European Telecommunication Standard Institute
FC	Fading Coefficient
FCC	Federal Communications Commission
FDD	Frequency Division Duplex
FDMA	Frequency Division Multiple Access
FEC	Forward Error Correction
GHz	Giga (10^9) Hertz
GSM	Global System for Mobile Communications
GUI	Graphical User Interface
HARQ	Hybrid ARQ
HOM	High Order Modulation
HSDPA	High Speed Downlink Packet Access
HS-DSCH	High Speed Downlink Shared Channel
<i>I</i>	In Phase (component)

IMT	I nternational M obile T elecommunication
IR HARQ	I ncremental R edundancy HARQ
IS-95/IS-136	I nterim S tandard 95/ I nterim S tandard 136
ITU	I nternational T elecommunication U nion
lcr	L evel- C rossing R ate
LDPC	L ow D ensity P arity C heck
LLR	L og- L ikelihood R atio
LOS	L ine of S ight
LSB	L east S ignificant B it
MAP	M aximum A P osteriori
MHz	M ega (10^6) H ertz
MIMO	M ultiple I nput M ultiple O utput
MRC	M aximum R atio C ombining
MSB	M ost S ignificant B it
MUD	M ultiuser D etection
NACK	N egative A cknowledgement
NMT	N ordic M obile T elephone
NV	N oise V ariance
OFDM	O rthogonal F requency D ivision M ultiplex
OOD	O bject O riented D esign
OOP	O bject O riented P rogramming
OVSF	O rthogonal V ariable S preading F actor
PCC	P arallel C oncatenated C ode
PCCC	P arallel C oncatenated C onvolutional C ode
pdp	P ower D elay P rofile
pdf	P robability D ensity F unction
PSTN	P ublic S witch T elephone N etwork
Q	Q uadrature (component)
QAM	Q uadrature A mplitude M odulation
QPSK	Q uadriphase S hift K eying, 4- PSK
RSC	R ecursive S ystematic C onvolutional
SAW HARQ	S top and W ait HARQ
SC	S election C ombining
SIR	S ignal p ower to I nterference p ower R atio
SISO	S oft- I nput S oft- O utput
SMAP	S implified M aximum A P osteriori
SOVA	S oft O utput V iterbi A lgorithm

STL	Standard Template Library
STTD	Space Time Transmit Diversity
TC	Turbo Code or Turbo Coding
TCM	Trellis Coded Modulation
TDD	Time Division Duplex
TDL	Tapped Delay Line
TDMA	Time Division Multiple Access
TTCM	Turbo TCM
TTI	Transmit Time Interval
UMTS	Universal Mobile Telecommunication System
USA	United States of America
WCDMA	Wideband Code Division Multiple Access

Chapter 1

Introduction

1.1 Introduction

The wireless mobile cellular communication systems that were based on analogue communication technology, such as the NMT (Nordic Mobile Telephone) system – the first cellular system ever operated, are commonly referred to as first generation systems. Limited quality, services and compatibility have driven the development of second generation systems, which are based on digital communication technology. These include GSM (Global System for Mobile Communications) that is adopted in Europe and most parts of the world, and IS-95 and IS-136 (Interim Standard 95 and 136) that are deployed mainly in the United States of America (USA).

From the point of view of data services, the second generation systems introduce new data services, but the maximum bit rate on offer is only up to 9.6 kbps (kilo bits per second). Improvements were made by extending the standards to support higher bit rates. Specifically in the GSM standard, such an extension is called the EDGE (Enhanced Data rates for Global Evolution) concept, which offers data rate of up to 384 kbps.

In the past few years, the ITU (International Telecommunication Union) conceived a third generation system, IMT-2000 (International Mobile Telecommunication 2000). In terms of data service capability, this system can support up to 2 Mbps (mega bits per second) data services. This system consists of two major standards, UMTS (*Universal Mobile Telecommunication System*) that is proposed by European countries and Japan, and cdma2000 that is proposed mainly by the USA. Both standards are based on the WCDMA (*Wideband Code Division Multiple Access*) technique, and their standardisation processes are managed by the 3GPP (3rd Generation Partnership Projects) consortium. In this thesis, the UMTS system is adopted.

To support even higher data rate services, an enhancement to the UMTS standard was made through the incorporation of the HSDPA (*High Speed Downlink Packet Access*) standard. Currently, this system is capable of providing up to 10 Mbps data services. The provision of high data rate is made possible by means of the adoption of 16-QAM (*16-ary Quadrature Amplitude Modulation*).

Modulation) and TC (*Turbo Code*) operated in conjunction with AMC (*Adaptive Modulation and Coding*) and HARQ (*Hybrid Automatic Retransmission reQuest*) techniques.

1.2 Motivation and Objectives of the Research

UMTS, including HSDPA, standard specifies primarily the transmitter. On the other hand, the choice of algorithms, techniques, and implementations for the receiver is largely up to the implementer. It is expected that the resulting competition will yield better and more affordable solutions.

In this thesis, the main issue to be addressed is the demodulation process at the UMTS and HSDPA receiver for the sake of maximising the performance of the TC. In addition, to simplify the overall implementation of the demodulation and decoding processes, mathematical modelling approaches differing from those found in the literature, will be adopted.

It is well known, for instance in [Hal98, Vuc00], that the TC decoder performs best in fading environments if CSI (*channel state information*), comprising FCs (*fading coefficients*) and NV (*noise variance*), is incorporated in the decoding process. However, in most of the literature, including [LeG94, Bar95, Hal98, Vuc00], the proposed solutions are carried out by modifying the constituent TC decoder, particularly when MAP (*maximum a posteriori*)-based algorithms are adopted. This implies that the CSI must be provided as a separate input to the decoder. Being a scalar, provision and handling of NV is quite easy. In contrast, the FC is a vector, the sequence order of which is the same as that of data. In UMTS and HSDPA, including their STTD (*space-time transmit diversity*) mode, there are up to nine sub-systems separating the demodulator and the TC decoder that alter the data sequence-order. Therefore, processing this extra vector in this way would incur considerable implementation resources and complexity.

Another point regarding the literature is that the Rayleigh channel FCs are commonly modelled as a real-valued vector, as opposed to the more realistic complex-valued vector [Sau99]. Taking into account this point and those in previous paragraph, the complex-valued approach will be adopted in this thesis.

Briefly stated, the aim of the research underlying this thesis is to devise and evaluate high performance yet low complexity soft demodulation methods of QPSK and 16-QAM for UMTS and HSDPA applications. Elaborated, the corresponding objectives are:

1. to derive a simple mathematical model of a wireless mobile communication downlink using complex-number notation (as opposed to the scalar-number notation, as used in the literature, for instance in [LeG94, Bar95, Hal98, Vuc00])

2. to include the CSI in each demodulated bit, hence eliminating the TC decoder's need for a separate CSI input. This helps the complexity of UMTS and HSDPA receiver (the chain from the demodulator up to the TC decoder, in the transport channel demultiplexing part) to remain low
3. to derive exact (analytical) soft-demodulation methods of the modulation schemes that are employed in the HSDPA standard, i.e., QPSK and 16-QAM
4. to derive low-complexity soft-demodulation methods while keeping the consequent TC performance degradation minimum by way of approximating the exact method
5. to estimate and compare the complexity of the devised soft-demodulation methods
6. to evaluate the performance of the devised soft-demodulation methods in different systems and channels (system and channel will be collectively referred to as *environment* hereinafter).

The scope of research will be limited to a single user coded BER (*bit error rate*) link performance based on the use of a conventional rake reception technique employing maximum ratio combining (MRC) method.

1.3 Original Achievements

The original achievements reported in this thesis can be summarised as follow:

1. Using the complex-number-based approach to the communication link system, exact soft-demodulation methods of QPSK and 16-QAM, applicable to different channels, are derived. These methods embed the CSI in every soft-demodulated bit (*soft-bit* hereinafter), hence simplifying HSDPA receiver implementation. This simplification is achieved through elimination of the otherwise unnecessary extra CSI input to the TC decoder as well as the elimination of the necessity to modify the TC constituent decoder.
2. Demonstration that the exact soft-demodulation method of QPSK, through the use of the complex-number-based approach, is already simple, regardless of the channel types. As a result, no further simplification is required.
3. Derivation of a low complexity soft-demodulation method of 16-QAM that performs almost as well as the exact method in different environments.
4. Complexity estimation of different soft-demodulation methods.

5. Performance evaluation and comparison of different soft-demodulation methods in different environments.
6. Application of different soft-demodulation methods in the HSDPA system, including HARQ, and their corresponding performance evaluation.
7. Application of HARQ to a microsatellite communication system.
8. A professional UMTS link simulator, the W-CDMA Version 3 for Microsoft Windows, as the original developer and principal author.
9. A professional UMTS-HSDPA link simulator, the HSDPA Version 0.6 for Microsoft Windows, as the principal author.

1.4 Organisation of the Thesis

The remainder of the thesis is organised as follows: Chapter 2 outlines the basic theories of the important elements making up a wireless mobile communication system under consideration. This includes QPSK and 16-QAM, wireless mobile channels, STTD, and WCDMA systems.

Chapter 3 describes the link simulator development. Also presented are uncoded and coded performance validation processes, by comparing the performance of the developed models with the theory, literature and manufacturers' publications.

In Chapter 4, various soft-demodulation methods of QPSK and 16-QAM are derived and evaluated in basic (non-CDMA) communication environments. The complex-valued modelling approach is adopted. The channels include AWGN, Uncorrelated and Correlated Rayleigh. Effects of bit interleaving, interleaving length and Doppler spread to different soft-demodulation methods' coded performance are evaluated.

In Chapter 5, modification and application of the devised soft-demodulation methods in WCDMA and STTD environments, along with their performance evaluation, are presented. In addition to the regular AWGN and Rayleigh channels, UMTS-HSDPA multipath channel is also used for evaluation.

In Chapter 6, application of the devised soft-demodulations to HSDPA HARQ system, and their performance evaluation, are presented. Performance is measured in terms of BER, block error rate (BLER) and retransmission efficiency.

Finally, conclusion and a discussion regarding future work are given in Chapter 7.

Chapter 2

Overview of the Elements of Wireless Mobile Communication Systems

2.1 Introduction

Analysis, derivation and evaluation of various soft-decision methods, as well as their application to wireless communication systems, will involve a complex model implemented as a link simulator. In particular, the UMTS downlink including its HSDPA mode is chosen as the system to be modelled. Operating this system over a certain wireless mobile channel makes up a wireless mobile environment.

In this Chapter, important elements of the above wireless mobile environment will be briefly explained. They include QPSK and 16-QAM modulation schemes, wireless mobile channels, STTD, WCDMA, UMTS, HSDPA and TC. Following this, a literature review will be presented regarding the latest advances of the soft-demodulation methods of QPSK and 16-QAM in conjunction with TC decoding.

More detailed elaboration about these elements can be consulted from [Pro00, Hay01, Skl01, Rap96, Sau99, Vuc00]. Meanwhile, more advanced subjects reviewed towards the end part of the chapter can be found in their respective cited references.

2.2 QPSK and 16-QAM Modulation Schemes

2.2.1 Introduction

To be able to send data through a wireless mobile channel in a certain frequency band, normally much higher than the information bit rate, a form of carrier modulation must be utilised. Phase modulation is the modulation of choice in current wireless systems. Unfortunately, its undesirable performance when modulation order becomes higher, limits its applicability for systems that require higher capacity and higher bit rate but limited available bandwidth. In fact,

even 8-PSK has been excluded in favour of 16-QAM in the UMTS and HSDPA development process [Hol02]. However, mainly due to high complexity and low performance, other higher order QAM schemes are also excluded. As a result, the adopted modulation schemes in these systems are QPSK and 16-QAM [TGP02c]. In the following sections, these modulation schemes will be briefly described.

2.2.2 QPSK

Using QPSK modulation, 2 bits construct a symbol, which is represented by carrier phases. Therefore, in every symbol period, there are 4 possible phases. Assuming a rectangular filter is used, number of bits per modulation symbol, k , is the same as spectral efficiency. It follows, for QPSK, $k = 2$. This number is also referred to as *modulation order* or *modulation index*. The number of possible symbols, also called *alphabet size*, is $M = 2^k$, hence the term M -ary modulation. For phase modulation, the term is M -PSK, so that for the case of $M = 4$, it is 4-PSK, or more commonly QPSK.

A QPSK modulated carrier waveforms can be represented as

$$u_m(t) = A g_T(t) \cos(2\pi f_c t + (2m + 1) \pi/4), \quad m = 0, 1, \dots, 3 \quad (2.1)$$

where $g_T(t)$ is the transmitting filter pulse shape and A is the signal amplitude. It can be shown that each M -PSK waveform has equal energy of E_s . For convenience of analysis, it is common to assume that $g_T(t)$ is a rectangular pulse lasting for $0 \leq t \leq T$, where T is signalling interval and $A = \sqrt{E_s}$. Therefore, equation 2.1 can be expressed as

$$u_m(t) = \sqrt{\frac{2E_s}{T}} \cos(2\pi f_c t + (2m + 1) \pi/4) \quad (2.2)$$

This equation can be decomposed into two orthogonal components as

$$\begin{aligned} u_m(t) &= \sqrt{E_s} g_T(t) \cos((2m + 1) \pi/4) \cos(2\pi f_c t) - \\ &\quad \sqrt{E_s} g_T(t) \sin((2m + 1) \pi/4) \sin(2\pi f_c t) \\ &= \sqrt{E_s} \cos((2m + 1) \pi/4) \psi_1(t) - \sqrt{E_s} \sin((2m + 1) \pi/4) \psi_2(t) \end{aligned} \quad (2.3)$$

where

$$\psi_1(t) = g_T(t) \cos(2\pi f_c t) \quad (2.4)$$

$$\psi_2(t) = g_T(t) \sin(2\pi f_c t)$$

are the orthogonal basis functions. Therefore, a phase-modulated signal can be viewed as two quadrature carriers with amplitudes that depend on transmitted phase in each signal interval. Represented geometrically as a two-dimensional vector yields:

$$s_m = \left(\sqrt{E_s} \cos((2m+1)\pi/4) \quad \sqrt{E_s} \sin((2m+1)\pi/4) \right). \quad (2.5)$$

A diagrammatical representation of this vector is shown in Figure 2-1. Due to better BER performance, Gray coding is implied in all modulation schemes, unless stated otherwise.

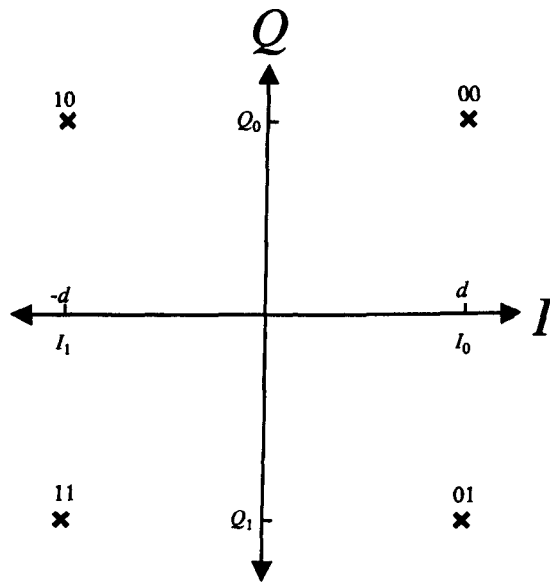


Figure 2-1: QPSK signal constellation.

2.2.3 16-QAM

As implied by its name, a QAM signal is constructed by two quadrature carriers, that is $\cos(2\pi f_c t)$ and $\sin(2\pi f_c t)$. The waveforms can be expressed as

$$u_m(t) = A_{mc} g_T(t) \cos(2\pi f_c t) + A_{ms} g_T(t) \sin(2\pi f_c t), \quad m = 0, 1, \dots, M-1 \quad (2.6)$$

where $\{A_{mc}\}$ and $\{A_{ms}\}$ are the sets of in-phase and quadrature amplitude levels, respectively, made up of combination of k bits. Represented in a single trigonometric form, it can be considered as a generalisation of QPSK, namely phase modulation combined with amplitude modulation. The waveforms take the form of

$$u_{mn}(t) = A_m g_T(t) \cos(2\pi f_c t) + \theta_n, \quad m = 0, 1, \dots, 2^{k_1}-1; \quad n = 0, 1, \dots, 2^{k_2}-1 \quad (2.7)$$

where $k_1 + k_2 = k$. In this case, it is possible to assign k_1 bits for phase modulation and k_2 bits for amplitude modulation. The geometric signal representation is

$$s_m = \begin{pmatrix} \sqrt{E_s} A_{mc} \\ \sqrt{E_s} A_{ms} \end{pmatrix}. \quad (2.8)$$

From this general expression, there are several possibilities of signal constellations, particularly when $k > 2$. However, owing to simplicity of implementation and analysis, only those that are I - Q separable (i.e., have identical and independent I and Q amplitude sets, square constellations) will be considered and employed in the research. Figure 2-2 illustrates the chosen 16-QAM constellation. This constellation is also adopted by 3GPP [TGP02c], and used earlier in [Web94].

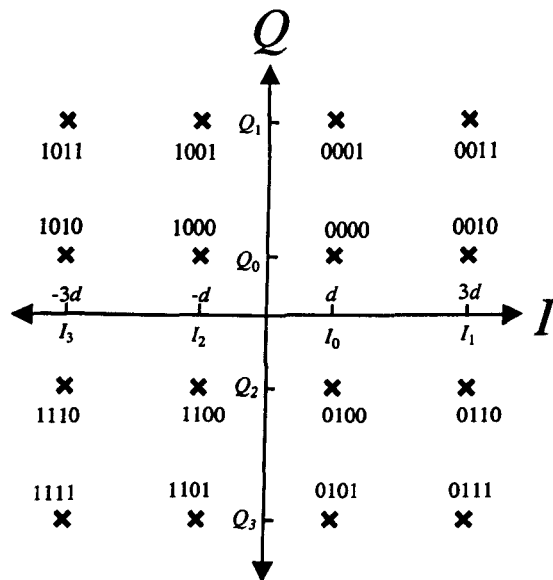


Figure 2-2: 16-QAM signal constellation.

2.3 Wireless Mobile Channels

2.3.1 Introduction

Wireless mobile radio communication (*mobile communication* for short) necessitates the use of transmit and receive antennas. The best possible medium separating them has been widely modelled as AWGN channel. In this case, the primary source of impairments is thermal noise that is unavoidably generated by the receiver. This channel usually serves as the simplest and the least

hostile channel model and is commonly used as a starting point in evaluating a newly designed communication system.

Another necessary element in mobile communication is the distance separating the antennas. In a perfect vacuum environment, the attenuation suffered by the transmitted signal follows a *free-space* or *path loss* model. In a practical mobile environment, however, the channel condition is generally more hostile than that modelled by AWGN and free-space loss. The mobility of the receiver and the presence of surrounding objects give rise to *multipath fading*.

According to Sklar [Skl97] (also Saunders [Sau99]), mobile radio propagation can be classified into *large-scale fading* and *small-scale fading*. Assuming that the transmitter site is stationary, large-scale fading is due to relative motion of the receiver over large areas and the direct path of the signal is obstructed by prominent objects, such as hills, and buildings. This condition is termed as *shadowing*. Meanwhile, small-scale fading occurs due to small changes of the receiver's relative position. Depending on whether or not there is a direct path (or, *line of sight*, LOS) between the transmit and receive antennas, the small-scale fading envelope (or, magnitude) can be described as having *Rician* or *Rayleigh* distribution, respectively.

Small-scale fading manifests through two categories: *time spreading* (or *signal dispersion*) and *fading rapidity*. Each manifestation can be viewed from time and frequency domain. Signal dispersion is categorised further as either *frequency-selective* or *flat* fading, while fading rapidity involves *fast* or *slow* fading.

Before proceeding further with the explanation of different multipath fading types, it is useful to review a few terminologies beforehand. *Maximum excess delay* T_m is defined as the time between the first and the last received multipath components. *Power delay profile* (*pdp*) or *multipath intensity profile* usually provides more comprehensive description in this regard. Viewed from frequency domain, the *pdp* gives *spaced-frequency correlation function*. From this function, information about *coherence bandwidth* f_0 can be obtained. This new term is defined as a statistical measure of the range of frequencies over which the channel passes all spectral components with approximately equal gain and linear phase. Note that T_m and f_0 are reciprocally related.

Another important term is *coherence time*, T_0 , that is defined as a measure of expected time duration over which the channel's response is essentially invariant. Its mathematical description is referred to as *space-time correlation function*. Normally, the frequency domain representation of this function is more widely known, namely, *Doppler power spectral density function*. The frequency-axis-projected width of this function is termed as *fading rate* or *Doppler spread*, f_d . This measure is reciprocally related to the coherence time.

Now, having reviewed the required terminologies, a channel is said to exhibit *frequency-selective fading* if the excess delay is larger than signal's symbol period, $T_m > T_s$. This condition causes *intersymbol interference (ISI)*. When $T_m < T_s$, the channel is referred to as *flat-fading*. Generally, this condition is better than frequency-selective fading, mainly because there is no ISI. However the phasor components can add up destructively to lead to SNR degradation. Viewed from the frequency domain, frequency-selective fading occurs when coherence bandwidth is less than signal bandwidth, $f_0 < W$.

Regarding fading rapidity, *fast fading* occurs whenever coherence time is less than symbol period, $T_0 < T_s$. Otherwise, it is referred to as *slow fading*. In other words, these terminologies indicate whether there is fading variation during a symbol period. Viewed from frequency domain, fast fading occurs if signalling rate (or signal bandwidth) is less than Doppler spread, $1/T_s < f_d$. Normally, fast fading is more hostile, as it causes signal pulses to be distorted that result in SNR loss.

2.3.2 Channel Modelling

For simulation purposes, the AWGN channel will be modelled using an Uncorrelated Gaussian sample generator. In this case, “uncorrelated” means that there is no correlation between successive samples generated from it. This generator is actually derived from another channel model, that is, Uncorrelated Rayleigh generator. This is due to the fact that the magnitudes of complex AGWN samples have Rayleigh distribution.

Correlated Rayleigh channel, characterised by Doppler spread and other parameters, can be obtained by filtering the output of the Uncorrelated Rayleigh samples. However, in this thesis, a more flexible modelling based on a certain deterministic algorithm known as Jakes' model [Jak74, Pae98] is adopted. The frequency-selectivity of the multipath channel is modelled by using a *tapped delay line* (TDL). This way, the power delay profile can be adjusted easily as required. A more detailed description about the implementation of these channel models is given in the next chapter, section 3.4.1.

2.4 Space-Time Transmit Diversity

2.4.1 Introduction

It is well known that using multiple antennas can improve the wireless link performance in fading channel [Jak74]. Although applying this concept at transmitter and receiver sides theoretically achieves better performance, in practice it is usually more straightforward to implement such a

concept at the base station, where implementation of multiple antennas is easier to achieve. This means, for downlink, it is more favourable to implement transmit diversity.

There are several types of spatially separated transmit antenna diversity, but the most common ones are those based on time and frequency. Both techniques exploit the facts that at different instances of time or frequency, the occurrence that both channels are in bad condition are less likely.

From an implementation point of view, transmit diversity can be divided into *open loop* and *closed loop* techniques. In the open loop technique, there is no signalling feedback from the receiver to enable transmitter configuration to adapt to the channel condition. This means, there is no signalling overhead, the complexity of the mobile terminal can be kept low, and the performance does not degrade too much when the channel variation is very high. Unfortunately, because there is no channel adaptation, when the channel variation is slow, the maximum attainable performance is not exploited.

There are several techniques that can be implemented in the open loop mode, namely phase-switched TD [Der02], time-switched TD [TGP02b], orthogonal TD [TIA00], space-time spreading TD [TIA00], and space-time TD (STTD) [Ala98]. STTD can be further divided into two techniques, namely block-coded [Ala98, Tar99] and trellis-coded TD [Bar00].

2.4.2 Block Coded STTD

STTD was originally designed to work for a quasi-static (meaning, fading coefficients remain constant for the STTD block-length duration) narrowband channel [Ala98]. However, provided that the channel exhibits some “quasi-staticity” and the rake receiver can extract multipath components, it will be shown that the technique works equally well for the wideband channel. Slightly modified, this technique has been adopted in the 3GPP standard [TGP02a, TGP02b].

Alamouti's, and thus 3GPP's, STTD encoding is a block code which can be represented by a 2×2 matrix, that is, 2-element time-dimension by 2-element space-dimension (i.e., transmit antennas). Representing time-dimension column-wise and space-dimension row-wise, Alamouti's STTD

encoder is denoted as $\begin{pmatrix} s_0 & -s_1^* \\ s_1 & s_0^* \end{pmatrix}$, whereas 3GPP's is $\begin{pmatrix} s_0 & s_1 \\ -s_1^* & s_0^* \end{pmatrix}$, where s_0 and s_1 are two

successive complex symbols and $*$ denotes complex conjugation operation. It is seen that 3GPP standard modifies the Alamouti's encoder by a simple time-to-space symbols swapping. Therefore, a similarly simple modification is employed at the decoder. Since Alamouti has clearly explained his technique [Ala98], only a mathematical description of the 3GPP's technique is presented here.

Assuming the quasi-staticity of every path of the multipath channels from both transmit antennas, similar to those of Alamouti, the fading coefficients of the paths corresponding to first and second transmit antennas can be expressed as

$$\begin{aligned}\alpha^{(0)} &= \alpha_t^{(0)} = \alpha_{t+T}^{(0)} \\ \alpha^{(1)} &= \alpha_t^{(1)} = \alpha_{t+T}^{(1)}.\end{aligned}\quad (2.9)$$

where T is the symbol duration. Assuming further that a perfect channel estimate is available at the perfect rake receiver, the received and despread symbols at time $t = 0$ and $t = 1$ at each rake finger can be expressed as

$$\begin{aligned}p_0 &= \alpha^{(0)} s_0 + \alpha^{(1)} (-s_1^*) + n_0 \\ p_1 &= \alpha^{(0)} s_1 + \alpha^{(1)} (s_0^*) + n_1\end{aligned}\quad (2.10)$$

where subscript and parenthesised superscript denote time and space dimensions, respectively. Performing STTD decoding on these received and despread symbols as follow:

$$\begin{aligned}s_0 &= \alpha^{(0)*} r_0 + \alpha^{(1)*} r_1 \\ s_1 &= -\alpha^{(1)*} r_0 + \alpha^{(0)*} r_1\end{aligned}\quad (2.11)$$

results in

$$\begin{aligned}s_0 &= (|\alpha^{(0)}|^2 + |\alpha^{(1)}|^2) s_0 + \alpha^{(0)*} n_0 + \alpha^{(1)*} n_1 \\ s_1 &= (|\alpha^{(0)}|^2 + |\alpha^{(1)}|^2) s_1 - \alpha^{(1)*} n_0 + \alpha^{(0)*} n_1.\end{aligned}\quad (2.12)$$

Summing all these symbol estimates over all L -rake receiver fingers, approximately L -fold diversity improvement is expected. (Overview of a rake reception technique is given in section 2.5.2.4).

2.5 WCDMA Mobile Communication Systems

2.5.1 Introduction

Radio communication was firstly introduced by Guglielmo Marconi in 1897. In fact, it was also the first mobile radio communication. It was not until World War II that portability became so important that mobile radio started to emerge. In 1964, non-military land mobile radio system “Radiotelephone” in the USA allowed users to be connected to PSTN (Public Switch Telephone Network). Due to inefficient use of the spectrum, within only tens of years the system reached saturation [Rap96].

In 1964, AT&T Bell Laboratories proposed the concept of cellular telephony to the Federal Communications Commission (FCC). Despite this, the first cellular system was the Nordic Mobile Telephone that was developed by Ericsson and began operation in Scandinavia in 1981. Following this success, there were various standards emerged in Europe and elsewhere in the world, which were based on analogue technology, and subsequently known as first generation cellular systems.

In early 1990s, second generation cellular systems, which were based on digital technology, began to be deployed throughout the world. Most systems, including the Pan-European Global System for Mobile Communications (GSM) standard, utilised TDMA techniques. A few years later in the USA, a similar system based on CDMA, i.e., IS-95, was also introduced.

As technology evolves, the need for higher data rate services is inevitable. While this demand can still be served to some extent by enhancing the capability of existing second generation cellular standards, such as the Enhanced Data rates for Global Evolution (EDGE) concept in GSM standard, there are many more mobile applications that require beyond the enhanced system's capability.

In the past few years, ITU conceived a third generation system, the IMT-2000. This system has recently crystallised into two major standards, UMTS and cdma2000. Both standards are based on WCDMA, and their standardisation processes are managed by the 3GPP consortium. UMTS is mainly supported by European countries and Japan, and this is what we adopt in this research work.

2.5.2 CDMA

2.5.2.1 Basic Concept

While a user is given a specific frequency band in FDMA or time slot in a TDMA system to obtain access, in a CDMA system one is given the whole frequency band at all times but a specific code. This code has much higher rate than the information rate and has very low cross-correlation with the other users' codes. Thus, when it is used for spreading the user's information signal, the spread signal has larger bandwidth and hence smaller power spectral density. At the receiver, cross-correlating this signal with the same spreading code recovers the original information signal, and renders the other interfering signals as background noise.

2.5.2.2 Basic Transmitter

A basic CDMA transmitter is made up of a spreading code generator that spread data signal and a wideband modulator that modulates the spread signal. The block diagram in Figure 2-3 depicts

such a transmitter. In an advanced CDMA transmitter, however, the modulation may take place prior to spreading.

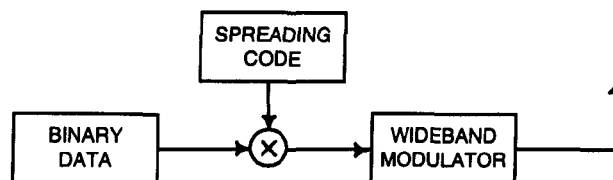


Figure 2-3: Basic CDMA transmitter.

2.5.2.3 Basic Receiver

A basic CDMA receiver consists of a spreading code generator identical to that at the receiver, a code synchroniser and tracker, and a demodulator. Recall from the concept of CDMA information recovery that the spread signal can be despread by means of resspreading, or equivalently, by cross-correlating. Code synchroniser and tracker play a crucial role here since a non-alignment between the locally generated code and the received code renders failure of information recovery. The receiver is depicted in Figure 2-4.

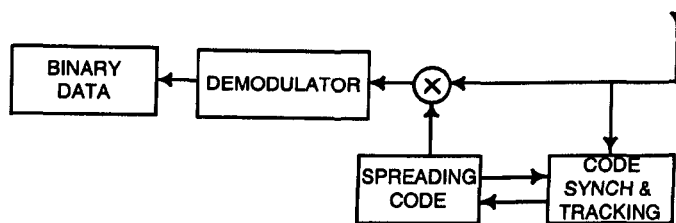


Figure 2-4: Basic CDMA receiver.

2.5.2.4 Rake Receiver

The rake receiver was conceived to combat the effect of a multipath channel, hence it is also called an anti-multipath receiver. The resulting merit is referred to as *multipath diversity*. From Figure 2-5, it can be seen that the rake receiver is an elaboration of the basic CDMA receiver.

Delay compensation is normally accomplished by using a sliding correlator. Each path, also termed *finger*, is despread separately. The results from these paths are then combined in combiner according to a particular combining method.

There are three popular methods: *selection combining* (SC), *equal gain combining* (EGC), and *maximum ratio combining* (MRC). The SC method selects whichever finger has the largest power, and ignores the rest. The EGC method compensates the phases of the signals at all fingers

and sums them with the same weights. In the MRC method, the signal processing is similar to that of EGC, but the summation is carried out by using signal strength of the corresponding finger as weights. A more elaborate exposition about the combining techniques can be found in [Sau99, Pro00].

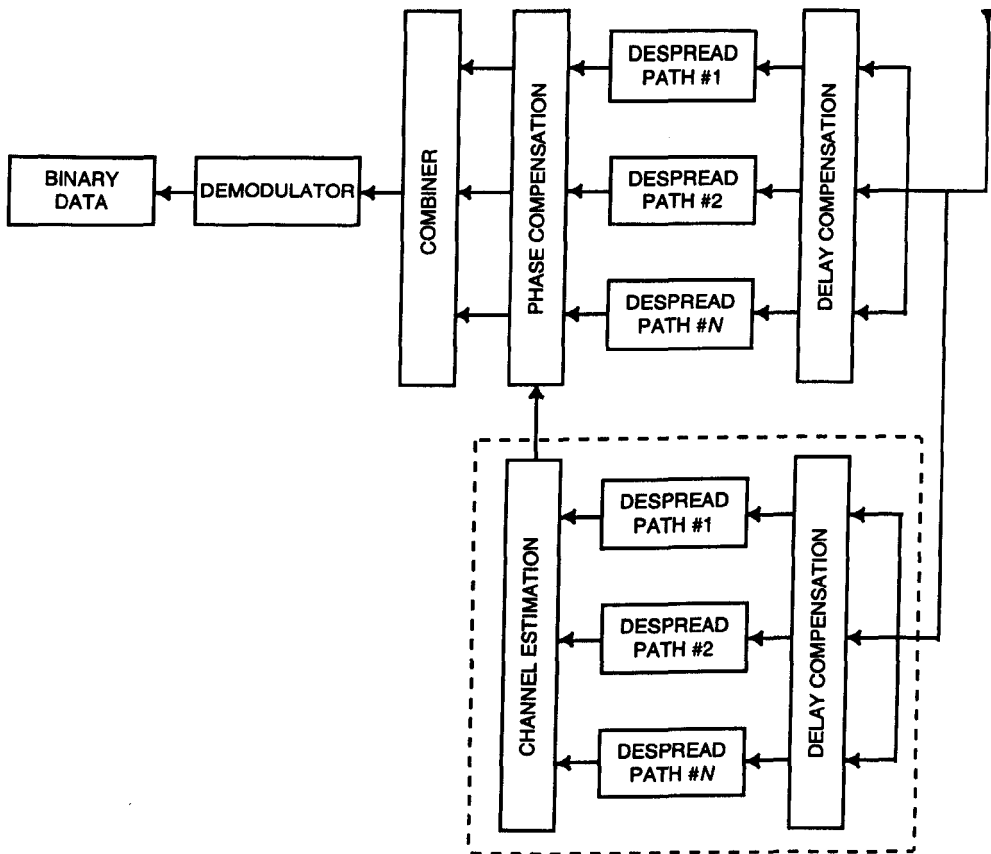


Figure 2-5: Rake receiver.

2.5.2.5 Other Features

There are many other features that are normally incorporated in a real CDMA network. Considering their lower relevance to the topic of the thesis, a few of them will just be briefly overviewed here.

Power Control: The power control concept arises because of the near-far problem, most importantly in the uplink. Due to propagation loss and fading effects, a signal from a nearby mobile terminal is received stronger than that from another farther away. To achieve maximum capacity, the signals arriving at the base station should ideally have the same power level. Power control is one method to deal with this issue.

Soft Handover: Signal from a communicating mobile terminal located in the cell boundary region can be received simultaneously by more than one base station. A mobile terminal enters a soft handover state when signals received from neighbouring base stations exceed a certain threshold but still below the one from the current base station. In this case, it is communicating to more than one base station, and macro diversity results. If the handover occurs in sector boundary (a cell can be divided into a 2 to 4 sectors), *softer handover* takes place. Another type of handover, termed *interfrequency handover*, can take place in a cell employing hierarchical cell structure or multicarrier method.

Multiuser Detection: Has many similarities with *joint detection* and *interference cancellation*, multiuser detection technique is a signal reception technique usually employed at base station by jointly detecting all incoming signals, so that the undesired signals appearing as interference can be systematically removed.

2.5.3 WCDMA

As the name implies, the most distinguishing property of WCDMA from the original CDMA is the occupancy of frequency spectrum. Unfortunately, the “wideband” designation does not officially state a specific bandwidth range, but conventionally it is at least 4 times wider than the bandwidth of IS-95 (a second generation CDMA wireless mobile standard), which is 1.25 MHz. With this bandwidth occupancy, coupled with the use of QPSK modulation, an application requiring up to 2 Mbps peak bit rate is possible. The higher the required bit rate the more restricted the mobility. In addition to bandwidth occupancy, the following are some important WCDMA properties listed in [Pra98, Hol02]:

- multirate services
- packet data
- coherent uplink using a user dedicated pilot
- additional pilot channel in the downlink for beamforming
- seamless interfrequency handover
- fast power control in the downlink
- optional multiuser detection

From the point of view of network synchronisation, WCDMA systems can be synchronous or asynchronous. Meanwhile, in terms of usage of carriers, it can employ single or multicarrier. The

frequency band requirement can be a pair in case of frequency division duplex (FDD), or just a single band for the time division duplex (TDD).

2.5.4 UMTS

UMTS is a candidate for the IMT-2000 being developed harmonically by Europe and Japan in the 3GPP consortium. As a standard, it will cover various aspects of wideband communication systems of the third generation. It is a WCDMA system with particular technical specifications that are different from the other candidates. A summary of the specified parameters is listed in Table 2-1.

Table 2-1: UMTS WCDMA Basic Parameters

Channel bandwidth	5 MHz
Downlink RF channel structure	direct spread
Chip rate	3.84 Mc/s
Roll-off factor of chip pulse shaping	0.22
Frame length	10 ms
Modulation	QPSK (downlink) Dual channel QPSK (uplink)
Coherent detection	User dedicated time multiplexed pilot (downlink and uplink) No common pilot in uplink
Channel multiplexing in uplink	Control and pilot channel time multiplexed I and Q multiplexing for data and control channel
Multirate	Variable spreading and multicode
Spreading factors	4 up to 512
Power control	Open and fast closed loop (1.5 kHz)
Spreading (downlink)	OVSF for channel separation; Gold sequences for cell and user separation (truncated cycle 10 ms)
Spreading (uplink)	OVSF for channel separation; Gold sequences for cell and user separation (truncated cycle 10 ms)
Handover	Soft handover Interfrequency handover
Channel coding	Convolutional codes for low data rate applications, e.g. speech and control. TC for high data rate applications

2.5.5 HSDPA

HSDPA is an enhancement to UMTS offering high bit rate downlink services up to 10 Mbps [TGP02b, Hol02] and higher when a MIMO technique is employed in the forthcoming standard release. This is achieved by incorporating adaptive modulation and coding (AMC) and Hybrid ARQ (HARQ), among others. The AMC involves QPSK and 16-QAM as modulation schemes, and an adaptive rate TC in conjunction with incremental redundancy (IR) HARQ. A compromise in reducing delay, maintaining relatively high throughput efficiency, and reducing implementation complexity is accomplished by shortening transmit time interval (TTI) to 2 ms (as opposed to 10 ms in UMTS) and employing parallel stop-and-wait (SAW) HARQ. All of these are implemented by introducing a new type of transport channel, called the High Speed Physical Downlink Shared Channel (HS-PDSCH), and other corresponding high speed control channels. 3GPP has revised the first HSDPA standard (Release 4 in 1999) to produce the current Release 5 published in 2002 [TGP02b], which is adopted in this research work.

A more elaborate exposition of HSDPA is presented in Chapter 6.

2.6 Turbo Codes

2.6.1 Introduction

TCs were introduced in 1993 by Berrou, Glavieux and Thitimajshima [Ber93]. A basic TC encoder consists of two identical recursive systematic convolutional (RSC) constituent encoders concatenated in parallel, linked by a pseudorandom interleaver. Correspondingly, a TC decoder comprises two constituent soft-input soft-output (SISO) decoders that exchange information iteratively. Owing to this arrangement, it is also referred to as Parallel Concatenated Convolutional Code (PCCC) [Ben95].

The turbo coding concept may be generalised to comprise more than two, non-identical, non-convolutional, non-binary constituent encoders of which inputs are linked through interleaver(s) coupled with appropriate decoders, hence more general terminology Parallel Concatenated Codes (PCC). In fact, the concept has been extended to form serial and hybrid concatenation schemes [Ben96a, Div97] and applied innumerable fields, such as spectrally efficient modulation [LeG94], equalisation [Dou95], multiuser detection [Jun94], and many others.

TCs have been receiving so much attention since their introduction as they exhibit astonishing BER performance. At BER of 10^{-5} , the first TC [Ber93] that applied 18 MAP decoding iterations was approximately 0.5 dB away from Shannon limit [Sha48], which is 0.2 dB (pragmatic limit for

BPSK [Ber93]). As the concept becomes more mature, these achievements improve with time. This includes the rejuvenation of similar codes, such as low density parity check (LDPC). As far as closeness to the Shannon limit is concerned, the current LDPC employing 10^7 -bit block length is only 0.04 (0.0045 in [Chu01]) dB away from the Shannon limit at BER of 10^{-6} [Big02 citing Chu01].

The main elements of the TC that we are considering are:

1. two rate-1/2 constituent RSC encoders, with typical memory length of 3 (equivalently, constraint length of 4)
2. an interleaver that decorrelates the information bit frames before entering the second constituent encoders
3. a puncturer that selects certain bits out of the entire coded bits for creating higher rate code
4. two constituent SISO decoders, the same interleaver and the corresponding deinterleaver for performing soft decision iterative decoding.

In terms of performance, TCs are exceptionally good in the region where E_b/N_0 is low. Beyond this, they exhibit a less favourable feature. This is commonly referred to as “error floor”, that is, when the slope of the performance curve becomes very small. In this region, increasing the E_b/N_0 does not significantly decrease the BER. A simple explanation for this is the fact that the weight property of TC is not high and that TC decoding is not optimum [Ben96d, Div95b]. Expressed in other words, this low weight property leads to low free distance property, as formulated in [Vuc00].

2.6.2 Encoding

The basic idea of turbo encoding is to produce codewords from combinations of two constituent codewords that are as uncorrelated as possible to one another and at the same time producing high weight codewords. It is the task of the interleaver to decorrelate (or to randomise) the codewords by rearranging the indices of the information sequence before putting it into the second constituent encoder.

Since these constituent encoders are fed by different input bit sequences (i.e., original and interleaved), the associated trellises may terminate at different states, so that extra bit sequences (also known as *tail bits*) to reset these states to zero states can consequently be different. This can be addressed through interleaver design or through tail biting. (Tail biting is an encoding process to ensure that the encoding will start and finish at the same trellis state, hence no tail bits are involved.) However, in favour of implementation simplicity, but at the expense of reduced

bandwidth efficiency and possibly performance, simply sending the complete tail bits is the most straightforward solution. This method is adopted by the UMTS standard [TGP02b].

Figure 2-6 depicts an example of a rate-1/3 TC(1, 15/13, 15/13) encoder. The notation $\text{TC}(1, 15/13, 15/13)$ denotes the use of systematic information and an identical RSC(1, 15/13) for both constituent encoders. The generator polynomials are in octal notation. The RSC(1, 15/13) itself has code generator of 15 for feedforward connections and 13 for feedback connections. Note that due to its recursive nature, the selected constituent encoder possesses an infinite impulse response (IIR) characteristic, which is one of the requirements for building good TCs [Div96].

Puncturing is further used to create higher rate codes. It is common to denote the puncturing pattern using a puncturing matrix. At the receiver, the deleted symbols will be replaced by neutral values by the depuncturer.

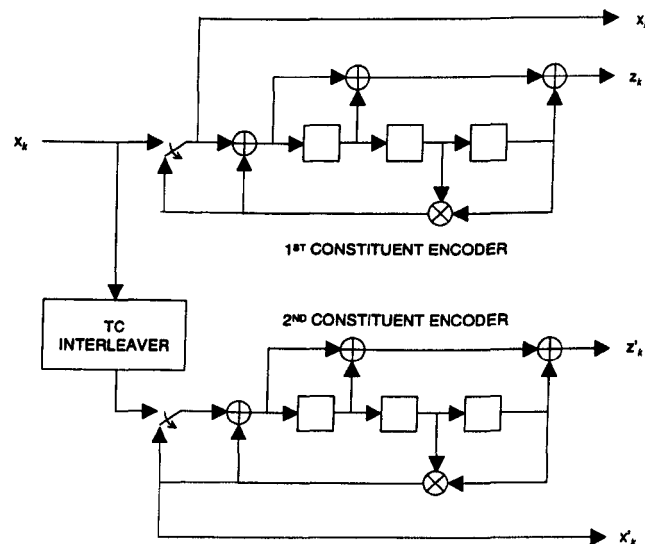


Figure 2-6: Turbo encoder.

2.6.3 Decoding

As opposed to the constituent encoder arrangement, the corresponding constituent SISO decoders are concatenated serially. Although any SISO decoders can be used as a constituent decoder, the most commonly used is that which employs MAP-based decoding algorithms, mainly due to superior performance. The Soft Output Viterbi Algorithm (SOVA) decoder is another alternative, with simpler implementation but inferior performance.

As seen from Figure 2-7, a constituent turbo decoder can be regarded as having two inputs and one output. However, the output can be subsequently extracted to produce two kinds of information: extrinsic information and soft decision of the decoded bits. The two inputs are *a priori* value and soft decision bits from the demodulator output.

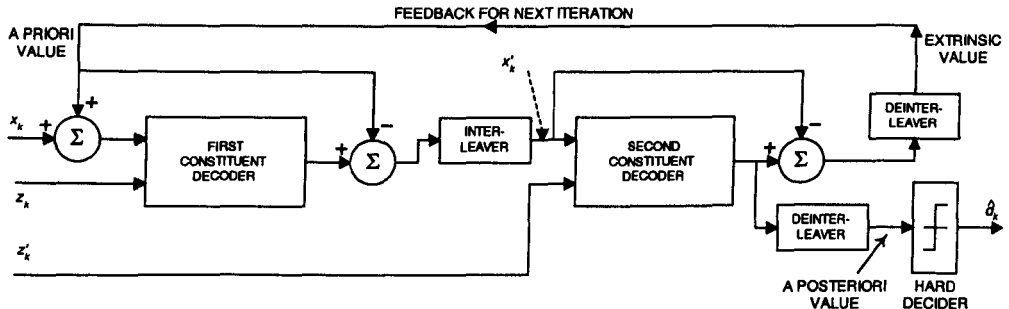


Figure 2-7: Turbo decoder.

The TC decoding is normally performed blockwise. This means that the decoder must wait until the whole information and coded blocks are received. To simplify the explanation, suppose the received input pair values are stored separately into two buffers. The depuncturer extracts, inserts neutral values, and demultiplexes soft decision bits belonging to the first and second constituent decoders. As with the constituent encoders, the first constituent decoder works on original information, while the second one works on the interleaved version. This fact explains the necessity of interleaver and deinterleaver.

The basic concept of turbo decoding can be described as follows: the first constituent decoder receives a pair of input blocks from demodulator and decodes. Thus, a better estimate of the transmitted information block results. Since this new estimate made use “*a priori* information” fed from the second constituent decoder (although at the beginning of iteration process it contains nothing), to make it “*extrinsic information*” for the second constituent decoder, the contribution needs to be omitted, hence the subtraction connection in Figure 2-7. After being made “*extrinsic*”, this newly decoded block is interleaved and fed to the second constituent decoder, hence an even better estimate is produced. The turbo decoder now completes one iteration. A further iteration is performed by feeding back this latest decoded block to the first constituent decoder, by applying the same “*extrinsic subtraction*”, and the second iteration starts. The iterations will continue until a stopping criterion is reached. The iteration stopping criterion can be a pre-set maximum number of iterations or other termination methods.

2.6.3.1 MAP and its Simplified Algorithms

The MAP algorithm, also known as BCJR algorithm to credit its inventors [Bah74], is well known to be complicated, hence it was largely ignored for almost two decades. Fortunately, its simplified and modified versions (SMAP) are available [Pie95, Vit98]. Despite the simpler approach, there is negligible degradation in terms of BER performance. The decoding characteristic is similar to that of Viterbi decoding algorithm, in that it requires large amount of memory and performs the same type of calculations repeatedly and serially. The main difference is that the Viterbi tries to find the “best possible sequence”, whereas MAP computes the “best possible symbols” constituting a sequence.

In describing the basic SMAP decoding algorithm, a BPSK modulation scheme, fading channel, and systematic convolutional encoder are assumed. As with the Viterbi algorithm, SMAP utilises a trellis for decoding. In the next section, the algorithm is described by using pseudocodes, so that it closely resembles its implementation. Its mathematical description counterpart can be found in literature, such as [Pie95, Vi98, Vuc00].

There are three types of actual implementations of the algorithm, as follows:

1. SMAP
2. logarithmic SMAP (LogSMAP)
3. minimum logarithmic SMAP (MinLogSMAP)

The SMAP is included for understanding and comparison. It can be seen later that it is not the best choice for implementation. The LogSMAP and MinLogSMAP are equivalent to the more popular LogMAP and MaxLogMAP algorithms [Rob97], respectively.

In the following description, the notations along with their definitions are listed in Table 2-2.

Table 2-2: Notations and conditions for the SMAP algorithm

Item	Notation or condition
Rate	$\frac{1}{2}$
Time index in trellis	K
Input bit (which is also systematic output bit) at time k	i_k
Coded bit at time k corresponding to input bit i at state m	$c_{k,i}(m)$

Memory length	v
Constraint length	$K = v + 1$
Number of states	$M = 2^v$
Interleaver or block length (including systematic tail bits)	N
Initial state	$S_0 = 0$
Final state (terminated)	$S_{N-1} = 0$
Modulation	BPSK
Channel Noise	Fading amplitude = a_k AWGN mean = 0 AWGN variance = σ^2
Received coded sequences, including tails	$r_{0..(N-1)} = \{x_{0..(N-1)}, y_{0..(N-1)}\}$
Fading amplitude sequence at time k	$\{a_{k0}, a_{ky}\}$
The state which if i is input leads to state m	$S_{b,i}(m)$
The state resulted from input i if current state is m	$S_{f,i}(m)$
Branch metric (in trellis) at time k state m , corresponding to input bit i	$\delta_{k,i}(m)$ or $\Delta_{k,i}(m)$
Forward metric (in trellis) at time k , state m , corresponding to input bit i	$\alpha_{k,i}(m)$ or $A_{k,i}(m)$
Forward metric (in trellis) at time k , state m , corresponding to input bit i	$\beta_{k,i}(m)$ or $B_{k,i}(m)$

2.6.3.1.1 SMAP

Step 1: Branch metric calculation

First of all, in order for a SMAP decoder to give maximum performance, an exact knowledge of channel noise variance σ^2 must be supplied. It is used in the form:

$$L_c = 2/\sigma^2 \quad (2.13)$$

Note that, this term (also in equation (2.22)) is applicable only for AWGN channel. For fading channels, there are modified to include the fading coefficients [LeG94, Hal98, Vuc00]. Most importantly, in Chapter 4 and Chapter 5, it will be shown that these factors can be embedded into individual soft-bits x_k and y_k .

For all trellis branches of the whole received bit sequence, calculate their branch metrics:

(2.14)

```

For k = 0..(N-1); m = 0..(M-1); i = 0,1:
     $\delta_{k,i}(m) = \exp\{ L_c (a_{kx} \cdot x_k \cdot i_k + a_{ky} \cdot y_k \cdot c_{k,i}(m)) \}$ 
    End
  
```

Step 2: Forward metric calculation

Having calculated the branch metrics, now we are ready to calculate the forward (state) metrics $\alpha_{k,i}(m)$. This is actually equal to $P(d_k = i, S_k = m, r_{1..k})$, that is, the probability of sent bit of being i , at state m , at a given time k , knowing we have partially received the bit sequence from the beginning up to k . Taking advantage of the fact that we know the initial state, for $k = 0$, we just give it known values for all the branches accordingly as follows:

2a. Initialisation

```

For k = 0; i = 0,1:
  For m = 0:   $\alpha_{k,i}(m) = \delta_{k,i}(m)$   End
  For m = 1..(M-1):   $\alpha_{k,i}(m) = 0$   End
    End
  
```

(2.15)

For the rest we need to calculate them recursively, starting from the known value of $k = 0$ until the end of the block.

2b. Forward recursion

```

For k = 1..(N-1); m = 0..(M-1); i = 0,1
   $\alpha_{k,i}(m) = \delta_{k,i}(m) \{ \sum_{j=0}^1 \alpha_{k-1,j}(S_{b,i}(m)) \}$ 
    End
  
```

(2.16)

Step 3: Backward metric calculation

This term is similar in nature to the previous one, but this time the recursion starts from the other end. Taking advantage of the fact that the end state is known, we start with the known values as follows:

a. Initialisation

```

For k = 0; i = 0,1:
  For m = 0:   $\beta_{N,i}(S_{b,i}(m)) = 1$   End
  For m = 1..(M-1):   $\beta_{N,i}(S_{b,i}(m)) = 0$   End
    End
  
```

(2.17)

For the other values of k , we calculate recursively in the reverse direction:

b. Backward recursion

For $k = (N-1)..1; m = 0..(M-1); i = 0,1$:

$$\beta_{k,i}(m) = \sum_{j=0}^1 \{ \delta_{k+1,j}(S_{f,i}(m)) \cdot \beta_{k+1,j}(S_{f,i}(m)) \} \quad (2.18)$$

End

Step 4: LLR calculation

Now, the LLR values for each k are easily calculated as follows:

4a. Soft-decision

For $k = 0..(N-1)$:

$$L(d_k) = \ln \frac{\sum_{m=0}^{M-1} \{\alpha_{k,1}(m)\beta_{k,1}(m)\}}{\sum_{m=0}^{M-1} \{\alpha_{k,0}(m)\beta_{k,0}(m)\}} \quad (2.19)$$

End

4b. Hard-decision

For $k = 0..(N-1)$:

$$\hat{d}_k = \begin{cases} 1, & \text{if } L(d_k) \geq 0 \\ 0, & \text{otherwise} \end{cases} \quad (2.20)$$

End

This step concludes the SMAP algorithm.

2.6.3.1.2 LogSMAP

This algorithm is a reformulation of the previous one with implementation simplicity in mind. The main difference is that in this particular algorithm, the probability calculations are carried out in the logarithm domain, hence no exponential operations, while multiplications and divisions

become additions and subtractions, respectively. Additions of probability values, however, need a new operator.

Step 0: Definition of new operator

For any probability values a and b , it is defined that:

$$\begin{aligned} a \Xi b &\equiv -\ln(\exp(-a) + \exp(-b)) \\ &\equiv \min(a, b) - \ln(1 + \exp(-\text{abs}(a - b))) \end{aligned} \quad (2.21)$$

This operator is similar to the \max^* operator used in some literature, for instance [Val01]. Also, this operator can be used recursively, for instance, $a \Xi b \Xi c = a \Xi (b \Xi c)$.

The rest of the calculations are essentially the same, just applying the corresponding new operator definitions to the calculations in the former algorithm. Therefore, it is not necessary to repeat the description of the steps.

Step 1: Branch metric calculation

The definition of L_c remains the same:

$$L_c = 2/\sigma^2 \quad (2.22)$$

$$\begin{aligned} \text{For } k = 0..(N-1); m = 0..(M-1); i = 0,1; \\ \Delta_{k,i}(m) = -L_c (a_{kx} \cdot x_k \cdot i_k + a_{ky} \cdot y_k \cdot c_{k,i}(m)) \\ \text{End} \end{aligned} \quad (2.23)$$

Step 2: Forward metric calculation

2a. Initialisation

$$\begin{aligned} \text{For } k = 0; i = 0,1; \\ \text{For } m = 0: A_{k,i}(m) = \Delta_{k,i}(m) \quad \text{End} \\ \text{For } m = 1..(M-1): A_{k,i}(m) = 0 \quad \text{End} \\ \text{End} \end{aligned} \quad (2.24)$$

2b. Forward recursion

$$\begin{aligned} \text{For } k = 1..(N-1); m = 0..(M-1); i = 0,1; \\ A_{k,i}(m) = \Delta_{k,i}(m) + \left\{ \sum_{j=0}^1 A_{k-1,i}(S_{b,i}(m)) \right\} \\ \text{End} \end{aligned} \quad (2.25)$$

Step 3: Backward metric calculation***3a. Initialisation***

```

For k = 0; i = 0,1:
  For m = 0:  BN,i(Sb,i(m)) = 1    End
  For m = 1..(M-1):  BN,i(Sb,i(m)) = 0    End
  End

```

(2.26)
3b. Backward recursion

```

For k = (N-1)..1; m = 0..(M-1); i = 0,1:
  Bk,i(m) =  $\sum_{j=0}^1 \{ \Delta_{k+1,j}(S_{f,i}(m)) \cdot B_{k+1,j}(S_{f,i}(m)) \}$ 
  End

```

(2.27)
Step 4: LLR calculation***4a. Soft-decision***

```

For k = 0..(N-1):
  L(dk) =  $\sum_{m=0}^{M-1} \{ A_{k,0}(m) B_{k,0}(m) \} - \sum_{m=0}^{M-1} \{ A_{k,1}(m) B_{k,1}(m) \}$ 
  End

```

(2.28)
4b. Hard-decision

```

For k = 0..(N-1):
   $\hat{d}_k = \begin{cases} 1, & \text{if } L(d_k) \geq 0 \\ 0, & \text{otherwise} \end{cases}$ 
  End

```

(2.29)
2.6.3.1.3 MinLogSMAP

The difference between this algorithm and LogSMAP is just in **Step 0**, that is, the definition of Ξ , which is as follows:

Step 0: Redefinition of new operator

$$a \Xi b \equiv \min(a, b) \quad (2.30)$$

It can be seen that equation 2.21 is actually equation 2.30 but without the correction term $-\ln(1 + \exp(-\text{abs}(a-b)))$. This reduction in complexity consequently results in a minor degradation of performance.

Step 1,2, and so on are the same as those of LogSMAP.

2.6.4 Parameter Selections

2.6.4.1 Constituent Encoder

Theoretically and empirically good RSC generator polynomials were chosen for constituent encoders. They are extracted from [Ber93, Ben96b, Ben96d, Div96], although some of them contradict each other. For example, the polynomial RSC(1, 21/37) which was the best for memory length $v = 4$ (constraint length $K = 5$) and long interleaver [Ber93] is not so for a shorter interleaver. It is not even listed as the best in [Ben96b], [Ben96d] or [Div96], which in turn also differ from each other. Further, those listed as the best are also not necessarily so when simulated. This fact is probably because of the incomplete understanding of TCs in general. As simulation results in the AWGN channel revealed, the best one for $v = 4$ and shorter interleaver turned out to be RSC(1, 35/23). Regardless of these inconsistencies among the researchers, the 3GPP standardisation process has decided to choose only TC(1, 15/13, 15/13) [TGP02b], which is adopted in this work.

2.6.4.2 Constituent Decoder

Since the MAP decoding algorithm offers the best performance, and the complexity has been reduced to a feasible level of roughly twice as complex as SOVA [Pie94, Vit98], its simplified variant, i.e., SMAP, was preferred. This has the advantages of enabling a further simplified MAP version, the MinLogSMAP. These decoders have been discussed in more detail in Section 2.6.3.

2.6.4.3 Interleaver

Interleavers play a crucial role in determining the TC performance. They are partly responsible for the error floor characteristic of TCs [Cro99, Vuc00]. A pseudorandom interleaver performs well in randomising the resulting codewords. However, if other properties are expected, other types of interleavers are viable. An optimisation procedure is involved in finding good interleavers. These interleaving issues are closely related to the trellis termination issue described in the next subsection. Having considered different proposals from different contributors, 3GPP decided to use a multistage interleaver, as described in [TGP02b].

2.6.4.4 Trellis Termination

Both MAP and SOVA perform better if their decoding trellises are terminated, that is, if the state is forced to 0. However, as the RSC constituent encoders have feedback connections and different sequences of input bits due to interleaving, clearing out both shift registers is not straightforward. Therefore, particular methods have to be devised.

A simple method for the foregoing purpose is by terminating both trellises using separate tail bits. This strategy is simple, but less efficient. This approach is adopted in 3GPP standard [TGP02b].

A better approach is by synchronising the encoder and the interleaver, and in some cases, the block length. Simile [Bar95] is a example of such synchronised approach. Unfortunately, the randomness property, complexity, or length restriction is inevitably sacrificed.

2.6.4.5 Iteration Stopping

By themselves, TCs do not know when to stop iteration. Utilising a CRC [Ros99] can be effective, but inefficient, since extra redundancy (and complexity) needs to be incurred. Cross entropy or another method based on neural networks have been shown to give less satisfactory results, as they tend to give false decisions when the codes operate at high E_b/N_0 [Buc99]. As this issue is related to the receiver, it is not standardised in 3GPP. However, most transport channels are CRC coded, so in this case a stopping criterion based on CRC can be employed. Nonetheless, in many 3GPP technical documents, most manufacturers simply apply a certain maximum number of iterations to stop the iteration.

2.6.4.6 Puncturing

The puncturing scheme does not seem to receive a lot of interest. In the original TC [Ber93], to produce a rate-1/2 from 1/3 TC, the authors simply used odd- and even-indexed puncturing of the first and second parity blocks, respectively. Simulating any combination of these odd and even puncturing, yields similar BER performance. The puncturing, however, becomes an important issue when the TC is employed in conjunction with ARQ, such as in [Ros99] and in 3GPP UMTS HSDPA [TGP02b].

2.6.4.7 Channel State Information (CSI)

TCs employing MAP (or its derivatives) decoders require CSI, including fading coefficients (FCs) and noise variance (NV), estimator to perform maximally. While such TCs are more tolerant to the NV [Ree97, Sum97], they are not so tolerant of the effect of the FCs. This issue is one of the driving issues of the research reported in this thesis. See section 1.2 and chapters following the current one for a more in-depth elaboration.

2.7 Current Developments in Soft-Demodulation Methods

The soft-demodulation issue has become more important since the introduction of TC a decade ago [Ber93]. The importance is even more when a binary TC is employed but the modulation schemes in use require symbol-to-multibit demapping at its demodulator. In this situation, soft-demodulated bits (soft-bits) should be extracted from soft-demodulated symbols (soft-symbols hereinafter).

The simplest representation of soft-bits, in the form of *neutral values*, has been in existence since the introduction of *erasure* and *puncturing* in block and convolutional decoding. However, a truer, infinite-level soft-decision issue firstly emerged when performance improvement was sought from convolutional codes' Viterbi decoders. In an AWGN channel, an improvement of up to 3 dB coding gain at BER of 10^{-6} can be obtained if the Viterbi decoder is supplied with and makes use of the soft-decision compared to hard-decision [Cla81, Mic85, Swe91, Swe02]. Most of the discussions regarding the soft-decision thereafter were largely regarding how the quantisation is carried out and its impacts on performance and complexity [Cla81, Mic85, Swe02]. The environment under discussion was still limited to binary modulation on AWGN channel.

While producing the soft-bits for the benefit of TC decoder from a binary modulation system and AWGN channel is straightforward, beyond this it is not so, particularly when maximum performance and less complicated implementation are sought. This maximum performance can be obtained when CSI is taken into account during demodulation and decoding.

There are different types of TC constituent decoders, but the most popular of them are of MAP and SOVA types [Ber93, Hag94, Vuc00]. Recall the discussion in section 2.6.3. SOVA decoder incurs less complexity but provides inferior performance. MAP, on the contrary, is just the opposite: more complex to implement, but offers better performance. In general, both of them can benefit from the CSI, as can be deduced from [LeG94, Vuc00], for instance.

The first publication that addresses the soft-decision for high order modulation (HOM) schemes, in particular 16- and 64-QAM, is due to Le Goff *et al.* [LeG94]. It is in this paper where a binary turbo coded HOM system (as opposed to symbol-based trellis coded modulation) is termed "pragmatic" TCM. This was published a year after the publication of the seminal paper on TC [Ber93], both were originated from the same institution. Therefore, it can be deduced that the soft-decision issue has been recognised earlier on, but there is not much in the literature.

In the First Symposium on TCs, Barbulescu *et al.* [Bar97] reported the implementation of the hardware 16-QAM modem in conjunction with the TC. However, apparently they just applied the soft-modulation method proposed earlier [LeG94].

In 1999, a book on TC by Heegard and Wicker [Hee99] was published. In addition to elaborating their original contribution, this reference also summarises many aspects of TC, but no specific discussion regarding the soft-demodulation. A year afterwards, Vucetic and Yuan published another book [Vuc00]. In this reference, there is indeed a discussion regarding HOM and other turbo coded trellis modulation (TTCM) types, but for the pragmatic TCM part, it is mainly reiteration of the work in [LeG94]. There is also a discussion about TC application in Rayleigh channel, but similar to the work of Barbulescu [Bar95] and Hall *et al.* [Hal98], a real-valued Rayleigh channel model in conjunction with BPSK or QPSK modulation scheme were adopted. Furthermore, the method necessitates separate CSI handling. As a result, modification of the TC constituent decoder to accommodate it also becomes necessary.

Recently, Hanzo *et al.* published two books [Han02a, Han02b] containing discussions regarding TC, non-AWGN channels, and HOM. These references summarise the works of hundreds other references. From the point of view of TCM, as in [Vuc00], there are discussions about different types of TCMs. Unfortunately, there is no explicit discussion about the provision of soft-bits.

From the literature about the QAM topic, for example in [Web94] and its revised edition [Han00], there is no specific discussion about the soft-demodulation for TC. Similarly, from a recent book of WCDMA [HoJ02] that includes a chapter on HSDPA, no such an explicit discussion about the matter.

In HSDPA part of 3GPP UMTS standard [TGP02b], there is only one binary TC encoder to use regardless of modulation types, that is, either QPSK or 16-QAM. In other words, 3GPP adopts pragmatic TCM. Therefore, a proper soft-bit demodulation is necessary to maximally exploit the TC's error correcting potential. This issue is in fact the main motivation of the research work reported in this thesis.

A foundation of the technique to tackle this issue for 16-QAM has been laid by Le Goff *et al.* [LeG94]. Using the same real-valued Rayleigh channel model, other researchers [Bar95, Hal98, Vuc00] have also partly complemented the technique, particularly for QPSK scheme. Unfortunately, compared to the implementation in UMTS and HSDPA, including its multipath channel models, this basic technique can no longer cope well, hence further development is required.

The approach of using a real-valued variable in modelling the Rayleigh channel in the above literature [LeG94, Bar95, Hal98, Vuc00] is too limiting for the application in more realistic

channels, such as in UMTS channels. Therefore, a complex-valued model is adopted in this work. Besides representing more realistic modelling [Sau99], this approach also enables easy extension for the diversity environment.

Regarding separate CSI handling and modification of TC decoder to accommodate this extra input, such as proposed in [LeG94, Bar95, Hal98, Vuc00], this would make the UMTS receiver unnecessarily complicated. Recall that in a typical TC receiver (the transmitter counterparts can be seen in section 3.2), there are at least nine subsystems separating the demodulator and TC decoder. All these subsystems alter the data-sequence order. Therefore, if the CSI was handled separately, the FC part of the CSI would need the same processing as data, since the sequence order is equally important in both cases. This issue represents the second motivation underpinning this research. In recapitulation, the research work will adopt complex-valued approach in system modelling and analysis and will embed the CSI on every soft-bit during soft-demodulation, for both QPSK and 16-QAM schemes. This way, the resulting methods will eliminate the necessity of separate CSI handling and TC decoder modification, hence a simpler UMTS receiver implementation results.

2.8 Summary

In this chapter, some concluding remarks can be drawn:

1. Basic principles of the subjects that are employed in the next chapters have been briefly explained.
2. Current development of the research topic has been reviewed.
3. The objectives of the research summarised in section 1.2 has thus become more obvious.

In the next chapter, a platform on which the devised methods are simulated and evaluated is developed. The basic principles reviewed here are used as a foundation for the implementation.

Chapter 3

Link Simulator Development

3.1 Introduction

Building a fully compliant 3GPP UMTS STTD and HSDPA link simulator software from scratch is a daunting task. From the bit source subsystem (of a transport channel) at the base station all the way to the bit error calculator subsystem at the mobile terminal, there are over 50 subsystems that must be developed. Yet, as this is the prerequisite of the research underpinning this thesis, a version of this, however simple, must be available. Since none was available, a simulator development was conducted.

In view of these thoughts, it becomes more valuable that resulting software be not only useful for the research but also immediately beneficial for the mobile communication industry, which at the moment is in the stage of designing, planning, assessing, and deploying 3G networks. Note that a calibrated and dependable link simulator plays a very crucial role in a system dimensioning. With this twofold goal in mind, the development task is even harder, as there are subsystems that are not required and can be simplified for the research purposes but they are required by industry. These include a user-friendly and professional graphical user interface (GUI) that makes the simulator software readily accessible by any physical link engineers in the industry.

Having been collaborating with industrial partners, one very important implication from achieving this twofold goal is that the validation process can be performed in parallel, with feedback and information exchange along the course, so the dependability of the resulting simulator is relatively high. Therefore, it can be stated confidently that the performance obtained from the simulator is calibrated and dependable.

As in an ordinary software development project, the succeeding step after the goal has been set is the design step. Considering the flexibility, degree of freedom, professionalism level of the output, and fast execution, an object-oriented design is chosen along with its object-oriented programming (OOP) paradigm for implementation. Finally, performance validation is conducted to ensure that everything is working properly as designed. Elaboration of all these steps is the main theme of this chapter.

3.2 Design

The top-level block diagram of the complete simulator is shown in Figure 3-1. As illustrated, the GUI part and its corresponding functionalities are not for research purposes, so they will not be touched upon. Below this is the part that simulates simplified upper layer functionalities, return link for HSDPA HARQ (and power control, for industrial purposes), and overall control of the simulator.

Going further down, on the left there are three bit framing blocks: 3GPP HSDPA, 3GPP UMTS, and *basic*. A more detailed block diagram of HSDPA bit framing has been reproduced from [TGP02b] to appear in Figure 3-3. Similarly, an elaboration of UMTS bit framing is shown in Figure 3-2. Note that in its original document [TGP02b], this bit framing is referred to as transport channel multiplexing structure for downlink. The detailed description of these UMTS and HSDPA bit framings can be found in [TGP02b], and will not be reproduced here. The last block of bit framing (the innermost in the figure) is the *basic* one. Further elaboration of this block appears as the transmitter part in the block diagram of Figure 4-1 or Figure 4-14. Out of these three bit framing blocks, the basic one is firstly used for the derivation of soft-demodulation methods presented in the next chapter, and their subsequent performance evaluations are performed utilising this part.

It is important to emphasise that despite clear block partitioning in this block diagram, in implementation they share some subsystems. One important shared subsystem worth mentioning is the TC encoder block.

In the bottom left corner of the picture, there are four transmitter blocks: *basic*, 3GPP UMTS, 3GPP HSDPA, and OFDM. The *basic* transmitter consists only of a modulator block, as illustrated in Figure 4-1 or Figure 4-14. In UMTS and HSDPA, they comprise among others modulator, STTD encoder and its dual transmitters, spreading, scrambling, parallel physical channel and multiuser functionalities, and multi base station functionalities. The OFDM block is included for performance comparison only; its discussion is outside of the scope of this thesis. As can be seen from the diagram, *basic* bit framing can utilise any of these transmitters.

Connecting the transmitter and receiver blocks is the channel block. In this block, there are different kinds of channel models, including AWGN, Uncorrelated Rayleigh, Correlated Rayleigh, Correlated Rician and multipath channels. The multipath channels are implemented using tapped delay line (TDL). One of the multipath channels that is used in validation process is 3GPP Case 1 [TGP02d], whereas the more severe ones and used for evaluating HSDPA system in the worst-case scenarios are Vehicular A [TGP02d, UMT98] and Vehicular B [UMT98].

Finally, the receiver blocks consist of the functionalities that reverse-process the corresponding ones at the transmitter blocks. Additionally, various channel estimation and signal to interference ratio (SIR) estimation techniques are implemented, but not used in this research.

All these blocks are designed with object-orientation in mind. In view of this design, these blocks are top-level large objects containing other smaller objects. Detailed elaboration of this design would take too much space. Further, this is not highly relevant to the research topic at hand. Therefore, the top-level block diagram illustrated in Figure 3-1 is considered adequate in this regard.

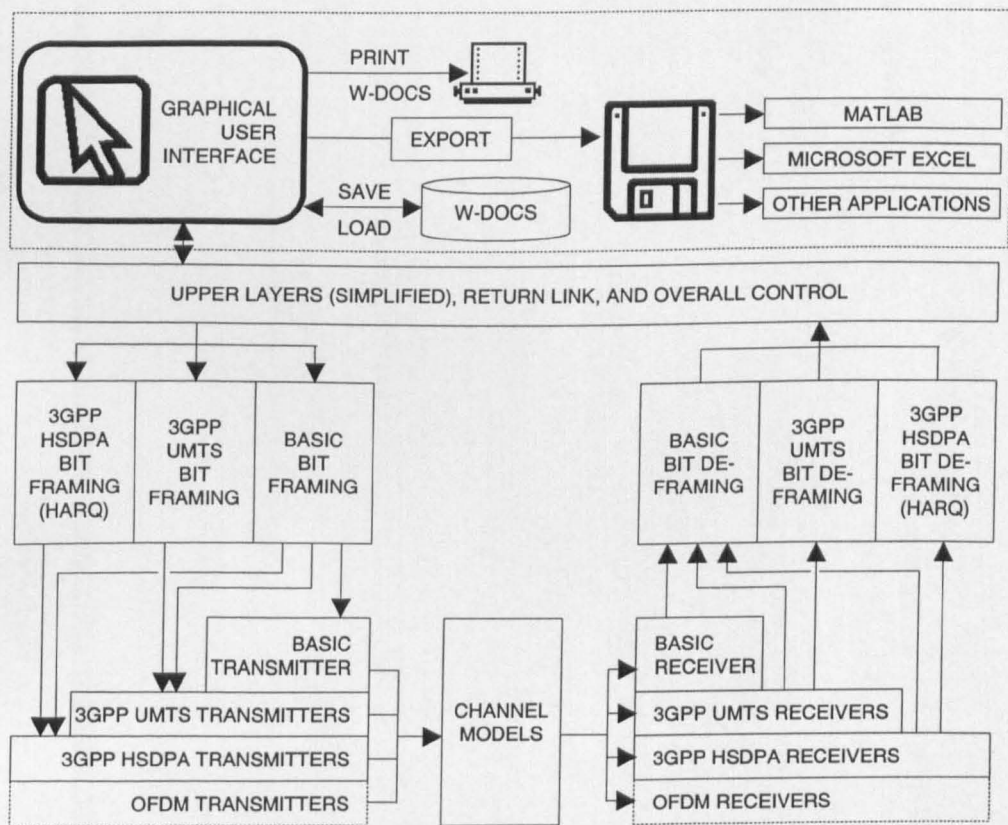


Figure 3-1: Simulator Structure.

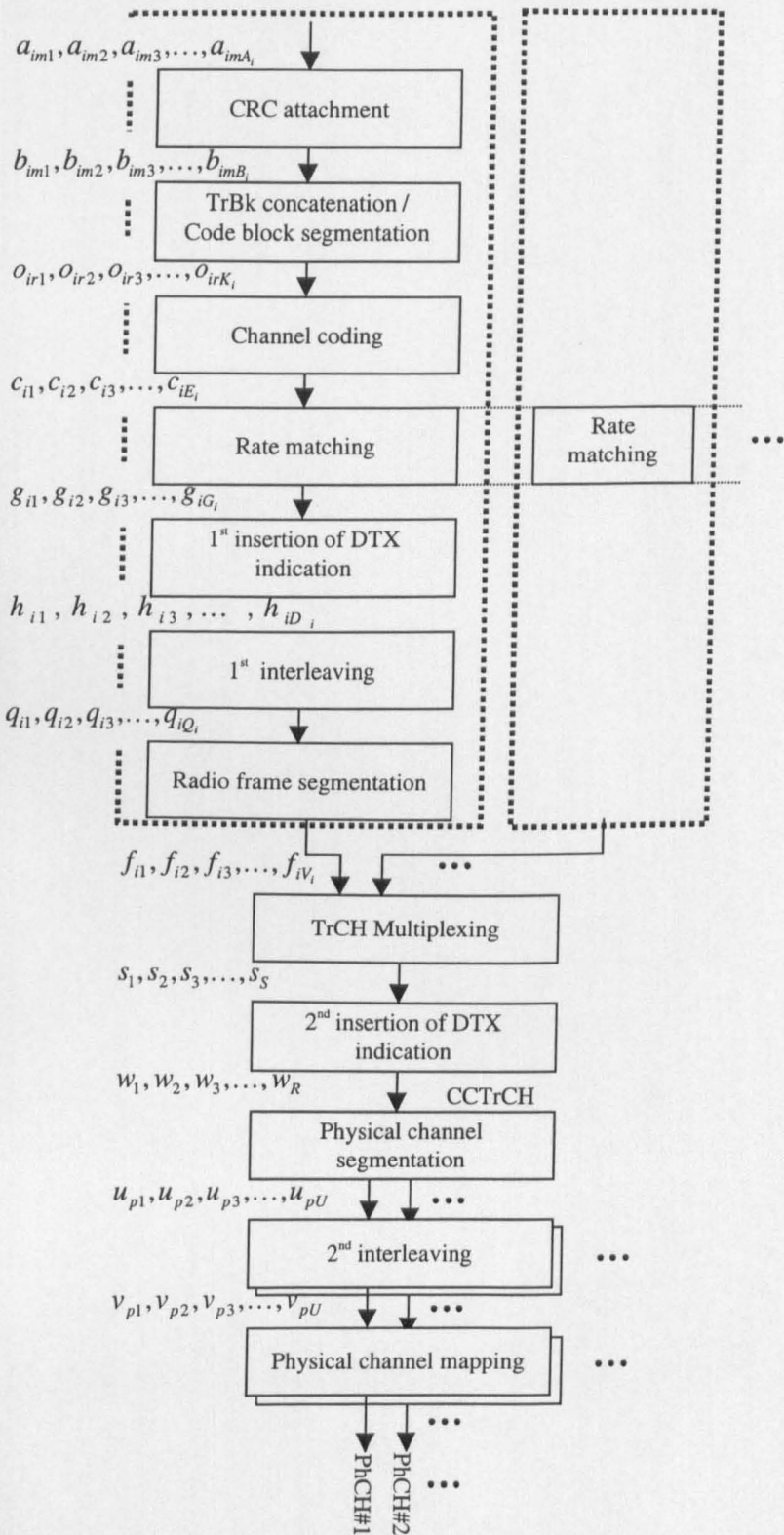


Figure 3-2: 3GPP UMTS bit framing [TGP02b].

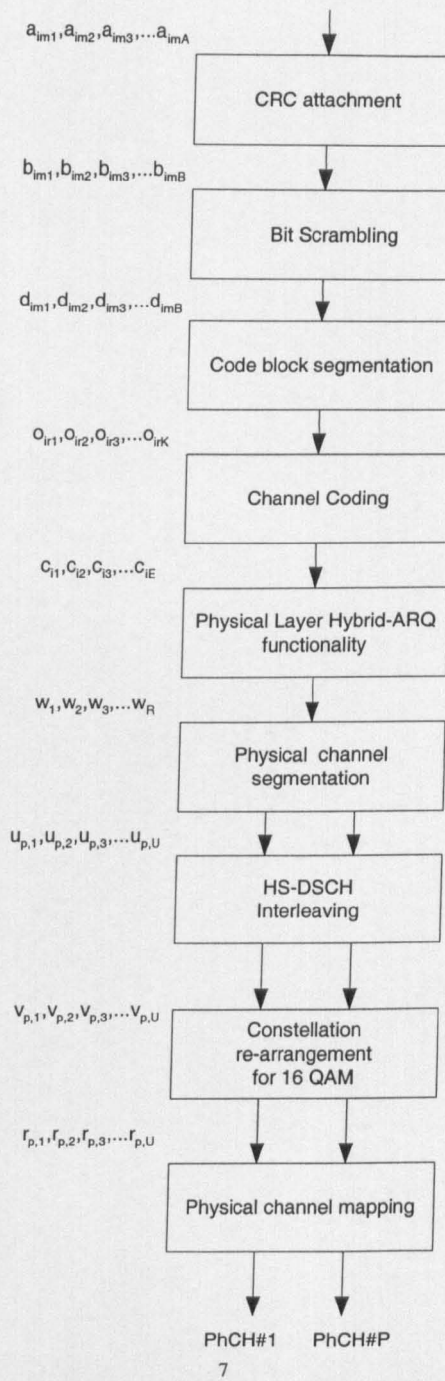


Figure 3-3: 3GPP HSDPA bit framing [TGP02b].

3.3 Implementation

The simulator software is implemented in C++ programming language using OOP paradigm. The implementation extensively exploits the benefits of standard template libraries (STL). In Microsoft Windows environment, Microsoft Visual C++ 6.0 is used for the development, including its GUI and its multithreading execution mode. A snapshot of the “Professional Edition” of the software – called W-CDMA, currently bearing version 3 – is shown in Figure 3-4.

For the UNIX/SunOS/Linux environment, there is no GUI yet developed. In this environment, only a “Research Edition” of the software is currently available. The user interface is via text-based terminal console, namely using keyboard or command line arguments as input, and screen text display and file as output. Development is mainly using XEmacs, g++, gdb, ddd, and Matlab.

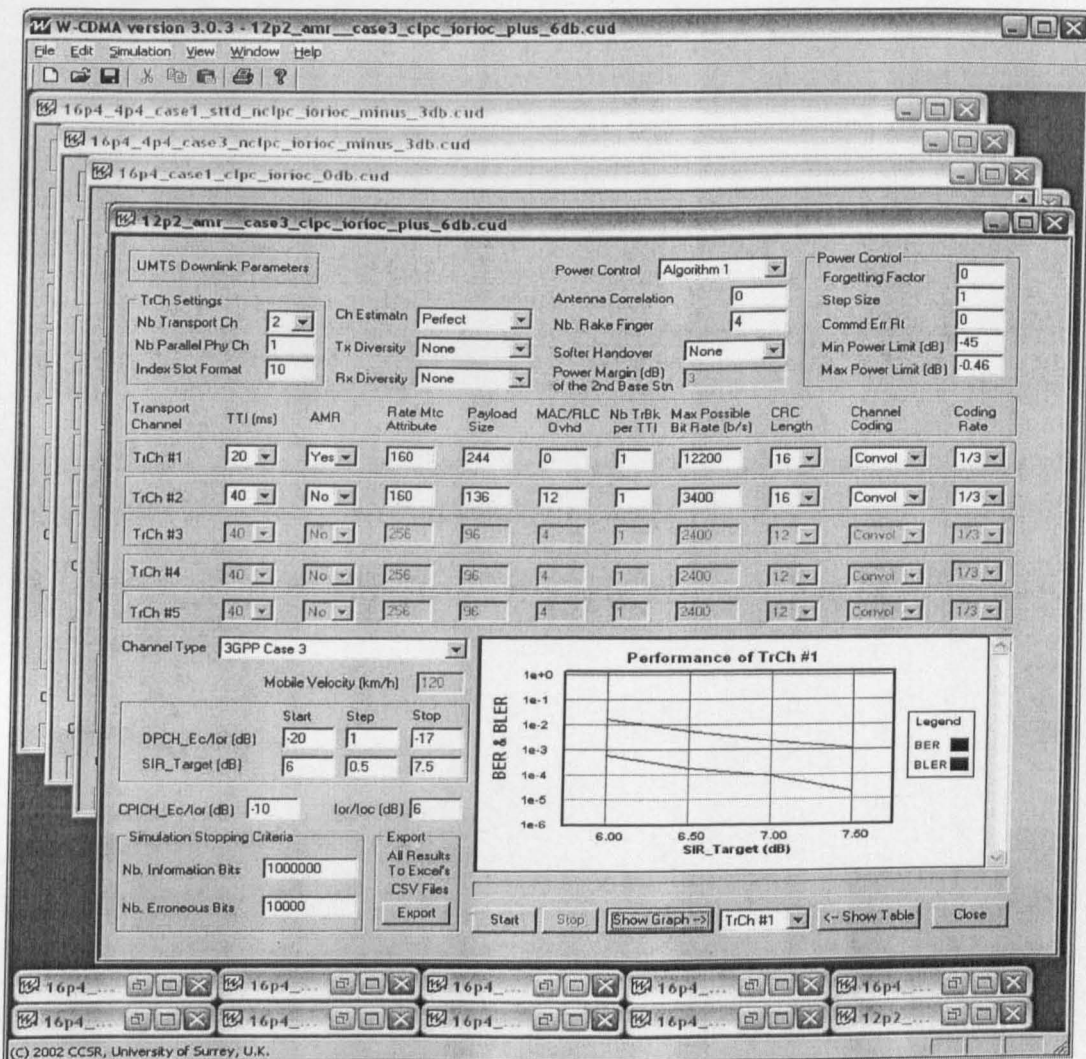


Figure 3-4: Snapshot of W-CDMA Version 3 for Windows 2000/XP.

3.4 Validation Process

This is the most time consuming and the most exhausting part of the simulator development. In a simulator of this size, there are so many blocks to be validated that a long overall development duration is needed. Considering the degree of relevance, only a few important validation steps are discussed here. These include channel block, basic uncoded BER performance in AWGN channel, and 3GPP performance validation process as described in [TGP02d]. Additional validation processes are conducted when new methods are devised and evaluated in the forthcoming chapters.

3.4.1 Channel Models

3.4.1.1 AWGN and Uncorrelated Rayleigh

The AWGN channel is an ever-present channel. On its own, it represents the least hostile channel. Hence, this channel is commonly used as the first step for a communication simulation. When other non-additive impairments are present, this channel is also implied. It is very common that, unless stated otherwise, the “AWGN” term implies zero mean AWGN. This convention is also adopted throughout the thesis. Its variance represents its average power.

To be more specific, there can be real-valued and complex-valued AWGN sample generators. Referring to [Pre92], to which the implementation of the AWGN and pseudorandom number generator in this work conforms, the native AWGN generator is a complex-valued one, as it is derived from the Uncorrelated Rayleigh sample generator. However, due to its independence (uncorrelated-ness) among generated samples, this complex-valued AWGN generator can be regarded as a real-valued one, by treating the samples from real and imaginary components as two successive samples. What matters most in this case is the variance. The variance of the complex-valued AWGN is twice that of the real-valued one (the variance can be measured only on either real or imaginary part), provided that the generator parameters remain unchanged.

Figure 3-5 depicts theoretical and simulation probability density function (pdf) plots of such a real-valued AWGN channel, with a variance of 0.25. The simulation plot is based on the statistics of 1 million samples. Calculated numerically, the samples give a mean of 0.0006 and a variance of 0.2505. These results indicate that the simulator conforms to the theory very closely.

Since AWGN and Uncorrelated Rayleigh channels share the same block, one validation step validates both. Auto and cross-correlation properties have also been tested and validated.

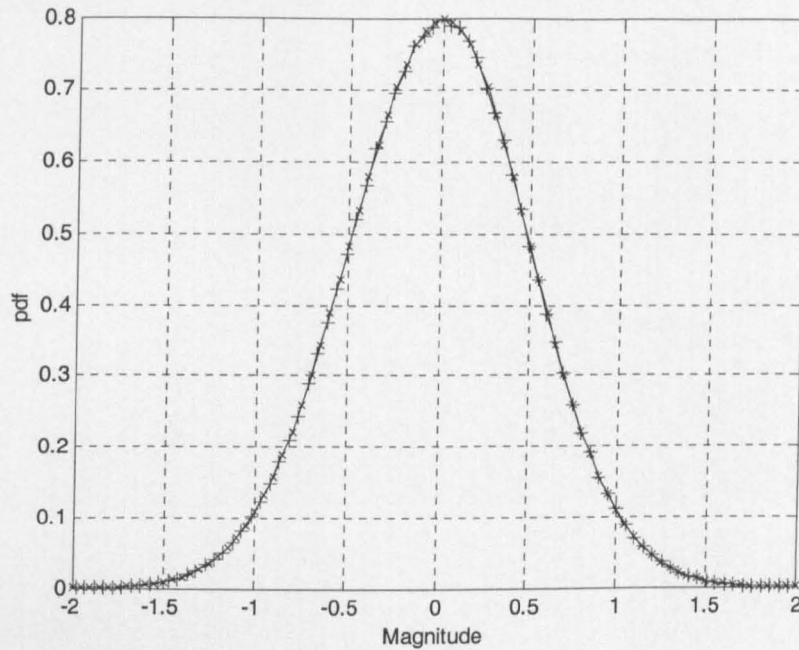


Figure 3-5: AWGN pdf, with mean = 0 and variance = 0.25.
Legend: + Theory, \times Simulation

3.4.1.2 Correlated Rayleigh

Implementation of the Correlated Rayleigh that is used on its own or in conjunction with TDL channel follows the description found in [Jak74] and particularly in [Pae98, Pae02]. Figure 3-6 shows a squared-magnitude plot of the resulting samples.

First and second order statistics are validated. Reference (or ideal) values and curves for these statistics are computed referring to [Sau99]. Although not shown here, the auto- and cross-correlation properties have also been validated. First order statistics validation includes the mean and variances of real and imaginary components and the mean and the variance of its magnitude. The resulting values are as follow:

Doppler spread : 222 Hz

(corresponds to carrier frequency of 2 GHz
 and mobile velocity of 120 km/h)

Sampling rate : 240 000 samples/s

(equivalent to HSDPA symbol rate, given that UMTS chip rate
 is 3.84 MHz and HSDPA spreading factor is 16)

Number of samples : 1 million
(corresponds to 4.17 s time duration)

Means : I and Q components, respectively:
Ideal : 0 and 0
Simulated: 0.005786 and 0.003828

Magnitude:
Ideal : 0.8862 (rounded to 4 decimal places)
Simulated: 0.8926

Variances : I and Q components, respectively:
Ideal : 0.5 and 0.5
Simulated: 0.5001 and 0.5010

Magnitude:
Ideal : 0.2146 (rounded to 4 decimal places)
Simulated: 0.2043

The resulting pdf along with the ideal one is plotted in Figure 3-7. From these numerical and graphical comparisons, it can be observed that despite relatively low number of samples, the first order statistics are very close to the ideal. It is worth mentioning that other models that are based on filtered Gaussian have also been implemented and evaluated, but the resulting statistics are not as good as this one.

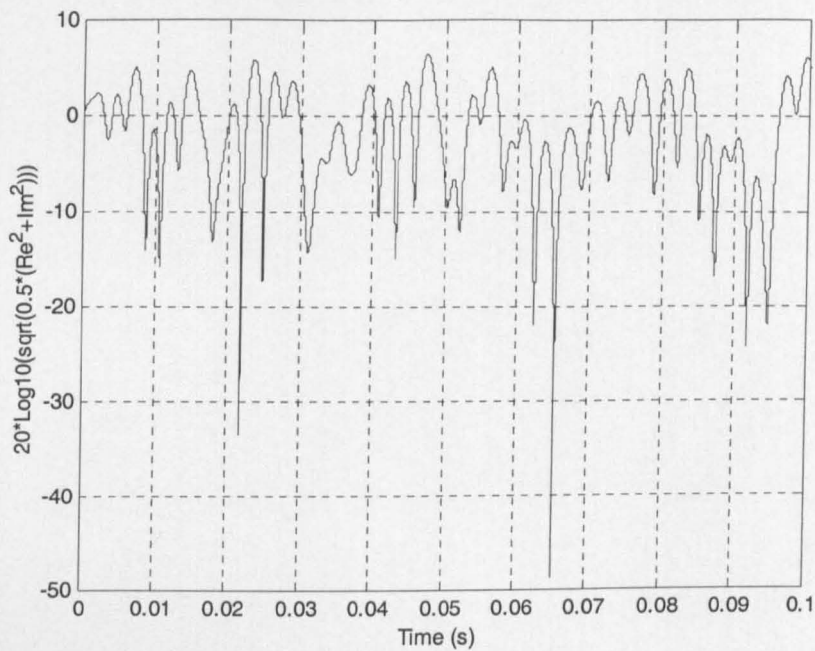


Figure 3-6: Correlated Rayleigh power plot.

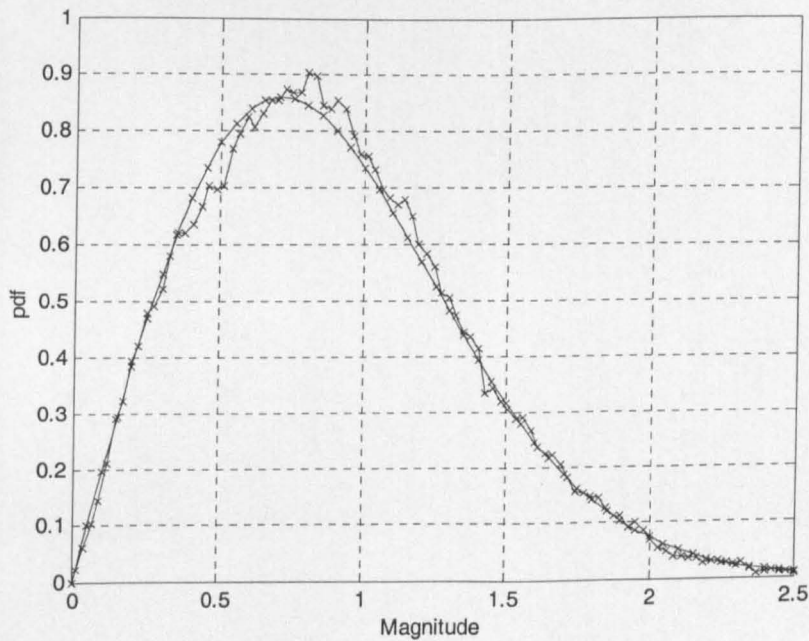


Figure 3-7: Correlated Rayleigh magnitude pdf.
Legend: + Theory, \times Simulation

The second order statistics include *level-crossing rate (lcr)* and *average fade duration (afd)*. Referring to [Sau99] while looking at Figure 3-6, the lcr is the number of positive-going crossings of a reference level in unit time, while the afd is the average time between negative and positive level-crossings. These statistics are used to evaluate the Doppler property of a channel. Figure 3-8 and Figure 3-9 show the plots of ideal and simulated lcr and afd, respectively. Despite relatively small number of samples, the lcr and afd curves are very close to the ideal ones.

The TDL implementation of the multipath channel has also been validated to work properly.

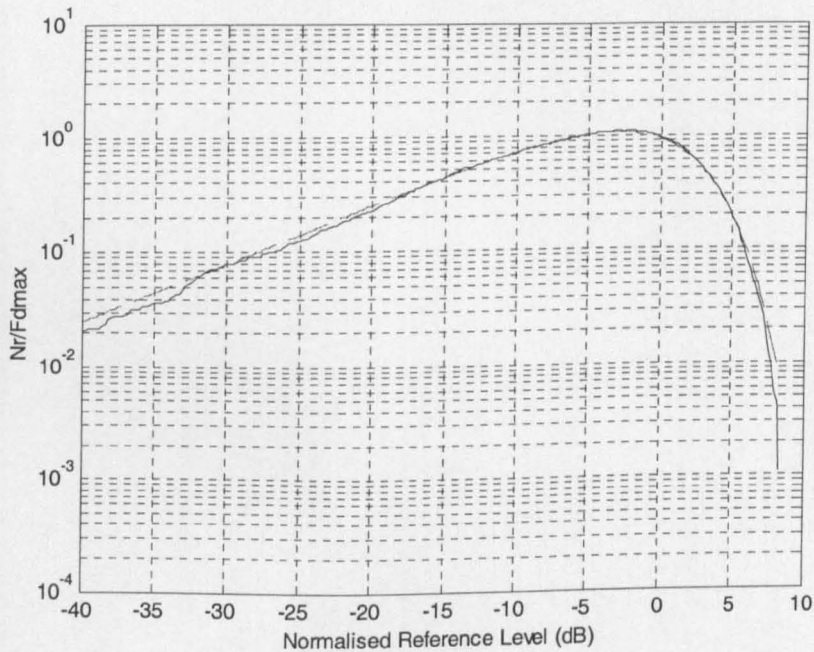


Figure 3-8: Correlated Rayleigh squared-magnitude lcr.
Legend: - - Theory, — Simulation

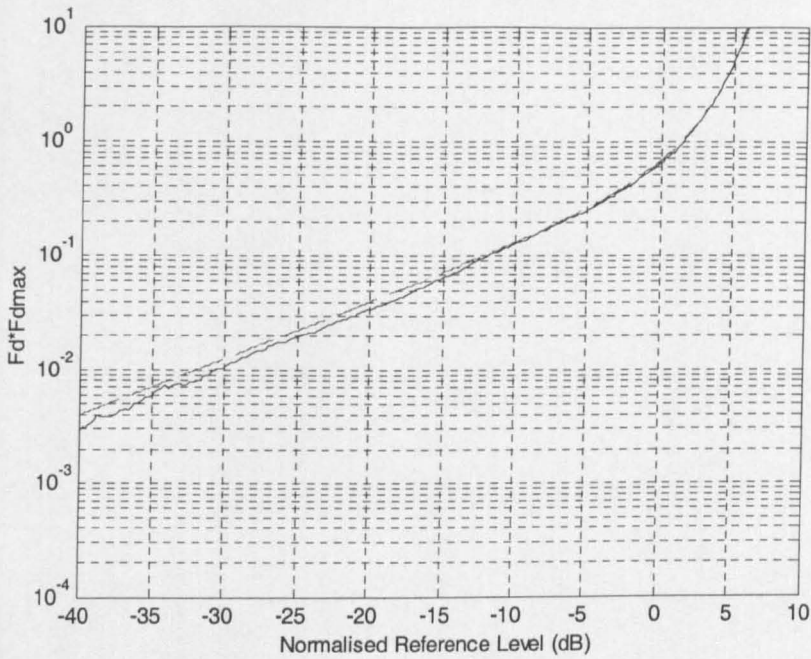


Figure 3-9: Correlated Rayleigh squared-magnitude afd.
Legend: - - Theory, — Simulation

3.4.2 Comparison of Uncoded BER Performance with Theoretical Analysis

Referring to [Pro00], the uncoded BER of Gray-coded QPSK in AWGN can be approximated by

$$P_b = Q\left(\sqrt{2\frac{E_b}{N_0}}\right). \quad (3.1)$$

The corresponding performance curve, plotted along with the simulation result, is depicted in Figure 3-10. A nearly perfect agreement between analytical and simulation results can be observed.

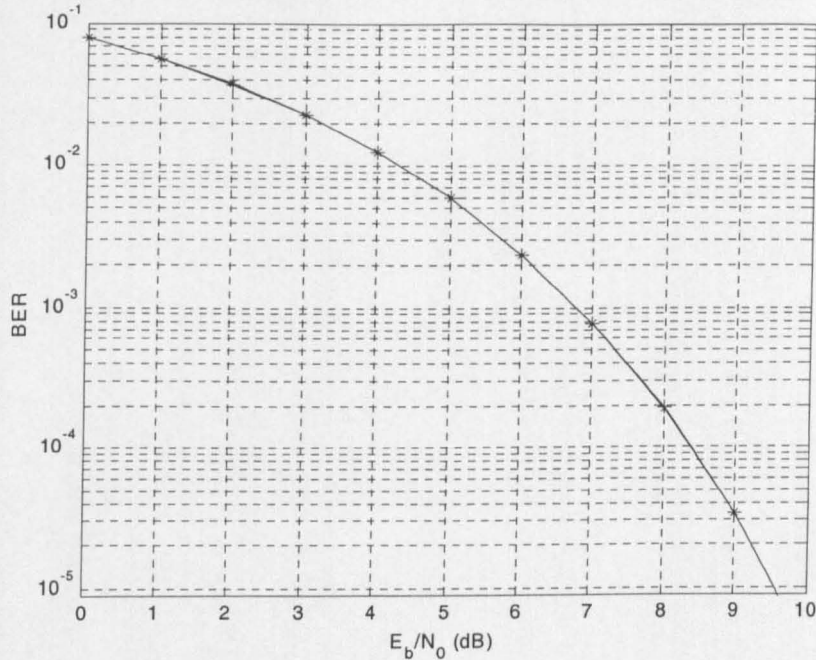


Figure 3-10: Performance of Uncoded QPSK in AWGN channel.
Legend: + Theory, × Simulation

Again, referring to [Pro00], the uncoded BER performance of the 16-QAM in AWGN can be tightly upper bounded by

$$P_b \leq Q\left(\sqrt{\frac{12 \cdot E_b}{15 \cdot N_0}}\right). \quad (3.2)$$

Plotted along with two other curves from simulation, the corresponding curve of this equation is shown in Figure 3-11 using “+” markers. When an arbitrary constellation is employed and Euclidean demodulation method is performed, the resulting performance curve, marked by “Δ”, is almost at the same spot as the upper bound. Employing Gray coded, I - Q separable constellation (as illustrated in Figure 2-2), and exact demodulation method (or its approximation methods), the performance is slightly better. This shows the superiority of the chosen constellation over an arbitrary one.

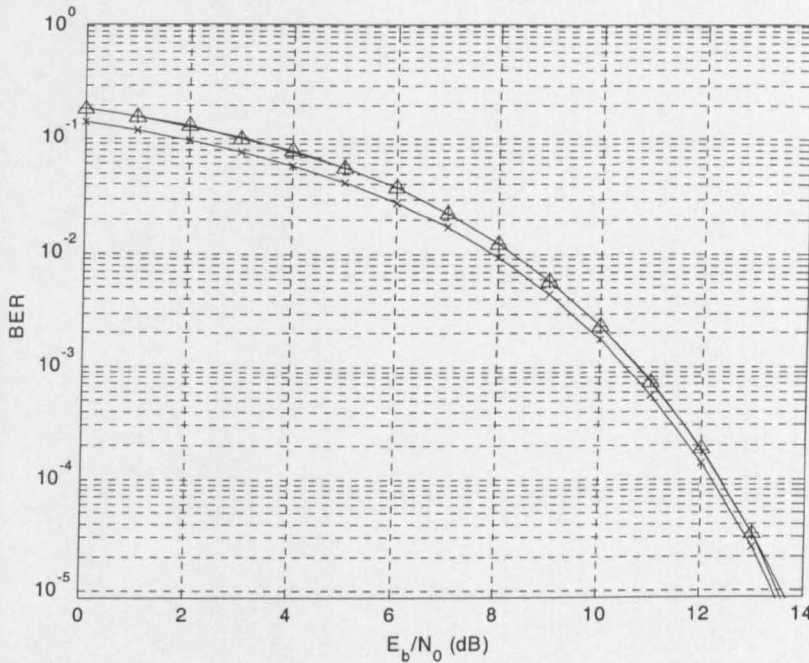


Figure 3-11: Performance of Uncoded 16-QAM in AWGN channel.

Legend: + Theoretical upper bound, \times Simulation using Gray constellation of Figure 2-2
 Δ Simulation using non-Gray constellation

3.4.3 Comparison of TC Performance with Literature

Validation of basic TC performance is carried out by comparing the developed TC performance against that found in literature. One of highly relevant references is [Val01], where the UMTS TC(1, 15/13, 15/13) employing UMTS TC interleaver [TGP02b], is evaluated. Two representative interleaver block lengths are evaluated: 640 and 5114 bits. The performance resulting from the use of LogMAP algorithm is used for comparison, as this is the decoding algorithm adopted throughout this thesis. Maximum TC decoding iterations are 10 when interleaver block length is 640, and 14 when the length is 5114. The modulation is BPSK and the channel is AWGN. All explicitly stated simulation parameters used in this reference are adopted. Simulated, the resulting performance is plotted along with that of the reference in Figure 3-12.

As can be seen from the figure, the performance of both TCs are generally in agreement. It differs slightly at certain places, most notably at low BER region. In this region, when the interleaver block length is 640 bits, the developed TC exhibits no apparent error floor, whereas when the interleaver block length is 5114 bits, the reverse phenomenon occurs.

Commenting on this performance difference, first, this can be due to different implicit parameters, such as the seeds of the random bit generator and AWGN noise generator. Second, different simulation stopping criteria can lead to different performance. At low BER region such as 10^{-7} , the simulation time becomes a hindrance to obtaining a reliable BER value. Third, it can be due to the different implementations of the MAP algorithms. The developed simulator adopts the simplified MAP algorithm of [Pie94, Pie95] described in 2.6.3.1.2. Lastly, variations in internal implementation of TC decoder, such as LLR normalisation and clipping, can also contribute to performance difference.

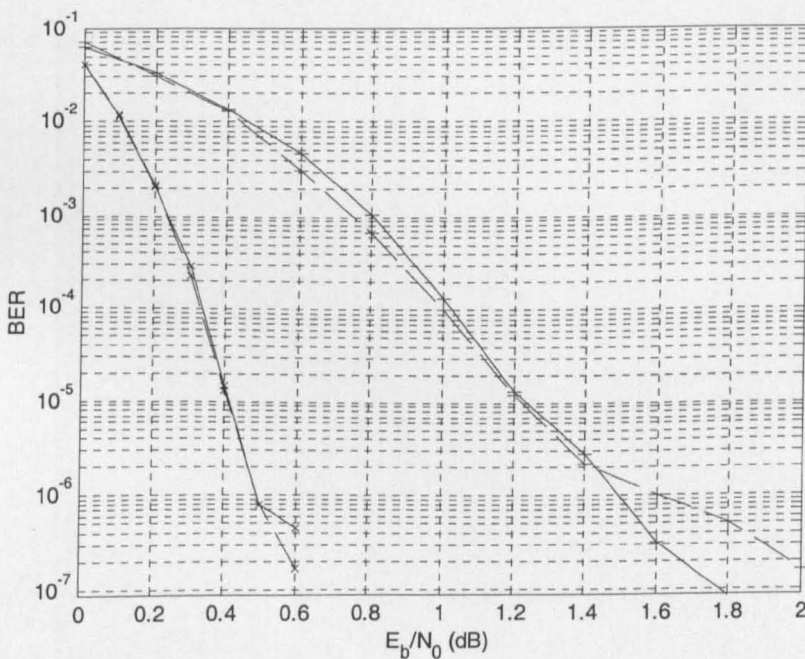


Figure 3-12: Performance of UMTS TC(1, 15/13, 15/13) in AWGN channel.

Legend: — Simulator, - - - [Val01]
+ Interleaving length of 640 bits, × Interleaving length of 5114 bits

To further validate the performance, comparison of basic TC(1, 5/7, 5/7) with that of [Woo00, Han02a] is performed. In these cited references, the TC utilises a pseudorandom interleaver, the length of which is 1000 bits. The performance is evaluated in AWGN channel, in conjunction with BPSK modulation. Adopted maximum number of LogMAP decoding iterations is 8. Coding rate of 1/3 and 1/2 are evaluated and compared. The rate-1/2 TC is produced by employing odd-even puncturing, such as used in [Ber93]. The resulting performance curves are plotted in Figure 3-13. As can be seen in the figure, the simulated and referenced TCs perform

comparably. Slight disagreement is expected to arise from the result of two entirely different implementations and independent statistical observations.

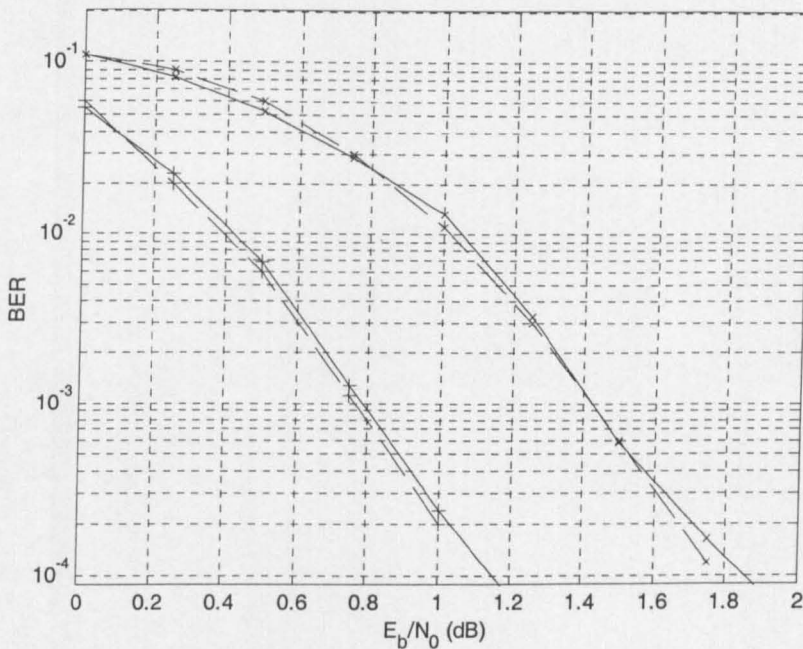


Figure 3-13: Performance of TC(1, 5/7, 5/7) in A WGN channel.

Legend: — Simulator, - - - [Woo00, Han02a]
+ Rate-1/2, × Rate-1/3

Considering the foregoing performance comparison, it is reasonable to state that the developed TC possesses the standard performance. In the next section, the performance of the TC that is used as part of the complete UMTS simulator will be compared to that published by Nokia and Ericsson.

3.4.4 Comparison of UMTS Simulator Performance with That of Nokia and Ericsson

The performance validation process presented here follows the steps outlined in 3GPP standard [TGP02d]. This document describes the details of bit framing (or transport channel multiplexing) and the environments on which the simulator (or any implementation of the standard) will be validated. However, these details are mainly the parameters of the transmitter, as those for the receiver are left to the manufacturers for them to compete with each other. Therefore, to be able to validate our simulator, additional parameters for the receiver are required. Reproduced as Table 3-1, in [TGP99a] and [TGP99b] we found these parameter details along with their

corresponding performance curves. Descriptions of the abbreviations and terms used can be found in the cited references [TGP99a, TGP99b], as well as in [Hol02].

Table 3-1: Simulation assumptions of Nokia and Ericsson [TGP99a, TGP99b]

Parameter	Explanation/Assumption			
Chip Rate	3.84 Mcps			
Closed loop Power Control	OFF			
AGC	OFF			
Channel Estimation	Ideal			
Number of samples per chip	1			
Propagation Conditions	As specified in Annex B of TS 25.101 v.2.2.0. Note that path delays in Case 1 and Case 2 have been moved to positions that are integer number of chips. The reason for this is the number of samples per chip used in simulations (1).			
Number of bits in AD converter	Floating point simulations			
Number of Rake Fingers	Equals to number of taps in propagation condition models			
Downlink Physical Channels and Power Levels	CPICH_Ec/Ior = -10 dB PCCPCH_Ec/Ior = -12 dB SCH_Ec/Ior = -12 dB (Combined energy of Primary and Secondary SCH) PICH_Ec/Ior = -15 dB OCNS_Ec/Ior = power needed to get total power spectral density (Ior) to 1. DPCH_Ec/Ior = power needed to meet the required block error rate (BLER) target			
BLER target	BLER target is not defined yet. Thus results for BLER from 0.5 to 10-3 are presented			
BLER calculation	BLER has been calculated by comparing with transmitted and received bits. So CRC is not used for BLER estimation.			
PCCPCH model	Random symbols transmitted, ignored in a receiver			
PICH model	Random symbols transmitted, ignored in a receiver			
DCCH model	Random symbols transmitted, ignored in a receiver			
TFCI model	Random symbols, ignored in a receiver but it is assumed that receiver gets error free reception of TFCI information.			
Used OVSF and scrambling codes	Codes are chosen from the allowed set.			
\hat{I}_{or} / I_{oc} values	Bit Rate	Case 1	Case 2	Case 3
	12.2 kbps	9, 12	-3, 0	-3, 0
	64 kbps	9, 12	-3, 0	-3, 0
	144 kbps	9, 12	3, 6	3, 6
	384 kbps	9, 12	6, 9	6, 9
Turbo decoding	MaxLogMap algorithm is used with 8 iterations			
SCH position	Offset between SCH and DPCH is zero chips meaning that SCH is overlapping with the first symbols in DPCH in the beginning of DPCH slot structure			
Measurement Channels	As specified in Annex A of TS 25.101 v2.2.0			
Other L1 parameters	As Specified in latest L1 specifications (July/August 1998 versions)			

Employing the same parameters as Nokia and Ericsson use, simulation was conducted. Some important results, along with those of Nokia and Ericsson, are plotted in Figure 3-14 to Figure 3-17. It can be seen that the performance of our simulator (the professional version, i.e., the W-

CDMA) is mostly in between those of Nokia and Ericsson. It is therefore reasonable to state that the simulator performs as well as expected.

The performance differences among the curves from different simulators can be attributed to the differences in the detailed implementation of various blocks (random number and noise generators, channel models, rake receivers and combiners, TC decoders, etc.) and number of accumulated total processed and erroneous bit to stop the simulation.

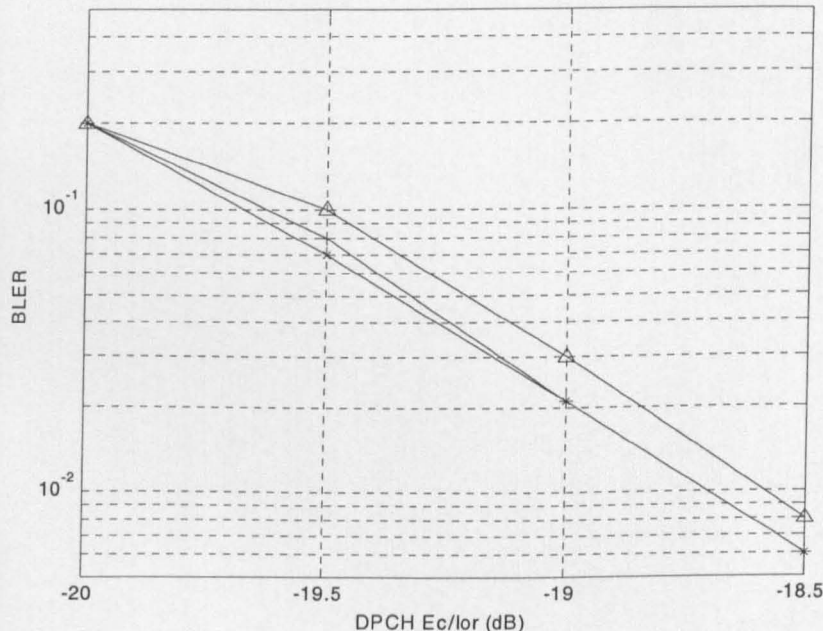


Figure 3-14: Simulator Performance of Speech 12.2 kbps Service in 3GPP Static (AWGN) channel.
Legend: + W-CDMA, × Ericsson, Δ Nokia

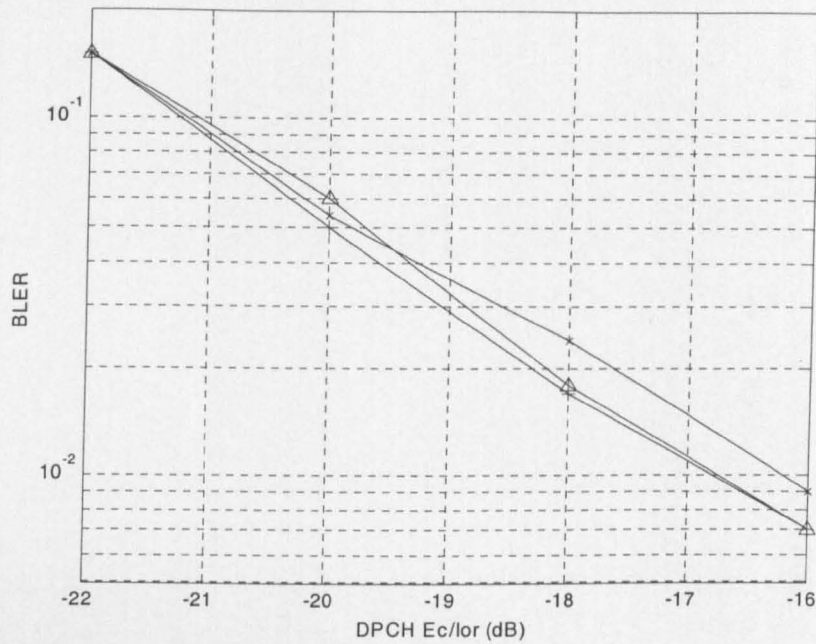


Figure 3-15: Simulator Performance of Speech 12.2 kbps in 3GPP Case 1 channel.
Legend: + W-CDMA, × Ericsson, Δ Nokia

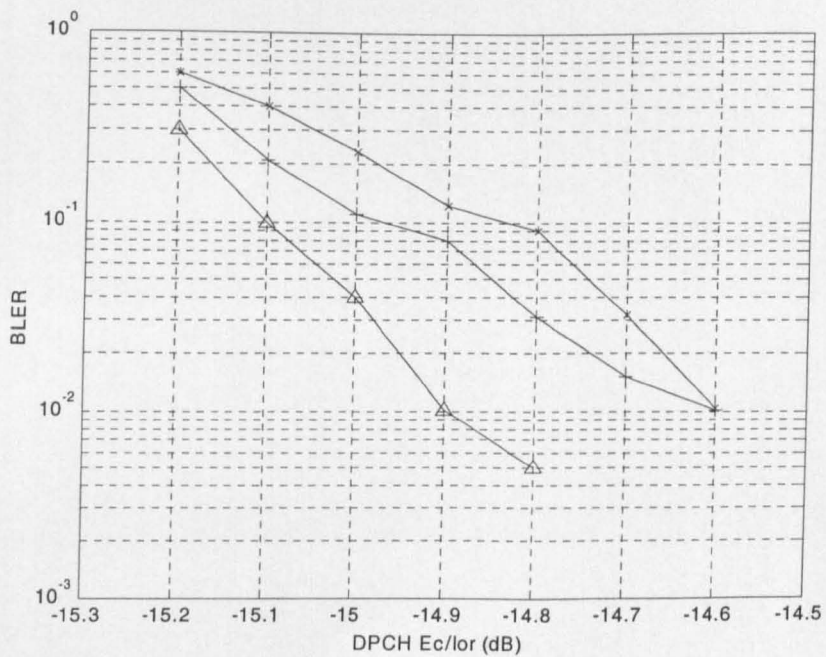


Figure 3-16: Simulator Performance in Data 64 kbps in 3GPP Static (AWGN) channel.
Legend: + W-CDMA, × Ericsson, Δ Nokia

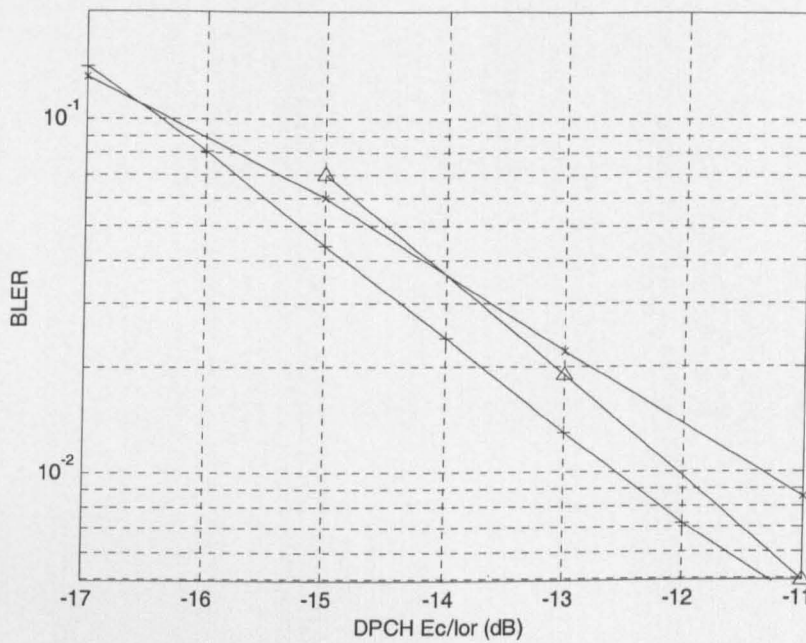


Figure 3-17: Simulator Performance of Data 64 kbps Service in 3GPP Case 1 channel.
Legend: + W-CDMA, × Ericsson, Δ Nokia

3.5 Summary

The simulator, which is used as the core platform for the next chapters, has been designed, implemented and validated. Several concluding remarks are worth mentioning:

1. The simulator is an output of the twofold implementation goal, that is, to be beneficial for research and industrial application purposes. Collaborative validation between academic and industrial researchers and engineers has speeded up the process and improved dependability.
2. Validation process and its consequent debugging sessions take up the largest portion of development time. Nevertheless, this has also opened the opportunity to understand better the system being simulated.

Chapter 4

Soft-Demodulation Methods

4.1 Introduction

Soft-demodulation, or more accurately soft-bit demodulation, is a demodulation process that estimates from the received demodulated symbols not only hard-bits (Boolean variable or binary digit: 0 or 1, or equivalently the polarity sign: positive or negative), but also their confidence levels. At the transmitter side, normally only hard-bits are involved, and they take the form of binary digits 0 or 1. However, at the receiver, particularly at the physical layer, these binary digits are more commonly represented as polarity signs, either negative or positive. Therefore, their confidence levels can simply be their magnitudes. In this case, the negative and positive polarities can be expressed as numeric values of -1 and +1, respectively.

There are two possibilities of interpreting the mapping of the binary digits to polarity signs: $\{0 \rightarrow -1, 1 \rightarrow +1\}$ or $\{0 \rightarrow +1, 1 \rightarrow -1\}$. The latter has the advantage that binary digit *XOR* operation is equivalent to the multiplication in bipolar domain. This convention is also adopted by 3GPP [TGP02c]. For these reasons, we adopt this convention as well in this work.

From the point of view of TC decoding, the soft-bit is the LLR value, i.e., the logarithmic ratio of probability of the bit of being 0 to the probability of the bit of being 1.

One important goal of the research work reported in this chapter is to devise exact as well as simplified or approximate soft-demodulation methods, particularly if the exact method is computationally complex. In the literature, for instance [LeG94, Hal98, Vuc00], when TC is operated in Rayleigh channels, the fading coefficients are modelled by real-valued variables. This approach is less realistic compared to another that adopts complex-valued variables [Sau99]. Most notably, at the receiver, CSI (comprising FC and NV) is supplied to TC decoder as an extra input while the TC decoder itself is also modified to accommodate this. This incurs extra complexity, particularly if there are many subsystems that separate soft-demodulator and the TC decoder. Being a scalar, provision and handling of noise variance is quite easy. In contrast, the fading coefficient is a vector, the sequence order of which is the same as that of data. In UMTS

and HSDPA [TGP02a], including their STTD mode, there are up to nine subsystems separating the demodulator and the TC decoder that alter the data sequence-order. Therefore, processing this extra vector would incur considerable implementation resources and complexity.

The remainder of this chapter will be devoted to the design, performance comparison and discussion of various soft-demodulation methods using complex-valued approach. In the design process, the CSI will be embedded in each demodulated bit, so that the resulting methods will eliminate the necessity of TC decoder from having extra CSI input and being modified, hence are simpler than those in [LeG94, Hal98, Vuc00]. A simple soft-demodulation method for binary modulation in the AWGN environment will first be described, followed by a more general approach that makes it applicable also in Rayleigh environments. Next is the soft-demodulation design for 16-QAM. This is the most important part of this chapter, wherein the devised methods are described in great detail. A summary section concludes the chapter.

4.2 Soft-Demodulation of Binary Modulation in an AWGN Environment

The soft-demodulation process is normally straightforward in the case of binary modulation schemes, for instance BPSK. This characteristic is also valid in any 4-ary modulation scheme that is *I-Q* separable, hence can be regarded as dual-binary modulation schemes, for example Gray-coded QPSK or Gray-coded 4-QAM schemes.

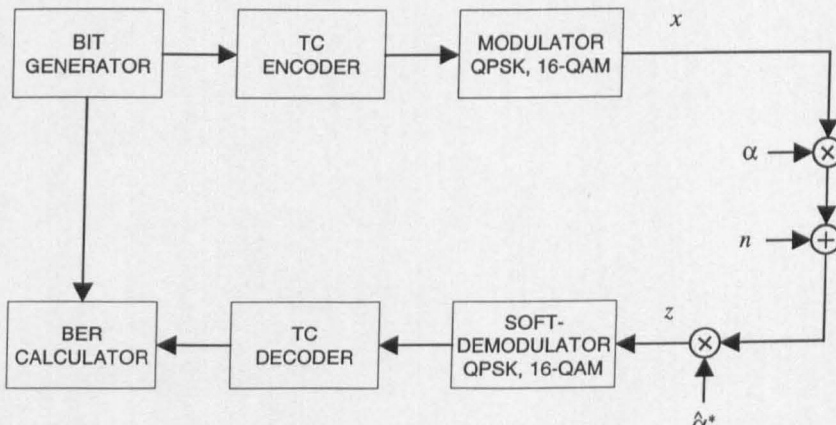
Let us examine a simple case, as depicted in Figure 4-1, of the Gray-coded QPSK link having a symbol energy $E_{av} = 1$ (hence, d in Figure 2-1 equals to $\frac{1}{\sqrt{2}}$) in an AWGN environment. For convenience, complex notation and operation are used. Now, suppose that a transmitter sends a modulated signal (low-pass equivalent) x through the AWGN channel n having zero mean and noise variance of σ^2 . Denoting the received signal as $r = r_I + j r_Q = x + n$, the LLR of the received soft-bit from the real (or in-phase) component r_I is [Skl01]

$$\begin{aligned}
L_c(b_I) &= \ln \left[\frac{p(b_I = 0 | r_I)}{p(b_I = 1 | r_I)} \right] \\
&= \ln \left[\frac{p(r_I | b_I = 0)}{p(r_I | b_I = 1)} \right] + \ln \frac{p(b_I = 0)}{p(b_I = 1)} \\
&= \ln \left(\frac{\frac{1}{\sigma\sqrt{2\pi}} \exp \left[-\frac{1}{2} \left(\frac{r_I - d}{\sigma} \right)^2 \right]}{\frac{1}{\sigma\sqrt{2\pi}} \exp \left[-\frac{1}{2} \left(\frac{r_I + d}{\sigma} \right)^2 \right]} \right) \\
&= \frac{2d}{\sigma^2} r_I \\
&= \frac{2}{\sigma^2} \frac{r_I}{\sqrt{2}}
\end{aligned} \tag{4.1}$$

assuming the event of selecting bit $b_I = \{0, 1\}$ for transmission is equiprobable. It follows that for imaginary (or quadrature) component case, substitute the subscript Q for I .

From this equation, it is evident that the LLR of a binary or dual-binary modulation scheme is just a simple function of the real or imaginary part of the received signal and its noise variance.

Unfortunately, the extraction of bit LLR, i.e., soft-demodulation, from a higher order modulation symbol is not a trivial issue. The coded BER performance difference between the optimum and the commonly used soft-bit demodulator in 16-QAM can be as high as 5 dB in the AWGN environment and even more in the Rayleigh environment, as will be shown later in this chapter.



Note: In AWGN environment, $\alpha = \hat{\alpha}^* = 1 + j 0$.

Figure 4-1: A Simple Low-Pass Equivalent Link Layer Model.

In the following sections, a design process for soft-demodulation methods will be carried out, starting with an exact method, which is referred to as “**Method E**”. This method is based on the calculation of “summation of exponentials”. To reduce the computational complexity, several approximation methods are envisaged. The first such method is termed “**Method M**”, which is based on a calculation taking the maximum of the arguments of the exponential summation. Second, a piece-wise linear approximation to the LLR curves is proposed, and then termed “**Method R**” for referencing convenience. This method can be regarded as an improvement to some widely used methods such as: (1) the approximation methods of Le Goff et al. [LeG94], which will be named “**Method L**”, and (2) the extension of the hard-demodulation method in [For92], which will be termed as “**Method F**”. Lastly, included for comparison purposes, “**Method C**”, represents a Euclidean soft-demodulation method, the soft-value of which is calculated intuitively by taking the reciprocal value of the distance between the received symbol to the nearest symbol in the constellation, i.e. the one that is chosen as the demodulated symbol. Owing to its inherent complexity, lack of analytical design and worse performance, the latter method will be included sparingly in the analysis. The purpose of this inclusion is to hint at the complexity and performance if a non-Gray method and non-*I-Q*-separable modulation scheme is employed.

An important point to note regarding Method L is that it is the LLR approximation of [LeG94] that is employed in the soft-demodulation process to include the CSI in every demodulated bit as the other methods under consideration.

4.3 Design of Soft-Demodulation Methods in Rayleigh Environments

The first line of equation (4.1) represents the basic principle of the bit LLR computation. To make it applicable to any *I-Q* separable modulation scheme working in a fading environment, let Y denote either I or Q and γ denote fading CSI that is represented by the estimated fading coefficient $\hat{\alpha}$. The j -th bit LLR can thus be expressed as:

$$L_c(b_Y^{(j)}) = \ln \left[\frac{p(b_Y^{(j)} = 0 | z_Y, \gamma)}{p(b_Y^{(j)} = 1 | z_Y, \gamma)} \right]. \quad (4.2)$$

In this case,

$$r = \alpha x + n \quad (4.3)$$

and

$$\begin{aligned}
z &= z_I + j z_Q \\
&= \hat{\alpha}^* r \\
&= \hat{\alpha}^* (\alpha x + n) \\
&= \hat{\alpha}^* \alpha x + \hat{\alpha}^* n
\end{aligned} \tag{4.4}$$

where * represents complex conjugation operation. Note that this multiplication process plays a crucial role, as this enables the inclusion of CSI in every demodulated bit. This process normally takes place in each finger of a rake receiver in a multipath channel, and can be referred to as channel compensation. Continuing the derivation, and assuming that the noise term $\hat{\alpha}^* n$ of (4.4) is Gaussian distributed, it can be shown that

$$\begin{aligned}
L_c(b_Y^{(j)}) &= \ln \left(\frac{\sum_{y \in y_0^{(j)}} \frac{1}{\sigma \|\hat{\alpha}\|^2 \sqrt{2\pi}} \exp \left[-\frac{1}{2\sigma^2 \|\hat{\alpha}\|^2} (z_Y - \|\hat{\alpha}\|^2 y)^2 \right]}{\sum_{y \in y_1^{(j)}} \frac{1}{\sigma \|\hat{\alpha}\|^2 \sqrt{2\pi}} \exp \left[-\frac{1}{2\sigma^2 \|\hat{\alpha}\|^2} (z_Y - \|\hat{\alpha}\|^2 y)^2 \right]} \right) \\
&= \mathbf{E}_{y \in y_0^{(j)}} \frac{-1}{2\sigma^2 \|\hat{\alpha}\|^2} (z_Y - \|\hat{\alpha}\|^2 y)^2 - \mathbf{E}_{y \in y_1^{(j)}} \frac{-1}{2\sigma^2 \|\hat{\alpha}\|^2} (z_Y - \|\hat{\alpha}\|^2 y)^2
\end{aligned} \tag{4.5}$$

where operator \mathbf{E} is defined as

$$\begin{aligned}
a \mathbf{E} b &\equiv \ln(\exp(a) + \exp(b)) \\
&\equiv \max(a, b) + \ln(1 + \exp(-|a - b|))
\end{aligned} \tag{4.6}$$

and $y \in y_0^{(j)}$ denotes the amplitude levels of the modulation symbol constellation projected to Y axis corresponding to bit $y^{(j)} = 0$. Y represents I or Q axis, so z_Y can mean either $\text{Re}\{z\}$ or $\text{Im}\{z\}$. If non-binary operation is involved, operator \mathbf{E} can be calculated recursively, for example

$$\begin{aligned}
\mathbf{E}_{i=1}^3 a_i &= a_1 \mathbf{E} a_2 \mathbf{E} a_3 \\
&= a_1 \mathbf{E} (a_2 \mathbf{E} a_3).
\end{aligned} \tag{4.7}$$

The method will become obvious when applied to the QPSK and 16-QAM cases that follow.

In QPSK case, there is only one member of y that satisfies $y \in y_0^{(j)}$, that is $y = +d$ (see Figure 2-1), so the LLR reduces to

$$\begin{aligned}
L_c(b_y^{(j)}) &= \frac{-1}{2\sigma^2\|\hat{\alpha}\|^2} (z_y - \|\hat{\alpha}\|^2)^2 + \frac{1}{2\sigma^2\|\hat{\alpha}\|^2} (z_y + \|\hat{\alpha}\|^2)^2 \\
&= \frac{\sqrt{2}}{\sigma^2} z_y. \\
&= \frac{2}{\sigma^2} \frac{z_y}{\sqrt{2}}
\end{aligned} \tag{4.8}$$

Now it is obvious that the exact soft-demodulation method of QPSK (i.e., Method E) has already been computationally simple, hence no simplified method is necessary.

In 16-QAM, however, there are two bits from each *I* and *Q* axes that make up a modulation symbol. Figure 2-2 is redrawn here as Figure 4-2 for referencing convenience. The constellation point on top right corner represents 0011 bits. Adopting $\{i_1 q_1 i_0 q_0\}$ bit arrangement, where letter *i* signifies that the bits originate from *I* axis, this constellation point is made up of $i_1 = 0, i_0 = 1$ bits from *I* axis and $q_1 = 0, q_0 = 1$ bits from *Q* axis. For further convenience, the bit with subscript 1 will be referred to as MSB, whereas the other with subscript 0 will be called LSB.

Referring to the bottom part of Figure 4-2 it is apparent that for MSB:

$$\begin{aligned}
y \in y_0^{(1)} &= \{d, 3d\} \\
y \in y_1^{(1)} &= \{-d, -3d\}
\end{aligned} \tag{4.9}$$

while for LSB

$$\begin{aligned}
y \in y_0^{(0)} &= \{-d, d\} \\
y \in y_1^{(0)} &= \{-3d, 3d\}.
\end{aligned} \tag{4.10}$$

Therefore,

for MSB:

$$L_c(b_y^{(1)}) = \underset{y=\{-d, -3d\}}{\mathbf{E}} \frac{-1}{2\sigma^2\|\hat{\alpha}\|^2} (z_y - \|\hat{\alpha}\|^2 y)^2 - \underset{y=\{d, 3d\}}{\mathbf{E}} \frac{-1}{2\sigma^2\|\hat{\alpha}\|^2} (z_y - \|\hat{\alpha}\|^2 y)^2 \tag{4.11}$$

and for LSB:

$$L_c(b_i^{(0)}) = \underset{y=\{-d, d\}}{\mathbf{E}} \frac{-1}{2\sigma^2\|\hat{\alpha}\|^2} (z_y - \|\hat{\alpha}\|^2 y)^2 - \underset{y=\{-3d, 3d\}}{\mathbf{E}} \frac{-1}{2\sigma^2\|\hat{\alpha}\|^2} (z_y - \|\hat{\alpha}\|^2 y)^2. \tag{4.12}$$

This is the Method E for 16-QAM. Note that this method is similar to the exact method in [LeG94], the main difference of which lies in the presence of the multiplicative variable K in the referred method.

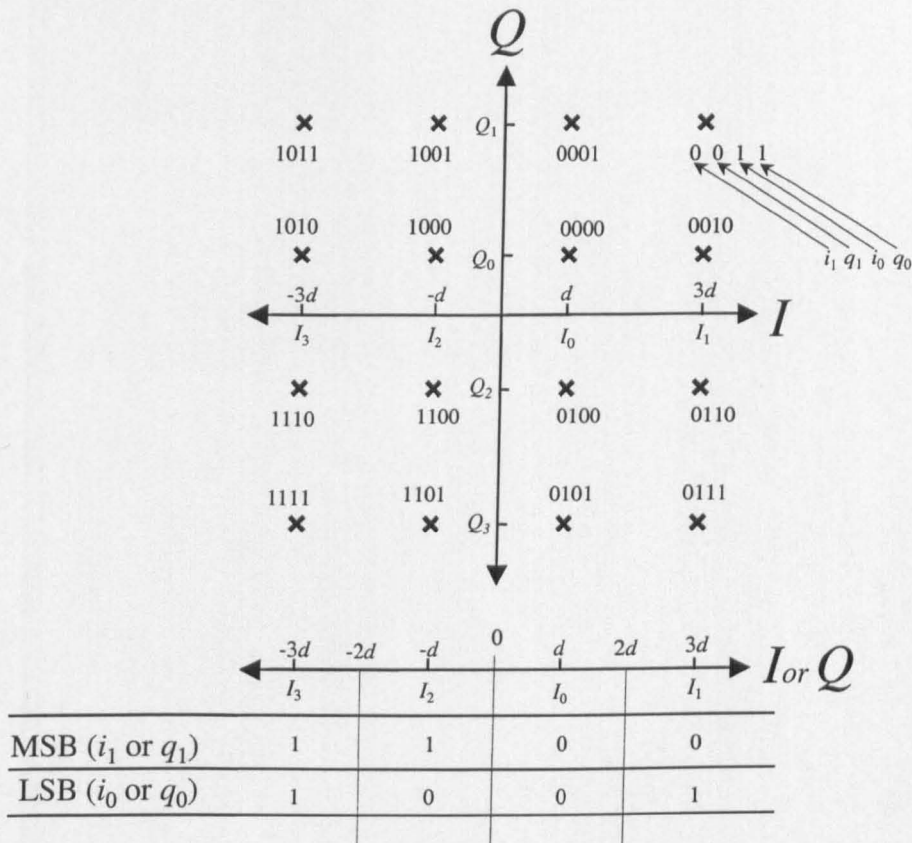


Figure 4-2: 16-QAM signal constellation and its corresponding 4-PAM

4.4 Approximation “Method M”

Due to simplicity of the exact soft-demodulation method for the QPSK case, there is no need of approximation. On the contrary, in the 16-QAM case, the calculation involves the computationally-intensive **E** operation. Therefore, in the following description and in the sections regarding the approximation methods, 16-QAM modulation is implied.

The most obvious and straightforward approximation for this operation is, popularly applied in *LogMAP* decoding algorithm to produce its simpler version *MaxLogMAP*, the “taking the maximum” operation defined as follows

$$a \text{ M } b \equiv \max(a, b). \quad (4.13)$$

Similar to the **E** operation, multiterm **M** operation can be performed recursively. Therefore, for MSB:

$$L_c(b_Y^{(1)}) = \underset{y=\{-d, -3d\}}{\mathbf{M}} \frac{-1}{2\sigma^2 \|\hat{\alpha}\|^2} (z_Y - \|\hat{\alpha}\|^2 y)^2 - \underset{y=\{d, 3d\}}{\mathbf{M}} \frac{-1}{2\sigma^2 \|\hat{\alpha}\|^2} (z_Y - \|\hat{\alpha}\|^2 y)^2 \quad (4.14)$$

and for LSB:

$$L_c(b_Y^{(0)}) = \underset{y=\{-d, d\}}{\mathbf{M}} \frac{-1}{2\sigma^2 \|\hat{\alpha}\|^2} (z_Y - \|\hat{\alpha}\|^2 y)^2 - \underset{y=\{-3d, 3d\}}{\mathbf{M}} \frac{-1}{2\sigma^2 \|\hat{\alpha}\|^2} (z_Y - \|\hat{\alpha}\|^2 y)^2. \quad (4.15)$$

4.5 Approximation ‘‘Method R’’

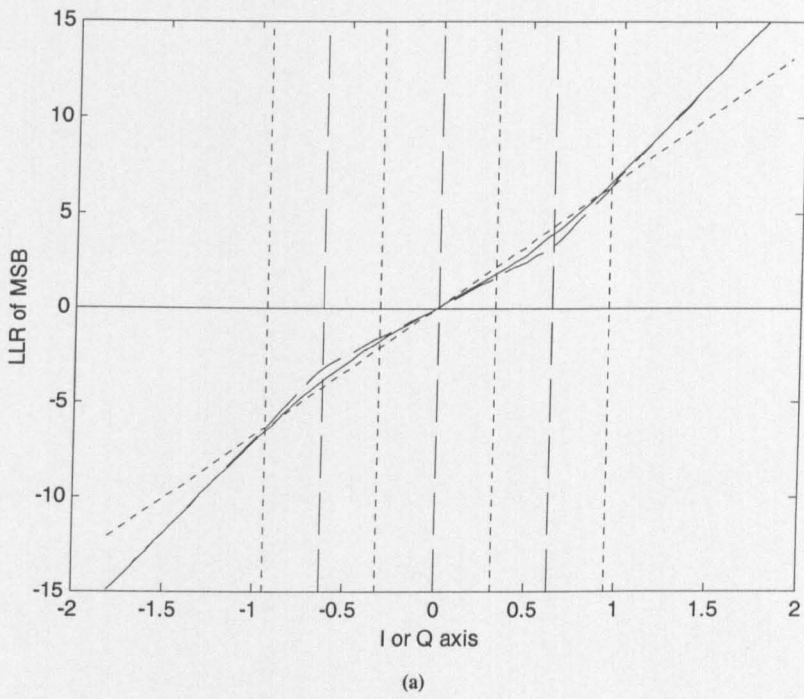
The approximation method introduced in this section can be regarded as an improvement to the basic hard-decision method introduced in [For92] or its extension by taking the distance to the appropriate decision boundary as a confidence level. Moreover, this can be regarded also as an improvement to the similar approximation method found in [LeG94].

The approximation is performed by employing a piecewise linear approach, by evaluating the approximate slopes of the Method M’s LLR curves. Examining Figure 4-3, where $E_{av} = 1$ hence $d \cong 0.3162$, it can be deduced that a linear approximation for MSB’s LLR will need just a single slope value for the whole range of z_Y , i.e., in the form of $y = m x$, where m denotes the slope. Substituting $3d$ and 0 for x into (4.14) results in $L_c(b_Y^{(1)}) = 16d^2/(3\sigma^2)$ and 0 , respectively. Applying the simple formula for finding the slope given two points in Cartesian diagram results in the slope for the MSB’s approximate LLR:

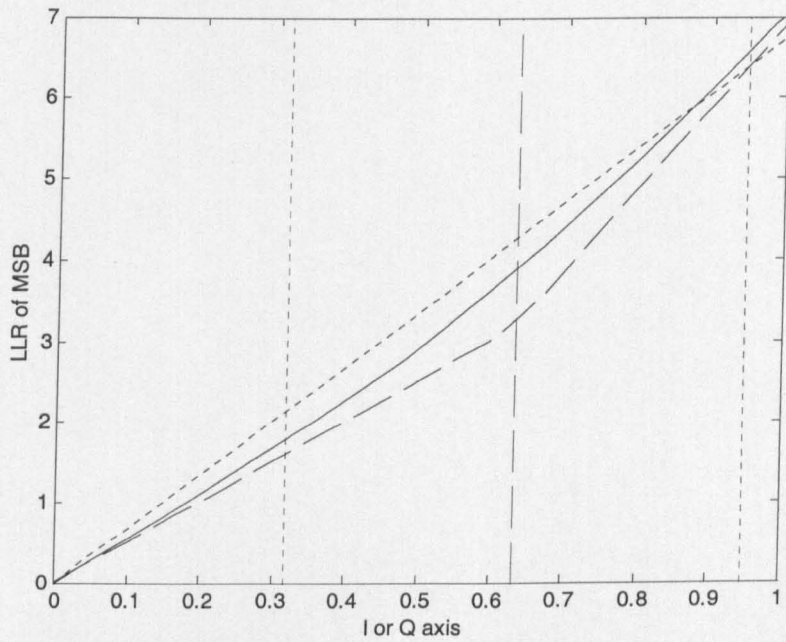
$$m^{(1)} = \frac{8d}{3\sigma^2}. \quad (4.16)$$

Therefore,

$$\begin{aligned} L_c(b_Y^{(1)}) &= m^{(1)} z_Y \\ &= \frac{8d}{3\sigma^2} z_Y. \end{aligned} \quad (4.17)$$



(a)



(b)

(a) z_I or z_O range = [-2, 2], (b) z_I or z_O range = [0, 1].

In the case of LSB, as can be deduced from Figure 4-4, the linear approximation is in the form of $y = m(z - |x|)$. Applying the same substitutions as for MSB case, i.e., substituting $3d$ and 0 for y into (4.15), we have $L_c(b_Y^{(0)}) = -2d^2/\sigma^2$ and $4d^2/\sigma^2$, respectively. Hence, the slope is

$$m^{(0)} = \frac{2d}{\sigma^2}. \quad (4.18)$$

and the corresponding LLR becomes

$$L_c(b_Y^{(0)}) = \frac{2d}{\sigma^2} (2d\|\hat{\alpha}\|^2 - \|z_Y\|). \quad (4.19)$$

For comparison, in Method F, $m^{(0)} = m^{(1)} = 1$, and in Method L, $m^{(0)} = m^{(1)} = 2d/\sigma^2$.

Figure 4-5 hints at the cause of the deviation of Method M's LLR curves from those of Method E, as can be observed in Figure 4-3 and Figure 4-4. For the MSB, the maximum deviation occurs at $z_Y = \pm 2d$, whereas for the LSB it takes place at $z_Y = \pm d$. As can be seen in Figure 4-5, at these points, the arguments of the E operator for the first and the second terms of LLR calculation for MSB (4.11) and LSB (4.12) are dominated by the second term of the E operator definition in (4.6) (this term is also referred to as "correction term"), and they do not cancel each other out. Therefore, at these points, the M operation (4.13) deviates by a large margin from the E operation (4.6).

Evaluation of LLR curves at $E_s/N_0 = 10$ and 20 dB are depicted in Figure 4-6 and Figure 4-7. It is interesting to note: (1) the ranges of LLR values are also multiplied by the same amount as E_s/N_0 , (2) the LLR curves of LSB become co-located, meaning that the approximate LLR's become accurate.

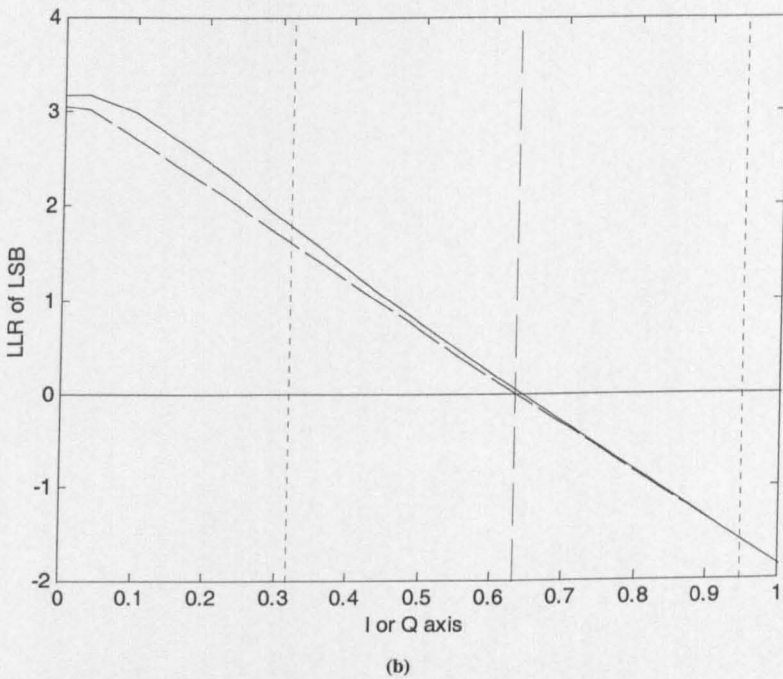
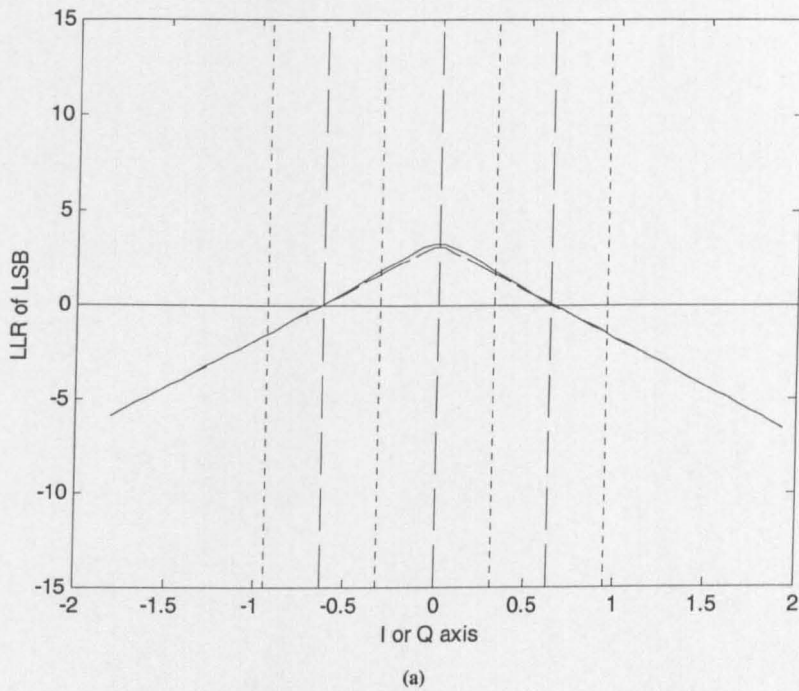
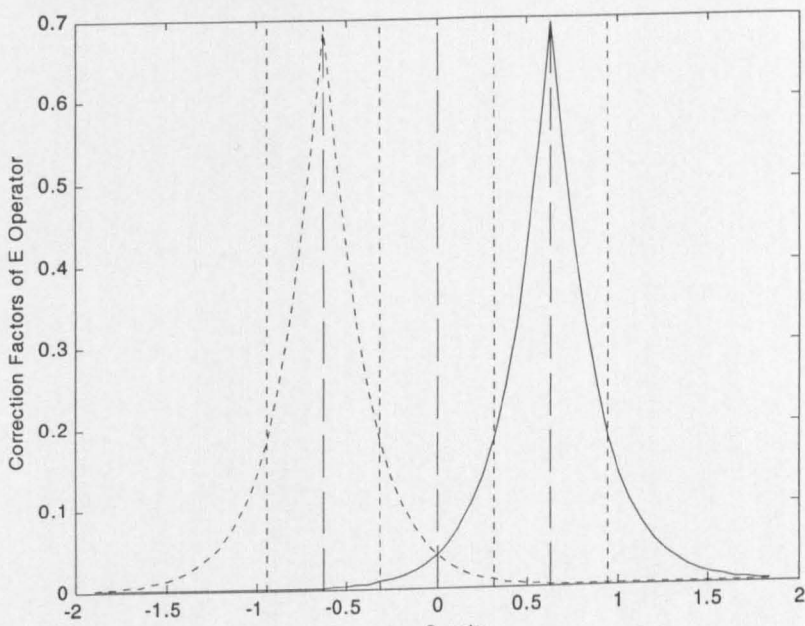
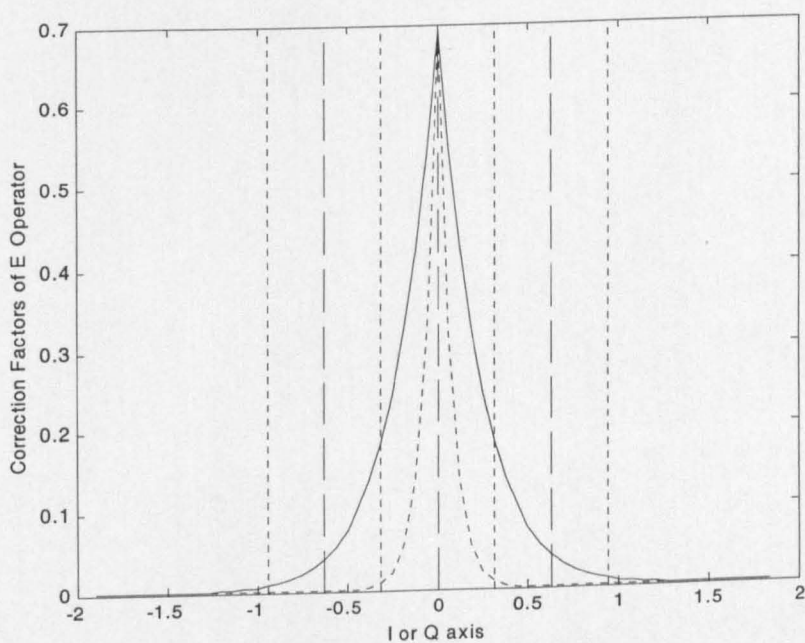


Figure 4-4: 16-QAM LLR of LSB at $E_s/N_0 = 0 \text{ dB}$.
Legend: — Method E, - - - Method M, ····· Method R
 The vertical grids are spaced d apart.
 (a) z_I or z_Q range = $[-2, 2]$, (b) z_I or z_Q range = $[0, 1]$.

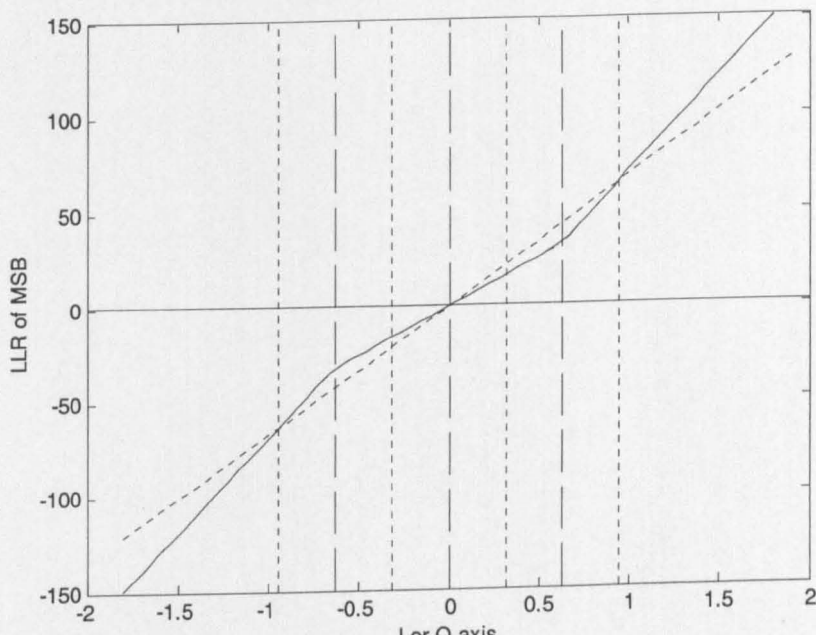


(a)

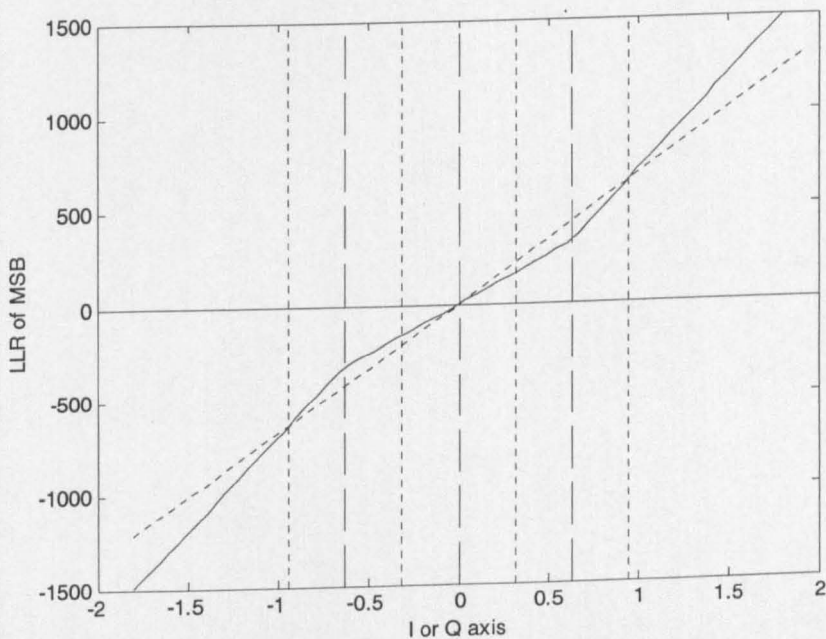


(b)

Figure 4-5: Correction factors of E operator in Method E at $E_s/N_0 = 0 \text{ dB}$
Legend: — The first term of eqn. (4.11), - - - The second term of eqn. (4.11)
 (a) MSB (b) LSB



(a)

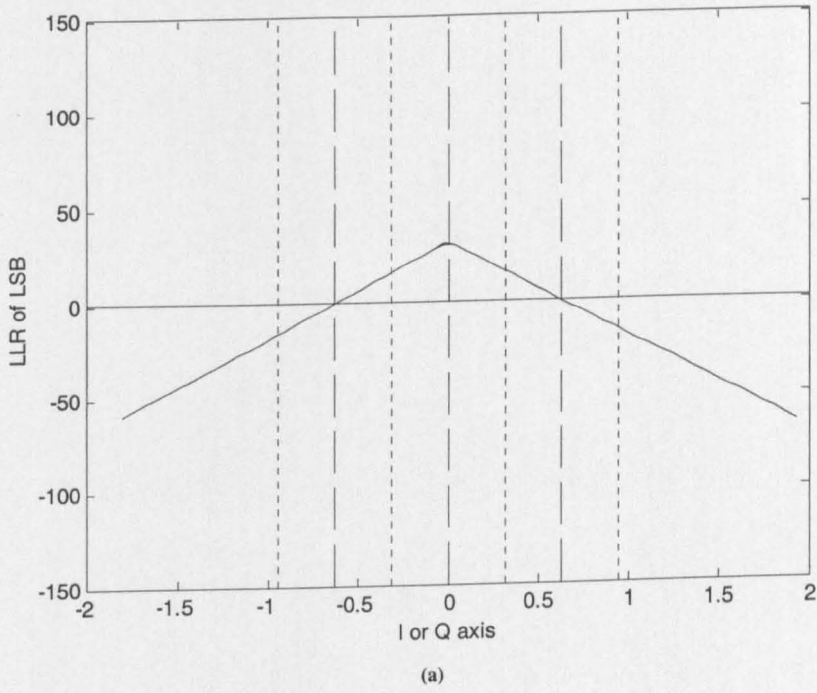


(b)

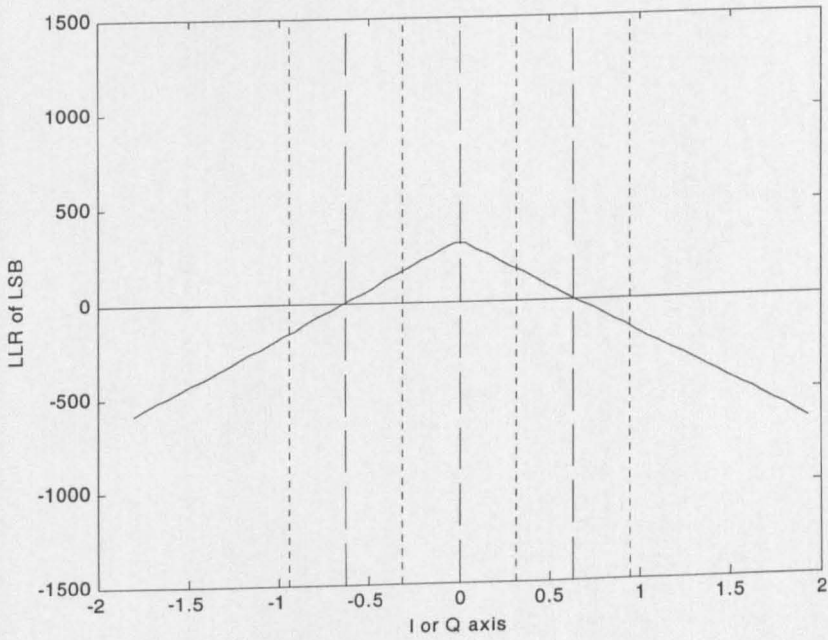
Figure 4-6: 16-QAM LLR of MSB at (a) $E_s/N_0 = 10$ dB and (b) $E_s/N_0 = 20$ dB.

Legend: — Method E, - - - Method M, ······ Method R

The vertical grids are spaced d apart.



(a)



(b)

4.6 Performance Evaluation

Referring to [Pro00, Hay01], the ratio of uncoded bit energy to the noise spectral density in a digital modulation system can be expressed as

$$\frac{E_c}{N_0} = \frac{E_{av}}{2 \cdot \log_2(M) \cdot \sigma^2} \quad (4.20)$$

where $E_{av} = 2d^2$ for QPSK and $E_{av} = 10d^2$ for 16-QAM (calculated based on Figure 4-2 or referring to [Pro00, Hay01]), M is the size of modulation symbol alphabet, and $N_0 = 2 \sigma^2$ is single-sided noise spectral density. However, for assessing the coded BER performance, it is the ratio of energy per information bit to the noise power spectral density, E_b/N_0 , that is normally used. Denoting R as code rate, $E_b = E_c / R$, hence

$$\frac{E_b}{N_0} = \frac{E_{av}}{2 \cdot \log_2(M) \cdot \sigma^2 \cdot R} \quad (4.21)$$

Having defined the E_b/N_0 relation, the coded performance of soft-demodulation methods described in the previous sections will be simulated and evaluated in different environments, namely AWGN, uncorrelated Rayleigh, and correlated Rayleigh channels. The simulator uncoded BER performance has been verified to comply with the theoretical one, such as that in [Pro00].

With regard to the channel coding, 3GPP's TC is employed [TGP02a]. It is a $[1, 15/13, 13/13]_8$ rate-1/3 code. The internal interleaver follows the one described in [TGP02a], by setting the block length to 1000, unless stated otherwise. Also adhering to 3GPP standard is the coded bit arrangement to form a single bit sequence. This bit sequence goes into a serial-to-parallel bit mapping, and in turn, these parallel bit sequences are respectively mapped to I and Q components of QPSK or 16-QAM modulator. The LogMAP algorithm with maximum number of iterations of 4 is applied at the decoder. Again, unless stated otherwise, there is no channel interleaving involved. Evaluation of performance using 3GPP's convolutional code (CC) is also performed to further validate the performance, particularly to examine the diversity benefit of TC compared to CC. In this section, perfect estimation of Rayleigh channel coefficient $\hat{\alpha} = \alpha$ and noise variance σ^2 is assumed.

As pointed out in Section 4.3, there is no advantage in envisaging a simplified soft-demodulation method for QPSK as the commonly used method has been simple and optimum. Nevertheless, simulation results will be shown to underline that the described soft-demodulation method includes CSI in every soft-bit, hence there is no necessity to provide separate CSI to the TC decoder.

As for 16-QAM, there will be discussions of performance evaluation, effects of interleaving type, effects of interleaving length, effects of Doppler spread, and performance versus complexity assessment.

4.6.1 QPSK

The performance of the soft-decision method will be simulated and evaluated in AWGN, Uncorrelated Rayleigh and Correlated Rayleigh channels.

4.6.1.1 AWGN Channel

The result depicted in Figure 4-8 is obtained from 3GPP rate-1/3 TC, with internal TC interleaving length of 1000 bits, simulated in AWGN channel. This graph shows that the simulator works as expected. The simulator shares the same engine with the professional version CCSR's "W-CDMA Version 3" [WCD03] that has been passed numerous performance validation stages and is used by a 3G operator in UK.

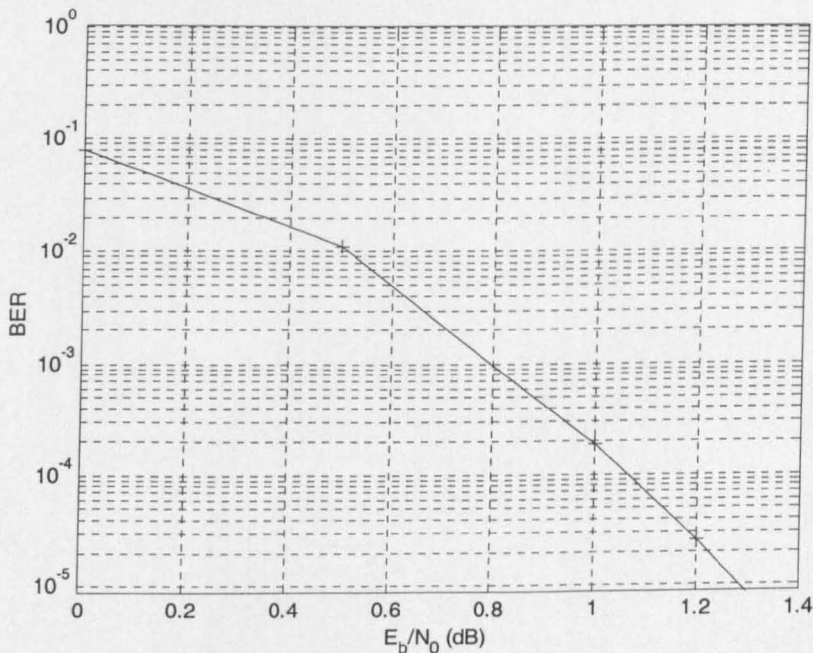


Figure 4-8: QPSK Performance in A WGN channel.

4.6.1.2 Uncorrelated Rayleigh Channel

In analysing and simulating uncorrelated and correlated Rayleigh environments, two approaches are used regarding the use of fading coefficients: either using complex-valued or real-valued

magnitude-only. We adopt the complex-valued coefficient approach, as it is more realistic and can be regarded as the superset of the real-valued approach.

In contrast, the approach adopted in [LeG94] or in [Vuc00] is real-valued approach. As a result, the soft-decision method in the Rayleigh environment, which involves the use of fading coefficients, is not straightforward. The fading coefficients need to be provided as a separate input to the TC decoder, so the method requires the modification of the MAP constituent decoder. This modification is not a simple task if there are many subsystems separating the soft-demodulator and the TC decoder, such as in a 3GPP receiver, where there are at least 9 separating subsystems [TGP02b]. The soft-demodulation, however, remains unchanged and is the same as the proposed one (4.8), but without multiplying it first by the conjugate of the estimated channel coefficient. We will refer to this method as “Method V” in the following discussion, also as the legend for the corresponding performance curves in Figure 4-9 and Figure 4-10.

The proposed method, termed Method E (see Section 4.3), has the advantage of keeping the TC decoder structure unchanged. It achieves this by embedding the fading coefficient in every soft-decoded bit, by way of multiplying the conjugate of the estimated channel coefficient with the received symbol, as expressed in (4.4).

Figure 4-9 shows simulation results. The two nearly co-located curves correspond to the Method E soft-demodulation employed in complex-valued and real-valued fading channels. Theoretically, both curves should be co-located at all places. The other curve, to the right by about 1.2 dB at BER of 10^{-5} , is when Method V is applied, but no separate fading coefficient given to TC decoder.

We can conclude that without changing the TC decoder, the coded performance provides 1.2 dB gain at BER of 10^{-5} . This is a typical gain resulting from the inclusion of CSI to the LogMAP TC decoder [Vuc00]. Expressed in other words, by using the proposed method, the gain can be obtained without the complexity of providing CSI as a separate entity to the TC decoder while keeping the TC decoder structure the same for all modulation schemes and channel types. It will be shown in the next chapter that this advantage is also applicable for multipath channels.

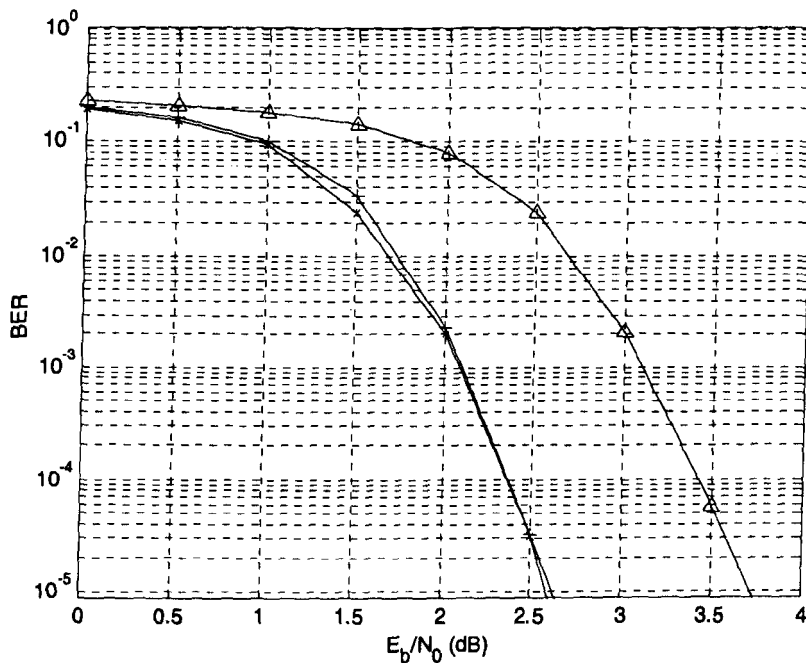


Figure 4-9: QPSK Performance in Uncorrelated Rayleigh channel.

Legend: + Method E, \times Method E, Magnitude-only Fading Channel,
 Δ Method V, Magnitude-only Fading Channel

4.6.1.3 Correlated Rayleigh Channel

The simulation results in a correlated Rayleigh channel are shown in Figure 4-10. Apart from the fact that the performance of all methods is much worse, similar analysis and conclusion discussed for uncorrelated channel in the previous section are applicable here. The bad performance is due to correlation between successive symbols entering the TC decoder. Bit interleaving and diversity techniques can be employed to improve the performance.

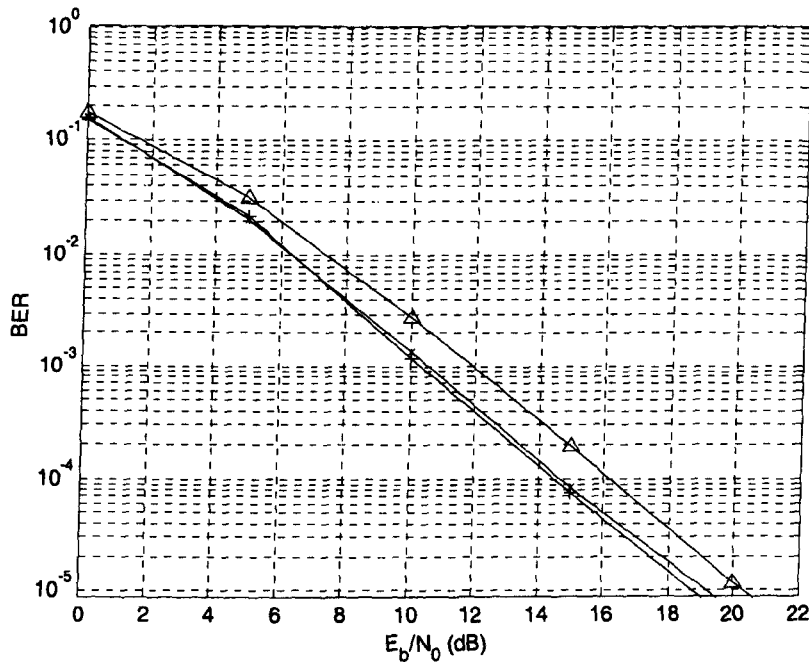
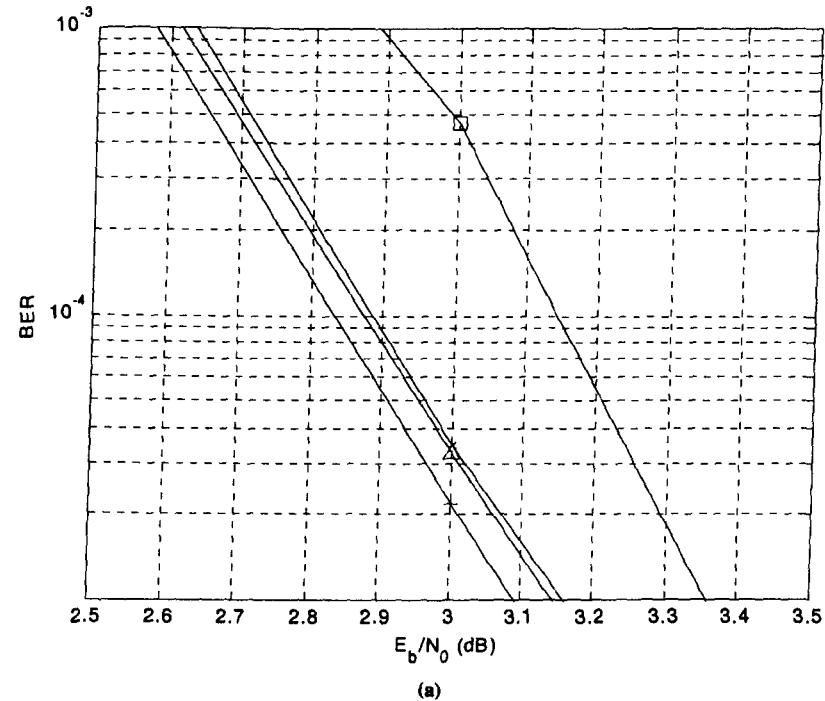


Figure 4-10: QPSK BER Performance in Correlated Rayleigh channel.
Legend: + Method E, \times Method E, Magnitude-only Fading Channel,
 Δ Method V, Magnitude-only Fading Channel

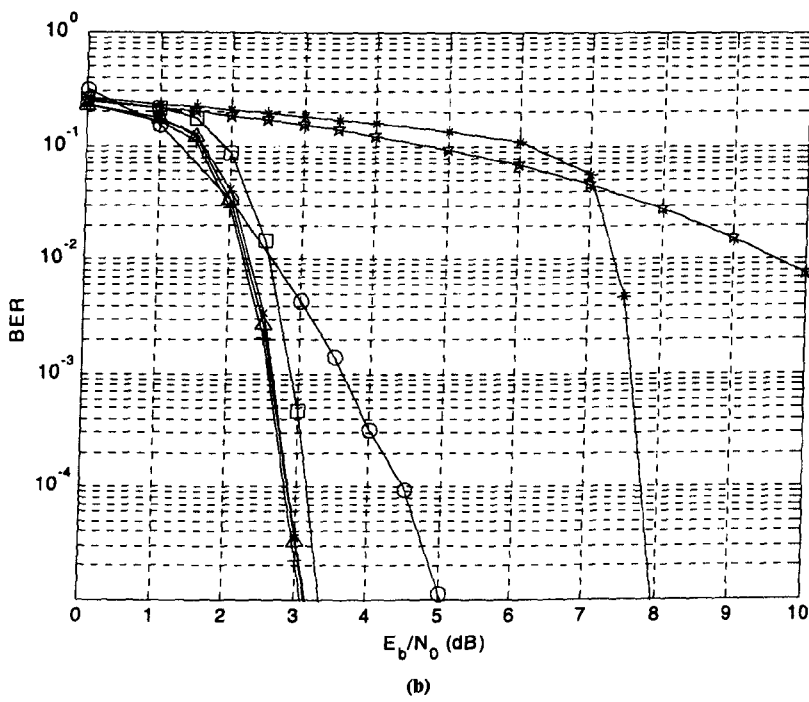
4.6.2 16-QAM

4.6.2.1 AWGN Channel

Performance evaluation in AWGN serves as a baseline for further evaluation in more complicated and more realistic environments. Figure 4-11 shows simulation results of such a performance evaluation. Part (a) of the figure can be considered as the zoomed version of part (b). Several points are worth noting, starting by examining part (a) at BER of 10^{-5} . First, the Method E gives the best performance, as expected. Second, despite being computationally simpler, Method R is slightly better than Method M, and is about 0.05 dB worse than Method E. The similarity in performance between Method M and R results from the similarity in LLR curves. Third, the Le Goff's approximation (Method L) is about 0.25 dB worse than Method E. This means, by revising the constant weighting factor of the Method L to form Method R, 0.2 dB improvement is gained. Further, the commonly used Method F is almost 5 dB worse than Method E. Finally, using reciprocal Euclidean distance as soft-decision value gives the worst performance. This hints that non-Gray mapping and non-I-Q-separable constellation may result in either complicated soft-demodulation method or worse performance if a comparable complexity soft-demodulation approximation is employed.



(a)



(b)

Figure 4-11: 16-QAM Performance in AWGN channel.

Legend: + Method E, \times Method M, Δ Method R, \square Method L
 \star Method F, $*$ Method C, \circ Method E using 3GPP Convolutional Code
(a) E_b/N_0 range = [2.5, 3.5] dB, (b) E_b/N_0 range = [0, 10] dB.

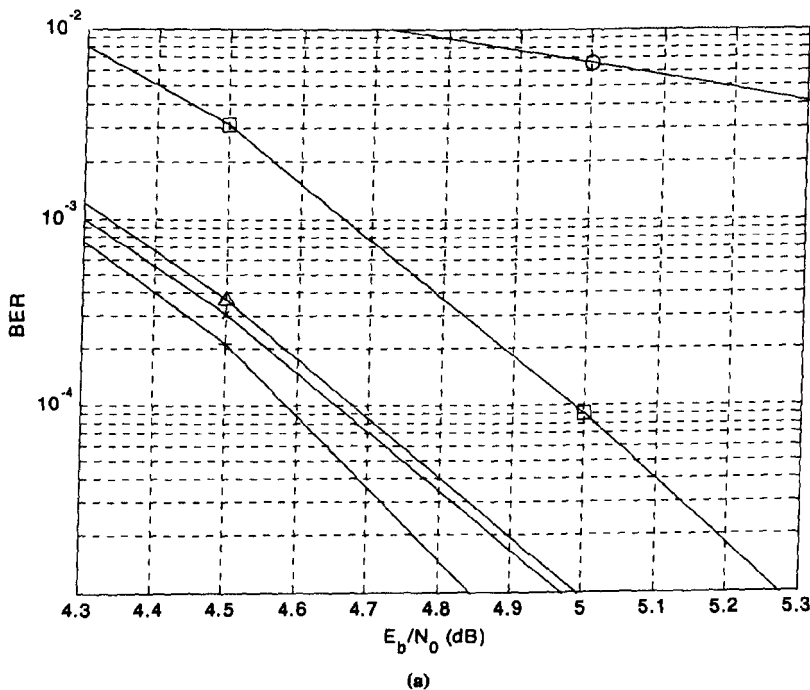
From the slope of the BER performance curve at high signal to noise values, an approximation of diversity order can be obtained. See, for instance the diversity comparison graphs in [Pro00]. Comparing the performance curve slopes of the TC and CC, we can deduce that TC has diversity as well as performance advantages, mainly due to internal interleaving and iterative decoding.

4.6.2.2 Uncorrelated Rayleigh Channel

The uncorrelated Rayleigh channel is also referred to as a fully-interleaved Rayleigh channel. The resulting coded performance can be regarded as the best possible performance out of a physical link communication system utilising single path, single transmit and single receive antennas working in a Rayleigh channel.

Examining Figure 4-12, starting with part (a), several points can be deduced. Let us concentrate on the case of BER equals 10^{-5} . First, the Method E performs the best, as expected. Second, the Method M is faintly better than Method R, both about 0.15 dB worse than Method E. Third, Method L is about 0.45 dB worse than Method E. Further, Method F is about 6.7 dB worse than Method E, whereas Method C is completely out of the question.

The performance of CC (employing Method E) has a similar trend with the case in AWGN channel: the diversity as well as the actual performance is worse than that of TC.



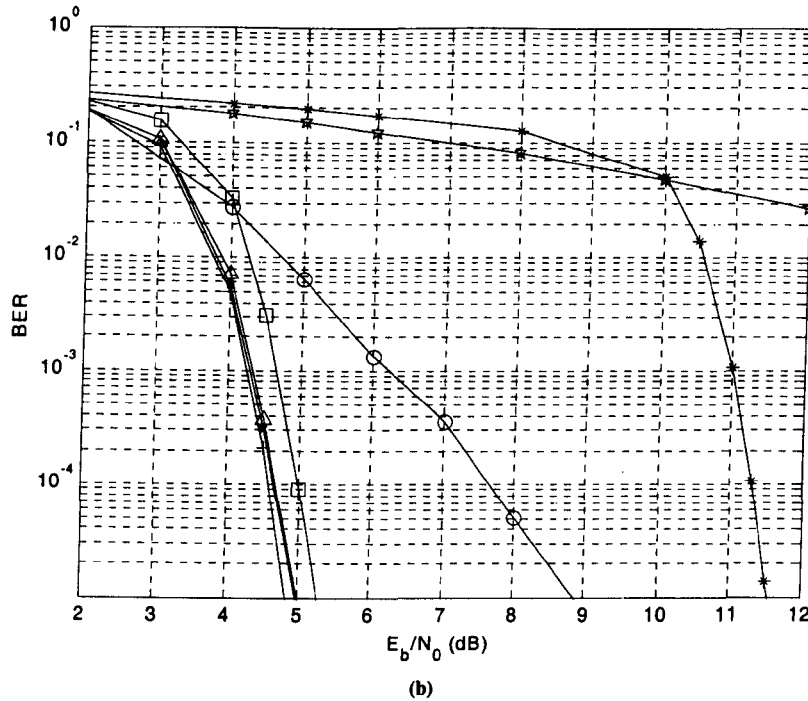


Figure 4-12: 16-QAM Performance in Uncorrelated Rayleigh channel.

Legend: + Method E, \times Method M, Δ Method R, \square Method L
 \star Method F, $*$ Method C, \circ Method E using 3GPP Convolutional Code
(a) E_b/N_0 range = [4.3, 5.3] dB, (b) E_b/N_0 range = [2, 12] dB.

4.6.2.3 Correlated Rayleigh Channel

This channel represents a more realistic channel. In fact, what is applied simulates the single path Rayleigh channel, resulting from a transmission with a carrier frequency of 2 GHz, mobile velocity of 120 km/h, hence Doppler spread of 222.2 Hz, sampled at 240000 samples/second. Note that there is no channel interleaving employed, so the performance will be much worse than that of the uncorrelated Rayleigh. Observing Figure 4-13, the performance of different methods follows the same trend as in the uncorrelated Rayleigh case. However, Method M, R, and L now perform similarly: about 0.6 dB worse than Method E. Method F is still about 4 dB worse than Method E, whereas Method C performs the worst as usual.

Similarly, the CC performance follows the same trend as in AWGN and uncorrelated Rayleigh channels.

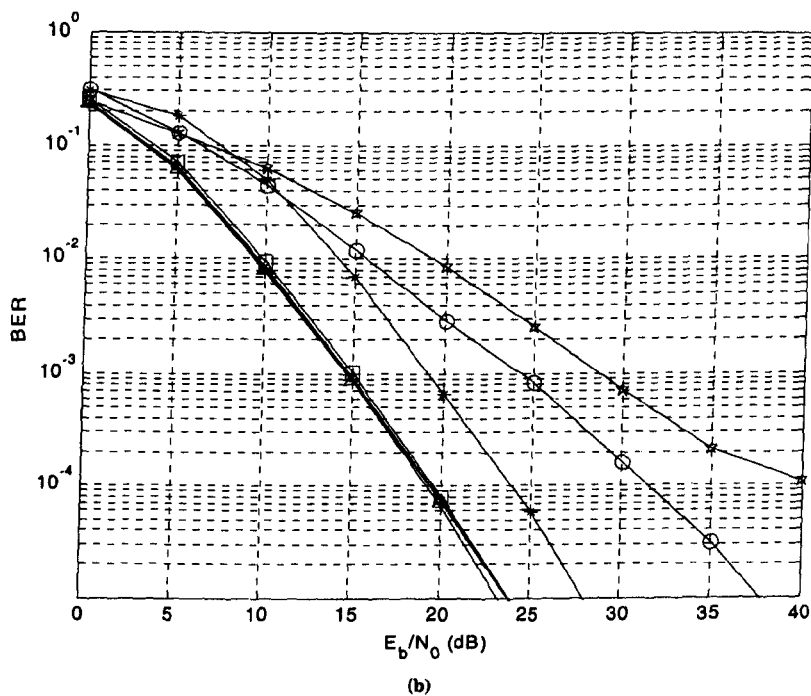
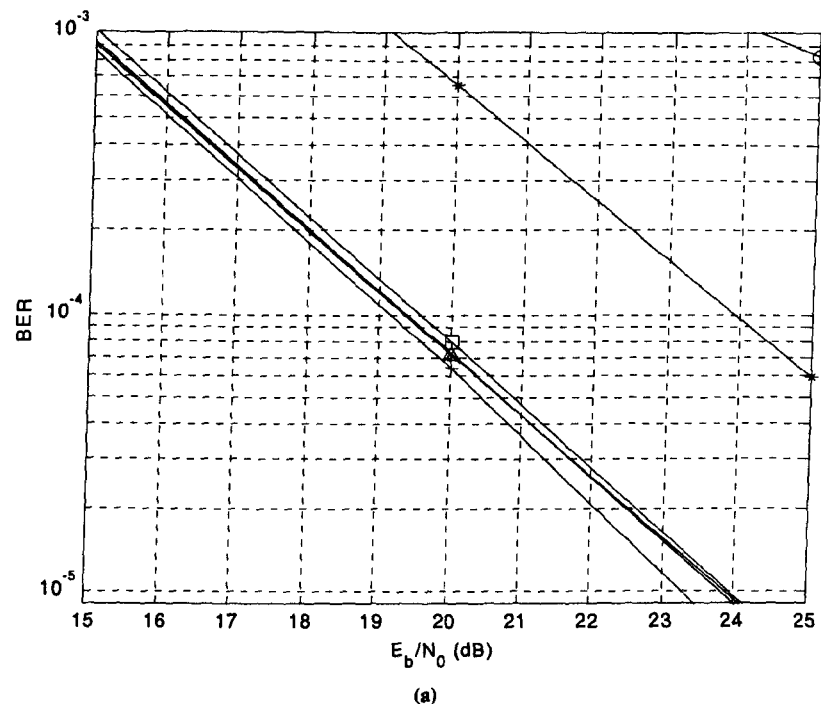


Figure 4-13: 16-QAM Performance in Correlated Rayleigh channel, $f_D = 222$ Hz.

Legend: + Method E, \times Method M, Δ Method R, \square Method L,
 \star Method F, $*$ Method C, \circ Method E using 3GPP Convolutional Code

(a) E_b/N_0 range = [15, 25] dB, (b) E_b/N_0 range = [0, 40] dB.

4.6.2.4 Effects of Bit Interleaving

The performance of 16-QAM in the correlated channel is very bad, mainly due to correlation between successive symbols, in addition to the correlation among bits extracted from a demodulated symbol which share the same fading channel coefficient. This issue can be regarded as a case of the bit-interleaved coded modulation (BICM) problem, a comprehensive treatment of which can be found in [Cai98]. Applying the BICM ideas to the system model results in a simple BICM model depicted in Figure 4-14. The interleaving type applied is either random bit-interleaving or 3GPP Second Channel Interleaving [TGP02b]. The interleaving length is calculated as follows: $3 \times TC_Interleaving_Length + TC_Tail_Bits$. For a 3GPP-compliance TC, TC_Tail_Bits is equal to 12. In this section, 1000 is used as $TC_Interleaving_Length$, so that the interleaving length becomes 3012.

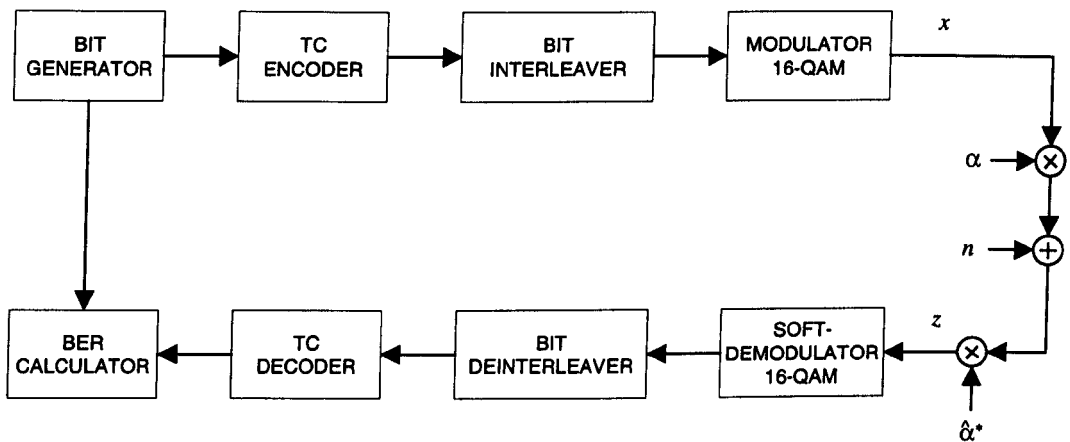
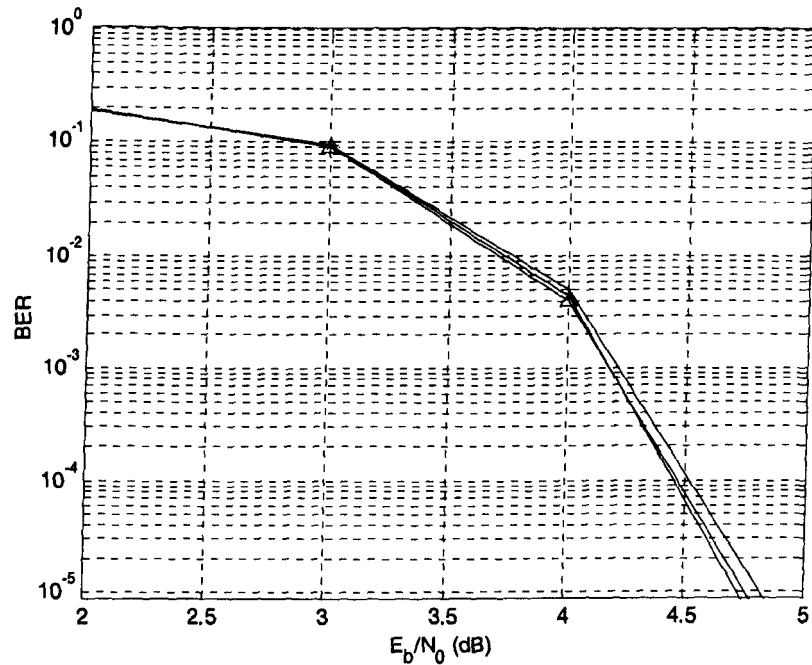
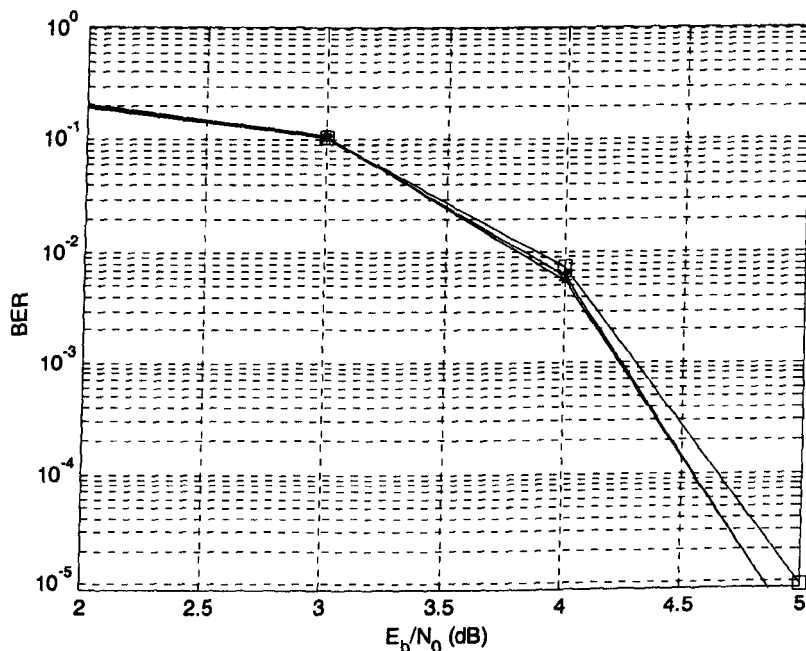


Figure 4-14: Basic Link Model Incorporating Bit-Interleaving

Figure 4-15 and Figure 4-16 show the simulation results from the investigation of the bit interleaving effects on the performance in AWGN channels using Method E and Method R soft-modulations, respectively. When Method E is employed, the performance improvement is negligibly small, less than 0.1 dB. Similarly, there is almost no performance difference resulting from employing random or 3GPP second interleavers. These results are in line with expectation, as nothing much can be gained from an already uncorrelated symbol sequence during TC decoding by this interleaving length. Minor improvement is due to the further decorrelation among bits extracted from the same symbol that otherwise share the same fading coefficient.



**Figure 4-15: Effects of Bit Interleaving on 16-QAM Performance
in Uncorrelated Rayleigh channel, using Method E soft-demodulation, Interleaving Length 3012.**
Legend: + No Bit-Interleaving, x Random Bit-Interleaving, Δ 3GPP 2nd Interleaving



**Figure 4-16: Effects of Bit Interleaving on 16-QAM Performance
in Uncorrelated Rayleigh channel, using Method R soft-demodulation, Interleaving Length 3012**
Legend: □ No Bit-Interleaving, ★ Random Bit-Interleaving, * 3GPP 2nd Interleaving

In contrast to the situation in uncorrelated channels, introducing bit interleaving improves the performance significantly, as shown in Figure 4-17 when Method E is employed, and in Figure 4-18 when Method R is employed. The improvements at BER of 10^{-5} are about 3.5 and 4 dB, respectively. In both situations, random and 3GPP 2nd bit-interleaving perform comparably.

Another point to note is that when bit-interleaving is incorporated, the performance of Method E and Method R is very similar. This is due to the fact that small difference from the soft-decision of each bit is not accumulated correlatedly to become a significant error in the process of TC decoding. Rather, it is possible that due to decorrelation process by bit-interleaving, this small difference is averaged out.

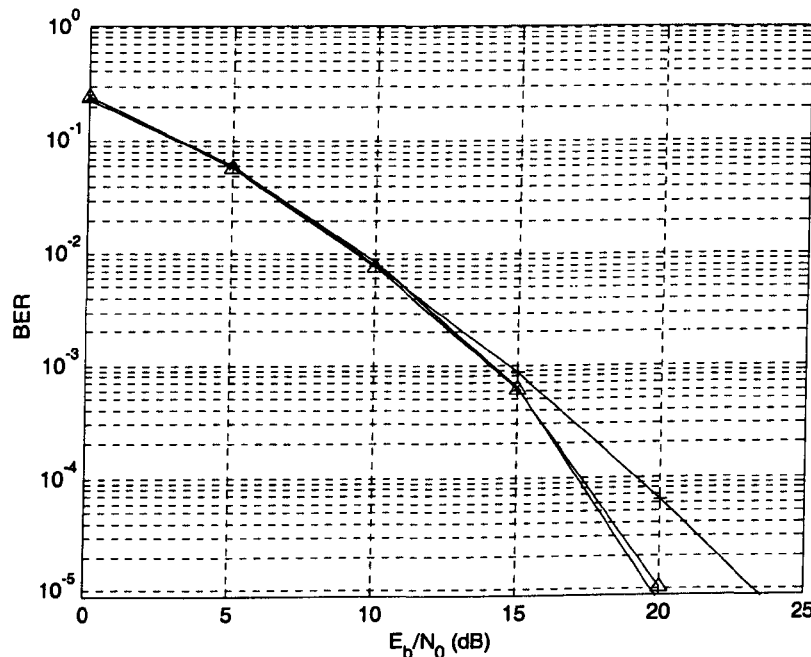


**Figure 4-17: Effects of Bit Interleaving on 16-QAM Performance
in Correlated Rayleigh channel, using Method E soft-demodulation, Interleaving Length 3012**
Legend: + No Bit-Interleaving, x Random Bit-Interleaving, Δ 3GPP 2nd Bit-Interleaving

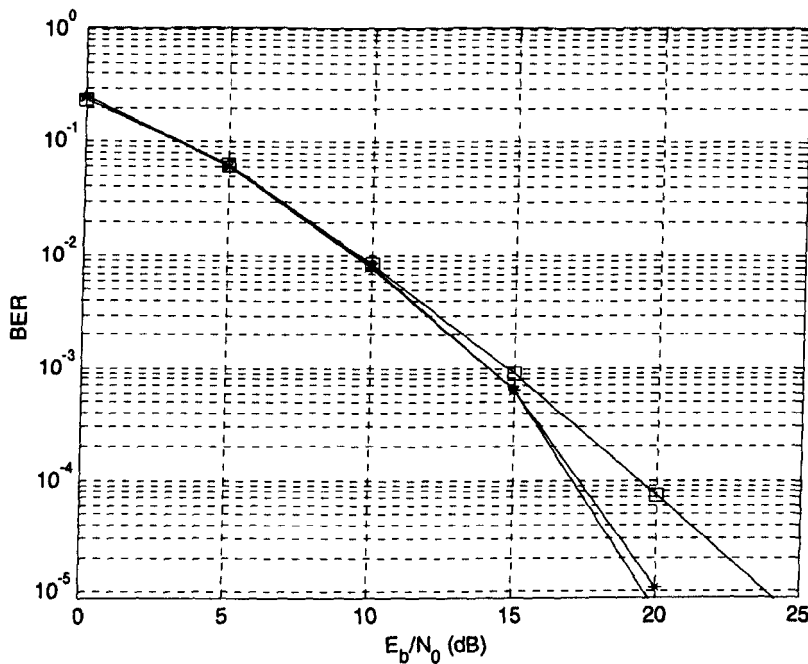


Figure 4-18: Effects of Bit Interleaving on 16-QAM Performance in Correlated Rayleigh channel, using Method R soft-demodulation, Interleaving Length 3012
Legend: □ No Bit-Interleaving, ★ Random Bit-Interleaving, * 3GPP 2nd Bit-Interleaving

4.6.2.5 Effects of Interleaving Length

Knowing from the results that there is not much difference between using Method E or Method R, and between using random or 3GPP 2nd interleaving, for the evaluation of interleaving length effects, Method R and random interleaving are chosen.

Multiplying the bit frame length entering the TC five times to 5000, hence the bit-interleaving length is now 15012, we can see there are further performance improvements. For comparison, the maximum length of TC internal interleaving in 3GPP is 5114 [TGP02a], that is, equivalent to channel bit interleaving length of 15354. Figure 4-19 depicts the results from the uncorrelated Rayleigh environment, whereas Figure 4-20 correspond to correlated a Rayleigh environment.

In the Uncorrelated Rayleigh environment, about 1 dB improvement is gained from lengthening the bit-interleaving by 5 times, whereas there is approximately 11 dB improvement in the Correlated Rayleigh environment. Compared to the uncorrelated performance, there is still about 5.5 dB gap. Increasing the interleaving length should close the gap.

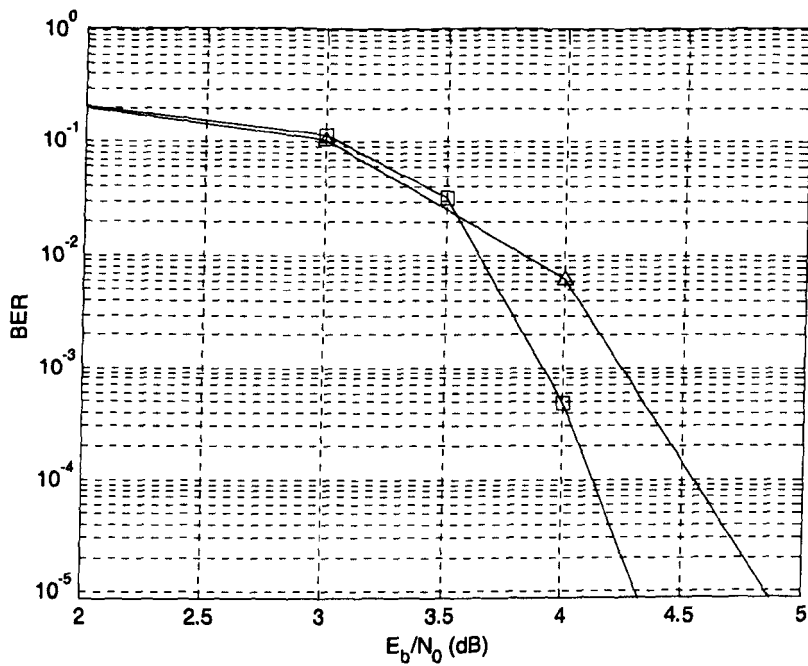


Figure 4-19: Effects of Interleaving Length on 16-QAM Performance in Uncorrelated Rayleigh channel.

Legend: Δ Interleaving Length = 3012 bits, \square Interleaving Length = 15012 bits

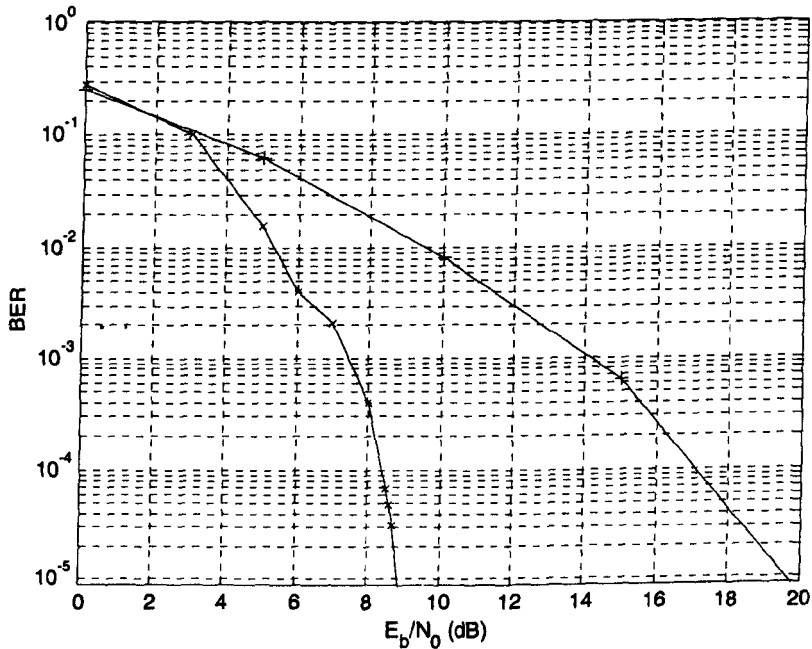


Figure 4-20: Effects of Interleaving Length on 16-QAM Performance in Correlated Rayleigh channel.

Legend: + Interleaving Length = 3012 bits, \times Interleaving Length = 15012 bits

4.6.2.6 Effects of Doppler Spread

Thus far, the correlated Rayleigh environments are simulated at 120 km/h mobile velocity (and 2 GHz carrier frequency), hence Doppler spread of $f_D = 222.2$ Hz. Obviously, sampled at 240,000 samples/second, the correlation is still high. Assuming perfect channel estimation and synchronisation, increasing the mobile velocity to 300 km/h (a common assumption for high speed train), or equivalently $f_D = 555.6$ Hz, there is an improvement of almost 6 dB for the employed interleaving length of 3012. In contrast, there is only about 2.6 dB improvement if the employed interleaving length is already high at 15012.

Summing up, the effect of correlation imposed by the channel to the bit sequence entering the TC decoder is very disadvantageous. The extreme, hence may not be realistic, performance difference at BER of 10^{-5} can be as high as 19.7 dB, namely when comparing the BER values of Figure 4-19 against that of Figure 4-13. In a more realistic environment, at a mobile velocity of 120 km/h, incorporating a bit interleaver having length of 15012 bits (maximum 3GPP equivalent is 15354, see section 4.6.2.5) can improve the performance by 15 dB.

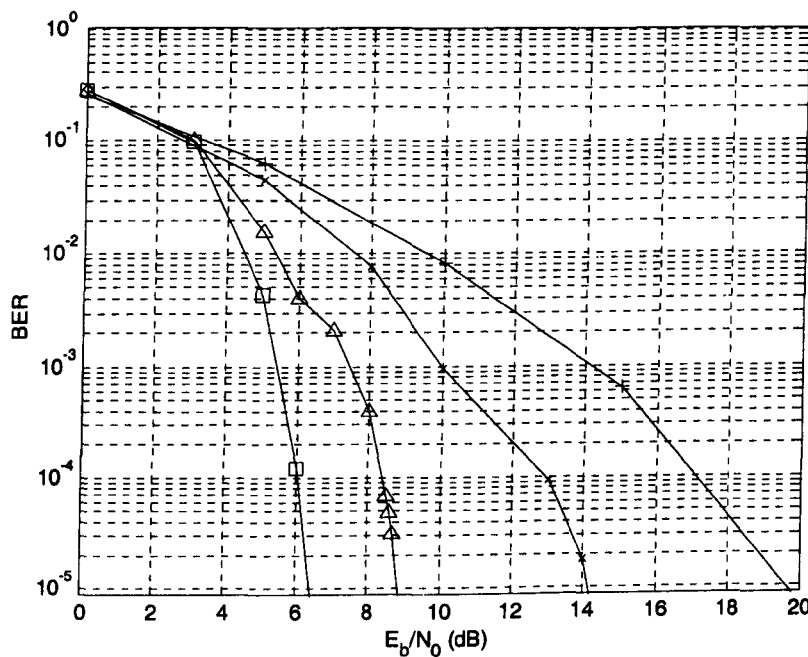


Figure 4-21: Effects of Doppler Spread on 16-QAM Performance in Correlated Rayleigh channel.

Legend: + L=3012 v120, × L=3012 v300, Δ L=15012 v120, □ L=15012 v300

4.6.3 Performance versus Complexity Assessment

The focus of discussion will be the Methods M and R, as their performance is almost the same, and both are just a fraction of a dB away from Method E, but the complexity, particularly Method R, is considerably less. The complexity of Method E itself is the most, at least equals to that of Method M plus additional complexity and memory requirement incurred from look-up table operation. This is assuming a lookup table method is adopted, otherwise, the *exp()* and *ln()* operations are computationally very intensive, hence the method itself.

Denoting:

- *add* as addition, equivalent to 1 cu (computation unit)
- *sub* as subtraction, equivalent to 1 cu
- *mul* as multiplication, equivalent to 2 cu
- *eop* as E-operation (4.6) by look-up table, equivalent to 2 cu
- *mop* as M-operation (4.13), equivalent to 1 cu
- *sqr* as square operation, equivalent to 2 cu

the complexity approximation and comparison in the following table can be performed.

Table 4-1: Approximate complexity calculation and comparison

Method	Number of computational operations per symbol demodulation, optimised disregarding memory requirement for buffering reusable variable
E	<p>MSB I or Q only</p> $ \begin{aligned} &= 1 \text{ weight mul} + 2 \text{ eop} + 4 \text{ sub} + 4 \text{ mul} + 4 \text{ sqr} + 1 \text{ sub} \\ &= 2 + 4 + 4 + 8 + 8 + 1 \text{ cu} \\ &= 27 \text{ cu} \end{aligned} $ <p>LSB I or Q only</p> $ \begin{aligned} &= \text{same as MSB} \\ &= 27 \text{ cu} \end{aligned} $ <p>Subtotal I or Q only</p> $ \begin{aligned} &= 54 \text{ cu} \end{aligned} $ <p>Total per symbol</p> $ \begin{aligned} &= 108 \text{ cu} \end{aligned} $

M	<p>MSB I or Q only</p> <p>= 1 weight mul + 2 mop + 4 sub + 4 mul + 4 sqr + 1 sub = 2 + 2 + 4 + 8 + 8 + 1 cu = 25 cu</p> <p>LSB I or Q only</p> <p>= same as MSB = 25 cu</p> <p>Subtotal I or Q only</p> <p>= 50 cu</p> <p>Total per symbol</p> <p>= 100 cu</p>
R	<p>MSB I or Q only</p> <p>= 1 weight mul = 2 cu</p> <p>LSB I or Q only</p> <p>= 1 sub + 1 weight mul = 1 + 2 cu = 3 cu</p> <p>Subtotal I or Q only</p> <p>= 5 cu</p> <p>Total per symbol</p> <p>= 10 cu</p>
L	<p>Total per symbol</p> <p>= same as Method R = 10 cu</p>
F	<p>MSB I or Q only</p> <p>= 0 cu</p> <p>LSB I or Q only</p> <p>= 1 sub = 1 cu</p> <p>Subtotal I or Q only</p> <p>= 1 cu</p> <p>Total per symbol</p> <p>= 2 cu</p>

Table 4-2: Summary of Relative Coding Gain and Approximate Complexity
Relative Coding Gain with respect to the Method E, Evaluated at BER = 10^{-5}

Method	Approx. Complexity (cu)	Relative Coding Gain (dB) w.r.t. Method E at BER = 10^{-5}		
		AWGN	Uncorr. Rayleigh	Corr. Rayleigh
E	108	0	0	0
M	100	-0.06	-0.15	-0.61
R	10	-0.05	-0.16	-0.62
L	10	-0.25	-0.45	-0.63
F	2	-5	-6.7	-4

As can be seen from the above table, Method R incurs just 10% complexity compared to Method M, and even less compared to Method E. Therefore, a conclusion can be drawn that for a narrowband channel application, Method R offers the best compromise between performance versus complexity. This advantage will be useful to be applied in a situation requiring the least complexity implementation without sacrificing too much of the performance, such as in the implementation of a small size power-limited mobile user terminal. Surely, when maximum performance is sought and complexity is not an issue, Method E offers the best option.

4.7 Summary

In this chapter, exact and approximate soft-demodulation methods for QPSK and 16-QAM have been devised and evaluated in AWGN, uncorrelated and correlated Rayleigh channels. A number of concluding remarks can be drawn:

1. Adopting complex-valued, instead of real-valued, approach offers some advantages: (1) it is a more realistic modelling [Sau99], (2) it enables us to embed the CSI into each modulated bit (by channel compensation process) that leads to less complex TC decoder implementation, (3) the method is readily applicable for multipath channel, which will be demonstrated in the next chapter.
2. Exact soft-demodulation method for QPSK has been simple, hence there is no simplification or approximation method is necessary.
3. Method R in 16-QAM offers best compromise between coded performance and complexity in AWGN, uncorrelated and correlated Rayleigh channels.
4. Incorporating bit interleaving prior to modulation in 16-QAM improves the performance, as it randomises the correlation otherwise exists among bits sharing the same channel

coefficient impairing a modulated symbol. The gain is very small in AWGN and uncorrelated Rayleigh channel, as the correlation between symbols has theoretically been zero. In contrast, the gain is maximum in correlated Rayleigh channel for the opposite reason applied for the other channels. The larger the interleaver size, the larger the performance gain.

5. The higher the Doppler spread, the more uncorrelated the fading coefficient, the better the performance. This is valid under the assumption that other issues of signal reception are not affected. In reality, there should be a compromise between the gain from the smaller correlation between successive modulated symbols and the difficulty in proper reception of the signal.
6. Approximate complexity calculation provides wider choices for the implementation, between performance and complexity. An obvious advantage shared by all of the devised methods over those in the literature are the elimination of separate CSI input to TC decoder and TC decoder modification.

Chapter 5

Soft-Demodulation Applications in WCDMA and STTD Coded Systems

5.1 Introduction

In this chapter, the soft-demodulation methods derived and evaluated in the basic communication environments of the previous chapter will be extended so that they can also be applied to more advanced and more realistic communication environments, such as WCDMA and STTD systems. In these systems, the channel characteristics will predominantly be multipath, so that the soft-demodulation will work in conjunction with a rake receiver, including STTD decoder(s) and a combiner. Being more realistic environments, there will not be an Uncorrelated Rayleigh channel. After deriving the extension of the methods, performance evaluation will be performed. This begins with the performance validation process in each environment under consideration. As in the previous chapter, there is not much to be discussed regarding QPSK soft-demodulation, as there is only one method associated with it, so the focus will be on the various soft-demodulation methods of 16-QAM. Different approximation methods of 16-QAM will be compared and evaluated, including the bit-interleaving effects.

5.2 Design of Soft-Demodulation Methods in WCDMA and STTD Systems

5.2.1 WCDMA System

In a WCDMA environment, specifically 3GPP UMTS downlink [TGP02a, TGP02b, TGP02c] that we adopt here, the modulated symbols are spread by different OVSF codes for different physical channels. When summed symbol-wise, they form a composite signal. For cell or sector separation purposes, this composite signal is scrambled by the Gold code prior to transmission.

Through an L -path channel (single path is just a special case), the composite signal from path- l arrives at the receiver and is processed inside a finger of the rake receiver. This can be expressed as

$$r_l = \alpha_l x + n_l. \quad (5.1)$$

We assume that the descrambling, despreading and channel estimation have been performed perfectly. Now, the channel compensation will take place at each rake finger (this is a basic feature of a rake receiver):

$$z_l = \hat{\alpha}_l^* r_l. \quad (5.2)$$

Comparing this equation with (4.4), it is straightforward to apply the soft-demodulation method of (4.5). Recall, however, that this would occur at each finger, whereas in a common rake receiver the demodulation is performed after rake combining. Considering that one of the goals of this research is to reduce complexity, soft-demodulating at each rake finger would undermine this goal. Therefore, we will approximate this by keeping using the common rake structure and soft-demodulating after rake combining. If MRC is employed, as customary in a current receiver, at rake output we have

$$\begin{aligned} z &= z_I + j z_Q \\ &= \sum_{l=1}^L z_l \\ &= \sum_{l=1}^L \hat{\alpha}_l^* z_l \\ &= \sum_{l=1}^L \hat{\alpha}_l^* (\alpha_l x + n_l) \\ &= \sum_{l=1}^L (\hat{\alpha}_l^* \alpha_l) x + \sum_{l=1}^L \hat{\alpha}_l^* n_l \\ &= \left(\sum_{l=1}^L \hat{\alpha}_l^* \alpha_l \right) \cdot x + \sum_{l=1}^L \hat{\alpha}_l^* n_l \end{aligned} \quad (5.3)$$

Comparing this equation with (4.3) and (4.4), and assuming that the noise term $\sum_{l=1}^L \hat{\alpha}_l^* n_l$ is Gaussian distributed, we can apply the soft-decision formula of (4.5) by substituting $\|\hat{\alpha}\|^2$ for

$$\rho = \sum_{l=1}^L \|\hat{\alpha}_l\|^2 \text{ to yield}$$

$$L_c(b_Y^{(j)}) = \sum_{y \in y_0^{(j)}} \frac{-1}{2\sigma^2\rho} (z_Y - \rho y)^2 - \sum_{y \in y_1^{(j)}} \frac{-1}{2\sigma^2\rho} (z_Y - \rho y)^2. \quad (5.4)$$

It can be observed that the same substitution can be applied to the other LLR definitions. It follows that, by using (4.8), the LLR remain unchanged for the QPSK, namely

$$\begin{aligned} L_c(b_Y^{(j)}) &= \frac{-1}{2\sigma^2\rho} (z_Y - \rho)^2 + \frac{1}{2\sigma^2\rho} (z_Y + \rho)^2 \\ &= \frac{2}{\sigma^2} z_Y. \end{aligned} \quad (5.5)$$

For 16-QAM, the same substitution can be applied to (4.11) for MSB and to (4.12) for LSB yielding

for MSB:

$$L_c(b_Y^{(0)}) = \sum_{y=(-d,-3d)} \frac{-1}{2\sigma^2\rho} (z_Y - \rho y)^2 - \sum_{y=(d,3d)} \frac{-1}{2\sigma^2\rho} (z_Y - \rho y)^2 \quad (5.6)$$

and for LSB:

$$L_c(b_I^{(0)}) = \sum_{y=(-d,d)} \frac{-1}{2\sigma^2\rho} (z_Y - \rho y)^2 - \sum_{y=(-3d,3d)} \frac{-1}{2\sigma^2\rho} (z_Y - \rho y)^2. \quad (5.7)$$

For approximation method M, the same substitution can also be applied to produce

for MSB:

$$L_c(b_Y^{(0)}) = \sum_{y=(-d,-3d)} \frac{-1}{2\sigma^2\rho} (z_Y - \rho y)^2 - \sum_{y=(d,3d)} \frac{-1}{2\sigma^2\rho} (z_Y - \rho y)^2 \quad (5.8)$$

and for LSB:

$$L_c(b_I^{(0)}) = \sum_{y=(-d,d)} \frac{-1}{2\sigma^2\rho} (z_Y - \rho y)^2 - \sum_{y=(-3d,3d)} \frac{-1}{2\sigma^2\rho} (z_Y - \rho y)^2. \quad (5.9)$$

Finally, for all other approximation methods, particularly Methods R and L, the LLR of MSB remains unchanged:

$$L_c(b_Y^{(0)}) = \frac{8d}{3\sigma^2} z_Y \quad (5.10)$$

whereas for LSB, the same substitution as in the case of Method E or M is performed, and this yields

$$L_c(b_l^{(0)}) = \frac{2d}{\sigma^2} (2d\rho - \|z_l\|). \quad (5.11)$$

5.2.2 STTD System

In an STTD system, each rake finger performs STTD decoding. For referencing convenience, the mathematical expression of the STTD decoded signal (2.12) will be reproduced here:

$$\begin{aligned} s_0 &= (|h^{(0)}|^2 + |h^{(1)}|^2) s_0 + h^{(0)*} n_0 + h^{(1)*} n_1 \\ s_1 &= (|h^{(0)}|^2 + |h^{(1)}|^2) s_1 - h^{(1)} n_0 + h^{(0)*} n_1 \end{aligned} \quad (5.12)$$

Assuming the noise parts of s_0 and s_1 in this set of equations are Gaussian distributed and has the same statistical characteristics, an equivalent expression of s_0 or s_1 for l -th rake finger can written as

$$z_l = \sum_{i=0}^1 \|\hat{\alpha}_{i,l}\|^2 s + \sum_{i=0}^1 n_{i,l} \quad (5.13)$$

where $\sum_{i=0}^1 \|\hat{\alpha}_{i,l}\|^2$ is used to approximate the $(|h^{(0)}|^2 + |h^{(1)}|^2)$ term in (5.12). It is important to stress that in an STTD mode, the rake MRC simply acts as a summer device, hence it is more appropriately termed as equal gain combining (EGC). At the rake output, we will have

$$z = \sum_{l=1}^L \sum_{i=0}^1 \|\hat{\alpha}_{i,l}\|^2 s + \sum_{l=1}^L \sum_{i=0}^1 n_{i,l} \quad (5.14)$$

Assuming the noise part is Gaussian distributed, and writing $\kappa = \sum_{l=1}^L \sum_{i=0}^1 \|\hat{\alpha}_{i,l}\|^2$, all the LLR expressions in section 5.2.1 are applicable for STTD case, by replacing every instance of ρ by κ . Knowing that this substitution is trivial, it is considered unnecessary to repeat the LLR expression of every method here.

5.3 Performance Evaluation in WCDMA System

The soft-decision methods that have been adapted for the WCDMA system in the previous section will be evaluated here. As is the case in the previous chapter, there is not much to investigate regarding the soft-decision methods for QPSK. Therefore, the focus will be on the performance evaluation and comparison of the 16-QAM soft-demodulation methods.

5.3.1 QPSK

5.3.1.1 Validation

This section compares the performance of the basic, i.e. non-WCDMA, simulator system with that of the WCDMA system. Theoretically, incorporating spreading and scrambling processes into a single user WCDMA system while keeping everything else equivalent to that of the basic system, should not change the performance. Figure 5-1 indicates such a performance consistency. In this figure, the performance of the soft-demodulation methods is evaluated over AWGN and Correlated Rayleigh channels in basic and WCDMA systems. As seen from the graph, the curves corresponding to the same channel but different system are almost co-located. Note that, due to UMTS WCDMA internal restriction, the interleaving length is 1596 bits, as opposed to 1000 bits that is used to produce Figure 4-8, hence there is a slight performance shift due to interleaving gain of the TC.

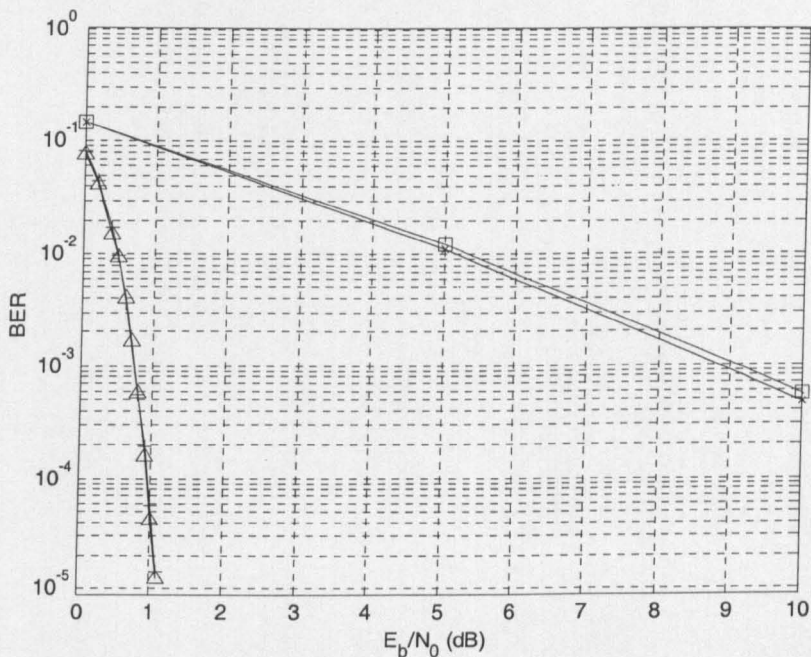


Figure 5-1: Turbo Coded QPSK Performance Validation

Legend: + Non-CDMA system AWGN channel,
 × Non-CDMA system Correlated Rayleigh channel,
 Δ CDMA system AWGN channel,
 □ CDMA system Correlated Rayleigh channel

5.3.1.2 Performance in Various Channels

The performance evaluation over different channels is carried out. The results are plotted in Figure 5-2. These are compliant with the expectation (theory). The multipath characteristic in Vehicular A and B that is captured constructively by the rake receiver to form diversity has improved the performance compared to the case of Correlated Rayleigh. This has brought the performance curves closer towards the AWGN curve. Notice that the performance in Vehicular A is slightly better than in Vehicular B. This is due to the fact that in Vehicular B channel the interpath interference is more pronounced, hence the orthogonality factor and diversity advantage is lower. As an additional note, the Vehicular B channel is not included in 3GPP standard, only in former ETSI UMTS standard candidate, but it is used here to examine the interpath interference effects it causes.

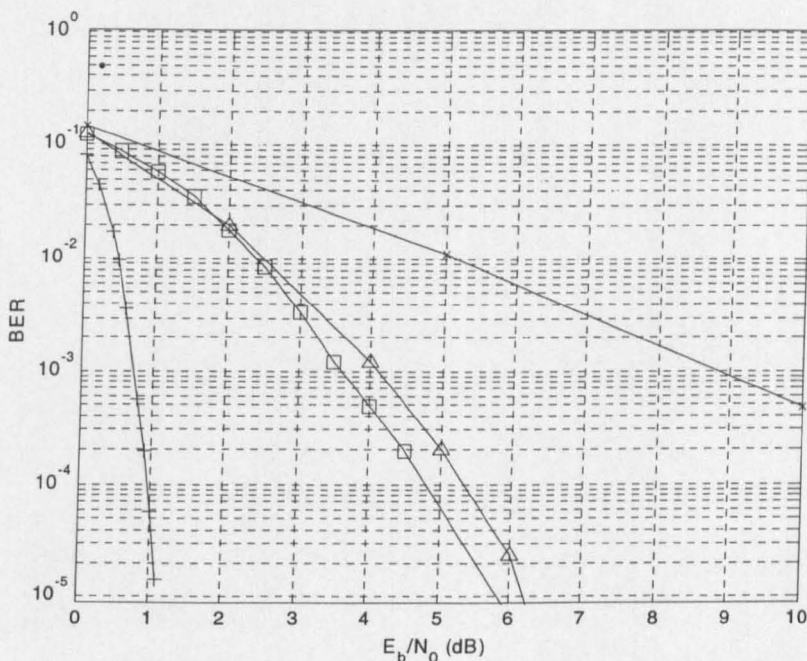


Figure 5-2: Turbo Coded QPSK Performance in CDMA environment.
Legend: + AWGN, \times Correlated Rayleigh, Δ UMTS Vehicular B, \square UMTS Vehicular A

5.3.2 16-QAM

5.3.2.1 Validation

Similar validation process as has been carried out for QPSK is performed, the results of which are depicted in Figure 5-3. As can be seen from the graph, the soft-decision performance is consistent regardless of the system it is applied to. In particular, the graph shows the results of Method E,

but other approximation methods will perform similarly. Comparing the AWGN performance curves of Figure 5-3 and of Figure 4-11, some performance shifts are observed. These are due to the fact that the interleaving length utilised in this chapter is 3196 instead of 1000 in Chapter 4. Bit framing in UMTS CDMA restricts arbitrary interleaving length, and this number (3196) is a result of a simple single transport channel multiplexing process.

Having been validated, the performance of various soft-demodulation methods will be assessed in different channels.

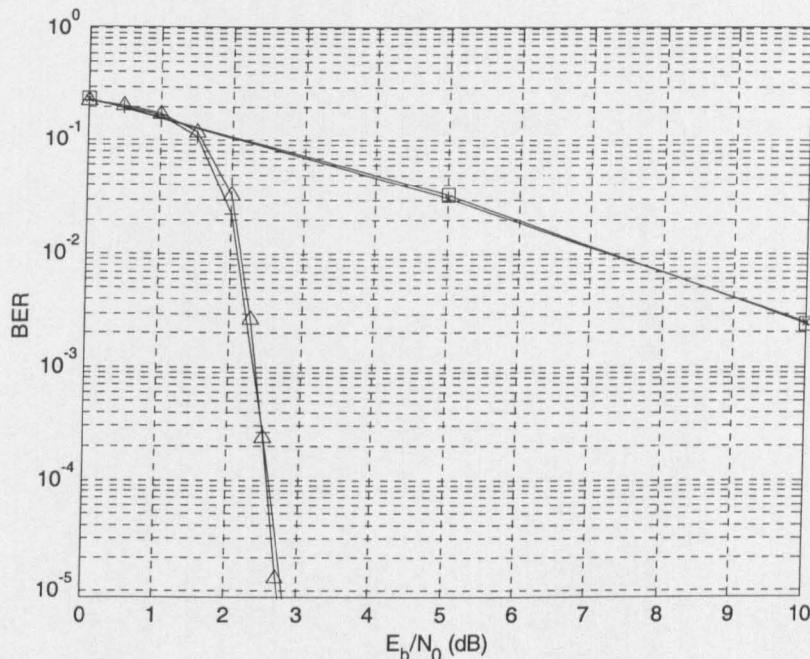


Figure 5-3: Turbo Coded 16-QAM Performance Validation.

Legend:

- + Non-CDMA environment AWGN channel,
- x Non-CDMA environment Correlated Rayleigh channel,
- △ CDMA environment AWGN channel,
- CDMA environment Correlated Rayleigh channel

5.3.2.2 AWGN

As the validation process has shown, the performance of the soft-demodulation methods in this type of channel as shown in Figure 5-4 will be the same as the one evaluated in a basic system (to within the simulation error tolerance). Therefore, analysis carried out for the basic system will also be applicable here. In brief, Method E offers the best performance, while Method R gives good compromise between performance and complexity.

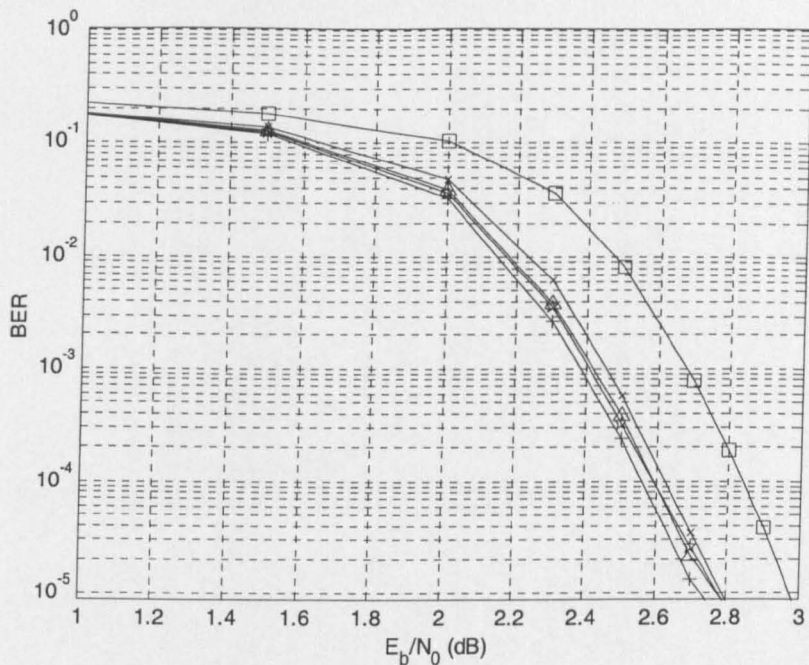


Figure 5-4: Turbo Coded 16-QAM Performance in A WGN channel.

Legend: + Method E, \times Method M, Δ Method R, \square Method L, \star Method E with Bit Interleaving

5.3.2.3 Correlated Rayleigh

Evaluated in the Correlated Rayleigh channel, Method E with bit interleaving stands out from the rest in performance, gaining over 6 dB improvement as can be seen in Figure 5-5. The effect of decorrelation in soft-bits entering the TC decoder is accountable for this performance improvement. The performance of different soft-demodulation methods without bit interleaving is very similar to each other, within 1 dB difference. Nonetheless, it still can be observed that Method E is the best in this group, whereas Method L is the worst. Additionally, the performance of Method F, not shown in the graph, is very bad. These results are consistent with expectation.

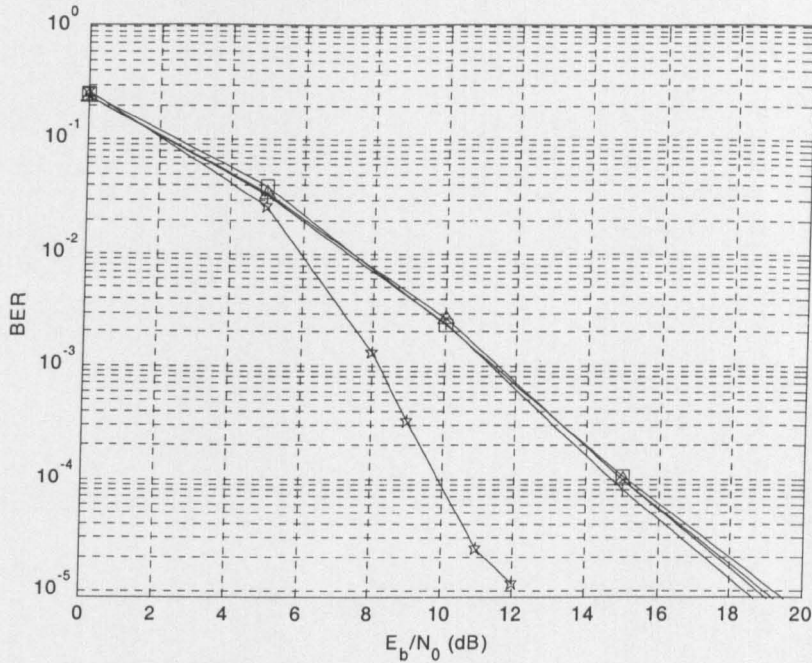


Figure 5-5: Turbo Coded 16-QAM Performance in Correlated Rayleigh channel
 Legend: + Method E, × Method M, Δ Method R, □ Method L, ★ Method E with Bit Interleaving

5.3.2.4 Vehicular A Environment

Figure 5-6 shows the performance of different soft-demodulation methods in Vehicular A channel. Compared to the performance in Correlated Rayleigh channel shown in the previous figure, the performance is much better for all methods. The performance of the bit interleaved Method E is also only marginally better than the rest. This phenomenon is mainly attributed to the diversity, which brings along with it the decorrelation in the successive demodulated symbols. Therefore, there is not much gain left for the bit interleaver. In spite of this, the performance of Method L is consistently the worst of the group.

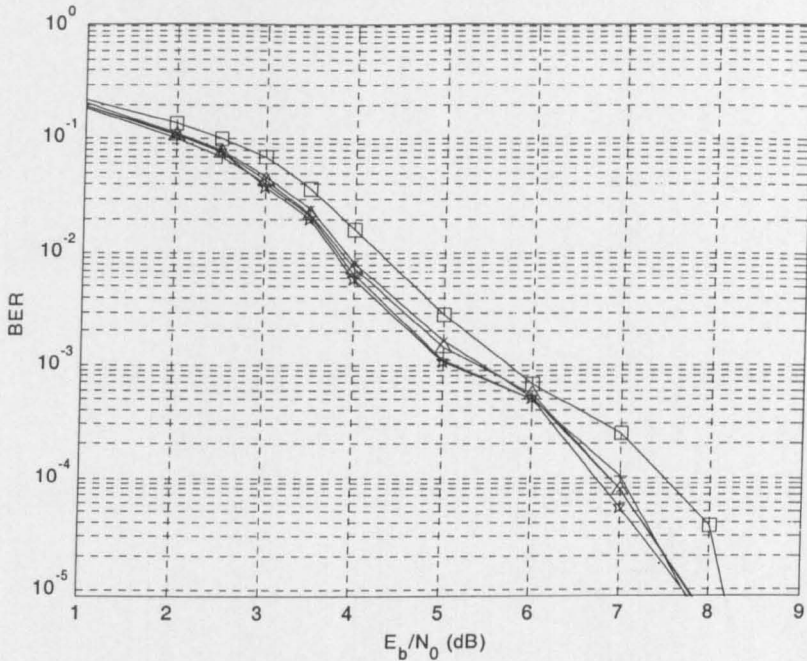


Figure 5-6: Turbo Coded 16-QAM Performance in Vehicular A channel.

Legend: + Method E, x Method M, Δ Method R, □ Method L, ★ Method E with Bit Interleaving

5.4 Performance Evaluation in STTD WCDMA System

We employ the STTD technique specified in 3GPP standard [TGP02c], by maintaining the total transmitter power emitted from both antennas to be the same as that with single antenna without STTD. As a result, in the AWGN channel the performance will remain the same. As usual, the performance of different soft-demodulation methods of QPSK and 16-QAM will be examined in various channels. Since there is only a single soft-demodulation variant in QPSK, the emphasis will be on 16-QAM.

5.4.1 QPSK

5.4.1.1 Validation

When STTD is enabled, the performance in the AWGN channel should be approximately the same as when it is disabled. The results of this examination are portrayed in Figure 5-7, specifically the two leftmost curves. As seen in this figure, the STTD performance is a little bit better. This is still normal, as the noise term in STTD is not purely AWGN, so a slight deviation is expected, particularly 16-QAM has a non-constant envelope characteristic, which may

contribute to noise averaging. Looking at the other two curves on the right hand side, we can see the impact of diversity brought about by the STTD in the Rayleigh channel. Utilising the rule of thumb for inspecting the diversity order, as used in section 4.6.2.1, it can be deduced that the diversity order of the performance curve corresponding to STTD is roughly twice the non-STTD one.

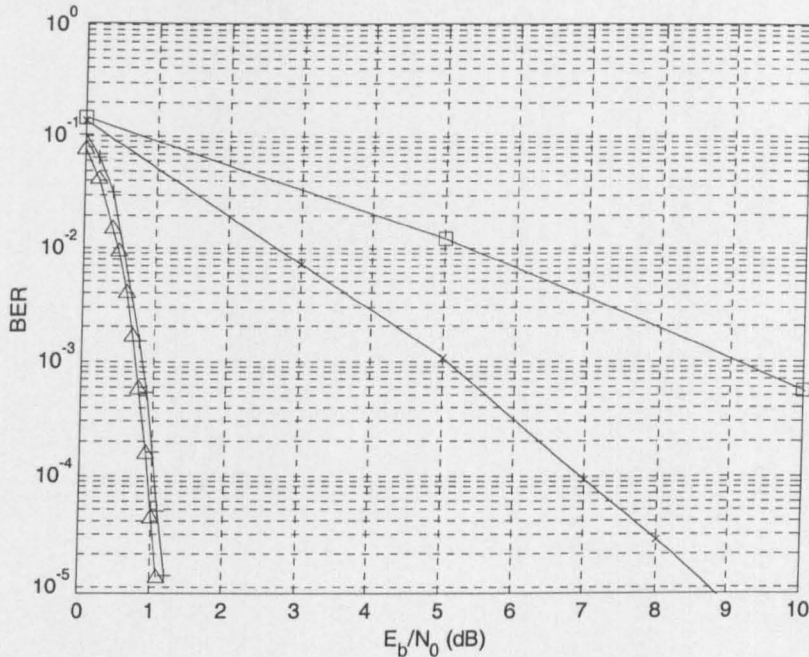


Figure 5-7: Turbo Coded QPSK Performance in AWGN channel.

Legend: + Non-CDMA, AWGN channel,
 × Non-CDMA, Correlated Rayleigh channel,
 △ CDMA STTD, AWGN channel,
 □ CDMA STTD, Correlated Rayleigh channel

5.4.1.2 Performance in Various Channels

As shown in Figure 5-8, the trend of the performance curves of the soft-demodulation methods in this environment is similar to that of the curves in Figure 5-7. Elaborating further, the performance in the AWGN channel is the same as that in the CDMA system. The performance decreases as the channel changes from AWGN to Vehicular A to Vehicular B and finally to Correlated Rayleigh. Thanks to extra diversity brought in by STTD, the performance curves for non-AWGN channels are always to the left of the corresponding ones in the CDMA environment. Performance in Vehicular A is better than in Vehicular B for the same interpath interference reason found in the CDMA case.

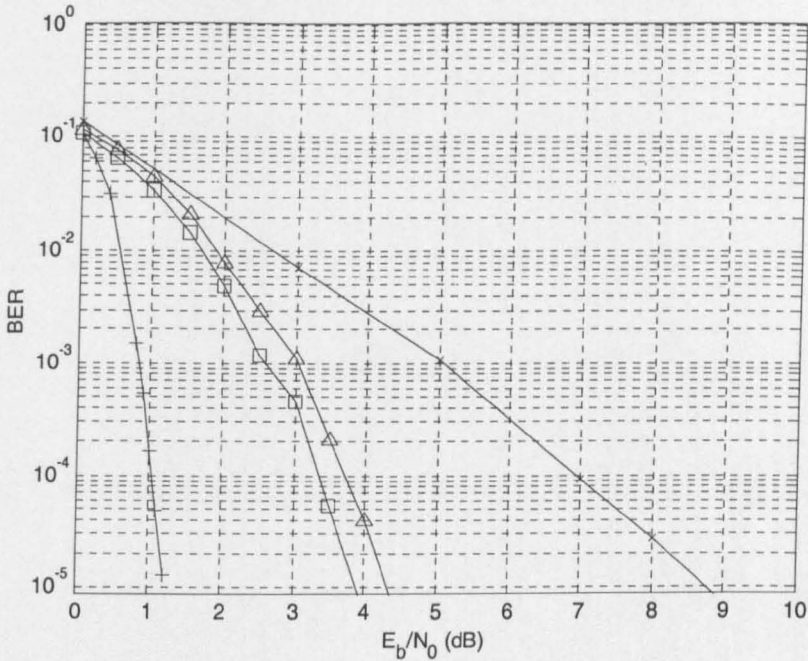


Figure 5-8: Turbo Coded QPSK Performance in STTD WCDMA system.
Legend: + AWGN, \times Correlated Rayleigh, Δ UMTS Vehicular B, \square HSDPA Vehicular A

5.4.2 16-QAM

5.4.2.1 Validation

Looking at the curves in Figure 5-9 and comparing them with those in Figure 5-3, a similar analysis can be given. First, the AWGN performance is the same regardless of the environment. Second, using the same rule of thumb as we did in QPSK case, it can be deduced that the diversity order has approximately doubled from that in the Correlated Rayleigh case, something that is expected from an STTD system. The next step is the examination of different soft-demodulation methods in different channels, which will be provided in the following sections.

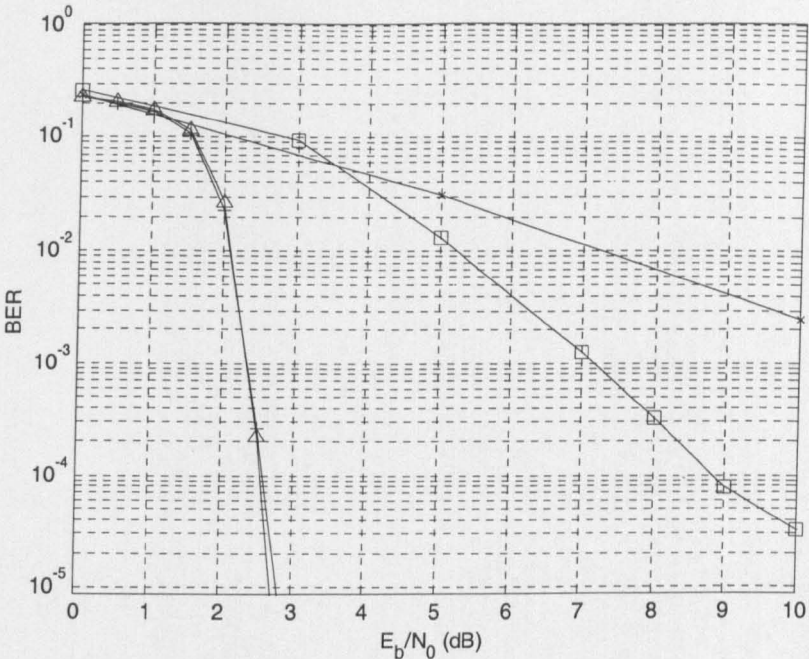


Figure 5-9: Turbo Coded 16-QAM Performance Validation.

Legend: + non-CDMA Non-STTD system, AWGN channel,
 × non-CDMA Non-STTD system, Correlated Rayleigh channel,
 △ CDMA STTD system, AWGN channel,
 □ CDMA STTD system, Correlated Rayleigh channel

5.4.2.2 AWGN

As expected, performance of the soft-demodulation methods in AWGN is independent of the environments. Comparing the corresponding curves in Figure 5-10 and in Figure 5-4, this fact becomes evident. What stands out in both graphs, however, is the fact that Method L is always the worst performer. Another point is that the bit interleaving does not improve the performance, due to the fact that the demodulated symbol has already been uncorrelated.

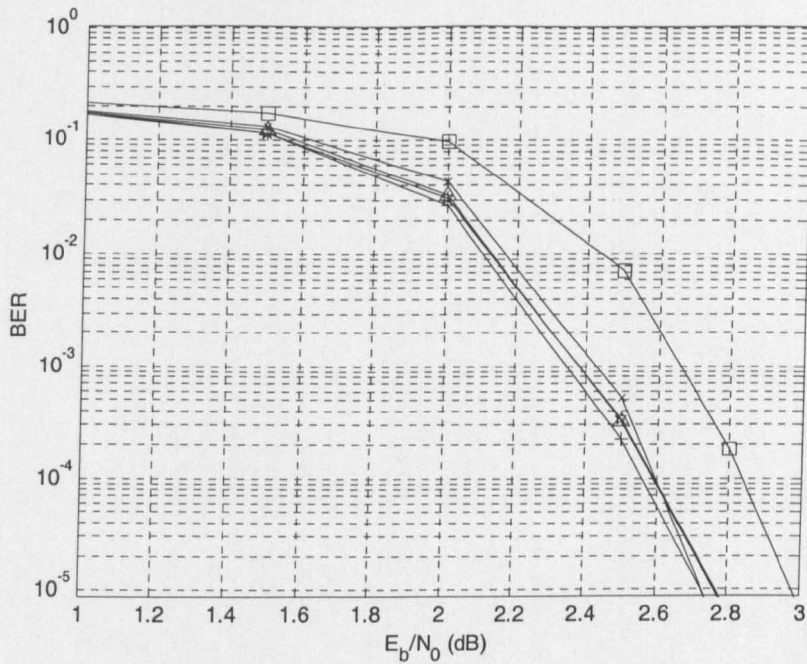


Figure 5-10: Turbo Coded 16-QAM Performance in STTD System, AWGN channel.
Legend: + Method E, \times Method M, Δ Method R, \square Method L, \star Method E with Bit Interleaving

5.4.2.3 Correlated Rayleigh

When evaluated in the Correlated Rayleigh channel, the positive impact of bit interleaving on the performance is apparent. See Figure 5-11. Also apparent is the inferior performance of Method L. The rest of the methods perform similarly. Significant coding gains, between 4 to 7 dB at BER of 10^{-5} , are observed when viewing these curves as a group and comparing them with those in Figure 5-5 where no STTD is employed.

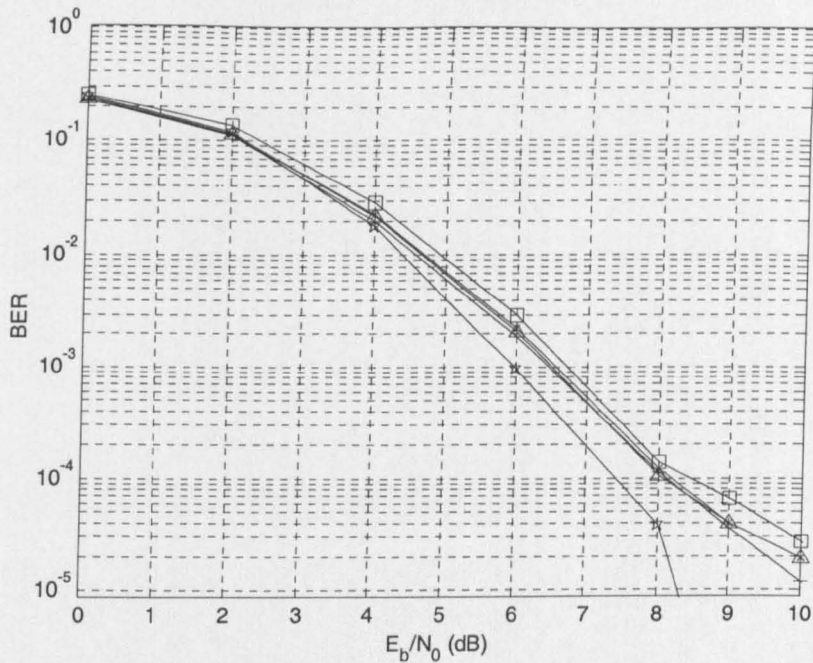


Figure 5-11: Turbo Coded 16-QAM Performance in UMTS STTD System, Correlated Rayleigh channel.

Legend: + Method E, \times Method M, Δ Method R, \square Method L
★ Method E and Bit Interleaving

5.4.2.4 Vehicular A Environment

In this channel, the effect of number of fingers in the rake receiver is also evaluated. Figure 5-12 and Figure 5-13 show the performance when 6 and 4 rake fingers are employed, respectively. In this ideal rake reception case, adding 2 fingers achieves about 0.2 dB gain.

Commenting on the performance of different soft-demodulation methods, it can be observed that the bit interleaved Method E performs the best, whereas Method L does the worst, as usual. Comparing these curves with the corresponding ones in Figure 5-6 where no STTD is employed, it can be seen that a gain of about 2 dB is obtained.

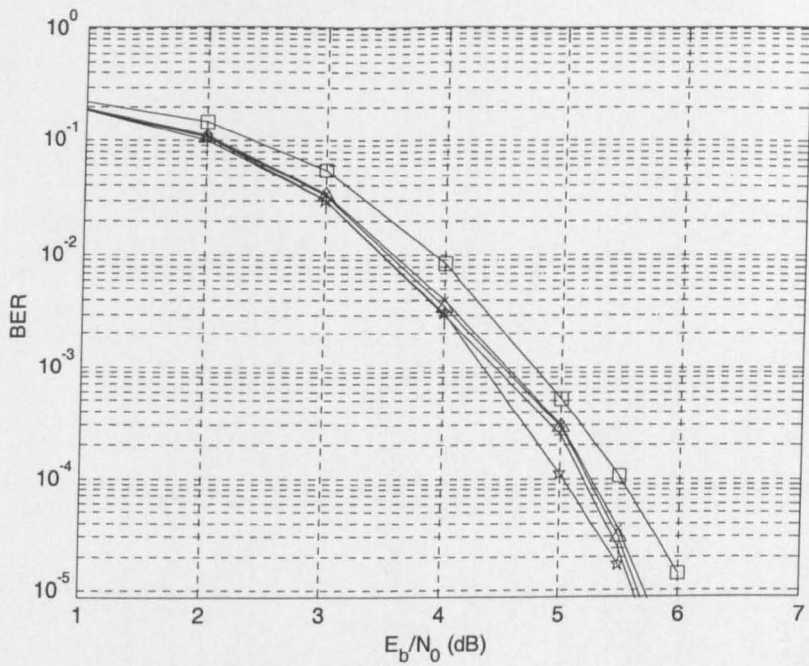


Figure 5-12: Turbo Coded 16-QAM Performance in STTD System,
Vehicular A channel, 6-finger rake.

Legend: + Method E, x Method M, Δ Method R, □ Method L, ★ Method E with Bit Interleaving

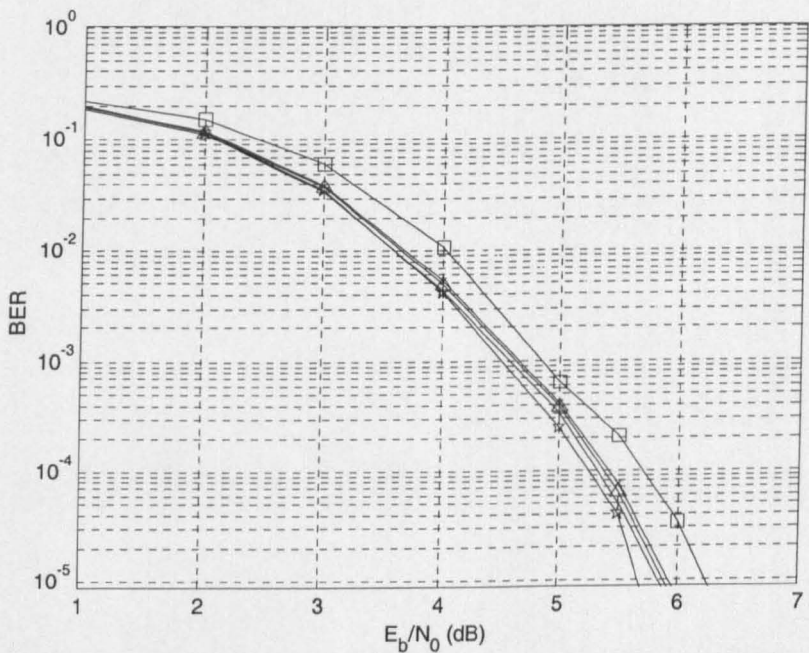


Figure 5-13: Turbo Coded 16-QAM Performance in STTD System,
Vehicular A channel, 4-finger rake.

Legend: + Method E, \times Method M, Δ Method R, \square Method L, \star Method E with Bit Interleaving

5.5 Summary

Having derived and examined the soft-demodulation methods in WCDMA and STTD environments, several points are worth summarising:

1. Although the soft-demodulation methods are no longer exact for these environments, the good performance and its consistency throughout different channels have indicated that the methods are very close to its otherwise complicated ideal counterpart. The poor performance of the pragmatic and non-analytical Method F (evaluated, but not included in any graph) is another indication.
2. Bit interleaving plays an important role in improving performance when the channel, hence the successive modulation symbols impaired by it, is highly correlated. However, in multipath channel where the rake receiver captures the inherent diversity and at the same time lowers the correlation, its impact is diminishing.
3. STTD improves the performance, mainly due to the doubling of the diversity order. The improvement is less than “doubling of the diversity order” if the non-STTD environment has exploited the multipath diversity already.
4. The devised soft-demodulation methods consistently perform better than any methods in the literature, including Method L. In addition, there would be a further problem or complexity to separately provide the CSI to the TC decoder in these kinds of environments where there are many subsystems separating the demodulator and the TC decoder.
5. Given the consistency in all tested environments, now it is safe to conclude that Method R offers the best compromise between performance and complexity. Having gained this confidence, in the remainder of the thesis, only Methods R or E will be employed.
6. Lengthy simulation time, mainly due to multipath channel processing, the most time consuming of which is in STTD environment, becomes a hindrance to obtaining very smooth waterfall-like performance curves, despite the fact that at least either (1) 5×10^7 (fifty million) information bits are transmitted and decoded or (2) 500 erroneous bits are collected for each point in all performance curves. Therefore, the error tolerances of the resulting performance curves are larger in these environments. This is one reason that the

performance gains among the soft-demodulation methods were not cited numerically when the values were small enough, e.g. less than 0.5 dB.

Chapter 6

Soft-Demodulation Applications in HSDPA HARQ System

6.1 Introduction

This chapter focuses on the discussion of performance of the proposed soft-demodulation methods when they are applied to an HSDPA HARQ system. The exposition will start with a description of an HSDPA system. Detailed descriptions will be given regarding the relevant functional blocks that significantly affect the link performance. This will be followed by description of a simplified link simulator of such a system and results of performance evaluation using this simulator. In addition to using BER, block error rate (BLER) will also be used as performance indicator in this chapter. As there is only one QPSK soft-demodulation method, performance evaluation and comparison will be performed only for 16-QAM. Effects of different rate-matching parameters, number of retransmissions and number of TC decoding iterations on performance will be examined. In addition, comparison of retransmission efficiencies will also be evaluated.

6.2 General Description of an HSDPA System

As outlined in section 2.5.5, the key element of the HSDPA system in the link level is the AMC in conjunction with an HARQ. Based on the statistics of positive and negative acknowledgements (ACKs and NACKs, respectively) and channel quality information (CQI) reported by a mobile receiver, the system-level controller decides what modulation scheme and coding rate to use for a certain subframe. (In UMTS documents, e.g. [TGP02a], the frame of HSDPA is referred to as a subframe; it is equivalent to 1/5 of the size of a UMTS frame.) For instance, a nearly-stationary mobile receiver located close to a transmitting base station (called Node B in 3GPP documents, e.g. [TGP02a]) will normally experience a good channel condition, hence the majority of its subframes will be assigned low power level, 16-QAM scheme and high TC rates. On the other hand, a fast-moving mobile receiver far away from the base station will most likely be assigned

normal power, QPSK scheme and low coding rates. As the channel condition changes, so will the modulation and coding parameters.

Note that the ACKs/NACKs and coding rate changes described in the previous paragraph are due to the use of an HARQ technique. In particular, code rate changes are due to the rate-matching and HARQ retransmission(s).

Mainly for simplicity, Stop-and-Wait (SAW) HARQ is adopted in the HSDPA standard. To improve the throughput efficiency, several parallel instances of such HARQ can be established, the number of which depends on the capability of the mobile receiver. An HARQ instance in this case is referred to as an HARQ process.

In the following sections, more detailed descriptions of the HSDPA HARQ functional blocks are presented. The majority of information is taken from the 3GPP documents [TGP02b, TGP03]. Note that only the most relevant information with respect to link performance is included.

6.2.1 The HSDPA HARQ

The HARQ functionality is controlled by *redundancy version* (RV) parameters. These parameters will determine whether *Incremental Redundancy* (IR), Chase combining [Cha85], or the combination of both modes is active in a certain period of time.

In IR combining mode, successive retransmissions gradually accumulate the coded bits at the receiver, effectively decreasing the effective code rate from a value of less or equal to 1 down to the mother code rate, which is 1/3 in HSDPA. In Chase combining mode, the effective code rate remains fixed, and can be any value between 1 and mother code rate. Successive retransmissions carry the same copy of the bits as the original transmission. Effectively, this combining mode introduces diversity. Chase combining is conceptually similar to the MRC of a rake receiver: the combination of diversity elements using SNR as weighting factor.

The HARQ functionality consists of two rate-matching stages and a virtual buffer as shown in Figure 6-1. The first rate matching stage matches the number of input bits to the virtual IR buffer, information about which is provided by higher layers. Note that, if the number of input bits does not exceed the virtual IR buffering capability, the first rate-matching stage is transparent.

The second rate matching stage matches the number of bits after first rate matching stage to the number of physical channel bits available in the High Speed (Physical) Downlink Shared Channel (HS-(P)DSCH) set in the Transmit Time Interval (TTI).

6.2.2 Soft-bit Calculation in HARQ Combining

It is important to note that the combining in HSDPA HARQ is performed at bit level, i.e. LLR combining. As a result, combining is straightforward: simply sum up the LLRs. Therefore, by assigning zeros to the receiver HARQ buffer at the beginning of a frame transmission instance, all possible HARQ combining modes (IR, Chase combining, or combination of both) can be performed using the same summation operation.

6.2.3 HARQ First Rate Matching Stage

The maximum number of soft-bits available in the virtual IR buffer is N_{IR} which is signalled from higher layers for each HARQ process. The number of coded bits in a TTI before rate matching is N^{TTI} ; this is deduced from information signalled from higher layers and parameters signalled on the High Speed Shared Control Channel (HS-SCCH) for each TTI. Note that HARQ processing and physical layer storage occurs independently for each HARQ process currently active.

If N_{IR} is greater than or equal to N^{TTI} (i.e. all coded bits of the corresponding TTI can be stored) the first rate matching stage is transparent. Note that no repetition is performed.

If N_{IR} is smaller than N^{TTI} the parity bit streams are punctured by setting the rate matching parameter $\Delta N_{il}^{TTI} = N_{IR} - N^{TTI}$ where the subscripts i and l refer to transport channel and transport format being processed. Note the negative value is expected when the rate matching implements puncturing.

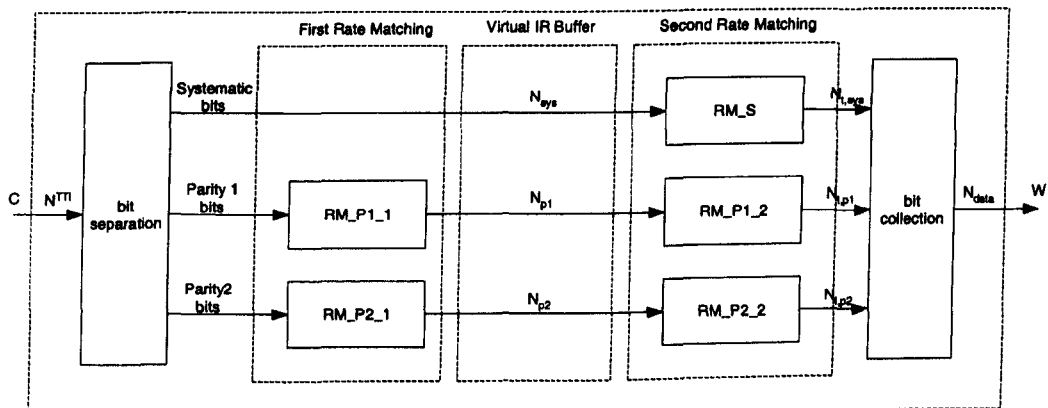


Figure 6-1: Two stage rate matching of the HS-PDSCH HARQ.

6.2.4 HARQ Second Rate Matching Stage

HARQ second stage rate matching for the HS-DSCH transport channel utilises the ordinary UMTS rate matching algorithm, but certain parameters are used.

The parameters of the second rate matching stage depend on the value of the RV parameters s and r . The parameter s can take the value 0 or 1 to distinguish between transmissions that prioritise systematic bits ($s = 1$) and non systematic bits ($s = 0$). The parameter r (range 0 to $r_{max} - 1$) changes the initial error variable e_{ini} in the case of puncturing. In case of repetition, both parameters r and s change the initial error variable e_{ini} . The parameters X_i , e_{plus} and e_{minus} are calculated as per Table 6-1. Note that the descriptions of these parameters can be found in [TGP02b].

Let us denote the number of bits before the second rate matching as N_{sys} for the systematic bits, N_{p1} for the parity 1 bits, and N_{p2} for the parity 2 bits, respectively. Denote also the number of physical channels used for the HS-DSCH by P . N_{data} is the number of bits available to the HS-DSCH in one TTI and defined as $N_{data}=P\times 3\times N_{data1}$, where N_{data1} is defined in [TGP02a]. The rate matching parameters are determined as follows.

For $N_{data} \leq N_{sys} + N_{p1} + N_{p2}$, puncturing is performed in the second rate matching stage. The number of transmitted systematic bits is $N_{t,sys} = \min\{N_{sys}, N_{data}\}$ for a transmission that prioritises systematic bits and $N_{t,sys} = \max\{N_{data} - (N_{p1} + N_{p2}), 0\}$ for a transmission that prioritises non systematic bits.

For $N_{data} > N_{sys} + N_{p1} + N_{p2}$ repetition is performed in the second rate matching stage. A similar repetition rate in all bit streams is achieved by setting the number of transmitted systematic bits to $N_{t,sys} = \left\lfloor N_{sys} \cdot \frac{N_{data}}{N_{sys} + 2N_{p1}} \right\rfloor$.

The number of parity bits in a transmission is: $N_{t,p1} = \left\lfloor \frac{N_{data} - N_{t,sys}}{2} \right\rfloor$ and

$N_{t,p2} = \left\lfloor \frac{N_{data} - N_{t,sys}}{2} \right\rfloor$ for the parity 1 and parity 2 bits, respectively.

Table 6-1 summarises the resulting parameter choice for the second rate matching stage.

Table 6-1: Parameters for HARQ second rate matching

	X_i	e_{plus}	e_{minus}
Systematic RM S	N_{sys}	N_{sys}	$ N_{sys} - N_{t,sys} $
Parity 1 RM P1_2	N_{p1}	$2 \cdot N_{p1}$	$2 \cdot N_{p1} - N_{t,p1} $
Parity 2 RM P2_2	N_{p2}	N_{p2}	$ N_{p2} - N_{t,p2} $

The rate matching parameter e_{ini} is calculated for each bit stream according to the RV parameters r and s using

$$e_{ini}(r) = \{(X_i - \lfloor r \cdot e_{plus} / r_{max} \rfloor - 1) \bmod e_{plus}\} + 1 \quad \text{in the case of puncturing,}$$

i.e., $N_{data} \leq N_{sys} + N_{p1} + N_{p2}$, and

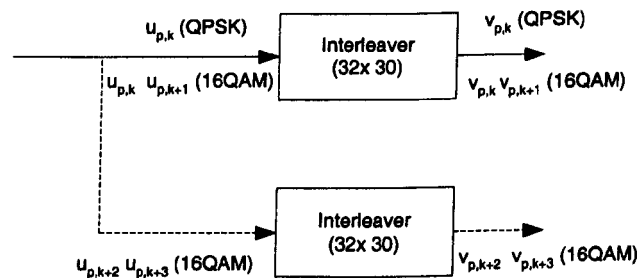
$$e_{ini}(r) = \{(X_i - \lfloor (s + 2 \cdot r) \cdot e_{plus} / (2 \cdot r_{max}) \rfloor - 1) \bmod e_{plus}\} + 1 \quad \text{for repetition, i.e.,}$$

$N_{data} > N_{sys} + N_{p1} + N_{p2}$. Where $r \in \{0, 1, \dots, r_{max} - 1\}$ and r_{max} is the total number of redundancy versions allowed by varying r . Note that r_{max} varies depending on the modulation mode, i.e. for 16-QAM $r_{max} = 2$ and for QPSK $r_{max} = 4$.

Note that the modulo operation used in the previous paragraphs the following clarification is used: the value of $(x \bmod y)$ is strictly in the range of 0 to $y-1$ (i.e. $-1 \bmod 10 = 9$).

6.2.5 Bit Interleaving for HS-DSCH

The interleaving of each physical channel is done according to the mechanism shown in Figure 6-2. The bits input to the block interleaver are denoted by $u_{p,1}, u_{p,2}, u_{p,3}, \dots, u_{p,U}$, where p is physical channel number and U is the number of bits in one TTI for one physical channel. For QPSK $U = 960$ and for 16-QAM $U = 1920$. The basic interleaver is as the second UMTS interleaver. The interleaver is of fixed size: R2=32 rows and C2=30 columns.

**Figure 6-2: HS-DSCH channel interleaving.**

For 16-QAM, there are two identical interleavers of the same fixed size $R2 \times C2 = 32 \times 30$. The output bits from the physical channel segmentation are divided two by two between the interleavers: bits $u_{p,k}$ and $u_{p,k+1}$ (MSBs) go to the first interleaver and bits $u_{p,k+2}$ and $u_{p,k+3}$ (LSBs) go to the second interleaver. Bits are collected two by two from the interleavers: bits $v_{p,k}$ and $v_{p,k+1}$ are obtained from the first interleaver and bits $v_{p,k+2}$ and $v_{p,k+3}$ are obtained from the second interleaver, where $k \bmod 4 = 1$.

It can be deduced that channel interleaving in the case of 16-QAM maintains the protection levels of the modulated bits. This is important, as the unequal protection level will be exploited for the benefit of the overall HARQ link performance by performing constellation re-arrangement, as described in the next section

6.2.6 Constellation Re-arrangement for 16-QAM

This function applies only to 16-QAM modulated bits. In case of QPSK it is transparent. Table 6-2 describes the operations that produce the different possible rearrangements. The bits of the input sequence are mapped in groups of 4 so that $v_{p,b}, v_{p,k+1}, v_{p,k+2}, v_{p,k+3}$ are used, where $k \bmod 4 = 1$

Table 6-2: Constellation Re-arrangement for 16-QAM

Constellation version parameter b	Output bit sequence	Operation
0	$v_{p,k} v_{p,k+1} v_{p,k+2} v_{p,k+3}$	None
1	$v_{p,k+2} v_{p,k+3} v_{p,k} v_{p,k+1}$	Swapping MSBs with LSBs
2	$v_{p,k} v_{p,k+1} v_{p,k+2} v_{p,k+3}$	Inversion of the logical values of LSBs
3	$v_{p,k+2} v_{p,k+3} v_{p,k} v_{p,k+1}$	Swapping MSBs with LSBs and inversion of logical values of LSBs

The output bit sequences from the table above map to the output bits in groups of 4, i.e. $r_{p,b}, r_{p,k+1}, r_{p,k+2}, r_{p,k+3}$, where $k \bmod 4 = 1$.

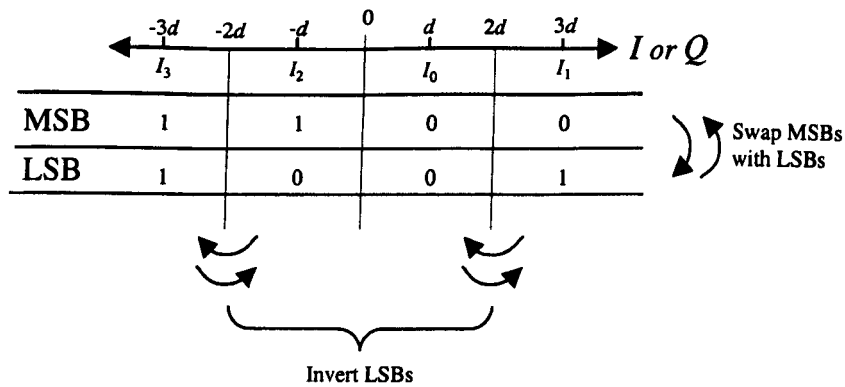


Figure 6-3: Illustration of Constellation Re-arrangement for 16-QAM.

Note that, by inspecting the 16-QAM constellation in Figure 6-3 (and Figure 4-2), MSBs are the most protected bits, while LSBs are the least protected bits. Swapping them swaps the protection levels. Similarly, there is a finer difference in protection level between the outer and inner bits of the LSBs. Inverting them swaps these protection levels.

6.2.7 Redundancy and Constellation Version Coding

The RV parameters r , s and constellation version parameter b are coded jointly to produce the final RV value. This is done according to Table 6-3 and Table 6-4 depending on the modulation mode used.

Table 6-3: RV Values for 16-QAM

RV Value	S	r	b
0	1	0	0
1	0	0	0
2	1	1	1
3	0	1	1
4	1	0	1
5	1	0	2
6	1	0	3
7	1	1	0

Table 6-4: RV Values for QPSK

RV Value	s	r
0	1	0
1	0	0
2	1	1
3	0	1
4	1	2
5	0	2
6	1	3
7	0	3

6.2.8 Parallel HARQ

Conceptually, parallel HARQ is simple: establish several instances of HARQ so that the otherwise idle time during the waiting the acknowledgements from the receiver of an HARQ instance is utilised for data transmission by other HARQ instances. Figure 6-4 (parts a and b) illustrates a scenario where four instances of such an HARQ are running in parallel. In this figure, while the base station is waiting for the ACKs/NACKs from the mobile receiver, it sends frames belonging to three other HARQ processes.

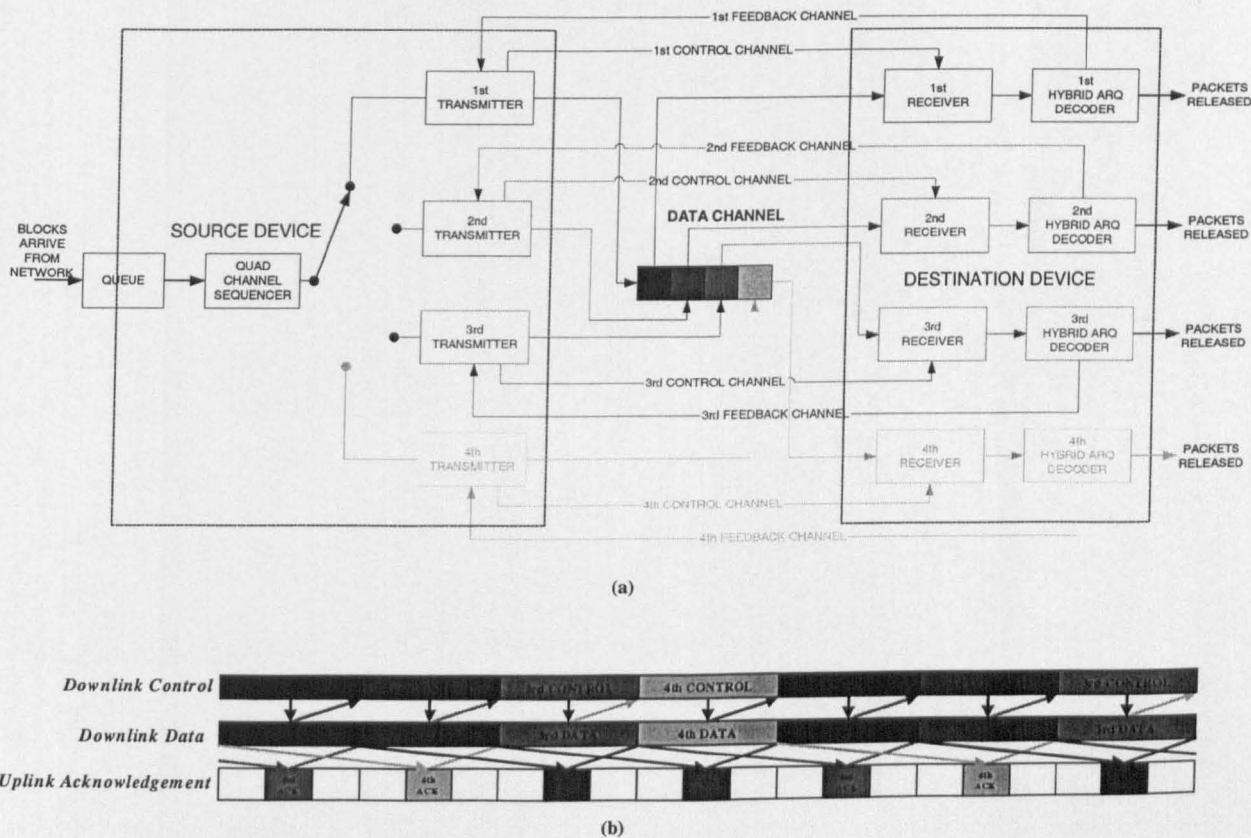


Figure 6-4: Parallel HARQ operation [TGP01].

From the point of view of BER or BLER performance, single or parallel instance HARQ is essentially the same. Therefore, for BER and BLER performance evaluation purposes, only single HARQ will be performed.

6.3 HSDPA HARQ Link Simulator

The HSDPA system is very complicated as it includes various kinds of advanced techniques in addition to the existing UMTS system. In other words, HSDPA operates as an extension of and simultaneously with a normal UMTS operation. For instance, the Common Pilot Channel (CPICH) and the Physical Dedicated Channels (PDCHs) of UMTS must co-operate simultaneously with any other HSDPA physical channels. PDCHs operate with full UMTS characteristics (e.g., TTI of 10, 20, 40 or 80 ms, power controlled), while HSDPA physical channels operate with full HSDPA characteristics (e.g., TTI of 2 ms, AMC, HARQ).

This complication is reflected in the modelling and simulation. In Figure 6-5, the timing relationship of the UMTS frames and HSDPA HARQ downlink and uplink subframes is illustrated. (Note: OCNS stands for Orthogonal Channel Noise Simulator.)

Since the main purpose of this chapter is performance evaluation of different soft-demodulation methods, developing such a complicated simulator incurs very long development time. Therefore, only the simplified one representing a single HS-PDSCH channel that is developed and used for evaluation.

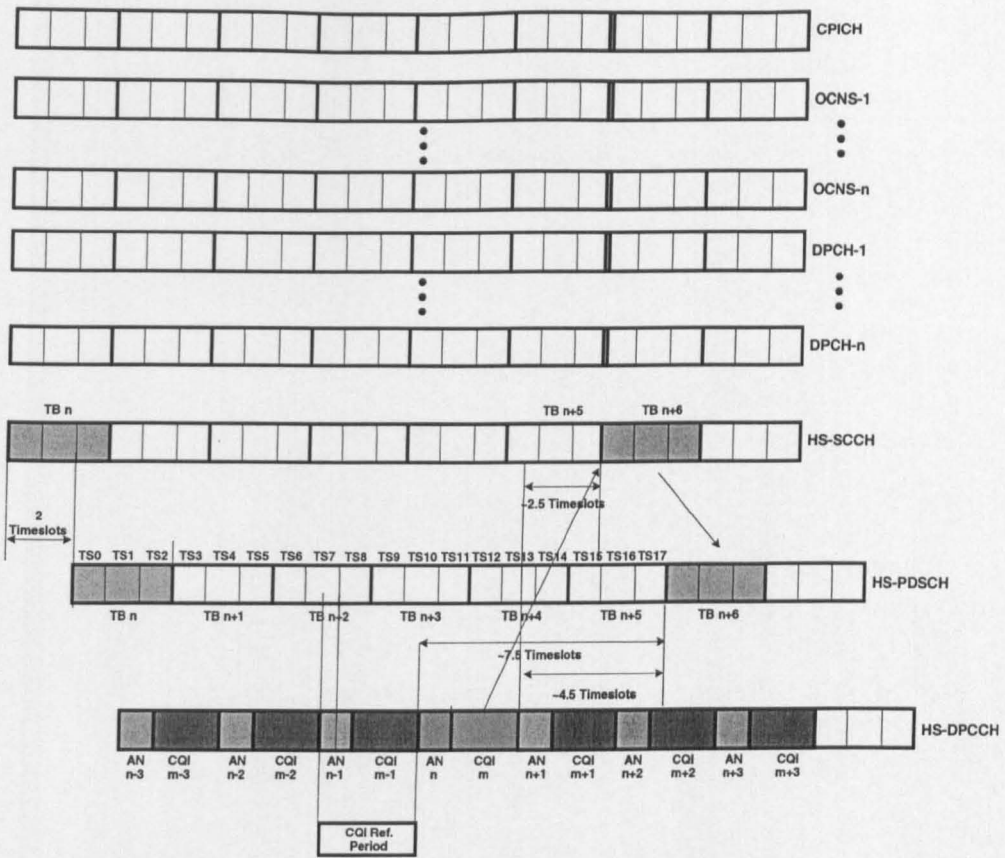


Figure 6-5: Timing relationship of UMTS and HSDPA frames implemented in the simulator.

6.4 Simplified HSDPA HARQ Link Simulator

To evaluate the generic performance of different soft-demodulation methods in HSDPA HARQ link, a simplified version of such a system is required. With this purpose in mind, a simulator as depicted in Figure 6-6 is developed. As different soft-demodulation methods exist only for 16-QAM, only this modulation scheme is involved. Also, only performance-sensitive functional blocks as described in the previous sections are involved. These include:

- HARQ First Rate Matching Stage (described in section 6.2.3): in transparent operation mode
- HARQ Second Rate Matching Stage (described in section 6.2.4)
- Bit Interleaving for HS-DSCH (described in section 6.2.5)
- Constellation Re-arrangement for 16-QAM (described in section 6.2.6)

- Redundancy and Constellation Version Coding (described in section 6.2.7)

The CRC check is by-passed and the corresponding CRC bits are treated as information bits. Performance is measured in terms of BER and BLER.

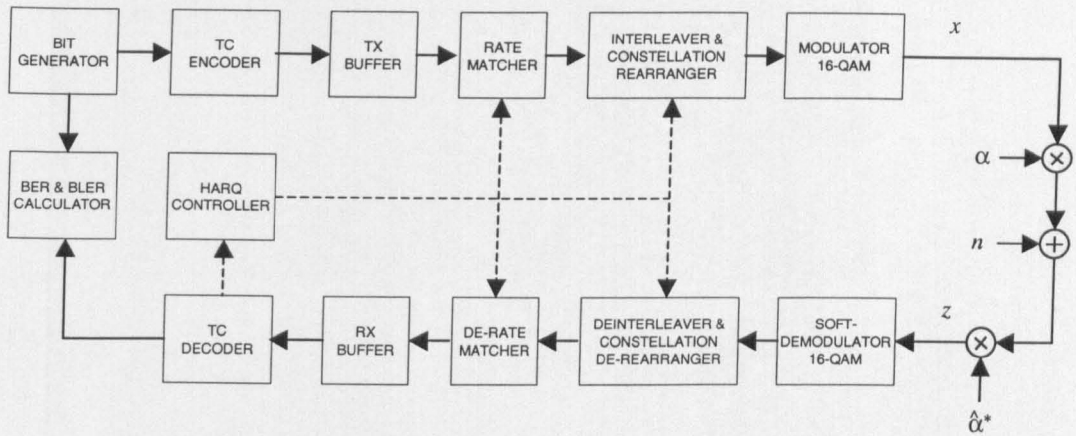


Figure 6-6: SAW HARQ model implemented in the simplified simulator.

Figure 6-7 illustrates the block sizes in different bit-framing stages of a case chosen for performance evaluation simulation. Note that these stages are a realisation of the HSDPA general bit-stages depicted in Figure 3-3 of Chapter 3. Adopted RV values for different retransmission instances are listed in Table 6-5. The actual operations of these RV values are summarised in Table 6-6 and Table 6-7. A few notes are worth mentioning in reading these tables:

1. Channel coding involved is only TC (as applicable in HSDPA), where coded bits can be identified as systematic, parity1, and parity2 blocks. Twelve tail bits are distributed evenly to these 3 blocks.
2. *Effective coding rate* is defined as the ratio of the number of systematic bits to the number of accumulated bits, disregarding whether Chase combining is involved.
3. *Retransmission efficiency* is defined as the ratio of the number of systematic bits to the number of accumulated bits taking into account the number of repeated bits due to Chase combining.
4. For the graphical illustration (in the rightmost column), the 1st row represents systematic bits, the 2nd row represents parity1 bits, the 3rd row represents parity2 bits. Shaded boxes represent that the bits have been received. Numbered shaded boxes denote that the bits

have been received repeatedly that many times by way of Chase combining. This graphical illustration has a similar purpose to the puncturing matrices commonly used in conjunction with HARQ technique, e.g. in [Ros99].

As can be deduced from Table 6-6, when particular settings of parameters as depicted in Figure 6-7 are employed, the 3GPP suggested of RV value sequence results in low retransmission efficiency 1/4 but high effective coding rate of 1/2. For a comparison, a logically more efficient RV sequence is proposed, as listed in the rightmost column of Table 6-5 and summarised in Table 6-7.

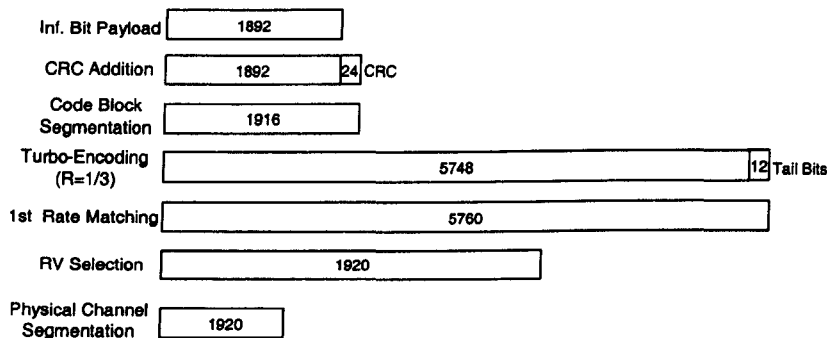


Figure 6-7: Block sizes in simplified SAW HARQ.

Table 6-5: RV Values for Maximum Number Retransmissions of 4
(0th retransmission denotes original transmission)

Retransmission instance	RV value	
	3GPP [TGP03]	Proposed
0	6	6
1	2	1
2	1	3
3	5	5

Table 6-6: Actual Operations of RV Value Sequence of (6, 2, 1, 5) used in [TGP03]
 (0th retransmission denotes original transmission)

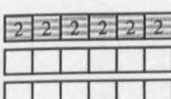
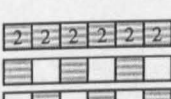
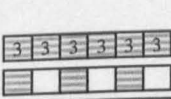
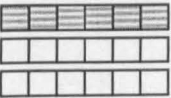
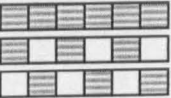
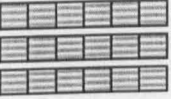
Retransmission instance	RV value	Actual operations	Accumulated coded bits at receiver (graphically)
0	6	<ul style="list-style-type: none"> - Send all systematic bits - Send no parity bits at all - Constellation re-arrangement: swap LSBs with MSBs, then invert LSBs - Effective coding rate so far = 1/1 - Rerransmission efficiency so far = 1/1 	
1	2	<ul style="list-style-type: none"> - Send all systematic bits - Send no parity bits at all - Constellation re-arrangement: swap LSBs with MSBs - Effective coding rate so far = 1/1 - Rerransmission efficiency so far = 1/2 	
2	1	<ul style="list-style-type: none"> - Send no systematic bits - Send odd-indexed bits of parity1 - Send even-indexed bits of parity2 - Constellation re-arrangement: do nothing - Effective coding rate so far = 1/2 - Retransmission efficiency so far = 1/3 	
3	5	<ul style="list-style-type: none"> - Send all systematic bits - Send no parity bits - Constellation re-arrangement: invert LSBs - Effective coding rate so far = 1/2 - Retransmission efficiency so far = 1/4 	

Table 6-7: Actual Operations of the Proposed RV Value Sequence of (6, 1, 3, 5)
(0th retransmission denotes original transmission)

Retransmission instance	RV value	Actual operations	Accumulated coded bits at receiver (graphically)
0	6	<ul style="list-style-type: none"> - Send all systematic bits - Send no parity bits at all - Constellation re-arrangement: swap LSBs with MSBs, then invert LSBs - Effective coding rate so far = 1/1 - Retransmission efficiency so far = 1/1 	
1	1	<ul style="list-style-type: none"> - Send no systematic bits - Send odd-indexed bits of parity1 - Send even-indexed bits of parity2 - Constellation re-arrangement: do nothing - Effective coding rate so far = 1/2 - Retransmission efficiency so far = 1/2 	
2	3	<ul style="list-style-type: none"> - Send no systematic bits - Send even-indexed bits of parity1 - Send odd-indexed bits of parity2 - Constellation re-arrangement: swap LSBs with MSBs - Effective coding rate so far = 1/3 - Retransmission efficiency so far = 1/3 	
3	5	<ul style="list-style-type: none"> - Send all systematic bits - Send no parity bits - Constellation re-arrangement: invert LSBs - Effective coding rate so far = 1/3 - Retransmission efficiency so far = 1/4 	

6.5 Performance Evaluation

The performance evaluation is performed for both RV value sequences, i.e., the 3GPP recommended one $\text{RV}(6, 2, 1, 5)$ and the proposed one $\text{RV}(6, 1, 3, 5)$. Since the proposed one has more potential to yield better overall performance and retransmission efficiency, as will be observed shortly, the discussion of performance evaluation using this sequence will be performed first.

In addition, retransmission efficiency as defined in the previous section will also be examined.

Performance evaluation is carried out over AWGN, Uncorrelated Rayleigh and Correlated Rayleigh channels. The Correlated Rayleigh channel has Doppler spread of 222 Hz, corresponding to a mobile velocity of 120 km/h using 2 GHz carrier frequency. The LogSMAP TC decoding algorithm described in section 2.6.3.1.2 is used throughout.

The effects on BER and BLER performance of different soft-demodulation methods from varying the number of TC decoding iterations and the number of maximum retransmissions will be examined. The BLER is also used as a performance indicator, as this is widely used in many publications related to HSDPA.

Two acronyms are used in the caption of each graph. First, “Itr” means “number of TC decoding iterations”. Second, “Retx” denotes “number of maximum retransmissions, with original transmission is counted as 1 retransmission”. The ranges of graphs’ axes remain fixed for a certain channel to ease comparison.

6.5.1 RV Value Sequence of (6, 1, 3, 5)

6.5.1.1 AWGN Channel

Figure 6-8 shows the performance of three soft-demodulation methods evaluated over the AWGN channel. Four TC decoding iterations are carried out and maximum number of retransmissions is set to 3. This means, from modulation and coding points of view, the settings are almost the same as the settings of an ordinary 16-QAM with rate-1/3 TC, the performance of which is depicted in Figure 4-11 (in Chapter 4). Comparing the performance of Method E, there is about 0.2 dB improvement. This can be attributed to the larger block length of information entering the TC encoder (hence longer TC interleaving size), 1892 against 1000 bits. The performance difference could also be due to the difference of TC interleaver types and operations. Figure 4-11 represents

the performance from a random interleaver whereas here the simulator uses UMTS interleaver. Moreover, there is constellation re-arrangement involved in the scheme being evaluated.

Examining the performance of Method R, the same analysis as given to the Method E is applicable. Note that despite being less complex, the performance difference between this method and the Method E is negligible.

In contrast, the performance of Method L is about 0.2 dB worse here. This may be due to the accumulation of inaccuracies of the approximation method.

The effects on BER and BLER performance of varying the number of TC decoding iterations and the maximum number of retransmissions represented by Figure 6-8 to Figure 6-15 are summarised in Table 6-8.

Table 6-8: Approximate E_b/N_0 Gain Relative to the Use of 3 Retransmissions, 4 TC Decoding Iterations in AWGN Channel at BER of 10^{-5} and BLER of 10^{-3}

No.	Number of retransmissions and TC decoding iterations in ($Retx, Itr$) format	Method R (dB)		Relative Gain of Method R to Method L at the same ($Retx, Itr$) settings (dB)	
		BER	BLER	BER	BLER
1	(3, 4)	0.00	0.00	0.77	1.85
2	(3, 8)	0.31	0.30	1.00	2.15
3	(4, 4)	1.50	1.15	1.15	1.54
4	(4, 8)	1.85	1.35	1.23	1.62

As can be seen from Table 6-8, increasing the number of TC decoding iterations from 4 to 8 gains over 0.3 dB E_b/N_0 improvement. Moreover, increasing the maximum number of retransmissions from 3 to 4 introduces around 1.5 dB improvement. The improvement achieved by BLER is slightly less. However, despite a larger gain obtained by increasing the maximum number of retransmissions, it will incur more delay due to retransmission process and less retransmission efficiency. In contrast, increasing the number of TC decoding iterations does not reduce retransmission efficiency, incurs less delay, and is probably easier to implement.

Comparing the performance of Methods R with that of Method L, the improvement is ranging from 0.77 up to 2.15 dB for different simulation settings. This is a significant improvement, knowing that the complexities of both methods are identical.

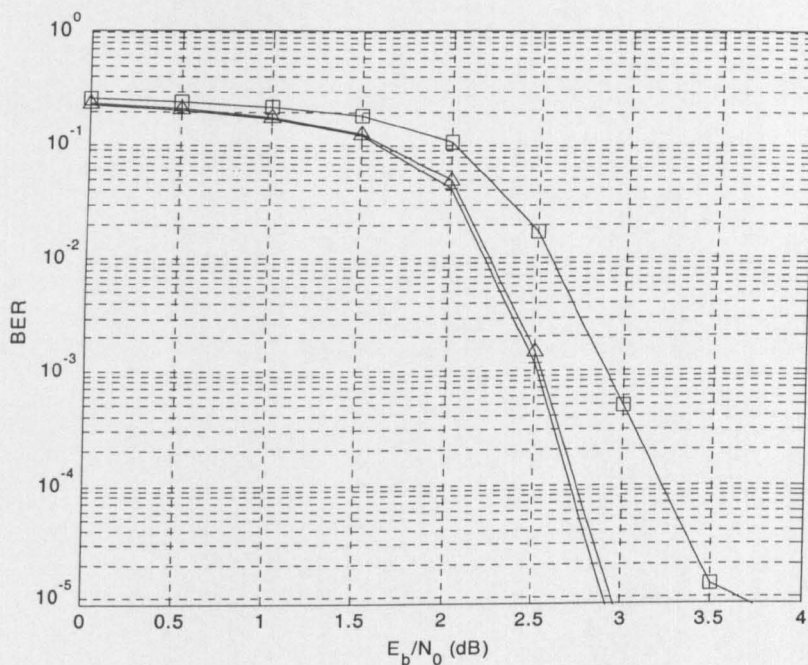


Figure 6-8: 16-QAM BER Performance in AWGN Channel, 3-Retx, 4-Itr
Legend: + Method E, Δ Method R, □ Method L

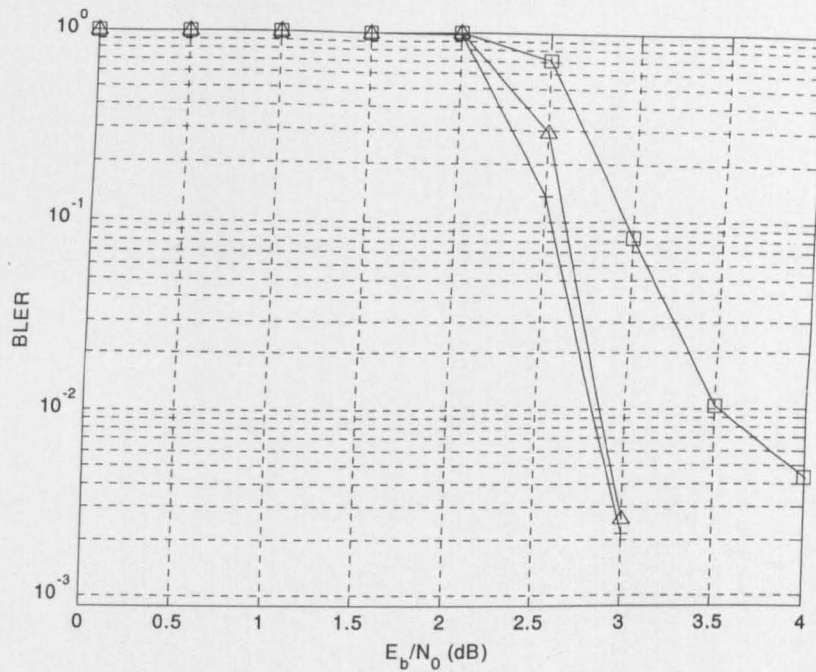


Figure 6-9: 16-QAM BLER Performance in AWGN Channel, 3-Retx, 4-Itr
Legend: + Method E, Δ Method R, \square Method L

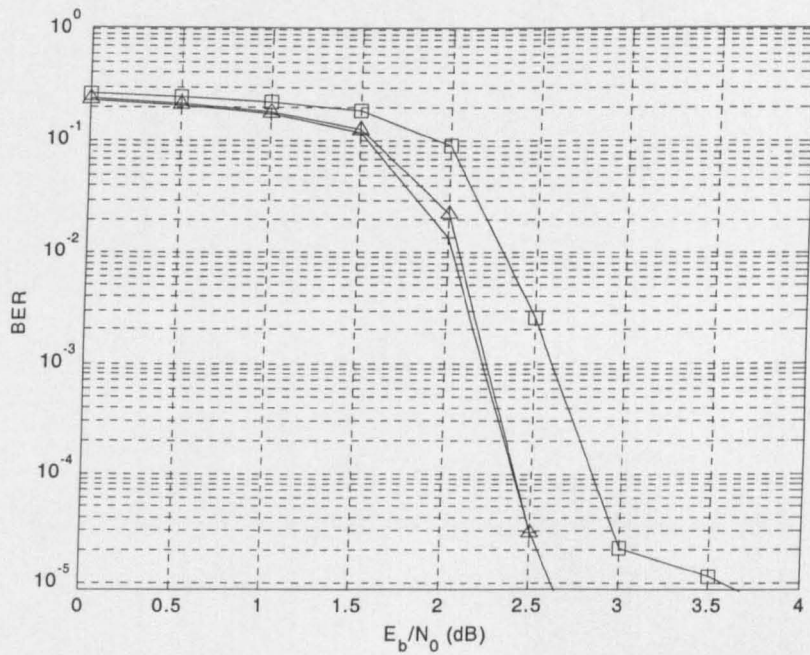


Figure 6-10: 16-QAM BER Performance in AWGN Channel, 3-Retx, 8-Itr
Legend: + Method E, Δ Method R, \square Method L

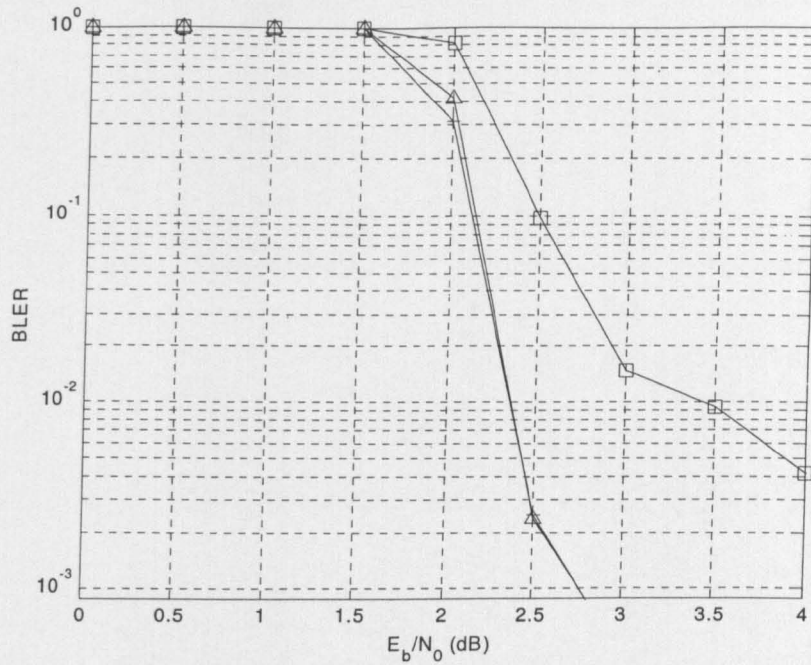


Figure 6-11: 16-QAM BLER Performance in AWGN Channel, 3-Retx, 8-Itr
Legend: + Method E, Δ Method R, \square Method L

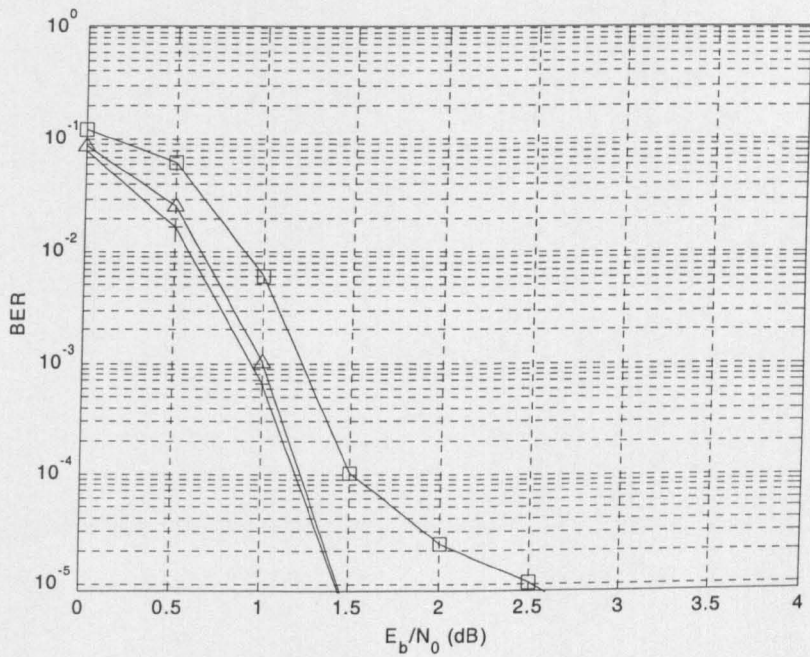


Figure 6-12: 16-QAM BER Performance in AWGN Channel, 4-Retx, 4-Itr
Legend: + Method E, Δ Method R, \square Method L

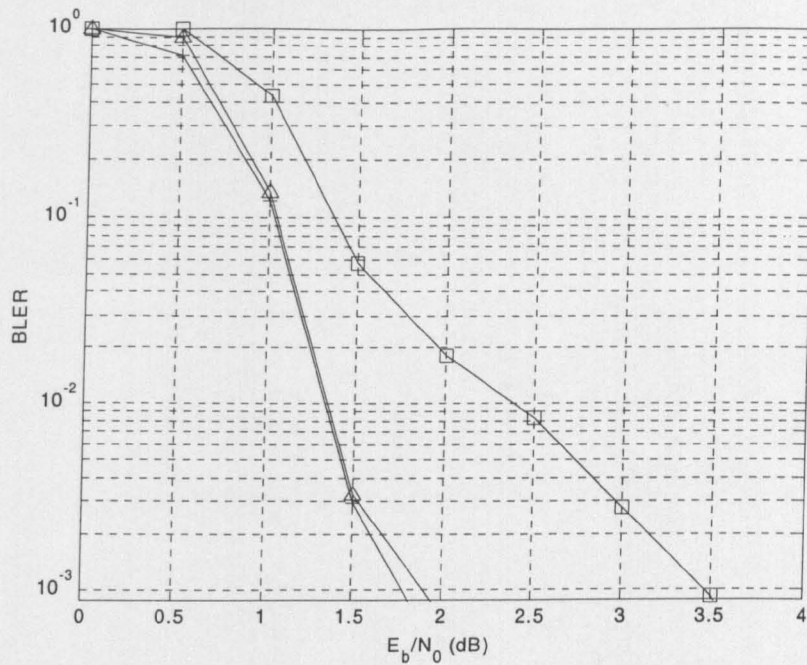


Figure 6-13: 16-QAM BLER Performance in AWGN Channel, 4-Retx, 4-Itr
 Legend: + Method E, Δ Method R, \square Method L

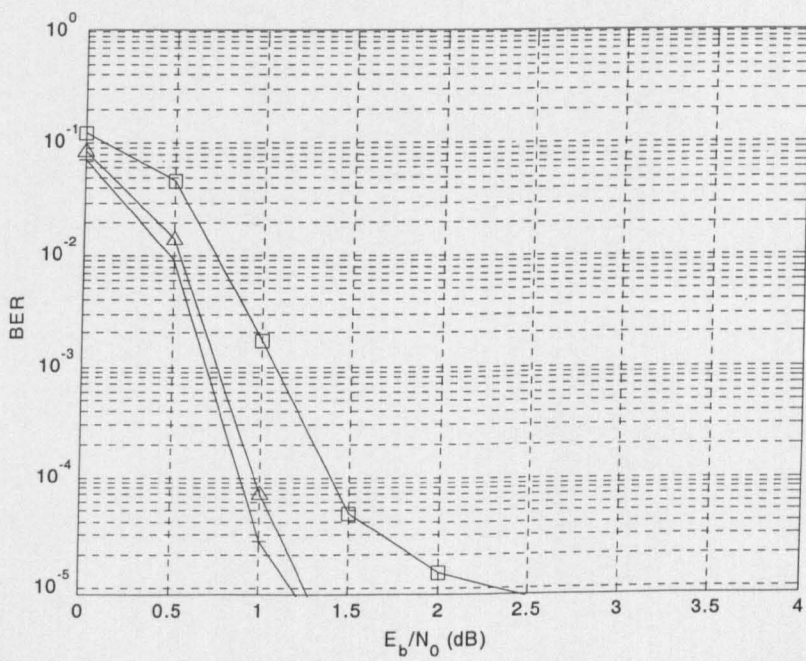


Figure 6-14: 16-QAM BER Performance in AWGN Channel, 4-Retx, 8-Itr
 Legend: + Method E, Δ Method R, \square Method L

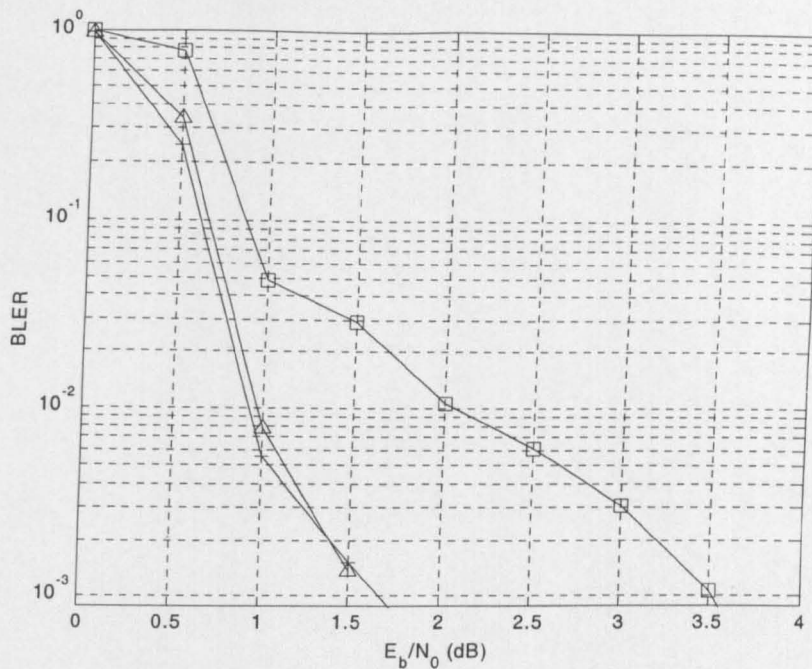


Figure 6-15: 16-QAM BLER Performance in AWGN Channel, 4-Retx, 8-Itr
Legend: + Method E, Δ Method R, □ Method L

Examining the retransmission efficiency graph depicted in Figure 6-16, it is further confirmed that the performance of Method R is very similar to that of Method E, whereas the performance of Method L is notably worse. Note that the performance of Method L in this graph is equivalent to the corresponding curve in [Wen02] for which the “constellation rearrangement” is applied. Here, it can be seen that the improvement in terms of E_b/N_0 gain in the previous figures (Figure 6-8 to Figure 6-15) appears as higher retransmission efficiency.

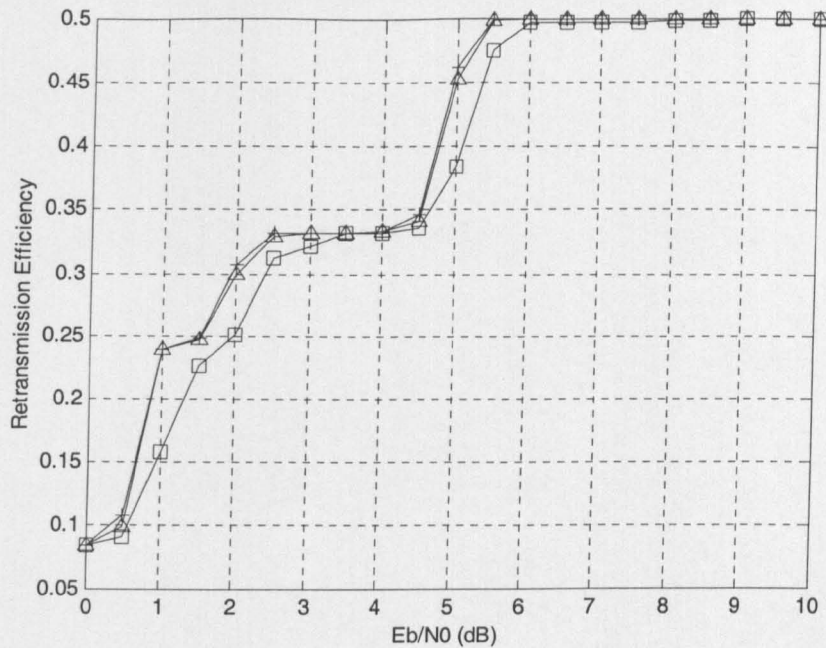


Figure 6-16: Retransmission Efficiency in AWGN Channel
Legend: + Method E, Δ Method R, □ Method L

6.5.1.2 Uncorrelated Rayleigh Channel

Comparing Figure 6-17 and Figure 4-12, a similar analysis as discussed previously for the case of AWGN channel can be applied. Briefly stated, the performance of different the soft-demodulation methods is as expected.

To aid the analysis, some important values displayed by Figure 6-17 to Figure 6-24 are summarised in Table 6-9.

In contrast to what is achieved in the AWGN channel, here in the Uncorrelated Rayleigh channel increasing the number of TC decoding iterations from 4 to 8 does not improve the gain, or improves only 0.12 dB in the case of BLER. However, increasing the maximum number of retransmissions increases the gain significantly: ranging from 1.52 to 1.95 dB.

Table 6-9: Approximate E_b/N_0 Gain Relative to the Use of 3 Retransmissions, 4 TC Decoding Iterations in Uncorrelated Rayleigh Channel at BER of 10^{-5} and BLER of 10^{-3}

No.	Number of retransmissions and TC decoding iterations in $(Retx, Itr)$ format	Method R (dB)		Relative Gain of Method R to Method L at the same $(Retx, Itr)$ settings (dB)	
		BER	BLER	BER	BLER
1	(3, 4)	0.00	0.00	0.82	2.76
2	(3, 8)	0.00	0.12	0.88	3.20
3	(4, 4)	1.82	1.52	1.35	2.29
4	(4, 8)	1.90	1.95	1.19	2.62

Commenting on the relative gain achieved by the Method R over the Method L, even greater gains than those in AWGN channel are obtained here. The gains of BER range from 0.82 to 1.35 dB, while those of BLER range from 2.29 to 3.20 dB.

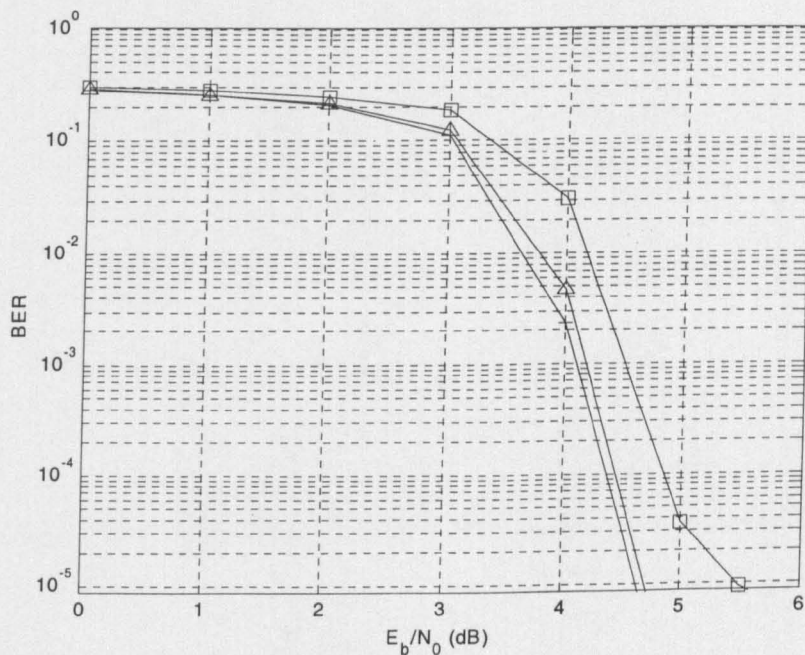


Figure 6-17: 16-QAM BER Performance in Uncorrelated Rayleigh Channel, 3-Retx, 4-Itr
Legend: + Method E, Δ Method R, □ Method L

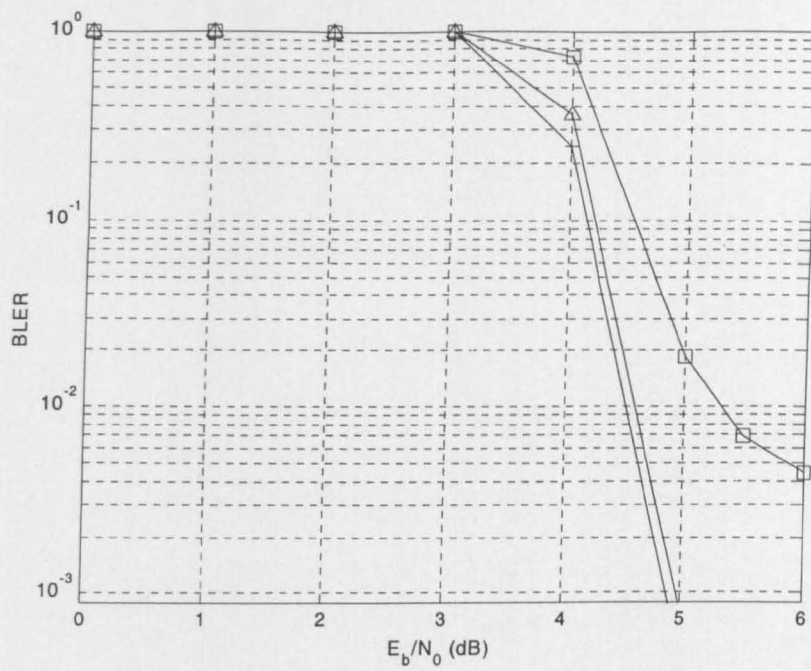


Figure 6-18: 16-QAM BLER Performance in Uncorrelated Rayleigh Channel, 3-Retx, 4-Ittr
 Legend: + Method E, Δ Method R, \square Method L

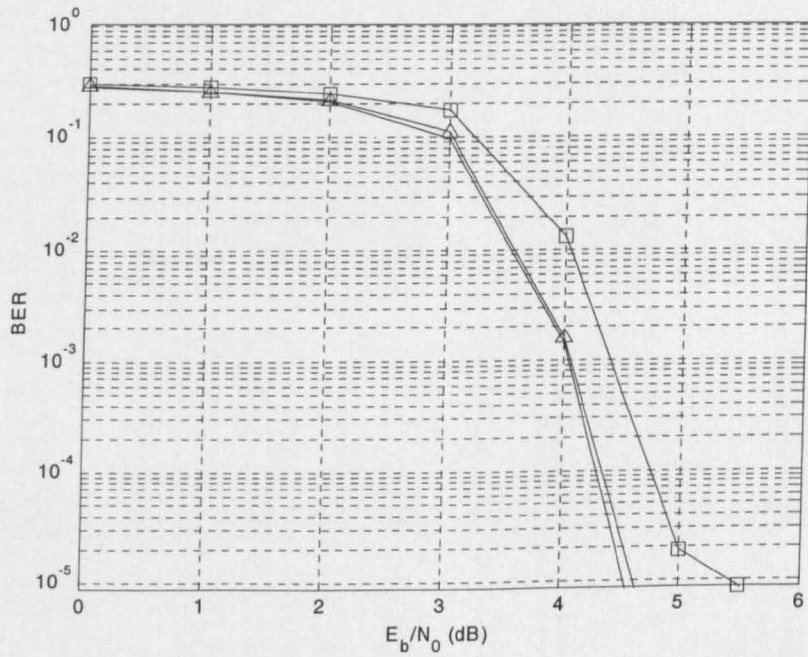


Figure 6-19: 16-QAM BER Performance in Uncorrelated Rayleigh Channel, 3-Retx, 8-Ittr
 Legend: + Method E, Δ Method R, \square Method L

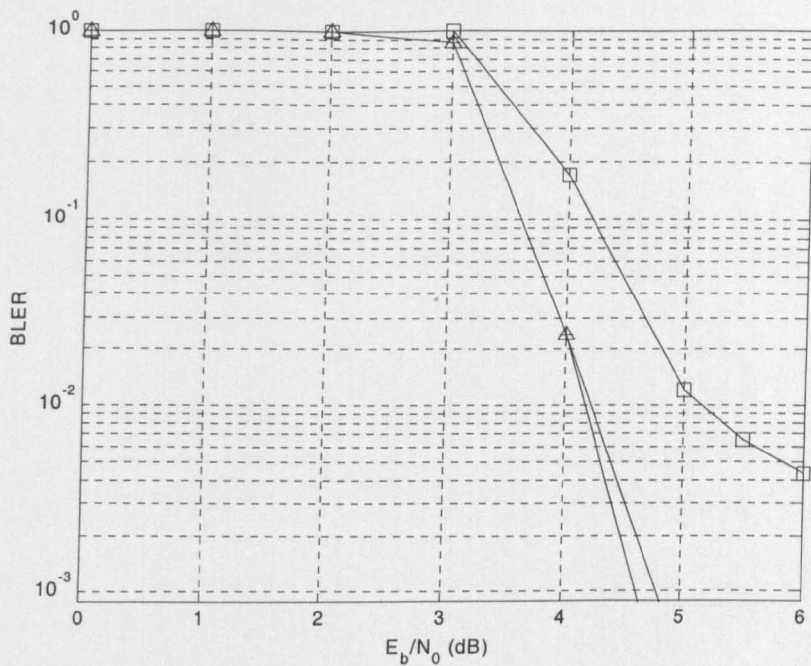


Figure 6-20: 16-QAM BLER Performance in Uncorrelated Rayleigh Channel, 3-Retr, 8-Itr
 Legend: + Method E, Δ Method R, \square Method L

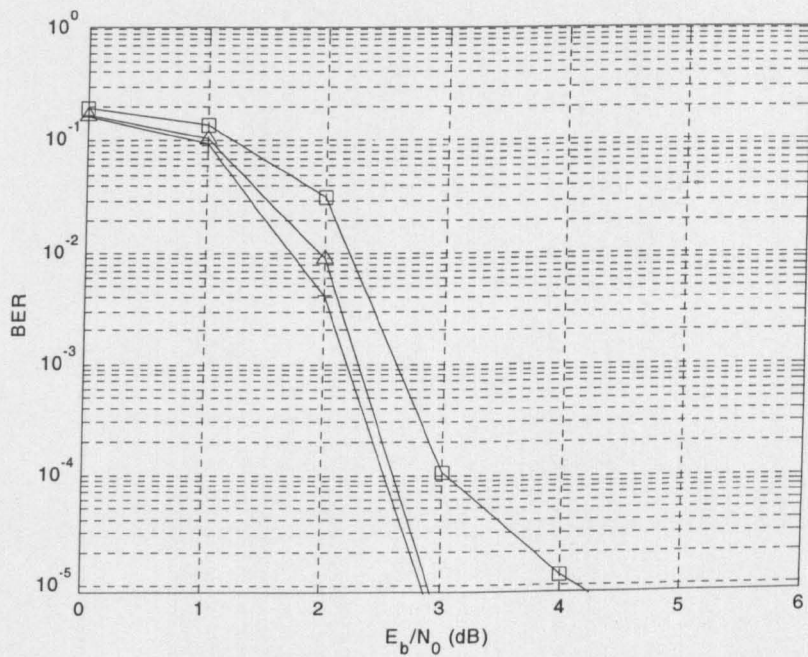


Figure 6-21: 16-QAM BER Performance in Uncorrelated Rayleigh Channel, 4-Retr, 4-Itr
 Legend: + Method E, Δ Method R, \square Method L

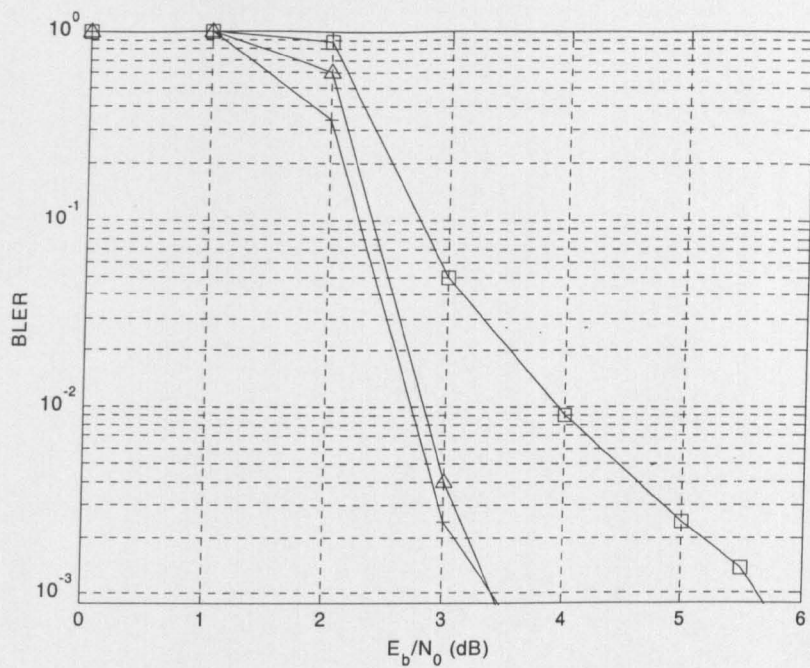


Figure 6-22: 16-QAM BLER Performance in Uncorrelated Rayleigh Channel, 4-Retx, 4-Itr
 Legend: + Method E, Δ Method R, \square Method L

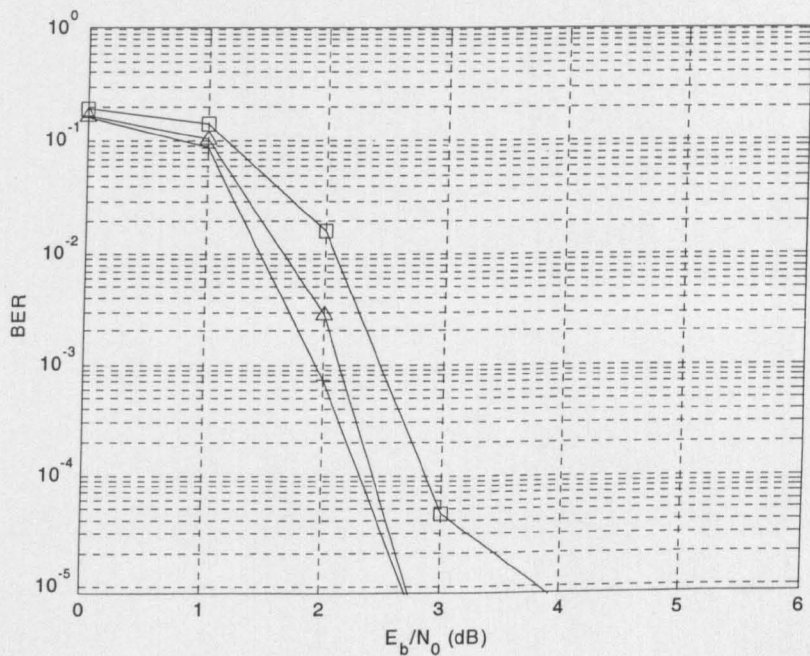


Figure 6-23: 16-QAM BER Performance in Uncorrelated Rayleigh Channel, 4-Retx, 8-Itr
 Legend: + Method E, Δ Method R, \square Method L

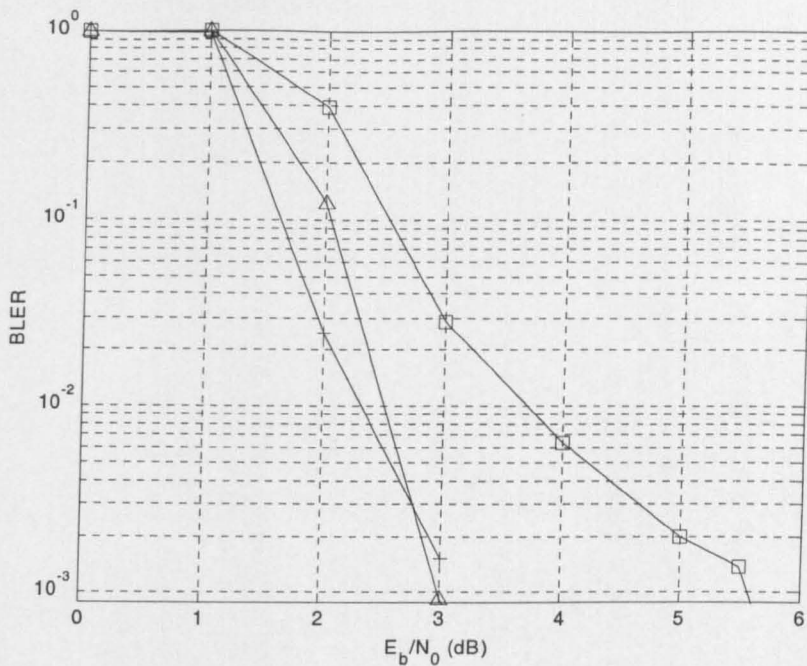


Figure 6-24: 16-QAM BLER Performance in Uncorrelated Rayleigh Channel, 4-Retx, 8-Itr
Legend: + Method E, Δ Method R, □ Method L

The corresponding retransmission efficiency plots are shown Figure 6-25. Here, it can be observed that the performance of Method R and E is very similar, whereas that of Method L is worse.

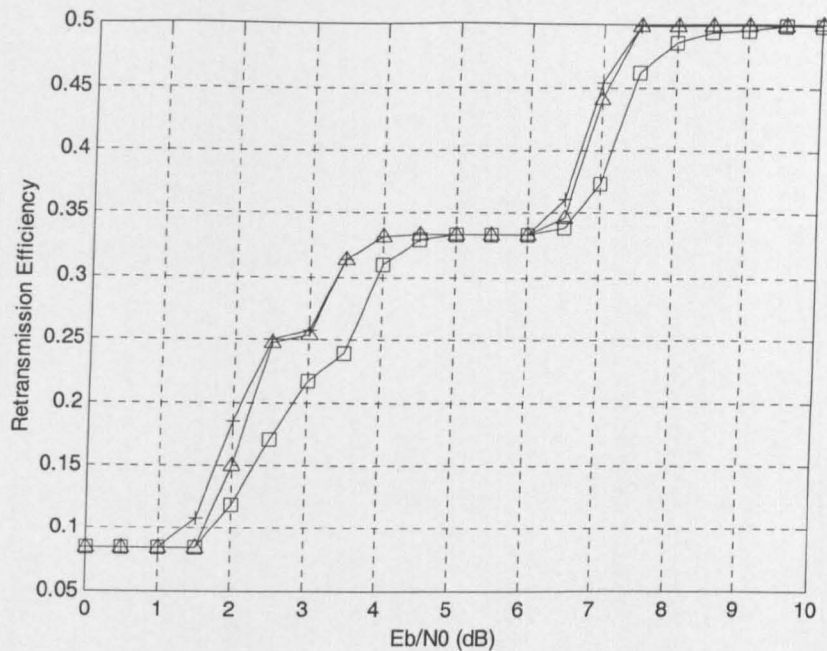


Figure 6-25: Retransmission Efficiency in Uncorrelated Rayleigh Channel
Legend: + Method E, Δ Method R, \square Method L

6.5.1.3 Correlated Rayleigh Channel

Comparing the performance of different soft-demodulation methods in Figure 6-26 and that depicted in Figure 4-13, it can be observed that there is about 10 dB improvement. Apart from the difference in the lengths of TC interleaver and the type of channel interleavers, this remarkable improvement can mostly be due to the lower correlation among the demodulated bits due to retransmissions.

Applying similar approach for simplifying the analysis, the performance evaluation results depicted in Figure 6-26 to Figure 6-33 have been summarised in Table 6-10.

Table 6-10: Approximate E_b/N_0 Gain Relative to the Use of 3 Retransmissions, 4 TC Decoding Iterations in Correlated Rayleigh Channel at BER of 10^{-5} and BLER of 10^{-3}

No.	Number of retransmissions and TC decoding iterations in $(Retx, Itr)$ format	Method R (dB)		Relative Gain of Method R to Method L at the same $(Retx, Itr)$ settings (dB)	
		BER	BLER	BER	BLER
1	(3, 4)	0.00	0.00	0.00	0.57
2	(3, 8)	2.72	0.72	0.72	0.00
3	(4, 4)	3.86	2.29	0.50	0.72
4	(4, 8)	3.29	1.72	1.00	0.29

As seen in Table 6-10, increasing the maximum number of iterations greatly increases the gain, particularly from the point of view of BER. The gain from the point of view of BLER is less. Also, if the number of TC decoding iterations has been set to 8, the improvement from increasing the maximum number of retransmissions is diminishing.

Increasing the number of TC decoding iterations, when the maximum number of retransmissions is equal to 3, greatly increases the gain. However, when the maximum number of retransmissions is equal to 4, increasing the number of TC decoding iterations decreases the gain. This decrement is likely to arise from the fact that, when the bits are correlated and have been partially recombined, TC decoding iterations saturate very rapidly, making 8 iterations excessive.

The relative gain achieved by Method L is not very consistent here; it ranges from 0.00 up to 1.00 dB. However, from the HSDPA standpoint, the use of 16-QAM for this channel condition is less likely. Therefore, the relative gain of Method R over Method L will be more favourable.

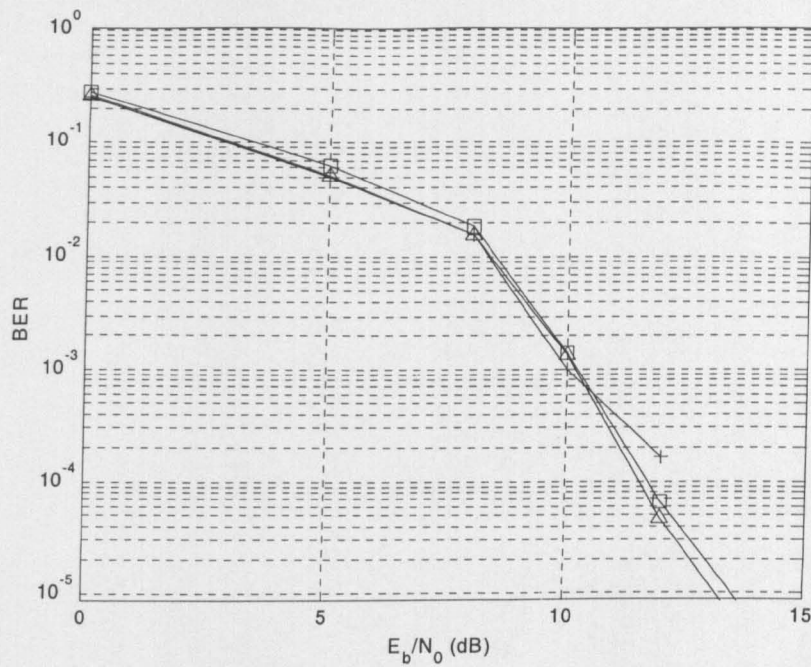


Figure 6-26: 16-QAM BER Performance in Correlated Rayleigh Channel, 3-Retx, 4-Itr
Legend: + Method E, Δ Method R, ◻ Method L

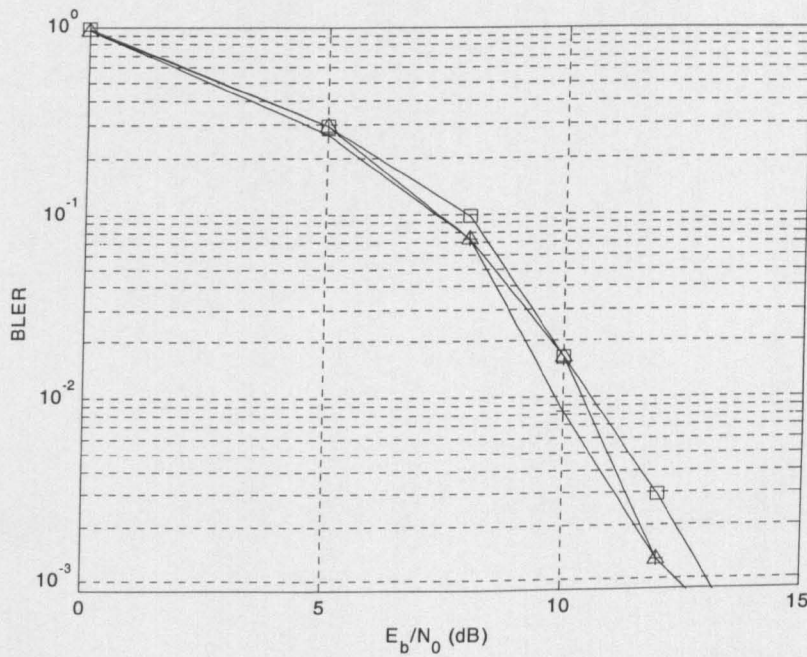


Figure 6-27: 16-QAM BLER Performance in Correlated Rayleigh Channel, 3-Retx, 4-Itr
Legend: + Method E, Δ Method R, ◻ Method L

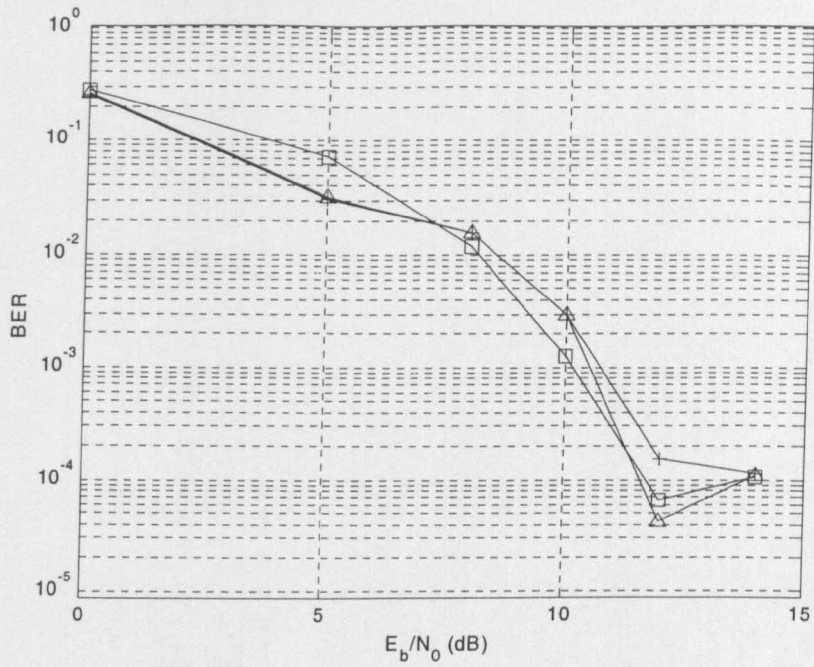


Figure 6-28: 16-QAM BER Performance in Correlated Rayleigh Channel, 3-Retx, 8-Ittr
Legend: + Method E, Δ Method R, \square Method L

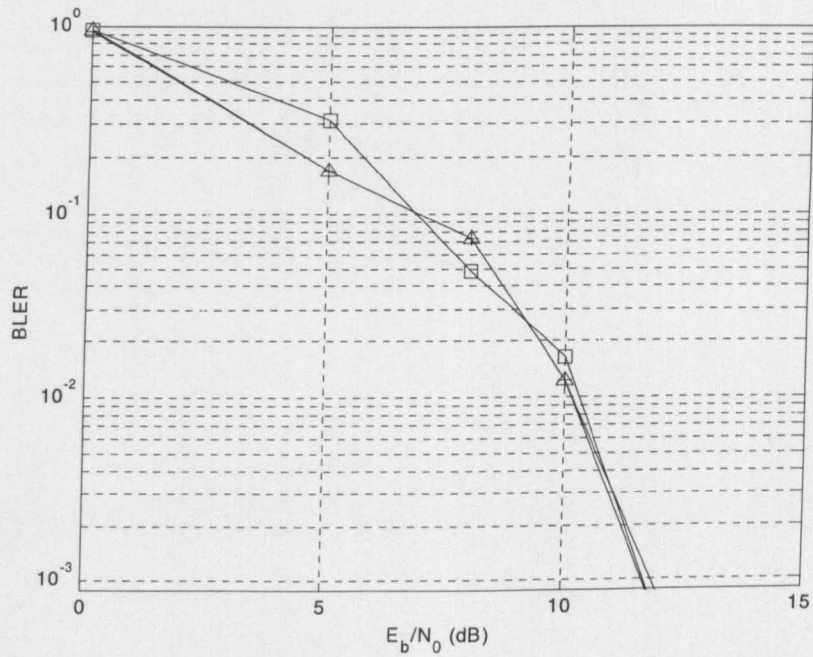


Figure 6-29: 16-QAM BLER Performance in Correlated Rayleigh Channel, 3-Retx, 8-Ittr
Legend: + Method E, Δ Method R, \square Method L

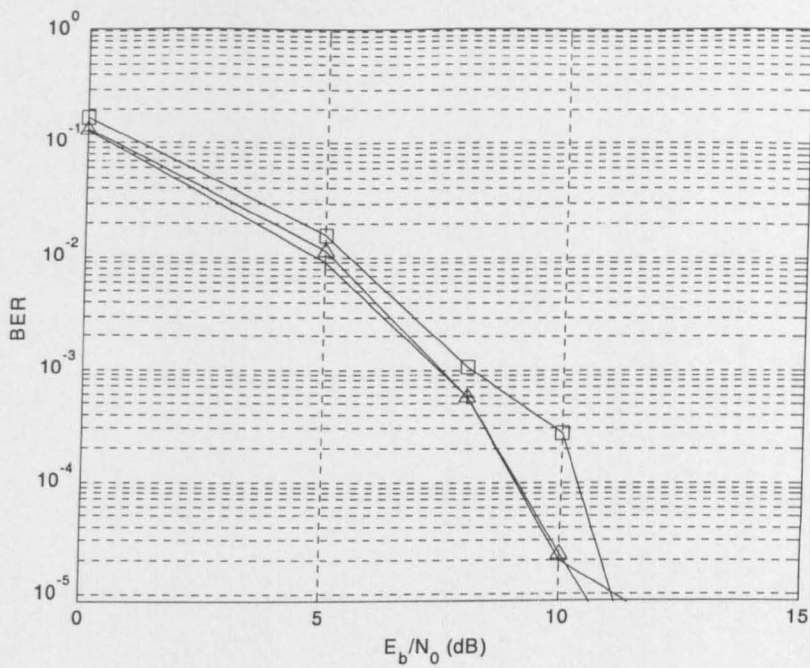


Figure 6-30: 16-QAM BER Performance in Correlated Rayleigh Channel, 4-Retx, 4-Itr
 Legend: + Method E, Δ Method R, \square Method L

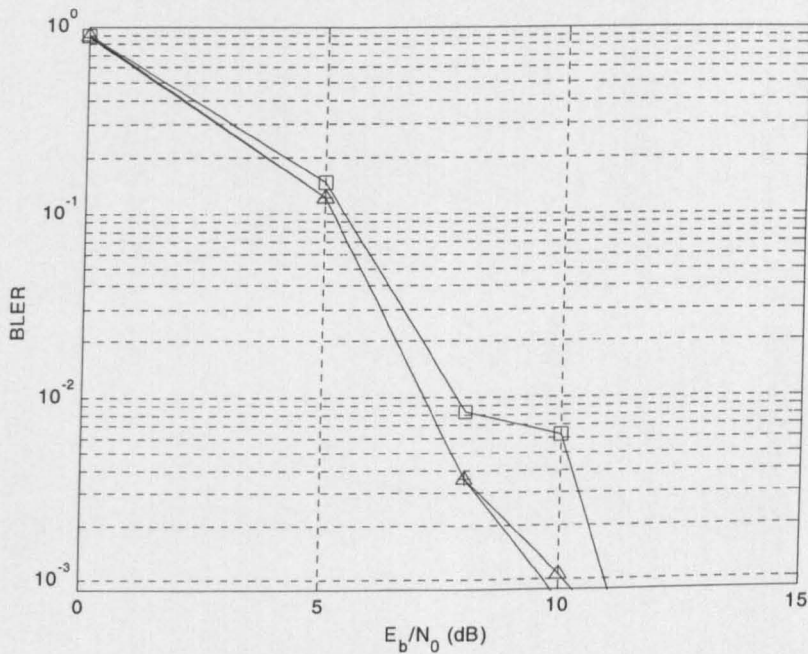


Figure 6-31: 16-QAM BLER Performance in Correlated Rayleigh Channel, 4-Retx, 4-Itr
 Legend: + Method E, Δ Method R, \square Method L

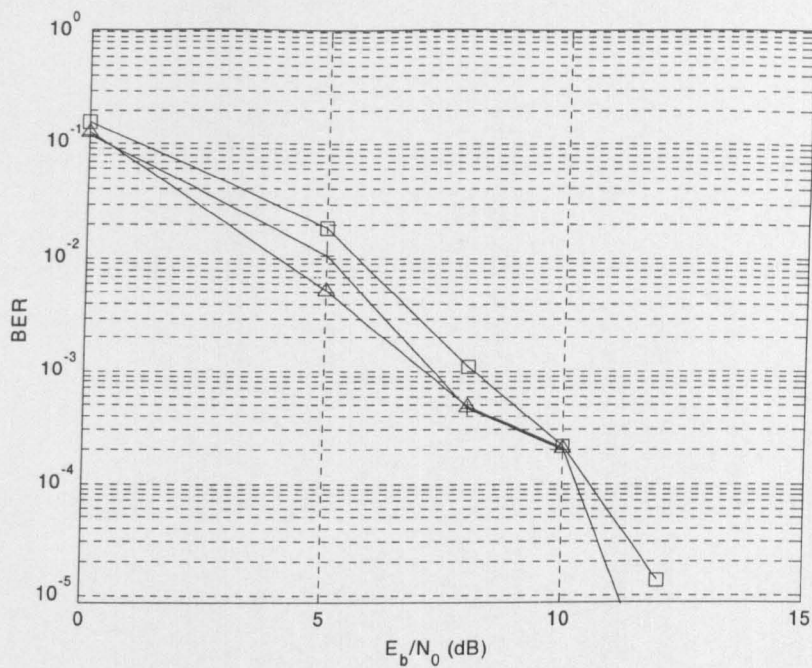


Figure 6-32: 16-QAM BER Performance in Correlated Rayleigh Channel, 4-Retx, 8-ItR
 Legend: + Method E, Δ Method R, \square Method L

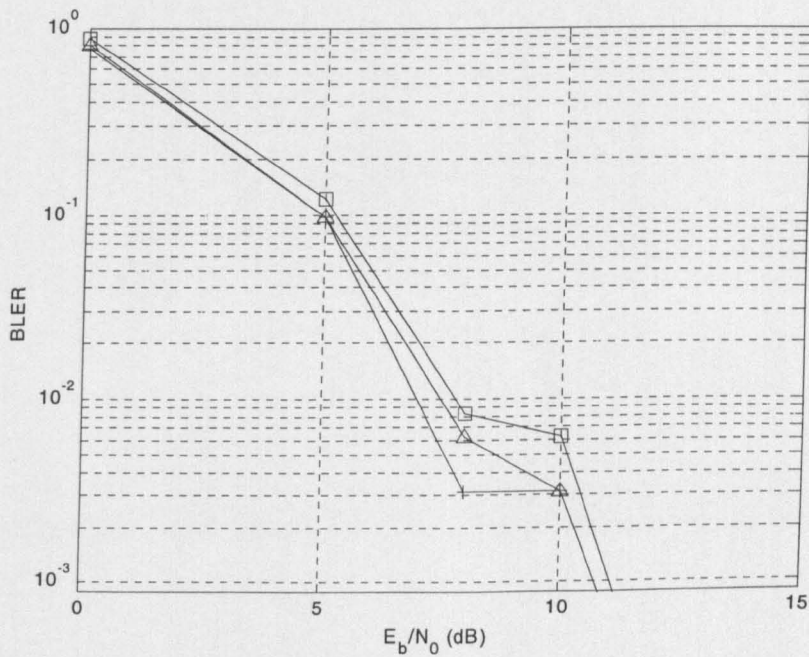


Figure 6-33: 16-QAM BLER Performance in Correlated Rayleigh Channel, 4-Retx, 8-ItR
 Legend: + Method E, Δ Method R, \square Method L

Unlike the performance in the cases of AWGN and Uncorrelated Rayleigh channels, the performance of the Method L here is not remarkably worse. However, the tendency is still worse.

It is interesting to note that the retransmission efficiency can go higher than 0.5. This means that, occasionally, the channel is good enough to make retransmission unnecessary.

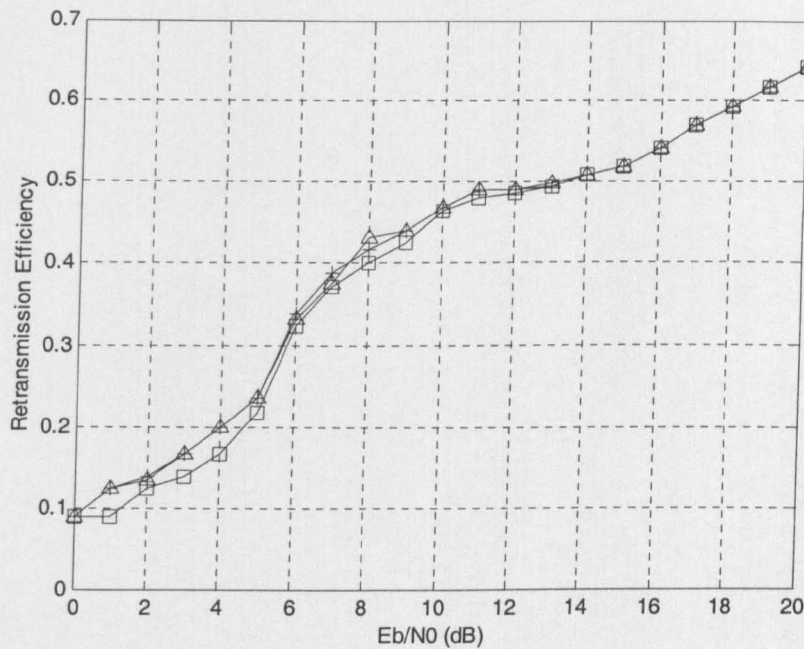


Figure 6-34: Retransmission Efficiency in Correlated Rayleigh Channel
Legend: + Method E, Δ Method R, □ Method L

6.5.2 RV Value Sequence of (6, 2, 1, 5)

Performance evaluation using this RV value sequence is mainly intended for comparison and completeness of the evaluation. As previously outlined, by examining the Table 6-6, it can be deduced that this sequence will lead to worse performance and retransmission efficiency, as the minimum effective coding rate is just 1/2. As a result, there will not be any detailed analysis performed.

6.5.2.1 AWGN Channel

Examining Figure 6-35 to Figure 6-42, and comparing them with the corresponding figures with RV(6, 1, 3, 5) in the previous section, it can be observed that there are losses of at least 1.2 dB. The loss suffered by the BLER is even greater.

However, one property is maintained throughout, that is, the performance of Method R is almost as good as that of Method E, whereas the performance of Method L is always worse.

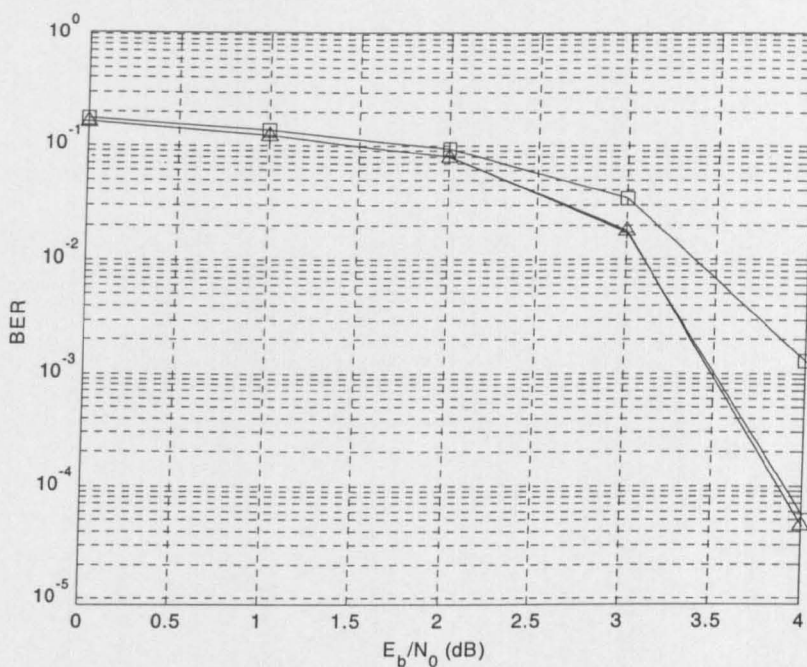


Figure 6-35: 16-QAM BER Performance in AWGN Channel, 3-Retx, 4-Ittr
Legend: + Method E, Δ Method R, □ Method L

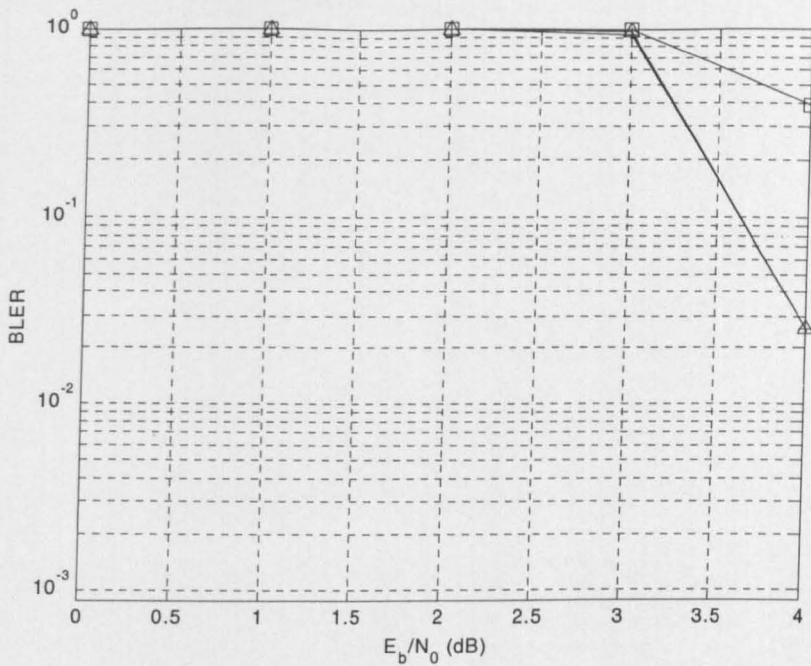


Figure 6-36: 16-QAM BLER Performance in AWGN Channel, 3-Retx, 4-Itr
 Legend: + Method E, Δ Method R, \square Method L

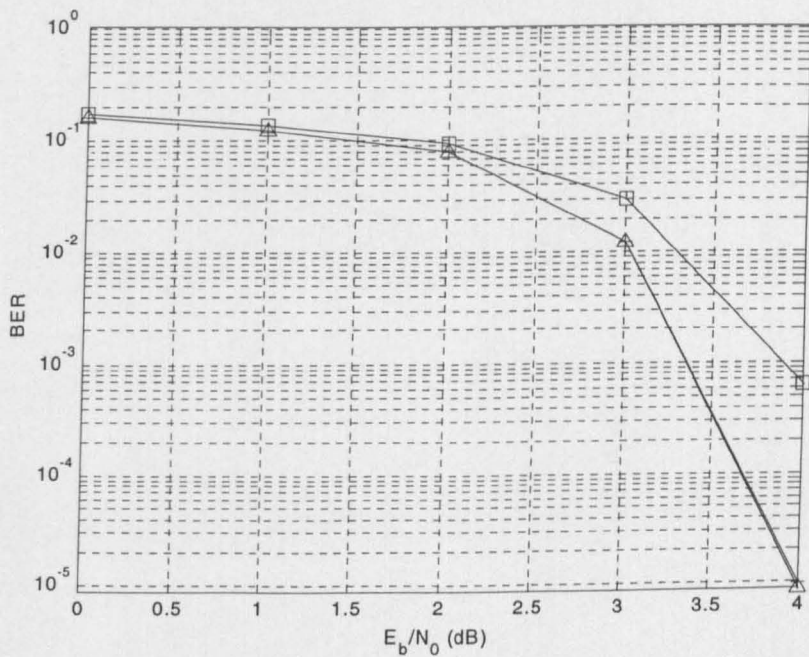


Figure 6-37: 16-QAM BER Performance in AWGN Channel, 3-Retx, 8-Itr
 Legend: + Method E, Δ Method R, \square Method L

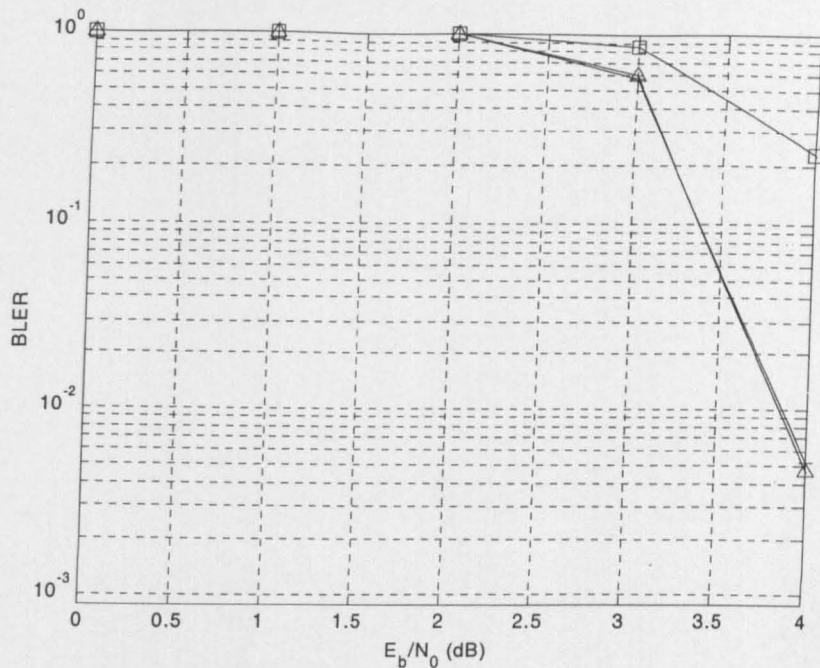


Figure 6-38: 16-QAM BLER Performance in AWGN Channel, 3-Rtx, 8-Itr
 Legend: + Method E, Δ Method R, \square Method L

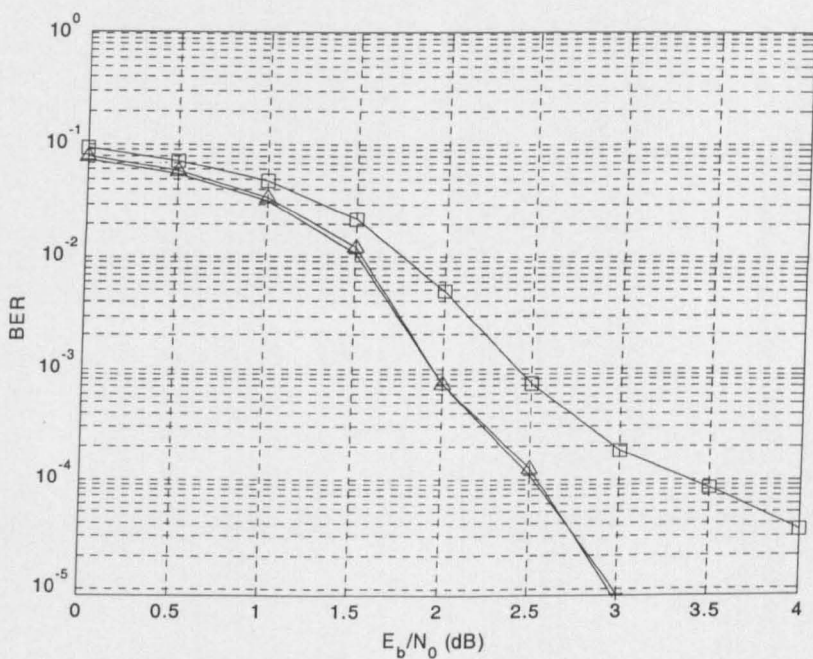


Figure 6-39: 16-QAM BER Performance in AWGN Channel, 4-Rtx, 4-Itr
 Legend: + Method E, Δ Method R, \square Method L

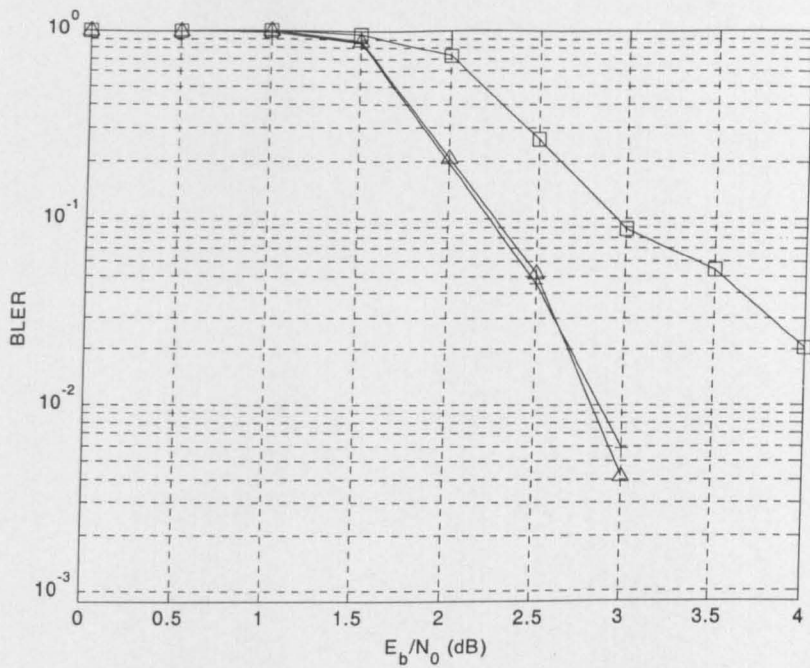


Figure 6-40: 16-QAM BLER Performance in AWGN Channel, 4-Retx, 4-Itr
Legend: + Method E, Δ Method R, \square Method L

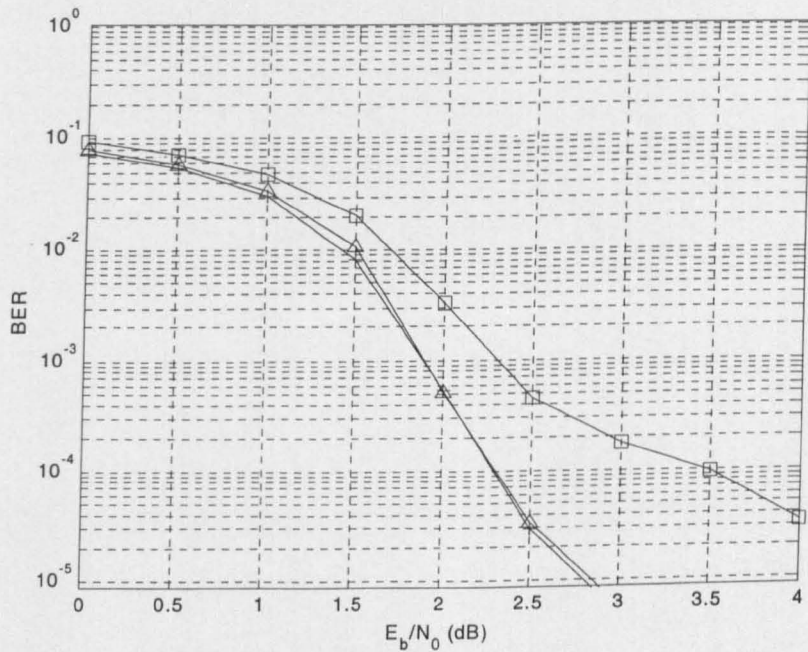


Figure 6-41: 16-QAM BLER Performance in AWGN Channel, 4-Retx, 8-Itr
Legend: + Method E, Δ Method R, \square Method L

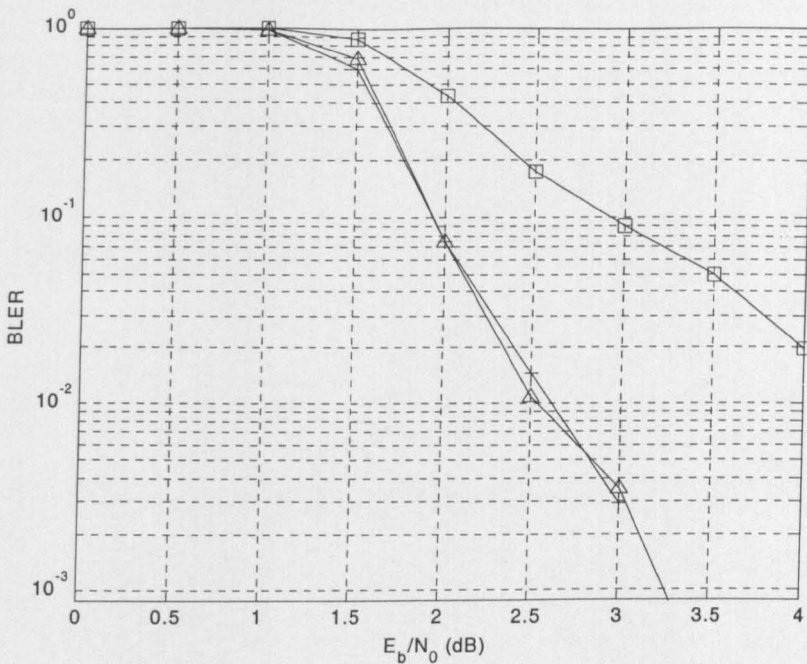


Figure 6-42: 16-QAM BLER Performance in AWGN Channel, 4-Retx, 8-Ittr
Legend: + Method E, Δ Method R, □ Method L

6.5.2.2 Uncorrelated Rayleigh Channel

The performance of the soft-demodulation methods employing the RV(6, 2, 1, 5) for different settings are depicted in Figure 6-43 to Figure 6-50. Compared to the performance of the RV(6, 1, 3, 5) counterpart, at least 1.2 dB loss is observed. These results confirm the logical analysis that the performance produced by RV(6, 2, 1, 5) for the settings depicted in Figure 6-7 is potentially worse than that produced by the RV(6, 1, 3, 5).

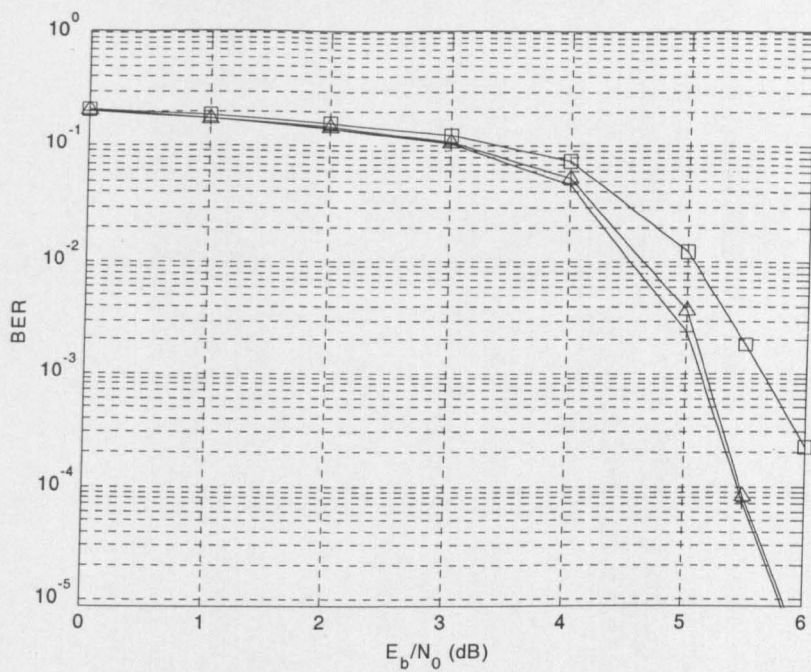


Figure 6-43: 16-QAM BER Performance in Uncorrelated Rayleigh Channel, 3-Retx, 4-Itr
 Legend: + Method E, Δ Method R, \square Method L

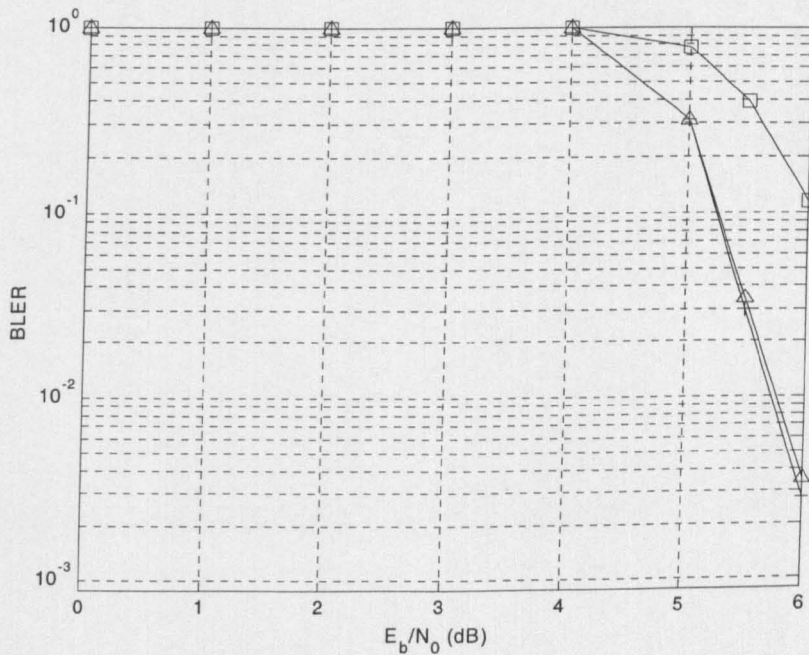


Figure 6-44: 16-QAM BLER Performance in Uncorrelated Rayleigh Channel, 3-Retx, 4-Itr
 Legend: + Method E, Δ Method R, \square Method L

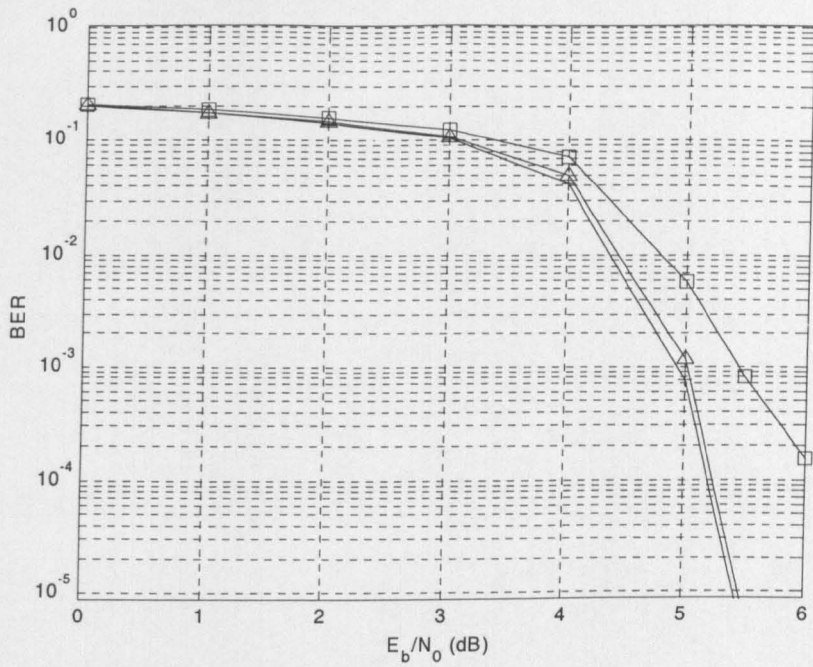


Figure 6-45: 16-QAM BER Performance in Uncorrelated Rayleigh Channel, 3-Retx, 8-Itr
 Legend: + Method E, Δ Method R, \square Method L

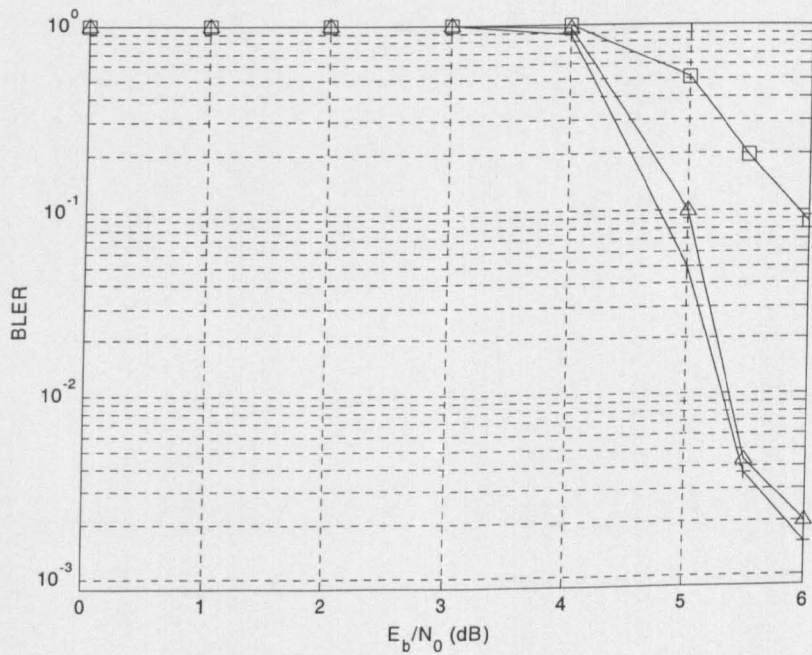


Figure 6-46: 16-QAM BLER Performance in Uncorrelated Rayleigh Channel, 3-Retx, 8-Itr
 Legend: + Method E, Δ Method R, \square Method L

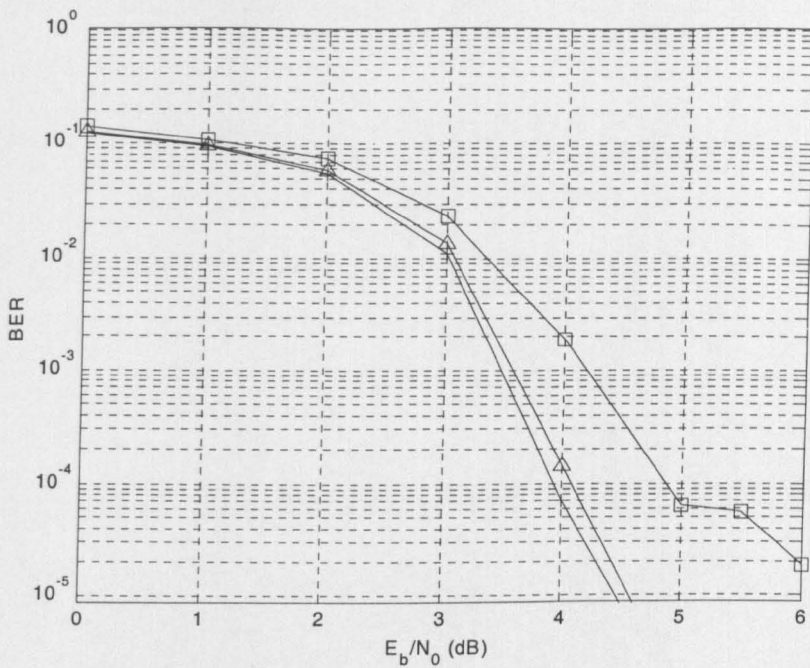


Figure 6-47: 16-QAM BER Performance in Uncorrelated Rayleigh Channel, 4-Retx, 4-Itr
 Legend: + Method E, Δ Method R, \square Method L

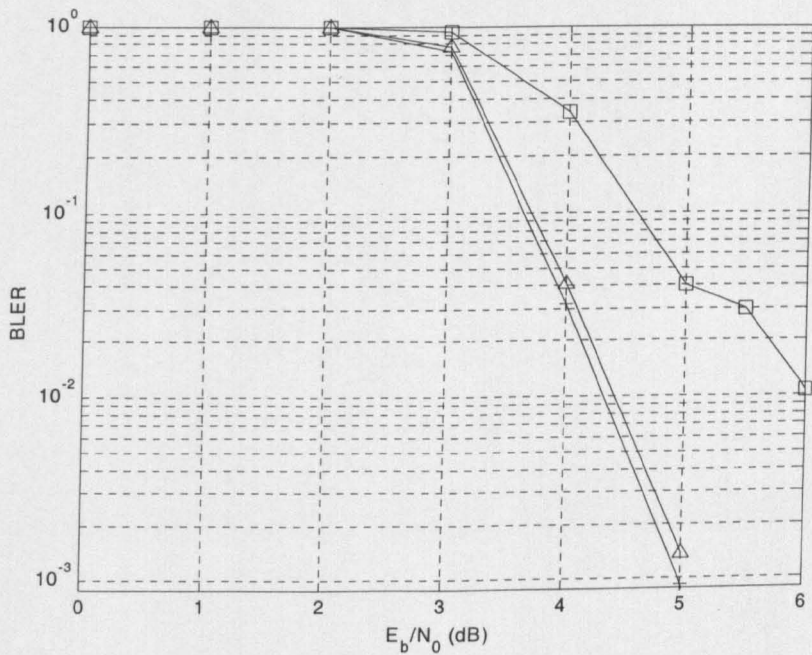


Figure 6-48: 16-QAM BLER Performance in Uncorrelated Rayleigh Channel, 4-Retx, 4-Itr
 Legend: + Method E, Δ Method R, \square Method L

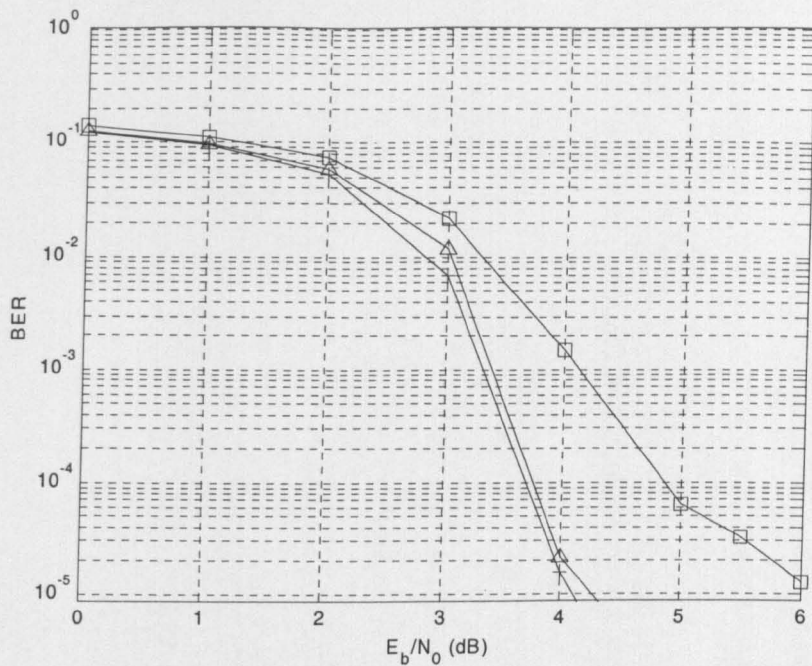


Figure 6-49: 16-QAM BER Performance in Uncorrelated Rayleigh Channel, 4-Retx, 8-Itr
 Legend: + Method E, Δ Method R, □ Method L

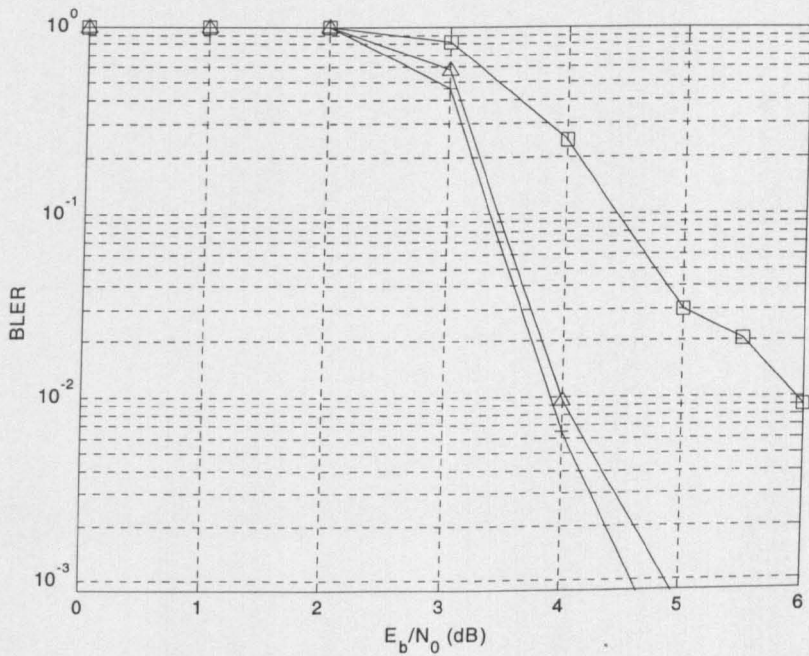


Figure 6-50: 16-QAM BLER Performance in Uncorrelated Rayleigh Channel, 4-Retx, 8-Itr
 Legend: + Method E, Δ Method R, □ Method L

6.5.2.3 Correlated Rayleigh Channel

A similar analysis to that applied to the cases of AWGN and Uncorrelated Rayleigh Channels can also be applied for the Correlated Rayleigh Channel case. Examining Figure 6-51 to Figure 6-58 and comparing them to the corresponding figures resulting from using RV(6, 1, 3, 5), it can be deduced that the losses are also experienced here. Therefore, the non-effectiveness of 3GPP RV value sequence compared to the proposed one is evident.

Nonetheless, it can be observed that the performance of Method R soft-demodulation tends to be consistently better compared to that of Method L.

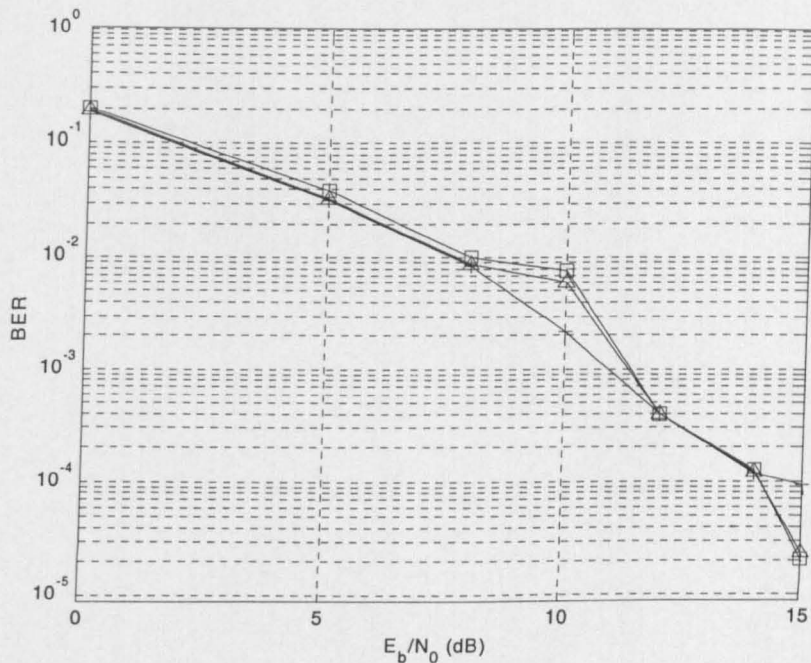


Figure 6-51: 16-QAM BER Performance in Correlated Rayleigh Channel, 3-Retx, 4-Itr
Legend: + Method E, Δ Method R, \square Method L

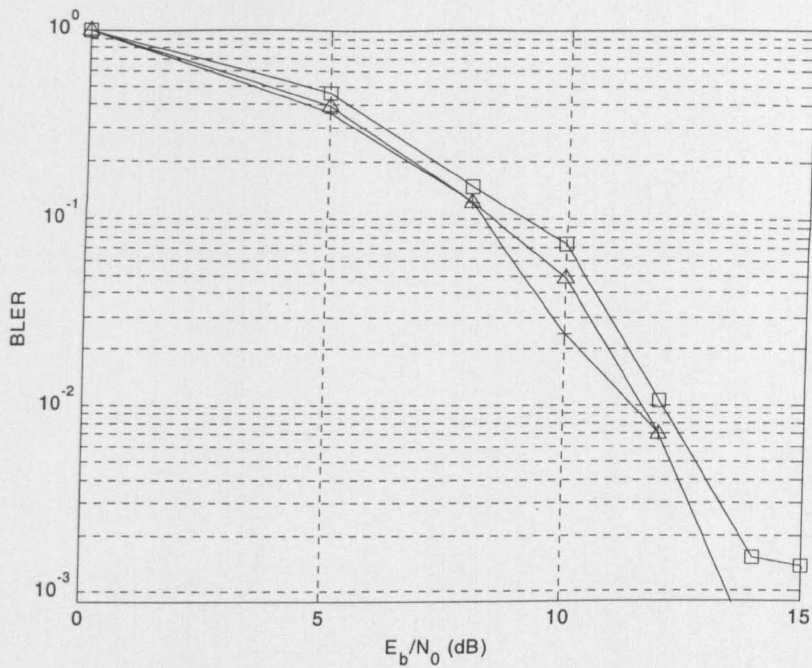


Figure 6-52: 16-QAM BLER Performance in Correlated Rayleigh Channel, 3-Retx, 4-Itr
Legend: + Method E, Δ Method R, \square Method L

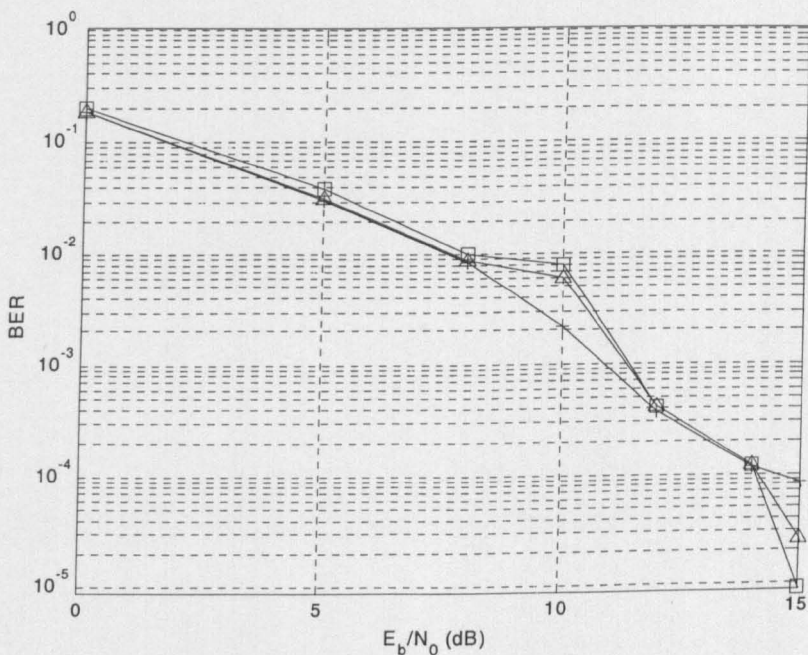


Figure 6-53: 16-QAM BER Performance in Correlated Rayleigh Channel, 3-Retx, 8-Itr
Legend: + Method E, Δ Method R, \square Method L

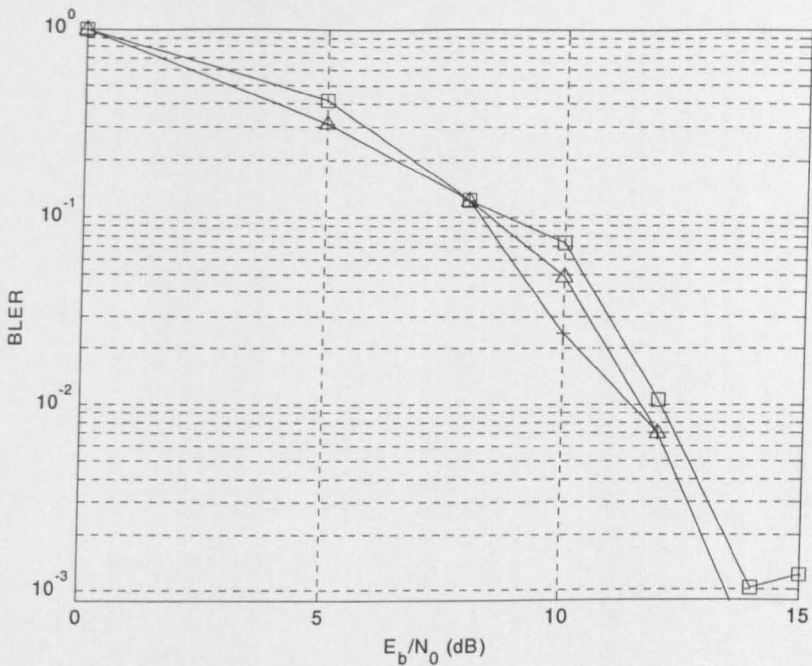


Figure 6-54: 16-QAM BLER Performance in Correlated Rayleigh Channel, 3-Retx, 8-Itr
 Legend: + Method E, Δ Method R, \square Method L

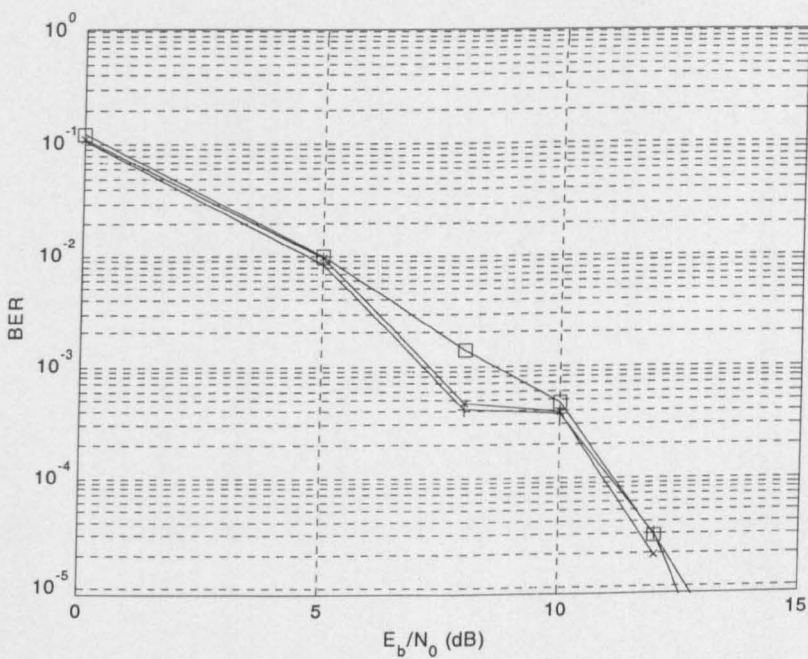


Figure 6-55: 16-QAM BER Performance in Correlated Rayleigh Channel, 4-Retx, 4-Itr
 Legend: + Method E, Δ Method R, \square Method L

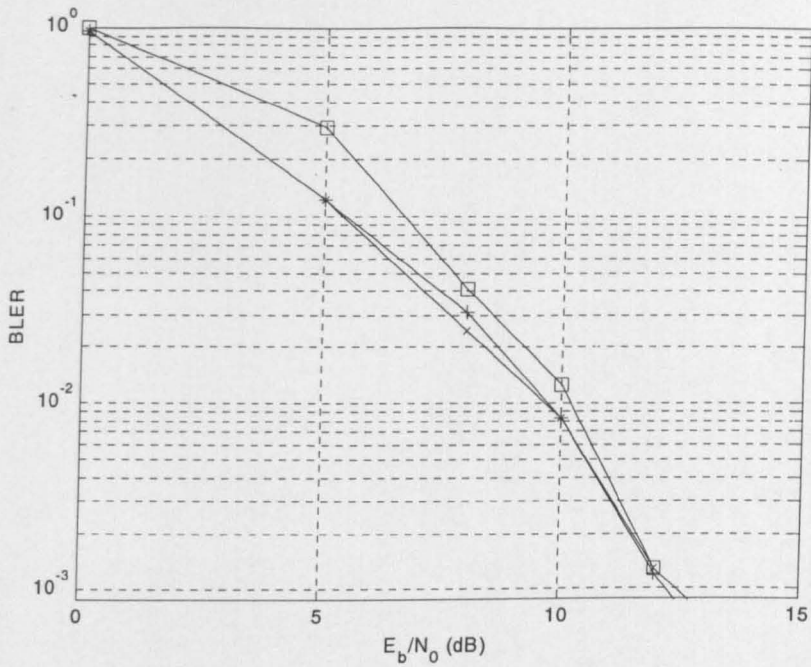


Figure 6-56: 16-QAM BLER Performance in Correlated Rayleigh Channel, 4-Retx, 4-Ittr
Legend: + Method E, Δ Method R, □ Method L

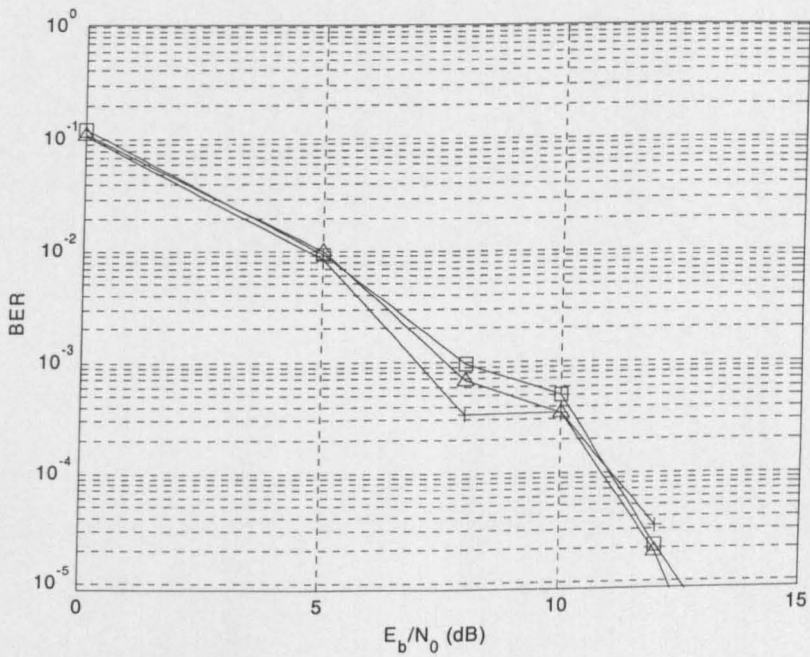


Figure 6-57: 16-QAM BER Performance in Correlated Rayleigh Channel, 4-Retx, 8-Ittr
Legend: + Method E, Δ Method R, □ Method L

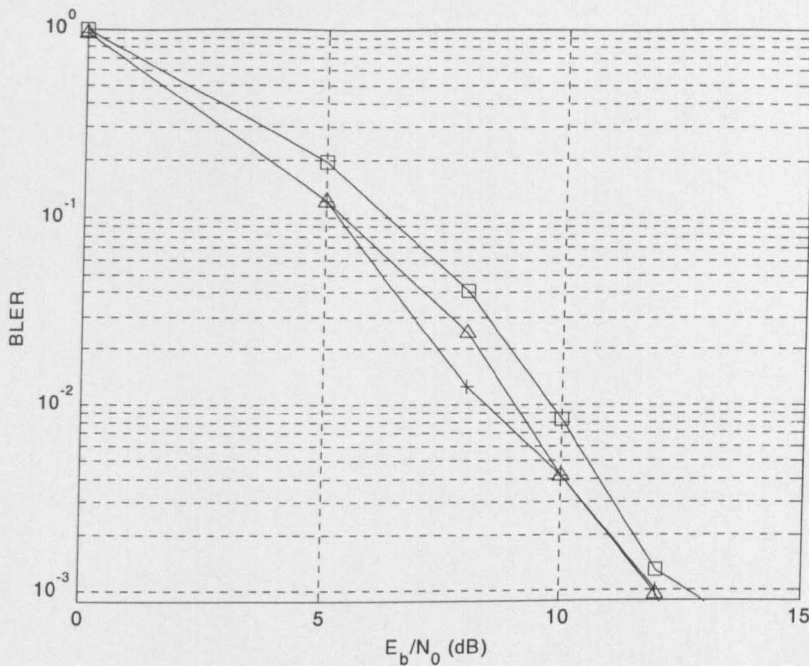


Figure 6-58: 16-QAM BLER Performance in Correlated Rayleigh Channel, 4-Retx, 8-Itx
Legend: + Method E, Δ Method R, □ Method L

6.6 Summary

Several concluding remarks are worth mentioning.

- HSDPA uses RV value sequence to determine HARQ settings, including the priority of bits to be transmitted, rate matching parameters and constellation re-arrangement.
- The choice of RV value sequence plays an important role in determining overall link performance and retransmission efficiency. It has been shown that for the chosen settings, RV(6, 1, 3, 5) performs better than RV(6, 2, 1, 5).
- In AWGN and Uncorrelated Rayleigh channels, the performance of Method E and Method R are almost the same, whereas the performance of Method L is consistently worse. In Correlated Rayleigh channel, however, the superiority of Method E is less consistent. Fortunately, 16-QAM is not particularly intended for use with high Doppler environment such as this.

Chapter 7

Conclusion

7.1 Conclusion

Motivations to undertake the research work have been identified, objectives have been set, literature has been surveyed, and possible solutions have been put forward, evaluated and compared. To summarise all these processes, several concluding remarks can be drawn as follow:

1. The introduction of TC has increased the importance of the soft-demodulation. This is particularly true when the TC is coupled pragmatically with high order modulation schemes, instead of in a more integrated way such as in a trellis-coded modulation mechanism. In this circumstance, there is a necessity to obtain bit (instead of symbol) level LLRs that can maximise the TC performance. Thus, a soft-demodulation issue arises.
2. To be able to offer high bit rate services, the HSDPA standard adopts a TC, coupled pragmatically with either QPSK or 16-QAM, in an adaptive modulation and coding scheme. This represents a realistic case where bit level soft-demodulation plays an important role in determining overall performance.
3. In the literature, detailed information regarding the soft-demodulation issue is still very limited. Moreover, the only modelling approach that can be found does not use complex-number notation. This is less realistic and leads to unnecessarily complicated implementation.
4. The adoption of complex-valued modelling approach to the communication link under consideration:
 - represents a more realistic modelling of the system, making it easier to analyse.
 - has enabled the derivation of soft-demodulation methods that are applicable in different systems and channels. Adoption of the methods for use in the single path and in multipath channels is straightforward.

- has enabled the proposed soft-demodulation methods to embed the CSI in every bit during the demodulation process. This leads to simpler overall UMTS and HSDPA implementation due to the fact that extra CSI handling and modification of constituent TC decoder become unnecessary.
5. Once the exact soft-demodulation method has been devised, various approximate methods can be derived by approximating its mathematical process. Method M is a result of such an approach. In addition, another set of approximation methods can also be derived by approximating the LLR curves. Method R is such an example.
 6. The exact soft-demodulation method for QPSK is already simple, hence no approximation method is necessary.
 7. With the inclusion of CSI during the decoding, TC performs better than when it is not included. In a single path Uncorrelated Rayleigh channel, performance improvement is approximately 1.1 dB at a BER of 10^{-5} . This evidence shows the importance of the CSI in maximising the TC performance.
 8. Particularly in 16-QAM, different soft-demodulation methods lead to significant differences in TC performance. In an AWGN channel at BER of 10^{-5} , the coding gain difference between the exact Method E and a reciprocal Euclidean method (Method C) is almost 5 dB. Even more, the difference between the extension of hard-decision method (Method F) and the exact method is estimated to be more than 10 dB. These differences are even greater in multipath channels.
 9. A channel bit-interleaver improves the TC performance. The improvement is more pronounced when the demodulated symbols are highly correlated. Similar to the characteristic of the TC internal interleaver, the longer the bit-interleaver, the larger the improvement.
 10. Using a simple approximation, the complexity of Method R is less than 10% of that of the exact method. Moreover, it performs almost as well as the exact method in many cases.
 11. The improvement offered by STTD is based on doubling the diversity order. However, it becomes less than “doubling” the diversity order as the receiver exploits more diversity by other means, for instance through rake reception in the multipath environment.
 12. In simplified HSDPA HARQ environments, the similarity of Method R to Method E, and the superiority over Method L is maintained in almost all the cases. The superiority can be expressed in terms of BER, BLER, E_b/N_0 gain or retransmission efficiency.

13. Developing a simulator from scratch requires a good understanding of the elements of the system to be simulated. Individual and overall performance validation is a very important step in order for the outputs to be valid and dependable. When a simulator becomes complicated, rendering a mathematical model intractable, validation can only be done by comparing the performance against publications in respectable literature.

Several publications as a result of the completed research work are listed in the List of Publications section, which immediately follows this chapter. It is worth noting that this research work is by no means exhaustive. A number of issues still need further investigation. These are left for future work, which are discussed in the next section.

7.2 Future Work

There are a number of issues worth investigating to complement the results reported in this thesis.

They include:

1. In order to lower the implementation complexity, the proposed approach augments the CSI estimates from different fingers and performs the soft-demodulation process after rake combining. However, in multipath channels at the rake receiver, it is possible to perform soft-demodulation at each rake finger, prior to combining. This way, the combining is carried out at LLR level. The main potential benefit of this approach is that the CSI is more relevant, which can lead to better overall performance. On the other hand, the complexity will be higher, since the soft-demodulation processes are repeated as many times as the number of rake fingers.
2. The proposed soft-demodulation methods have been applied to QPSK and 16-QAM in WCDMA environments. These methods can be applied to higher modulation orders operated in different environments, for instance in OFDM (orthogonal frequency division multiplex) and multicarrier CDMA. As technology evolves, it is very likely that 64-QAM will soon be employed too, so that formulation of the soft-decision for this modulation scheme will soon be more relevant.
3. Other advanced techniques such as Multi Input Multi Output (MIMO) and multiuser detection (MUD) can improve the overall HSDPA performance further. Application of the soft-demodulation methods in such environments will be an interesting research subject. Contribution of performance improvement to the overall performance is an issue that can be investigated.

4. The evaluation of the soft-demodulation methods in a more realistic environment involving multiple users will provide better demonstration of the performance and complexity benefits offered by the proposed methods.
5. In this thesis, only floating point numbers are used to represent LLR. In practice, fixed point implementation involving a certain quantisation technique is more likely. Therefore, it is interesting to investigate the quantisation effects on the performance.
6. Finally, to translate the concept to reality, a hardware implementation is necessary. This way, the gained performance improvement and complexity reduction can be easily demonstrated.

List of Publications

Journal Papers

1. Y. Rosmansyah, S.R. Saunders, P. Sweeney, R. Tafazolli, "Equivalence of flat and classical Doppler sample generators", *Electronics Letters*, vol. 37, Issue 4, pp. 243-244, 15 Feb., 2001.
2. Y. Rosmansyah, P. Sweeney, and M. Sweeting, "Efficient turbo coded ARQ for low earth orbit microsatellites", "Coding, Communications and Broadcasting", eds.: Farrell P, Darnell M, Honary B, Research Studies Press Ltd., Hertfordshire, ISBN: 0863802591, England, pp. 325-329, April, 2000.
3. Y. Rosmansyah, P. Sweeney, and M. Sweeting, "A turbo coded hybrid ARQ for low earth orbit microsatellite communications", *Int. J. Sat. Commun.*, vol. 17, no. 6, pp. 367-381, November-December, 1999.

Conference Papers

1. Y. Rosmansyah, "Evaluation of Optimal and Sub-Optimal Soft-Demodulation Methods for QPSK and 16-QAM using a Feature-Rich Link Simulator", CCSR Awards for Research Excellence 2003, <http://www.ee.surrey.ac.uk/CCSR/Research/Prizes/2003/>, May, 2003.
2. Y. Rosmansyah, "A new soft-demodulation method for QPSK, 16-QAM and 64-QAM that reduces turbo decoder implementation complexity", CCSR Awards for Research Excellence 2002, <http://www.ee.surrey.ac.uk/CCSR/Research/Prizes/2002/>, March, 2002.
3. C. C. Robin, Y. Rosmansyah, P. Sweeney, "SOVA for Serial Concatenated Convolutional Codes", Coding Workshop, Germany, 2001.
4. Y. Rosmansyah, P. Sweeney, R. Tafazolli, "Air interface techniques for achieving high data rates for UMTS", in Proc. 2nd Int. Conf. On 3G Mob. Communs. Technologies, U.K., pp. 368-372, 26-28 March, 2001.
5. D.R.B. Burgess, P. Sweeney, Y. Rosmansyah, S. Wesemeyer, "Low Complexity Soft-Decision decoding of Reed-Solomon Codes for a Range of Channel Conditions", in Proc. Int. Symp. On Coding an Its Application, U.K., pp. 455-458, 2001.

6. Y. Rosmansyah, C. Valadon, B.G. Evans, "Adaptive Modulation and Coding for Ka-band Satellite Air interfaces", in Proc. *IEE Seminar on Broadband Satellite*, U.K., pp. 19/1-19/6, Oct., 2000.
7. H. Herbrig, L. Lundheim, N.K. Rossing, T. Hentschel, M.-H. Silly, Y. Rosmansyah, R. Thiruvathirai, "The SORT 1 Project - Software-Radio Demonstration", Proceedings of the *1st Karlsruhe Workshop on Software Radios*, pp. 59-67, (Karlsruhe University, Germany) 29-30 March, 2000.
8. Y. Rosmansyah, P. Sweeney, and M. Sweeting, "An efficient turbo coded ARQ for low earth orbit microsatellites", Proc. *5th Int. Symp. Coding Theory and Appl.* (ISCTA'99), (Ambleside, UK), pp. 29-31, 11-16 July, 1999.
9. C. Valadon, Y. Rosmansyah, R. Tafazolli, B.G. Evans, "The SWAID Project: Deriving Powerful Modulation and Coding Schemes for Future Satellite Multimedia Satellite Systems", Proc. *6th Int. Mob. Sat. Conf.* (IMSC'99), (Ottawa, Canada), pp. 262-267, 1999.
10. C. Valadon, Y. Rosmansyah, R. Tafazolli, B.G. Evans, "Performance evaluation of FEC Coding Schemes for Future Broadband Satellite Systems", *5th Ka Band Utilization Conf.*, 1999.
11. Y. Rosmansyah, P. Sweeney, and M. Sweeting, "An investigation of the application of turbo codes for LEO microsatellite applications", Proc. *13th AMSAT-UK Colloq.*, (Guildford, UK), pp. 40-46, 1998.

References

- [Ala98] S.M. Alamouti, "A Simple Transmit Diversity Technique for Wireless Communications", *IEEE JSAC*, vol. 16, pp. 1451-58, Oct., 1998.
- [Bah74] L.R. Bahl, J. Cocke, F. Jelinek, and J. Raviv, "Optimal decoding of linear codes for minimizing symbol error rate", *IEEE Trans. Inform. Theory*, vol. 20, pp. 284-7, Mar., 1974.
- [Bar00] S. Baro, G. Bauch, and A. Hansmann, "Improved Codes for Space-Time Trellis-Coded Modulation", *IEEE Commun. Lett.*, vol. 4, pp. 20-2, Jan., 2000.
- [Bar95] A.S. Barbulescu, "Iterative decoding of turbo codes and other concatenated codes", *Ph.D. Thesis*, Univ. South Australia, 1995.
- [Bar97] A.S. Barbulescu, W. Farrell, P. Gray, M. Rice, "Bandwidth efficient turbo coding for high speed mobile satellite communications", Proc. *Int. Symp. Turbo codes*, Brest, 1997.
- [Ben95] S. Benedetto and G. Montorsi, "Performance evaluation of turbo-codes", *Electronics Letters*, vol. 31, pp. 163-5, Feb. 2nd, 1995.
- [Ben96a] S. Benedetto and G. Montorsi, "Iterative decoding of serially concatenated convolutional codes", *Electronics Letters*, vol. 32, pp. 1186-8, June 20th, 1996.
- [Ben96b] S. Benedetto and G. Montorsi, "Design of parallel concatenated convolutional codes", *IEEE Trans. Commun.*, vol. 44, pp. 591-600, May, 1996.
- [Ben96c] S. Benedetto and G. Montorsi, "Unveiling turbo codes: Some results on parallel concatenated coding schemes", *IEEE Trans. Inform. Theory*, vol. 42, pp. 409-28, Mar., 1996.
- [Ben96d] S. Benedetto, R. Garello and G. Montorsi, "Systematic encoders for convolutional codes and application to turbo codes", Proc. *IEEE Global Telecommun. Conf. (GLOBECOM)*, *Commun. Theory Mini Conf.*, pp. 6-10, London, Nov. 18-22, 1996.
- [Ber93] C. Berrou, A. Glavieux, and P. Thitimajshima, "Near Shannon limit error-correcting coding and decoding: Turbo-codes", *Proc. IEEE Int. Conf. on Commun.*, pp. 1064-70, May, 1993.
- [Ber96] C. Berrou and A. Glavieux, "Near optimum error correcting coding and decoding: Turbo-codes", *IEEE Trans. Commun.*, vol. 44, pp. 1261-71, Oct. 1996.
- [Big02] E. Biglieri, "Digital Transmission in 21st Century: Conflating Modulation and Coding", *IEEE Commun. Mag.* 50th Commemorative Issues, pp. 128-137, May, 2002.
- [Buc99] M.E. Buckley and S.B. Wicker, "A neural network for predicting decoder error in turbo decoders", *IEEE Commun. Lett.*, vol. 3, no.5, pp. 145-147, May 1999.
- [Cai98] G. Caire, G. Taricco, E. Biglieri, "Bit-Interleaved Coded Modulation", *IEEE Trans. Inf. Theory*, Vol. 44, No. 3, May, 1998.
- [Cha85] D. Chase, "Code Combining, A maximum likelihood approach for combining an arbitrary number of noisy packets", *IEEE Trans. Commun.*, vol. COM-33, pp. 385-393, May, 1985.
- [Chu01] S.-Y. Chung, *et al.*, "On the design of Lowd-Density Parity-Check codes within 0.0045 dB of the Shannon Limit", *IEEE Commun. Letters*, vol. 5, no. 2, pp. 58-60,

Feb., 2001.

- [Cla81] G.C. Clark and J.B. Cain, *Error-correction coding for digital communication*, Plenum, 1981.
- [Cro99] S. Crozier, J. Lodge, P. Guinand, A. Hunt, "Performance of turbo-codes" with relative prime and golden interleaving strategies", *Proc. 6th Int. Mobile Sat. Conf.*, (Ottawa, CAN), pp. 268-275, June 1999.
- [Dah98] E. Dahlman, B. Gudmundson, M. Nilsson, and J. Skold, "UMTS/IMT-2000 Based on Wideband CDMA", *IEEE Commun. Mag.*, pp. 70-80, September 1998.
- [Der02] R.T. Derryberry, S.D. Gray, D.M. Ionescu, G. Mandyam, B. Raghethaman, "Transmit Diversity in 3G CDMA Systems", *IEEE Commun. Mag.*, pp. 68-75, April 2002.
- [Div95a] D. Divsalar, S. Dolinar, F. Pollara, and R.J. McEliece, "Transfer function bounds on the performance of turbo codes", *JPL TDA Progress Report*, vol. 42, pp. 44-55, Aug. 15, 1995.
- [Div95b] D. Divsalar and F. Pollara, "On the design of Turbo Codes", *JPL TDA Progress Report*, vol. 42-123, pp. 99-121, Nov. 15, 1995.
- [Div96] D. Divsalar and R.J. McEliece, "Effective free distance of turbo codes", *Electronics Letters*, vol. 32, pp. 445-6, Feb. 29, 1996.
- [Div97] D. Divsalar and F. Pollara, "Serial and hybrid concatenation codes with applications", *Proc. Int. Symp. on Turbo Codes and Related Topics*, (Brest, France), pp. 80-7, Sept., 1997.
- [Dol95] S. Dolinar and D. Divsalar, "Weight Distributions for Turbo Codes using Random and Nonrandom Permutations", *TDA Progress Report*, no. 44-122, August 15, 1995.
- [Dou95] C. Douillard, M. Jezequel, C. Berrou, A. Picart, P. Didier, and A. Glavieux, "Iterative correction of intersymbol interference: Turbo-equalization", *European Trans. Telecommun.*, vol. 6, pp. 507-11, Sept./Oct., 1995.
- [For92] P.-M. Fortune, L. Hanzo, R. Steele, "On the computation of 16-QAM Performance in Rayleigh-Fading Channels", *IEICE Trans. Commun.*, Vol. E75-B, No. 6, June, 1992.
- [Gil91] K.S. Gilhousen, I.W. Jacobs, R. Padovani, A.J. Viterbi, L.A. Weaver, Jr., and C.E. Wheatley III, "On the capacity of a cellular CDMA System", *IEEE Trans. V. Tech*, vol. 40, no. 2, May 1991.
- [Hag94] J. Hagenauer, P. Robertson, and L. Papke, "Iterative (turbo) decoding of systematic convolutional codes with the MAP and SOVA algorithms", *Proc. ITG Conf.*, Sept., 1994.
- [Hag97] J. Hagenauer, "The turbo principle: tutorial introduction and state of the art", *Proc. Int. Symp. on Turbo Codes and Related Topics*, (Brest, France), pp. 1-11, Sept., 1997.
- [Hal98] E Hall and S.G. Wilson, "Design and Analysis of TCs on Rayleigh Fading Channels", *IEEE JSAC*, Vol. 16, No. 2, Feb., 1998.
- [Han00] L. Hanzo W.T. and Webb, *Single- and Multi-carrier Quadrature Amplitude Modulation*, John Wiley & Sons, 2000.
- [Han02a] L. Hanzo, T.H. Liew, M.S. Yee, *Turbo Coding, Turbo Equalisation and Space-Time Coding*, John Wiley & Sons, 2002.
- [Han02b] L. Hanzo, C.H. Wong, M.S. Yee, *Adaptive Wireless Transceivers*, John Wiley &

- Sons, 2002.
- [Has93] T. Hashimoto, "A Coded ARQ Scheme with the Generalized Viterbi Algorithm", *IEEE Trans. Inform. Theory*, Vol. 39, No. 2, pp. 423-432, Mar. 1993.
 - [Hay01] S. Haykin, *Communication System*, John Wiley & Sons Inc., 2001.
 - [Hee99] C. Heegard and S.B. Wicker, *Turbo Coding*, Kluwer Academic, 1999.
 - [Hol02] H. Holma and A. Toskala, *WCDMA for UMTS*, 2nd ed., Wiley, 2002.
 - [Jak74] W.C. Jakes, *Microwave Mobile Communications*, IEEE Press, New York, 1974.
 - [Jun94] P. Jung, M. Nasshan, and J. Blanz, "Application of turbo-codes to a CDMA mobile radio system using joint detection and antenna diversity", *Proc. IEEE Veh. Tech. Conf.*, pp. 770-4, 1994.
 - [LeG94] S. LeGoff, A. Glavieux, and C. Berrou, "Turbo-codes and high spectral efficiency modulation", *Proc. IEEE Int. Conf. On Commun. (ICC)*, pp. 645-9, May, 1994.
 - [Mic85] A.M. Michelson and A.H. Levesque, *Error-control techniques for digital communication*, John Wiley & Sons, 1985.
 - [Pae98] M. Paetzold, U. Killat, F. Laue, Y. Li, "On the statistical properties of deterministic simulation models for mobile fading channels", *IEEE Trans. Veh. Technol.*, pp. 254-269, Feb., 1998.
 - [Pae02] M. Paetzold, *Mobile Communications Channels*, Wiley, 2002.
 - [Pie94] S.S. Pietrobon and A.S. Barbalescu, "A simplification of the modified Bahl decoding algorithm for systematic convolutional codes", *Proc. Int. Symp. on Info. Theory and Applications*, (Sydney, Australia), pp. 1073-7, Nov. 1994.
 - [Pie95] S.S. Pietrobon, "Implementation and performance of a serial MAP decoder for use in an iterative turbo decoder", *Proc. IEEE Int. Symp. on Inform. Theory (ISIT)*, p. 471, 1995.
 - [Pra98] R. Prasad and T. Ojanpera, "An overview of CDMA Evolution toward Wideband CDMA", *IEEE Commun. Surveys*, <http://www.comsoc.org/pubs/surveys>, vol. 1, no. 1, pp. 2-29, Fourth Quarter, 1998.
 - [Pre92] W.H. Press, S.A. Teukolsky, W.T. Vetterling, B.P. Flannery, *Numerical Recipes in C*, Cambridge Univ. Press, 1992.
 - [Pro00] J. G. Proakis, *Digital Communications*, 3rd. ed., McGraw-Hill, 2000.
 - [Rap96] T. Rappaport, *Wireless Communications, Principles and Practice*, Prentice-Hall, 1996.
 - [Ree97] M.C. Reed and J. Asenstorfer , "A novel variance estimator for turbo code decoding", *Proc. Int. Conf. Telecommun.*, pp. 173-178, April 1997.
 - [Rob97] P. Robertson, P. Hoeher, and E. Villebrun, "Optimal and sub-optimal maximum a posteriori algorithms suitable for turbo decoding", *European Trans. on Telecommun.*, vol. 8, pp. 119-25, Mar./Apr., 1997.
 - [Ros99] Y. Rosmansyah, P. Sweeney, and M. Sweeting, "A turbo coded hybrid ARQ for low earth orbit microsatellite communications", *Int. J. Sat. Commun.*, vol. 17, no. 6, pp. 367-381, Nov.-Dec., 1999.
 - [Sau99] S.R. Saunders, "Antennas & Propagation for Wireless Commun. Sys.", Wiley, 1999.
 - [Sha48] C.E. Shannon, "A mathematical theory of communication", *Bell Syst. Tech. J.*, vol. 27, pp. 379-423, 1948.

- [Skl97] B. Sklar, "Rayleigh fading channel in mobile digital communication systems: Part I characterization", and "Part II Mitigation", *IEEE Commun. Mag.*, pp. 136-55, Sep., 1997.
- [Skl01] B. Sklar, *Digital Commun.*., 2nd ed., Prentice-Hall, 2001.
- [Sum97] T.A. Summers and S.G. Wilson, "SNR mismatch and on-line estimation in turbo decoding", *IEEE Trans. Commun.*, vol. 46, no.4, pp. 421-423, Apr., 1998.
- [Swe91] P. Sweeney, *Error Control Coding, An Introduction*, Prentice-Hall, 1991.
- [Swe02] P. Sweeney, *Error Control Coding, From Theory to Practice*, John Wiley & Sons, 2002.
- [Tar99] V. Tarokh, H. Jafarkhani, A.R. Calderbank, "Space-Time Block Codes from Orthogonal Designs", *IEEE Trans. Info. Theory*, vol. 45, pp. 1456-67, Jul. 1999.
- [TGP99a] 3GPP, TSGR4#7(99)578, "Simulation results for DL performance, 1999.
] requirements",
- [TGP99b] TSGR4(99)584, "Simulation results for UE Performance Tests", 1999.
]
- [TIA00] TIA/EIA, "IS-2000 Physical Layer Specification for CDMA Spread Spectrum Communications System", June, 2000.
- [TGP01] 3GPP, "UTRA High Speed Downlink Packet Access", Release 4, TR 25.950, V4.0.0, 2001.
- [TGP02a] 3GPP, "Physical Channels and Mapping of Transport Channels onto Physical
] Channels (FDD)", Release 5, TS 25.211, V5.0.0, 2002.
- [TGP02b] 3GPP, "Multiplexing and Channel Coding (FDD)", Release 5, TS-25.212, V5.1.0,
] 2002.
- [TGP02c] 3GPP, "Spreading and Modulation (FDD)", Release 5, TS 25.213, V5.1.0, 2002.
]
- [TGP02d] 3GPP, "UE Radio Transmission and Reception (FDD)", Release 5, TS 25.101,
] V5.3.0, 2002.
- [TGP03] 3GPP, *High Speed Downlink Packet Access: UE Radio Transmission and Reception (FDD)*, Release 5, TR 25.890, V1.3.0, Feb., 2003.
- [UMT98] UMTS-ETSI, "Selection procedures for the choice of radio transmission technologies of the UMTS", TR 101.112, V3.2.0, 1998.
- [Val01] M.C. Valenti and J. Sun, "The UMTS Turbo Code and an Efficient Decoder Implementation Suitable for Software-Defined Radios", *Int. J. Wireless Inf. Net.*, Vol. 8, No. 4, Oct., 2001.
- [Vit98] A.J. Viterbi, "An intuitive justification and a Simplified Implementation of the MAP Decoder for convolutional Codes ", *IEEE J. Select. Areas Commun.*, vol. 16, no.2, pp. 260-264, Feb, 1998.
- [Vuc00] B. Vucetic and J. Yuan, *Turbo Codes: Principle and Applications*, Kluwer Academic Publishers, 2000.
- [WCD03] WCDMA Version 3, 3GPP WCDMA Link Layer Simulator, CCSR, 2003.
]
- [Web94] W.T. Webb and L. Hanzo, *Modern Quadrature Amplitude Modulation*, Pentech Press Publishers, 1994.
- [Wen02] C. Wengerter, A.G.E.v. Elbwart, E. Seidel, G. Velev, M.P. Schmitt, "Advanced

- Hybrid ARQ Technique Employing a Signal Constellation Rearrangement”, Proc. *IEEE Veh. Tech. Conf.* (VTC2002-Fall), 24-28 Sept., 2002.
- [Woo00] J.P. Woodard and L. Hanzo, “Comparative Study of Turbo Decoding Techniques: An Overview”, *IEEE Trans. Vehic. Tech.*, Vol. 49, No. 6, pp. 2208-2233, Nov., 2000.

